Development of Online High Speed Capillary Electrophoresis Fluorescence Assays for 3', 5'-cyclic Guanosine Monophosphate (cGMP) and Pharmacokinetic Monitoring of Intranasal Administration of Drugs to the Mammalian Brain

A DISSERTATION
SUBMITTED TO THE FACULTY OF THE GRADUATE SCHOOL
OF THE UNIVERSITY OF MINNESOTA
BY

Anne Pershing Mohns

IN PARTIAL FULFILLMENT OF THE REQUIREMENTS
FOR THE DEGREE OF
DOCTOR OF PHILOSOPHY

Michael T. Bowser, Research Advisor

May 2011

ACKNOWLEDGMENTS

I would like to thank my research advisor, Dr. Michael T. Bowser, for his inspiration and guidance provided throughout my career as a graduate student. Dr. Bowser's enthusiasm for exploring new ideas and encouragement to think in nontraditional and critical ways has contributed immensely to my growth as a researcher and a person overall. Throughout this process I was encouraged to "tell a story" and feel that my ability to do so now is in large part due to his skills as a scientist, teacher, and writer. Thank you to Dr. Jared Fine, Dr. William Frey II, Dr. Leah Hanson, and the team at the Alzheimer's Research Center at Regions Hospital in St. Paul, MN. Their efforts and contributions in the field of developing therapies and elucidating the pathology of Alzheimer's disease are inspiring and bring hope to the individuals, friends, and families affected by a debilitating disease. Thank you for broadening my understanding of neuroscience and providing new avenues of exploration in analytical chemistry. I would also like to thank the members of the Bowser research lab over the years. It has been a pleasure to work with such distinguished and creative colleagues and friends. Dr. Chanda Ciriacks Klinker introduced me to MD-CE-LIF and taught me the value of patience and creative troubleshooting with specialized instrumentation. Mrs. Emily Resar observes life with a much appreciated frankness, and her friendship and dinner conversations throughout the years have been valued. Mr. Eric Castro has a wonderfully dry sense of humor and is not afraid to speak with forthrightness. I cannot thank him enough for his friendship and encouragement throughout graduate school.

Thank you to my friends and family for their amazing love and support. My mother Alison Mohns, and father Steven Mohns, have encouraged me to follow my dreams and aspirations. The contributions that they have made over the years to my educational path and life are too many to count. I have been encouraged to learn and appreciate the opportunities that life presents. There are not enough words to express the gratitude, love, and thanks that I feel for them. I have achieved my success through their belief in and support of me, and through the confidence and belief in myself that I learned from them. My brother Carl Mohns has become a person that I admire, with a wonderful family, Lindsey, Alice and David, that have proved to be an inspiration for me. I am thankful to have Carl as a brother, and friend. My grandmother Pearle Schultz, and grandfather Dr. Harry P. Schultz hold a special place in my heart. My love of literature and chemistry have stemmed from them. Their encouragement has been life long, and I keep Grandpa Hawk's mantra in mind: "Work hard. Have fun. Keep pushing back the frontiers of science." Thank you to my aunts and uncles Dr.s Tor and Emily Schultz, and Stephanie and Dick Buehler, for their wonderfully encouraging letters and phone calls; and my cousin Charlotte, to whom I wish all the best as she continues her successful graduate career, and who is a sister in my heart. A special thanks to the Bobich and Weekly families, who have given me a home and family away from home, and to Kate Janowek, for her friendship and much appreciated company at yoga class.

I offer my utmost and heartfelt thank you to Joshua Bobich, my best friend, and the person with whom I take these next steps into the future with. His love, support, and genuine appreciation for the humor in life have been constant throughout graduate

school, especially when research was challenging. Josh understands my quirks, challenges me, and inspires me to be a better person and to continue to grow. I am thankful to have met him and I officially concede the title of "The Funny One" to Josh in our marriage.

To my mother and father: for their love, encouragement,

and the gifts of Beethoven and science.

ABSTRACT

An innovative analytical system coupling online high speed microdialysis (MD) to capillary electrophoresis (CE) with laser induced fluorescence (LIF) detection has been developed for *in vivo* monitoring of chemical dynamics in the mammalian brain. Previously used for simultaneous *in vivo* monitoring and analysis of amino acid neurotransmitters; my research applied this powerful technique to the development of novel fluorescence assays for 1) the detection and monitoring of the intracellular messenger 3', 5' cyclic Guanosine Monophosphate (cGMP) and 2) monitoring pharmacokinetics of intranasal administration of drugs to the rat brain.

cGMP plays a significant regulatory role in numerous biological processes, including modulation of protein phosphorylation. Of specific interest is cGMP's proposed significance in the glutamate nitric oxide (NO) signaling pathway. As a downstream indicator of NO activity, the study of cGMP may lead to a greater understanding of the steps involved in reduction of oxidative stress and excitotoxic effects associated with human diseases and neurologically related disorders. Development of the cGMP assay was performed using a custom self built online, high speed MD-CE-LIF instrument. Derivatization was carried out in an online reaction with the guanine selective fluorogenic reagent phenylglyoxal (PGO). A flow gated interface was used to load the sample onto the separation capillary. Fluorescence was excited using the 364 nm line of an argon-ion laser in a sheath flow detector cell. Emission was collected at 90^{o}, passed through a band-pass filter, and collected on a photomultiplier tube. Optimization and characterization of the cGMP assay was carried out to achieve

maximum sensitivity, selectivity, resolution, and speed of analysis. Online detection limits of 14-19 nM (sample collected through an in-house manufactured microdialysis probe) have been achieved. cGMP was resolved at nanomolar concentrations with a temporal resolution on the order of 25-50 seconds. *In vivo* characterization of cGMP was performed in the rat striatum. Application of pharmacological agents via reverse microdialysis was performed to induce the stimulation of cGMP production. Experiments were carried out with high-K^+ aCSF, glutamate, phosphodiesterase inhibitor 3-isobutyl-1-methylxanthine (IBMX), and nitric oxide donor 2-(N-N-Diethylamino)-diazenolate-2-oxide (DEANO). Studies to establish the pharmacology of cGMP are done for two reasons: 1) confirm the identity of the cGMP peak, and 2) test current hypotheses regarding cGMP's function *in vivo.*

Working in concert with the Alzheimer's Research Center at Regions Hospital in St. Paul, we developed a novel fluorescence assay for the detection and monitoring of fluorescein in the rat brain following intranasal (i.n.) administration. A significant challenge in the development of clinical therapies for central nervous system (CNS) diseases and injuries is difficulty in delivering the agents directly to the target CNS regions due to blood brain and blood-cerebrospinal fluid barriers. The precise mechanisms underlying nose to brain transport post i.n. administration are not completely understood. MD-CE-LIF analysis of i.n. administered fluorescent compounds may elucidate possible pathways and mechanisms underlying transport from the nasal passages to the CNS and aid clinical development of drug therapies capable of directly targeting CNS regions associated with the pathology of neurological damage and

neurodegenerative diseases. Development of the fluorescein assay was performed using the custom built online high speed MD-CE-LIF instrument. A flow gated interface was used to load the sample onto the separation capillary. Fluorescence was excited using a 488 nm solid state laser in a sheath flow detector cell. Emission was collected at 90^{o}, passed through a band-pass filter, and collected on a photomultiplier tube. Optimization and characterization of the fluorescein assay was carried out to achieve maximum sensitivity, selectivity, resolution, and speed of analysis. The developed fluorescein assay achieved an online (sampled through an in house manufactured microdialysis probe) limit of detection (LOD) of 34 ± 4 pM with a temporal resolution on the order of 50 seconds. Electrophoretic separation of fluorescein was complete in 17-23 seconds at 23 kV. Animal protocol development and *in vivo* animal handling was carried out to characterize the fluorescein assay *in vivo* post intranasal administration of fluorescein. Fluorescein has been detected in the rat brain at picomolar to nanomolar concentrations and the first high temporal resolution pharmacokinetic profile of fluorescein in the rat olfactory bulb was achieved.

The optimized fluorescein assay was used to study the effectiveness of chitosan and hydroxypropyl-β-cyclodextrin (HPβCD) as nasal absorption/nasal mucosal membrane permeability enhancers of intransally delivered fluorescein with brain pharmacokinetics measured in the rat olfactory bulb via MD-CE-LIF. Whole blood samples were drawn and analyzed via microdialysis to elucidate fluorescein's likely nose to brain delivery pathways. Pharmacokinetic profiles of fluorescein in the olfactory bulb were attained with a temporal resolution not previously demonstrated or published in any

intranasal drug delivery study. Initial chitosan experiments did not indicate increased absorption and detection of fluorescein in the rat olfactory bulb. HPβCD demonstrated significant fluorescein enhancement in the brain relative to intransally administered fluorescein without an absorption enhancer.

The temporal resolution advantages associated with MD-CE-LIF allowed information to be measured on a time scale not possible in previous cGMP assays, and provided the first high temporal pharmacokinetic profile of fluorescein in the rat olfactory bulb. A high potential is indicated for application of MD-CE-LIF to brain pharmacokinetic study in the development of future intranasal drug therapies directly targeting the central nervous system.

TABLE OF CONTENTS

LIST OF TABLES

CHAPTER 1

CHAPTER 2

CHAPTER 3

CHAPTER 4

LIST OF FIGURES

CHAPTER 1

CHAPTER 2

CHAPTER 3

CHAPTER 4

LIST OF ABBREVIATIONS

AUC→40	Area Under the Curve to 40 minutes
AUC→120	Area Under the Curve to 120 minutes
aCSF	Artificial Cerebrospinal Fluid
AD	Anoxic depolarization
AMPA	amino-3-hydroxy-5-methyl-4-isoxazole-propionic acid
A/P	Anterior/Posterior
AMP	Adenosine Monophosphate
ADP	Adenosine Diphosphate
ATP	Adenosine Triphosphate
ACN	Acetonitrile
α-CD	Cyclodextrin
BBB	Blood Brain Barrier
BTP	Breakthrough Pain
cAMP	cyclic Adenosine Monophosphate
CBF	Ciliary Beat Frequency
CBQCA	3-(4-carboxybenzoyl) quinoline-2-carboxaldehyde
CE	Capillary Electrophoresis
cGMP	3', 5' cyclic Guanosine Monophosphate
Cmax	Maximum Concentration
CNS	Central Nervous System
CNQX	6-cyano-7-nitroquinoxaline-2, 3-dione
CZE	Capillary Zone Electrophoresis
DAAO	D-amino Acid Oxidase
DEANO	2-(N-N-Diethylamino)-diazenolate-2-oxide
DNS	Dansyl 5-methylaminonapthalene-1-sulfonyl chloride
DC	Deoxycholate
DMPG	3, 4-dimethoxyphenylglyoxal
DMSO	Dimethylsulfoxide

DMβCD	Dimethyl-β-cyclodextrin
DTI	Drug Targeting Index
DTP%	Drug Transport Percent
D/V	Dorsal Ventral
EOF	Electroosmotic Flow
FD	Fluorescein Isothiocyanate Labeled Dextran
FITC	Fluorescein-5-isothiocyanate
FA	Fluorescamine
FQ	3-(2-furoyl)-quinoline-2-carboxaldhyde
GABA	γ-Aminobutyric Acid
GDP	Guanosine diphosphate
GTP	Guanosine Triphosphate
GMP	Guanosine Monophosphate
GO	Glyoxal
GTP	Guanosine Triphosphate
HPLC	High Performance Liquid Chromatography
HPβCD	Hydroxypropyl-β-cyclodextrin
HPγCD	Hydroxypropyl-γ-cyclodextrin
IBMX	3-Isobutyl-1-methylxanthine
IGF-I	Insulin-like growth factor
I.N.	Intranasal
I.V.	Intravenous
KCN	Potassium cyanide
K^+-aCSF	High potassium artificial cerebrospinal fluid
LIF	Laser Induced Fluorescence
LOD	Limit Of Detection
LPC	L-α-lysophosphatidylcholine
MD	Microdialysis
MEKC	Micellar Electrokinetic Chromatography
M/L	Medial/Lateral

MWCO	Molecular Weight Cutoff
MGO	Methylglyoxal
MDPG	3, 4-methylenedioxyphenylglyoxal
MDQ-CE	Commercial Capillary Electrophoresis System
MRP	Multidrug Resistance Proteins
MS	Mass Spectrometry
NaAc	Sodium Acetate
NBD-F	4-fluoro-7-nitro-2, 1, 3-benzoxadiazole
NDA	Naphthalenedialdehyde
NMDA	N-methyl-D-aspartate
NGF	Nerve Growth Factor
NT-I	Cobtrotoxin
nNOS	neuronal Nitric Oxide Synthase
NO	Nitric Oxide
OB	Olfactory Bulb
OPA	o-Phthaldialdyde
ORN	Olfactory Receptor Neurons
PDE	Phosphodiesterase
PGO	Phenylglyoxal
PKG	cGMP dependent protein kinases
PMT	Photomultiplier Tube
PO	Peppermint Oil
RIA	Radioimmunoassay
sGC	soluble Guanylyl Cyclase
STDHF	Sodium Taurohydrofusidate
SDC	Sodium deoxycholate
SNAP	S-nitroso-N-penicillamine
SNP	Sodium nitroprusside
TEER	Transepithelial Electrical Resistance
TJ	Tight Junctions

Tmax	Time to maximum concentration
TMPG	3, 4, 5-trimethoxyphenylglyoxal
TDC	Taurodeoxycholate
TMPP	2, 3, 5, 6-Tetramethylpyrazine
UV	Ultraviolet
WGA-HRP	Horseradish Peroxidase

Chapter 1:

Introduction to Secondary Neuromessenger Cyclic Guanosine Monophosphate and Intranasal Drug Delivery

INTRODUCTION

cGMP plays an important regulatory role in numerous biological processes, including modulation of protein phosphorylation.[3, 4] Of specific interest is cGMP's proposed significance in the glutamate N-methyl-D-aspartate (NMDA) nitric oxide (NO) signaling pathway. Glutamate is the most abundant excitatory neurotransmitter in the brain with release into >50% of all brain synapses.[4] Elevated concentrations of extracellular glutamate are associated with neural injury, such as stroke.[5] and are toxic to neurons. Anti-excitotoxic drugs targeted at reducing glutamate activity however, have been shown to induce serious harmful psychomimetic and/or cardiovascular side effects.[6] As a result research is now focusing on other neurochemicals related to the glutamate/NMDA/NO interaction. Common disorders associated with cGMP/NO production or impairment include hypertension, hypercholesterolemia, diabetes, erectile dysfunction, heart failure, epilepsy, cerebral ischemia (stroke), and neurodegenerative diseases e.g. Parkinson's disease.[7-12] Research involving the study of cGMP is essential in the effort to understand the pathogenesis of human diseases and the treatment of neurologically related disorders. As a downstream indicator of glutamate and nitric oxide (NO) activity, the study of cGMP may also lead to a greater understanding of the steps involved in reduction of oxidative stress and excitotoxic effects associated with the glutamate/NMDA/NO pathway.

Previous *in vivo* microdialysis studies have utilized a radioimmunoassay (RIA) for cGMP analyses. Experiments based on RIA analysis have established basal levels of cGMP in the rat striatum between 6-9 nM.[13, 14] Though sensitive, these RIAs have

significant limitations. Long sampling times are required, once every 20 minutes, and the production of radioactive waste introduces unwanted health and hazardous waste disposal concerns.[13, 15, 16] Development of a high speed assay incorporating increased sensitivity and time resolution over conventional RIA methods and utilizing non radioactive materials will greatly benefit *in vivo* studies of cGMP. Until now, there was no assay allowing cGMP to be resolved or detected with high temporal resolution.

This thesis first focuses on the development and optimization of a cGMP assay (Chapter 2) capable of resolving and detecting cGMP in the rat brain with a temporal resolution on the order of seconds, instead of tens of minutes. Development of the cGMP assay was performed using a custom built online, high speed MD-CE-LIF instrument. Derivatization was carried out in an online reaction with the guanine selective fluorogenic reagent phenylglyoxal (PGO). Optimization and characterization of the cGMP assay was carried out to achieve maximum sensitivity, selectivity, resolution, and speed of analysis. Detection limits capable of resolving cGMP at nanomolar levels with a temporal resolution on the order of seconds have been achieved. This time scale offers a significant improvement over previous cGMP *in vivo* microdialysis. A more definitive picture of cGMP's role as a secondary messenger can be gained through the use of this powerful technique.

Continuing the study of brain dynamics with high temporal resolution, Chapter 3 shifts focus to explore the potential of applying high speed online MD-CE-LIF to the study of intranasal drug delivery pharmacokinetics. Development and optimization of a MD-CE-LIF fluorescein assay was carried out and characterized *in vivo* in the rat

olfactory bulb post intranasal administration. The work is part of a collaborative project with the Alzheimer's Research Center at Regions Hospital in St. Paul, MN to determine whether the MD-CE-LIF system is compatible with research involving *in vivo* analysis of intranasally administered drug therapies. Frey, Hanson, Thorne and coworkers have developed a careful characterization of nose to brain transport, indicating the existence of a direct nose to brain pathway post intranasal administration.[17-27] Poor temporal resolution typically limits pharmacokinetic profiles of drug absorption and clearance in the brain, however. Using MD-CE-LIF, high temporal resolution pharmacokinetic profiles of fluorescein in the olfactory bulb were achieved. These results demonstrate high potential for application of the MD-CE-LIF system to other intranasal drug development studies.

The final chapter of this thesis (Chapter 4) focuses on whether the application of nasal absorption enhancement compounds to intranasally administered drugs may increase the bioavailability of the drug in target regions of the CNS at therapeutically relevant levels and what effect enhancers have on the rate at which a drug can reach the CNS. Fluorescein was co administered with two separate nasal absorption and permeation promoters: Hydroxypropyl-β-cyclodextrin (HPβCD) and Chitosan, and delivered intranasally. Application of HPβCD and absorption enhancer increased the bioavailability of intranasally administered fluorescein in the rat olfactory bulb; chitosan did not demonstrate any advantage over fluorescein administered intranasally alone.

In contrast to the poor temporal resolution and 15-20 minute separations in HPLC, and radioimmunoassay analysis of intranasally administered compounds, the MD-

CE-LIF instrument is capable of 20-30 second separations by CE.[28-34] This dramatic improvement in temporal resolution will demonstrate the importance of high speed separations for the monitoring of *in vivo* pharmacokinetic dynamics and the high potential application of MD-CE-LIF to high throughput analysis and development of pharmacokinetic drug profiles with the best temporal resolution available to current drug therapy research.

BACKGROUND

3', 5'-cyclic Guanosine Monophosphate

Cyclic guanosine monophosphate (Figure 1.01) is a downstream intracellular messenger in the proposed glutamate NMDA signaling pathway[35-37] (Figure 1.02). Extracellular cGMP has been found to play a significant role in intracellular messaging

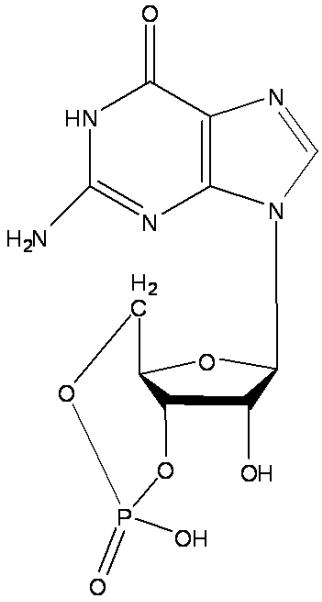

Figure 1.01. Structure of cGMP

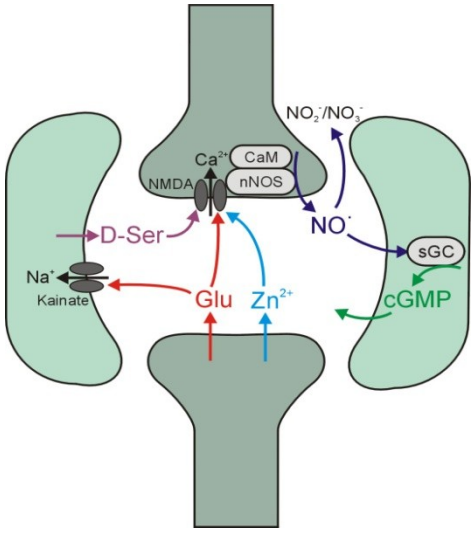

Figure 1.02. Proposed neuromessenger pathway

and communication,[38] smooth muscle relaxation, neutrophil degranulation, inhibition of platelet aggregation, and promoting modulation of protein phosphorylation.[15, 39] Initiation of the glutamate/NMDA/NO pathway begins when the NMDA receptor is activated by the binding of glutamate and co activation of the glycine site. At depolarized potentials, Mg^{2+}, bound in the pore of the NMDA channel, is driven out of the pore, opening the ion channel. Ca^{2+} enters the intracellular region via the receptor operated ion channels,[13] generating an action potential in the receiving neuron. Binding of calcium to calmodulin then occurs. This binding event activates the enzyme neuronal nitric oxide synthase (nNOS) which catalyzes the generation of NO from the amino acid L-arginine. Rather than acting directly on a cell surface receptor, NO diffuses readily through membranes, and binds to the heme moiety of soluble guanylyl cyclase (sGC).[40] Activation of sGC causes the catalytic conversion of guanosine triphosphate (GTP) into cGMP. Increased levels of cGMP in the intracellular region activate cGMP-dependent protein kinases (PKG) and cGMP-gated ion channels. cGMP can then undergo degradation via hydrolysis by a phosphodiesterase (PDE) or is exported from the cell into the extracellular environment via multidrug resistance proteins (MRP).

Ashman et al.[41] first discovered cGMP in a biological system via its isolation in rabbit urine in 196. The identification of cGMP as a natural component of mammalian tissues however was difficult due to the lack of sufficiently sensitive analytical methods.[42] Six years later Goldberg et al. developed a sequential enzymatic cycling system to generate and fluorimetrically measure pyruvate, a downstream product of the converted cGMP. cGMP was isolated in the liver, kidney and brain.[42] cGMP's

importance in the mammalian brain was revealed in studies performed soon after its identification in tissue samples. Initial experiments involved the isolation and identification of cGMP in the cerebellum and retina[43] and the activation of glutamate receptors and consequent increase in cGMP concentrations.[16, 44, 45] Further clarification of the physiological steps involved in the production and degradation of cGMP is needed. The over stimulation of receptors for excitatory neurotransmitters, a process known as excitotoxicity, is neurotoxic and linked to neural damage. High concentrations of glutamate and other excitatory neurotransmitters can also result in cell death. Manipulation of the downstream components of the proposed signaling pathway, like cGMP, may lead to the treatment of injury induced by excessive glutamate.

Nitric Oxide

In order to understand how the manipulation of cGMP may reduce excitotoxic glutamate effects, it is necessary to clarify the steps and chemical interactions of the neuromessenger pathway that link glutamate to cGMP. In addition to the excitotoxicity associated with excessive glutamate stimulation, radicals like NO can cause heavy damage to brain tissues and neurons. Due to the short half life of NO, most research has focused on measuring NO's downstream oxidation products, nitrite and nitrate. cGMP monitoring may prove a more ideal indicator to NO activity and allow the downstream effect of NO to be studied. cGMP production from sGC undergoes an amplification process due to signaling cascades. As a result of the large number of cGMP molecules produced for every NO that binds to sGC nNOS activity is amplified. Monitoring of cGMP may allow better detection of subtle changes in nNOS activity.

Current research studies are attempting to clarify cGMP's role in physiological processes.[38, 14, 46-48,68-73] It is theorized that cGMP collected during *in vivo* microdialysis reflects NO synthase activity,[14] further lending credence to the NMDA receptor → nitric oxide (NO) → cGMP pathway. Treatment of mice with NMDA or non-NMDA receptor agonists has been found to increase cGMP levels in the brain and the process was inhibited by NOS inhibitors.[49] Another study found the effects of NO mediated by cGMP, resulting in reduced neuronal damage associated with toxic effects of excess NO. NO toxicity is further enhanced via its reaction with superoxide to form peroxynitrite, an even more toxic free radical. Investigation of cGMP and its neurological role are necessary to understanding cGMP related physiological processes, and also clarify the results of altered activity in the proposed neuromessenger pathway.

Soluble Guanylyl Cyclase

cGMP synthesis is catalyzed by the activation of soluble guanylyl cyclase (sGC) resulting in the enzymatic conversion of guanosine triphosphate (GTP) to cGMP. Cellular cGMP levels are maintained by the rate of synthesis by soluble guanylyl cyclases. sGC is highly expressed in Purkinje cells, with lower expression found in stellate, basket, Golgi and granule cells.[40] Guanylyl cyclases have important roles in the cardiovascular and nervous system, vision, and bone development.[50] sGC is a heterodimer composed of an alpha and beta subunit, each containing a regulatory domain, a coiled-coil domain, and a cyclase domain.[40] Though the steps involved in the intermediate and latter activation of sGC are still not well known[40] the initial step involves the binding of NO to sGC to form

a nitrosyl-heme complex. This causes sGC to increase its activity by 100-300-fold, catalyzing the conversion of guanosine triphosphate into cGMP.

Phosphodiesterase and Multidrug Resistance Protein

Elimination of cGMP from the cell occurs via metabolic degradation by phosphodiesterases (PDE) as well as export into the extracellular region by membrane bound proteins like multidrug resistance proteins (MRP). The mechanism by which cGMP is exported from the intracellular to the extracellular region was not initially well understood. Recent research by Jedlitschky et al. has provided evidence that the cellular efflux of cGMP occurs via the multidrug resistance protein isoform MRP5, and to a more limited extent MRP4.[15, 46, 51-55] Boadu et al.[56] believe that other proteins may also contribute to cGMP efflux from human erythrocytes in addition to the highly specific MRP5.

Studies of cellular transport of cGMP into the extracellular region suggest that extracellular cGMP concentrations are indicative of sGC activity within the cell.[8] The clearance mechanisms of cGMP are important for the time course of cGMP activity within the cell.[40] In the family of phosphodiesterases, PDE5, PDE6, and PDE9 are highly cGMP specific. Phosphodiesterases were first detected by Sutherland and coworkers in 1958.[12] PDEs are highly involved in the cellular regulation of cGMP levels. A 2-4 fold increase in cGMP concentration will induce a significant physiological response leading to a reduction of cGMP levels. The regulation of cGMP by phosphodiesterases keeps cGMP concentrations within a narrow range.[12] Activation of PKGs can lead to the

inhibition of calcium influx into smooth muscle cells and mediate vasorelaxation and protein phosphorylation.

MICRODIALYSIS

In order to increase the understanding of cGMP's physiological role in the glutamate/NMDA/NO pathway, it will be necessary to develop methods for the sampling and detection of cGMP in biological samples. Microdialysis is a sampling technique frequently used for measuring extracellular concentrations of low molecular weight compounds in tissues. It may serve as an ideal tool for biological studies involving cGMP. Analysis is frequently performed *in vivo*, and has been extensively applied to the field of pharmacological and metabolic study.[57] Many studies have proven its sensitivity in sampling the extracellular space in discrete brain locations and monitoring the action of exogenous substances e.g. neurotransmitters.[13, 28, 48, 57-66] Sampling occurs by means of a small probe equipped with a semi permeable dialysis membrane with a low molecular weight cutoff, usually 5-30 kDa[67] (Figure 1.03). Commercially available microdialysis probes have polymeric membranes (cuprophan, polyacrylonitrile, and polyethersulfone) with molecular weight cutoff (MWCO) values that range between 5 and 100 kDa.[68] Typical pore sizes in a dialysis

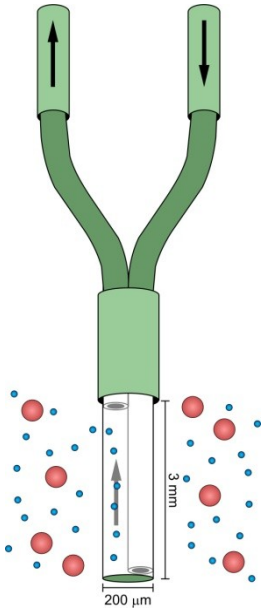

Figure 1.03. Side by side microdialysis probe. Amino acids and other small molecules (blue particles) diffuse across the membrane on the left side of the probe. Proteins and macromolecules (red particles) are prevented from diffusing. Polyimide resin seals the microdialysis membrane and prevents diffusion. Black arrows represent flow of artificial cerebral spinal fluid (aCSF) through the probe.

probe allow free diffusion of analytes such as amino acids,[69] and prohibits protein and macromolecule diffusion, simplifying sample clean up.[57, 70] After introduction into the target area of tissue analysis, perfusion buffer is pumped through the probe. Artificial cerebrospinal fluid (aCSF) is typically used as the perfusate in brain microdialysis experiments. The ionic composition of the perfusate closely matches that of the fluid in the extracellular region. Small molecules diffuse from the surrounding area, cross the membrane, and enter into the perfusion solution. The concentration of neurotransmitters collected using a microdialysis probe are limited by analyte properties such as molecular weight and diffusion rate in the surrounding medium, membrane properties, flow rate of solution through the probe and the size of the sampling region.[67] An equilibration time of approximately 1 hour prior to data collection allows the tissue area surrounding the probe to recover from damage and stress induced by the probe implantation procedure. Microliter sized fractions are collected from the outlet of the probe for analysis.[70] Temporal information, including changes in analyte concentration over time, can be gathered. A number of advantages are associated with the microdialysis technique. No sample fluid is removed from the physiological system, allowing multiple replicate measurements to be made,[67, 70-75] simultaneous monitoring of multiple compounds can be performed, and damage to the tissue area under study is minimized.[64, 69] Four designs of microdialysis probes are in common use today for sampling biological matrices.[69] These types are linear, loop, concentric, and side-by-side. The linear probe is typically used in peripheral tissues and is a flexible tubular construct. The loop probe is useful for subcutaneous tissue or peritoneal sampling. It has a longer membrane (2-4 cm) vs. the

typical 2-4 mm used in other designs. The loop probe is also a variation of the concentric probe. Concentric probes are often used for *in vivo* microdialysis of the brain, vasculature, and systemic tissues. These probes are useful for stereotaxic implantation of the probe and placement into precise tissue locations, due to the rigid structural nature of the probe. The usage of side-by-side probes (Figure 1.03) is most frequently applied to brain dialysis studies.[69] The flexibility of the side-by-side probe is beneficial for experiments incorporating behavior of live test animals that may move around during sampling. Microdialysis probes are generally less than 1 mm in diameter.[64]

A number of advantages are associated with the microdialysis technique. Typical pore sizes in a dialysis probe allow free diffusion of analytes in a 20-50 kDa molecular weight range.[69] This prohibits protein and macromolecule diffusion, simplifying sample clean up.[57, 70] No sample fluid is removed from the physiological system, allowing multiple replicate measurements to be made,[67, 70] simultaneous monitoring of multiple compounds can be performed, and damage to the tissue area under study is minimized.[64, 69]

A common limitation to microdialysis is poor temporal resolution. Temporal resolution is defined by the amount of time taken for a 10%-90% step change in the baseline when introduced to a change in analyte concentration. Temporal resolution can be affected by two components: 1) the perfusion rate through the microdialysis probe and 2) the quantity of sample mass required for the analytical detection system.[76] Temporal resolution is on the order of minutes for small volume probes. This is due to limited perfusion rates of a few microliters per minute.[70] Sample handling is a particular concern.

The dialysate fractions collected were usually separate from the analytical detection system. Samples are subject to 1) a high amount of evaporation,[77] and 2) sample loss due to adhesion of the liquid to the tube during sample transfer.[76] Broadening of samples zones due to Taylor dispersion as they are transferred from the MD probe to an analytical system is a significant contribution to poor temporal resolution. Large sample volumes of brain dialysate are frequently collected to obtain a sufficient amount of the analyte detectable by the analytical instruments due to mass sensitivity of the specific detection system. Physiological events that occurred on small time scales are therefore difficult to record due to sample collection times of 30-40 minutes.[69] At present, 5-15 minute sample collection fractions are common for radiochemical and high performance liquid chromatography (HPLC) analysis.[78-80] These off-line microdialysis analysis systems do not provide the temporal resolution necessary to measure neurological events that occur on a rapid time scale.

PREVIOUS CYCLIC GUANOSINE MONOPHOSPHATE ASSAYS

A major focus in current research couples off-line microdialysis sample collection and radioimmunoassay (RIA) analysis to monitor cGMP levels.[8, 38, 47, 75, 81] RIA can measure very small amounts of cGMP with high sensitivity and specificity. The RIA is an assay based on the reversible and non-covalent binding of an antigen by a specific antibody employing radioactivity labeled antigen to measure the fraction of the antigen (hapten) bound to a substoichiometric amount of antibody.[82] Early RIA were used to detect the first reported isolation of cGMP in mammalian tissues.[43] In 1993, Vallebuona and Raiteri[13] carried out initial studies utilizing the radioimmunoassay method for

detection of cGMP in the rat brain. They found 6.7 nM cGMP basal levels in the cerebellar cortex region based on a cGMP radioimmunoassay with a temporal resolution of 20 minutes. Multiple RIA microdialysis experiments have concurred on a range of the basal values of cGMP between 6 to 9 nM. More recent research however suggests that basal extracellular cGMP levels in the brain are considerably lower than previously thought, at low, 100-200 pM, levels.[83]

While the RIA is extremely sensitive, allowing detection in the nano to pico molar range of some biological molecules, it is a labor intensive process involving radioactive materials and expensive equipment. A technique capable of measuring changes in cGMP levels upon addition of pharmacological drugs that affect the cGMP pathway in seconds, like high speed online microdialysis (MD) capillary electrophoresis (CE) with laser induced fluorescence (LIF) detection, would provide a distinct advantage over the low temporal resolution of conventional RIA methods.

MICRODIALYSIS CAPILLARY ELECTROPHORESIS WITH LASER INDUCED FLUORESCENCE DETECTION

The development of online microdialysis has greatly reduced temporal resolution issues associated with off-line analysis systems. Online coupling of microdialysis and capillary electrophoresis with laser induced fluorescence detection has become a powerful technique with applications in determining dynamic interactions in the study of neurotransmitters. Higher temporal resolution associated with MD-CE-LIF may allow monitoring of rapid changes in the chemical dynamics of cGMP in the glutamate/NMDA/NO pathway. CE is a technique based on the application of high-

electric field on a narrow bore fused silica capillary to separate molecules in small volume samples.[84] CE has high mass sensitivity and the potential for high speed separations with high efficiency.[78, 85] Separation is driven by the electrophoretic mobility of the analyte. The inner surface of fused silica capillary consists of negatively charged silanol groups at pH > 3. Filling the capillary with a buffer will cause solvated buffer cations to be attracted to the negatively charged capillary walls. Application of an electric field on the layer of charge at the inner capillary wall generates electroosmotic (EOF) flow; the bulk flow of liquid inside a capillary as the solvated cations move toward the negatively charged cathode. Charged analytes in electrolytic solution will move in the same direction as the EOF and will migrate based on their charge to mass ratios.

Utilizing LIF detection in CE offers one of the most sensitive detection modes available for the analysis of biomolecules and has been applied to the study of amino acids, peptides, proteins, carbohydrates, and DNA.[86-89] The development of online sampling and detection systems with enhanced mass detection limits associated with CE-LIF allows higher sensitivity and throughput leading to improved temporal resolution.[88] Initial studies of electrophoresis separations in open tubular silica capillaries were reported by Jorgenson and co-workers in 1981.[90, 91] The first coupling of MD to CE-LIF was reported by Hogan and Lunte et al.[77] in 1994. High speed micellar electrokinetic chromatography (MEKC) separation was performed for monitoring the metabolite SR 4233 *in vivo* and separating it from its main metabolite, SR 4317. Resolution of the two compounds was achieved in less than 60 seconds, with overall temporal resolution of 90 seconds.

The first microdialysis system to generate high recoveries and good temporal resolution simultaneously for multiple neurotransmitters was developed by Lada and Kennedy.[88, 92, 93] Capillary zone electrophoresis (CZE) and micellar electrokinetic chromatography (MEKC) were coupled to LIF to analyze online derivatized primary amines.[94] Higher efficiency separations with high sample throughput were achieved by the addition of a flow-gated interface to the CZE system (Figure 1.04 A). The flow gate allowed automatic injection of dialysate samples directly onto the separation capillary. The interface consisted of a Lucite block that held the outlet of the reaction capillary and the inlet of the separation capillary aligned with a 75 μm gap between them. During a separation, a gating flow of electrophoresis buffer was pumped at 0.34 mL/min through the gap between the capillaries. This flow prevented derivatized dialysate from entering the separation capillary. To perform an injection, the gating flow was stopped by a pneumatically actuated gating valve. While the gating flow was stopped, the injection voltage was applied. Once the injection was complete, gating flow was resumed, and the separation voltage applied. This system allowed operation at low microdialysis flow rates and fast sampling times, increasing the relative recovery of analytes through the microdialysis probe resulting in improved detection limits. The low flow rate system also showed the potential to couple smaller microdialysis probes which could improve spatial resolution and decrease effects

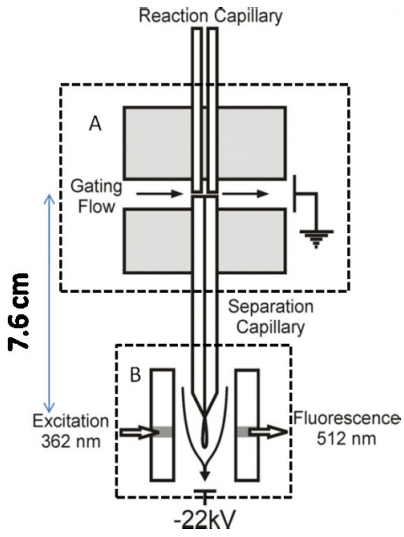

Figure 1.04. Flow gate injection interface (A) and sheath flow cuvette cell (B).

of probe damage on the tissue area of study. The emitted radiation was collected by an objective, passed through a dichroic mirror, and filtered with a 450 nm interference filter. Light passing through the interference filter was measured using a DCP-2 photometer system equipped with a R928 photomultiplier tube. Basal concentrations of aspartate and glutamate were determined in the rat striatum. A temporal resolution of 45 seconds was achieved. Multiple primary amines were also monitored with a 3 min temporal resolution. Other initial online microdialysis CE assays for neurotransmitters focused on glutamate and aspartate[65, 76, 95, 96] with temporal resolution further improved to 12 seconds.[95] Bowser et al.[78] have achieved nM limits of detection (LOD) for a number of amines (Table 1.01). An online high speed microdialysis CE-LIF analysis system was developed for the simultaneous monitoring of the neurochemicals glutamate, GABA, glycine, aspartate, serine, taurine, glutamine and dopamine. Temporal resolution was 10 seconds. This was a significant improvement over the resolution of previous microdialysis CE experiments.

Amine	*In Vivo* Dialysate Under Basal Conditions (nM)	*In Vitro* Probe Recovery (%)	*In Vivo* LOD (nM)
Glutamate	55 ± 85	57 ± 2	45
Aspartate	173 ± 19	64 ± 6	49
GABA	174 ± 42	64 ± 1	17
Glycine	1250 ± 114	76 ± 1	13
Dopamine	Not Detected	83 ± 1	36

Table 1.01. Basal concentrations and LODs of OPA derivatized amines.[78]

Recent research utilizing high speed online microdialysis CE-LIF analysis for primary amines includes that of O'Brien et al.[32, 33] and Ciriacks-Klinker et al.[28, 29, 97] for the analysis of D-serine and other neurotransmitters. The novel difference between these two lines of research involves *in vivo* monitoring in the retina vs. the brain. Separations were carried out in less than 22 seconds while sampling larval tiger salamander retinal

homogenates. The retina is a part of the central nervous system and shares many similar neurotransmitters with those found in the brain.[98] Experiments involving the glutamate/NMDA/NO neuromessenger pathway were performed to monitor changes in extracellular D-serine in the rat striatum.[99] The effects of the application of pharmaceutical agonists and antagonists to the NMDA receptor were studied. Temporal resolution in these studies on the order of 12-15 seconds was achieved. The current MD-CE-LIF system used incorporates a sheath flow detection cell[100-102] (Figure 1.04 B) for improved sensitivity of detection. A sheath flow buffer flowing around the outside of separation capillary, ground to a fine tip, induces a laminar flow profile to samples exiting the separation capillary into the sheath flow stream. A laser can be focused onto the narrow stream of derivatized analytes exiting the separation capillary, and fluorescence detected 90^{o} from excitation, via a photomultiplier tube. This technique reduces background scatter that was commonly associated with on capillary methods of detection. Application of the high speed online MD-CE-LIF technique shows a high potential for the improved sensitivity and time resolution needed for *in vivo* cGMP studies.

FLUORESCENCE DERIVATIZATION OF PRIMARY AMINES

A cGMP assay utilizing fluorescent derivatization must be able to detect cGMP near basal levels established in RIA. Amine derivatization with MD-CE-LIF offers the possibility of reaching the appropriate limit of detection (LOD) for cGMP. Laser induced fluorescence detection allows for extremely high sensitivity, the lowest reported detection limits, and a wide linear dynamic range.[103] Using a laser as the excitation source in CE

offers many advantages. The laser can be focused, allowing the excitation energy to be applied to very small sample volumes,[104] it offers simpler spectral backgrounds, better monochromicity, and excitation power can frequently be varied over a wide range for optimization for a particular analyte under study.[103] Selection of the appropriate fluorogenic reagent is important. The LOD achieved with some reagents may not be low enough for a cGMP assay, where expected basal levels of cGMP are 6-9 nM.

Derivatization of biomolecules involves the labeling of a desired analyte with a fluorescent moiety. Derivatization is necessary for high speed online microdialysis CE-LIF analysis when the desired analyte of interest, like cGMP, is not intrinsically fluorescent, or the analyte is not natively fluorescent enough for detection by the analytical system. Extensive fluorescence derivatization research has been carried out, particularly for amines in HPLC and CE-LIF analyses. Fluorophores investigated include

Compound	$\lambda_{excitation}$ (nm)	$\lambda_{emission}$ (nm)	$\varepsilon \times 10^{-3}$	Reaction Time
Fluorescamine	381	470	7.6	Ms
Dansyl Isothiocyanate	335	536	4.2	Several hours
OPA	334	455	5.7	5 minutes
NDA	462	520	Not determined	< 1 hour
FQ	486	591	Not determined	1 hour
CBQCA	465	560	Not determined	1 hour
NBD-Fluoride	465	535	8.0	5-10 minutes, 60°C[107]

Table 1.02. Common fluorophores for the analysis of low molecular weight amines.[105, 106] Reaction time occurs at room temperature, unless otherwise noted.

dansyl (DNS) 5-dimethylaminomapthalene-1-sulfonyl chloride, o-phthaldialdehyde (OPA), naphthalene-dialdehyde (NDA), fluorescein isothiocyanate (FITC), and fluorescamine. 4-Chloro-7-nitrobenzofuran (NBD) has been utilized in the derivatization of n-alkylamines[91] (Table 1.02). While many of these fluorogenic reagents have been

used to derivatize primary amines, there is no precedence in literature indicating these fluorophores have been used for the derivatization of cGMP or any other guanine containing compound.

Naphthalene-2, 3-dicarboxaldehyde and o-pthaldialdehyde

The homologous aromatic dialdehydes o-pthaldialdehyde (OPA) and naphthalene-2, 3-dicarboxaldehyde (NDA) are nonfluorescent until their reaction with a primary amine in the presence of excess cyanide or a thiol, yielding a fluorescent isoindole. The mechanism for isoindole formation is still not determined, though multiple proposals have been made.[108] OPA has been used in CE-LIF neurochemical analyses with micro to nanomolar detection limits.[95, 97, 98, 106] It reacts rapidly at room temperature to form fluorescent derivatives, is not inherently fluorescent and does not break down or react to form fluorescent side products when present in excess.[106] These characteristics make OPA and NDA a desirable possibility in the derivatization of cGMP.

(3-(4-carboxylbenzoyl))quinoline-2-carboxaldehyde (CBQCA) and (3-(2-(furoyl) quinoline-2-carboxaldehyde

(3-(4-carboxylbenzoyl)) quinoline-2-carboxaldehyde (CBQCA) and (3-(2-(furoyl) quinoline-2-carboxaldehyde (FQ) react with primary amines in the presence of cyanide or a thiol to produce isoindole products. CBQCA and FQ form charged conjugates that can easily be analyzed by electrophoresis techniques. Amine detection for capillary zone electrophoresis LIF detection has sensitivity in the subattomole range ($< 10^{-18}$ moles) for CBQCA and the subfemtomole range, (10^{-15} moles) for FQ.[109] Reaction time with amines, one hour, may be reduced upon the application of heat. The sensitivity, and

temporal resolution needed for a cGMP assay may not be reached. Solubility issues are also a concern. While CBQCA and FQ are soluble in ethanol and methanol, they are not very soluble in water. Precipitation reactions in the capillary during separation would be detrimental to a cGMP assay.

7-Nitrobenz-2-oxa-1, 3-diazole

7-Nitrobenz-2-oxa-1, 3-diazole (NBD) derivatives are another option for detecting amines via MD-CE-LIF. NBD chloride and NBD fluoride[28] both react with primary and secondary aliphatic amines. Nucleophilic substitution by the primary amine occurs on the fluorophore via an S_N2 type reaction. Adducts of aromatic amines are mostly nonfluorescent.[109] The fluorescence quantum yield in water of NBD adducts of amines can be very low. Anilines, phenols, and thiols yield weakly or nonfluorescent derivatives.[110] NBD methods are typically selective toward aliphatic amines. This could be prohibitive in its use as a fluorogenic reagent for the derivatization of cGMP.

Fluorescamine

Fluorescamine (FA) is an excellent reagent for the detection of primary amines in the picomolar range[111] and yields a blue green fluorescent derivative. Fluorescence results from the hydrolysis of the peptide amide bond. The fluorophores are stable over a period of hours. Labeling conditions are mild (pH=9), can occur at room temperature, and the reaction occurs very rapidly, $t_{1/2} \approx$ ms. The reactants are fluorescent, but will react with water, on a timescale of seconds to minutes, to become nonfluorescent. This requires fluorescamine be stored in a non-protic solvent until reaction. FA is considered to be less sensitive than NDA in the detection of primary amines.[108]

While extensive research has been carried out involving the derivatization of primary amines and amino acids, this is not true of labeling of aromatic amines. Chemical assays that react a fluorophore and compounds similar to cGMP are greatly needed. Previous work and experiments utilizing fluorophore and primary amine reactions may provide an initial step in developing an assay for cGMP. Compounds that readily react with primary amines may also react with cGMP.

Glyoxal

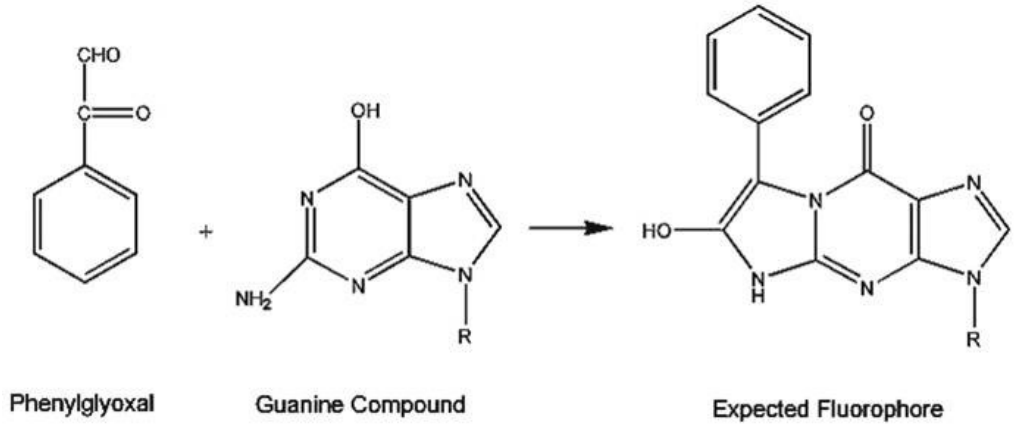

Figure 1.05. Derivatization of guanine containing compound by PGO

More recent studies of fluorogenic reagents include that of the glyoxal family of compounds. Glyoxal analogues which have a phenyl moiety substituted with electron-donating methoxyl group(s) or a methylenedioxyl group have been found to selectively and easily derivatize guanine containing compounds[80, 112-115] (Figure 1.05). Glyoxal (GO) and methylglyoxal (MGO) as aliphatic glyoxals, and 3,4-dimethoxyphenylglyoxal (DMPG) and 3,4-methylenedioxyphenylglyoxal (MDPG) and methoxyphenylglyoxal (MPG) and 3,4,5trimethoxyphenylglyoxal (TMPG) as PGO analogues substituted with

electron donating alkoxy group(s) have been explored as possible derivatizing reagents of guanine compounds.[112]

Initial studies of nucleic acid bases and their nucleosides and nucleotides involved measurement of their ultraviolet absorption after chromatographic separation.[116, 117] These methods were nonspecific and had low sensitivity. Fluorogenic reagents later found to be capable of selectively derivatizing guanine were initially used for derivatization of adenine. These experiments utilized fluorimetry, but had problems with a high level of noise in the signal due to Raman and Rayleigh scattering from the radiation light source.[118]

In order to provide further insight into the biomedical and physiological impact of guanine nucleosides and nucleotides, Kai et al.[117] developed the first pre column derivatization of guanines using the selective fluorescent reagent phenylglyoxal (PGO). PGO contains an aldehyde and a ketone functional group. In its anhydrous form it is a yellow liquid, and forms a colorless crystalline hydrate in water. Derivatization was carried out in a test tube and heated for 30 minutes at 60 ^{o}C. Excitation and emission maxima of derivatized products were around 365 and 510 nm, respectively. This reaction was also highly selective for guanine compounds, as the reaction conditions did not produce fluorescence products from other nucleic acid bases such as adenine, cytosine, uracil and thymine, and their nucleosides and nucleotides. A detection limit of 47-310 nM was achieved.

Isumi et al.[119] carried out the first application of PGO derivatization of cGMP. Their studies modified Kai et al.'s PGO guanine assay with resulting sensitivities lower

than the current radioisotope method. The activity of soluble guanylyl cyclase in the neuroblastoma N1E-115 cell was measured by tracing the peak height of cGMP synthesized from the conversion of GTP.

Once PGO cGMP assays were initially established in the literature, research began to focus more intently on clarifying the role of cGMP. Derivatization reactions by PGO of guanine compounds were used to study guanylate cyclase activity[120] and cyclic nucleotide phosphodiesterase (PDE) activity[121] in human blood platelets. Ohba et al.[113] performed studies in the rat brain. They reported the use of another glyoxal derivatizing reagent, (3, 4-dimethoxyphenyl) glyoxal, as a sensitive and selective reagent for guanine and its nucleosides and nucleotides using reversed phase HPLC separation. The HPLC measurement of PDE activity in the rat cerebral cortex was explored. Derivatization occurred at 30 ^{o}C over a 20 minute period of time in a sodium phosphate buffer at pH 6.0.

Application of the glyoxal family of derivatizing reagents may provide the sensitivity and reaction conditions ideal for derivatizing cGMP using the homebuilt MD-CE-LIF instrument. A number of advantages are associated with MD-CE-LIF in comparison to the microdialysis HPLC systems currently in use. One is a higher column efficiency[122] and the ability to simultaneously monitor multiple analytes with high throughput. CE also has a high mass sensitivity with LIF detection. This allows faster sampling rates to monitor rapid changes in pharmacological information and a significantly increased temporal resolution. The sample volume in CE is ≈ 1000 fold smaller than that used in HPLC.[123] This decrease is advantageous for *in vivo* sample

monitoring. MD-CE-LIF provides a strong potential for analysis of dynamic properties associated with *in vivo* cGMP.

Selectivity for the cGMP assay will be achieved as a result of the specific derivatization reaction for cGMP and analysis by CE. Currently there are a number of primary amines commonly found in brain dialysate, detectable by high speed online MD-CE-LIF and the commercial CE. Table 1.03 lists 25 of these amines. It is possible that the assay developed for cGMP will also derivatize a number of other compounds in the brain dialysate, e.g. guanosine triphosphate (GTP), adenosine triphosphate (ATP), GMP, cyclic adenosine monophosphate (cAMP), to name a few.

L-arginine	L-β-ABA	L-Histidine	L-Threonine	L-Glutamate
Serotonin	D-β-ABA	α-ABA	L-Tyrosine	D-Aspartate
Dopamine	βAlanine	Glycine	Phosphoethanolamine	L-Aspartate
L-Norepinephrine	Taurine	L-Glutamine	Glutathione	L-Asparagine
GABA	L-citrulline	L-Alanine	2-aminoadipic acid	L-Serine

Table 1.03. Primary amines commonly found in brain dialysate.[55]

High speed online MD-CE-LIF analysis indicates a high potential for *in vivo* monitoring of cGMP. The high temporal resolution associated with this analytical technique is capable of measuring brain pharmacokinetics on a scale not previously demonstrated in cGMP analysis. This is of particular importance in the development of drug therapies and elucidating brain dynamics associated with neurologically related diseases. As a downstream indicator of nitric oxide (NO) activity, the study of cGMP will lead to a greater understanding of the steps involved in reduction of oxidative stress and excitotoxic effects associated with the glutamate NMDA pathway.

INTRANASAL DRUG DELIVERY

In the study of brain pharmacokinetics and development of drug therapies, it is essential to apply analytical methods capable of measuring chemical dynamics as they occur in the brain. Our very understanding of the brain is restricted and defined by the sensitivity and speed of the analytical systems and methodologies used in these studies. Analytical techniques with high temporal resolution are essential for the generation of accurate pharmacokinetic profiles of compounds as they enter and exit the brain. High speed online MD-CE-LIF has the potential to be used not only in the effort of elucidating the pathogenesis of neurologically related disease and damage, but also elucidating mechanisms by which drug delivery to the brain and central nervous system occur for treatment of central nervous systems damage and disease. Clinical therapies designed to target diseases like Alzheimer's or Parkinson's, and treatment of pain in the CNS focus particularly on the potential of nose to brain transport delivering therapeutically relevant concentrations. This involves rapid transport of a drug across the olfactory region in the nasal cavity directly into brain tissue, e.g. the olfactory bulb or the CSF. Barrier properties of the olfactory epithelium and limited diffusion of the blood brain barrier inhibit the ability of drugs to enter into the brain. Intranasal (i.n.) administration of drugs provides a non invasive and convenient method to rapidly and directly deliver drugs to the CNS, bypassing the blood brain barrier (BBB).[19, 21, 24, 25, 124-132] The intranasal route of administration is not a new approach for drug delivery to the systemic circulation. The novelty lies in using this noninvasive method to rapidly deliver drugs directly from the nasal mucosa to the brain and spinal cord with the aim of treating CNS disorders while

minimizing systemic exposure.[23] Drug delivery via the nasal cavity offers many advantages over more traditional methods of drug delivery. The large surface area, uniform temperature, high permeability and extensive vascularity of the nasal mucosa[133] and its ease of access facilitate rapid systemic absorption of intranasally administered drugs. Additionally, intranasal delivery represents a needle-free, relatively non invasive, patient-friendly route of administration in contrast to painful intramuscular injections intravenous delivery.[21, 134] Intranasal administration also avoids first pass elimination of a drug, through the kidneys, and liver, increasing the bioavailability of the drug in the CNS.

Early research demonstrated that tracers, such as wheat-germ agglutinin conjugated to horseradish peroxidase (WGA-HRP), were transported within olfactory nerve axons to reach the olfactory bulbs in the CNS.[135] These findings were subsequently confirmed in a quantitative study comparing intranasal and intravenous administration of WGA-HRP.[23, 27] Direct intranasal delivery of therapeutics to the brain was first proposed and patented in 1989 by William H. Frey II of the Alzheimer's Research Center. (Frey WH II. 1991. In: WPTO, editor. Neurologic agents for nasal administration to the brain. US: Chiron Corporation, and Frey WH II. 1997. In: USPTO, editor. Method of administering neurologic agents to the brain. US: Chiron Corporation.) Transport of [125I]-labeled insulin-like growth factor-I (IGF-I; 7.6 kDa), nerve growth factor (NGF) (26.5 kDa) and IFN-_1b to the cervical lymph nodes, olfactory bulb, brainstem and many other CNS areas has been observed to occur less than one hour after intranasal application in rats.[17-19, 136] Intranasal IGF-I and NGF have been also been effective in rodent models of ischemic stroke[137, 138] and Alzheimer's disease.[139, 140] Nerve growth

factor,[17, 141-143] fibroblast growth factor-2,[144] insulin,[145, 146] vasoactive,[147, 148] estradiol,[149] and growth factor analogs[150] are able to gain access to or have effects in brain tissue or CSF following i.n. administration.[19]

Development of minimally invasive techniques capable of targeting neurotrophic factors or neuroprotective peptides to the CNS are needed to aid in the development of clinical therapies, particularly in the treatment of chronic conditions and neurodegenerative diseases where repeated dosing would be necessary.[19, 20, 24, 151] Neurotrophic factors are a family of proteins essential to the support, maintenance and growth of neurons in the central nervous system. Neurotrophins are hydrophilic, typically basic, monomeric or dimeric proteins, mostly in the size range of 5 to 30 kDa and have been found to elicit biological effects at concentrations in the nanomolar to femtomolar range.[20] Thorne et al.[18] have shown rapid transport into the CNS following i.n. administration of insulin-like growth factor-I (IGF-I), a 7.65 kDa protein neurotrophic factor. The proposed mechanism for [^{125}I]-IGF-I transport into the CNS following i.n. administration is rapid delivery to the CNS by extracellular bulk flow transport.[18] Their results suggest the existence of two distinct extracellular transport pathways associated with peripheral components of the olfactory and trigeminal systems. Intranasally applied proteins are rapidly transported into CNS tissue by a formerly identified pathway associated with the peripheral olfactory system connecting the nasal passages and OB/rostral brain, and a newly identified pathway associated with the peripheral trigeminal system connecting the nasal passages and the brainstem, in addition to one

branch of the trigeminal nerve that enters the cranial cavity through the cribriform plate along with the olfactory axons.[18]

Intranasal delivery of peptides and proteins has resulted in several promising research studies as well as marketed products. These include anti-migraine drugs sumatriptan from GlaxoSmithKline, zolmitriptan from AstraZeneca, ergotamine from Novartis, and butorphanol from BristolMyersSquibb as well as a range of peptides such as calcitonin from Novartis, desmopressin from Ferring, and buserelin from Aventis.[152] Additional nasal products in development include nasal morphine and ketamine[134, 152, 153] for the treatment of breakthrough-pain (BTP) in patients with chronic pain resulting from diseases such as cancer. Results indicated that intranasal administration of ketamine provides rapid, safe and effective relief for BTP. Intranasally administered insulin has been found to improve memory in healthy humans[154-156] as well as cognitively impaired humans with Alzheimer's disease.[157-159] In a rodent model of diabetes, intranasal insulin prevented cognitive decline, cerebral atrophy and white matter changes in the brain.[155, 160] Insulin like growth factor (IGF-I), delivered intranasally, is a promising treatment for stroke.[161 162 163]

Significant barriers of nose to brain transport exist, limiting the effectiveness of nasally administered drugs and compounds. The blood brain barrier restricts passage of all but small (<500 Da), lipophilic molecules from the bloodstream to the CNS.[164, 165] Methods that bypass this barrier often involve surgically invasive procedures (e.g. intracerebroventricular or intraparenchymal input) and can result in surgery-related side-effects.[18, 19, 166] Neurotrophic factors are not orally bioavailable and most exhibit short *in*

vivo half-lives[20] with inactivation by gastrointestinal enzymes. In addition, a fundamental problem with these approaches is the limited diffusion coefficients associated with the movement of peptide and protein drugs from the initial site of intrathecal/intracerebroventricular injections.[166] In order to develop effective drug therapies, improving the potential of drug delivery via nose to brain transport requires an understanding of the structure of the nasal cavity and processes that limit intranasal absorption. Elucidating the functions and mechanisms will lead to improved approaches to overcoming the barriers involved in intranasal drug delivery.

NOSE TO BRAIN PATHWAY

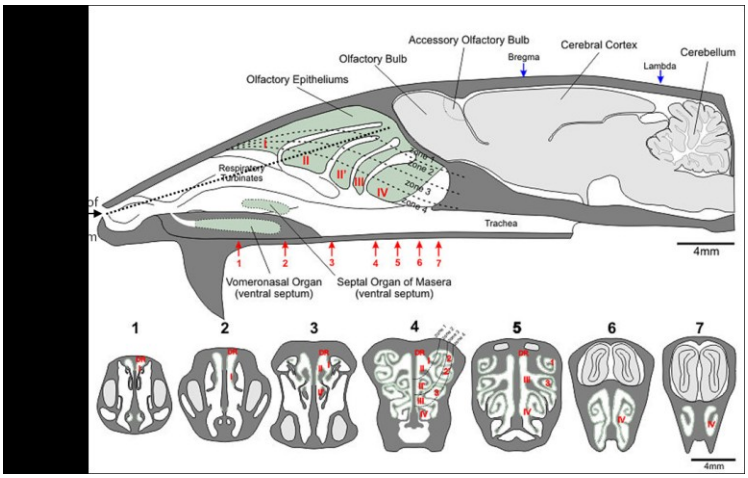

Figure 1.06. Drawing of a medial view of the rat nasal cavities and brain with cross-section views at different levels of the nasal cavity. Adapted from a drawing by Adam C. Puche, copyright Academic Press.[1]

The nasal cavity (Figure 1.06) possesses many advantages as a site for drug delivery. It has a large surface area for absorption with a sub epithelial layer that is highly vascularised. In addition, blood is drained directly from the nose into the systemic circulation, thereby avoiding first pass metabolism by the liver and kidneys.[167, 168] The

nasal cavity serves an important protective role in that it filters, warms and humidifies inhaled air before it reaches the lower airways. Inhaled particles and microorganisms are trapped by hairs in the nasal vestibule or by a mucus layer that coats the respiratory area of the nasal cavity.[152] The mucus layer carries particulates to the back of the throat, down the esophagus and into the gastrointestinal tract via a mucociliary clearance mechanism. Cilia are long (4-6 um in humans) thin projections, mobile, and beat with a frequency of 1000 strokes per minute. The cilia move in the soluble layer that lies beneath mucus, propelling mucus toward the posterior part of the nasal cavity. Due to this movement, the mucus layer is renewed every 15-20 minutes[152] in humans, with the nasal mucociliary clearance half life in rats around 5 minutes.[169] The olfactory mucosa is a region containing receptors for the sense of smell. Metabolic processes in the mucosa convert endogenous materials into compounds that are more readily cleared and eliminated. The nasal cavity is separated from the cranial cavity by the cribriform plate of the ethmoid bone, the principle supporting structure of the nasal cavities.[170] Just below the ethmoid bone the olfactory epithelium is situated between the nasal septum and the lateral wall of each side of the two nasal cavities. A midline septum divides the human nasal cavity into two non-connected parts, each consisting of three regions: First, the region just inside the nostrils, second, the olfactory region, which is situated in the roof of the nasal cavity in humans and the back of the nasal cavity in rats, and third, the respiratory region. Turbulent air flow ensures increased contact between inhaled air and mucosal surface. Stratified squamous epithelium cover the nasal cavity, gradually changing posteriorly into a psuedostratified columnar epithelium that covers the respiratory epithelium.[152]

Olfactory epithelium also contains olfactory receptor cells and neurons.[4, 152, 153, 171] At the basal end, the neuron ends in a fine non-mylelated axon that joins with other axons into a bundle surrounded by glial cells, and CSF, and penetrates into the cranial cavity through small holes in the cribriform plate (Figure 1.07, Box A).[23] The dendrites of olfactory receptor neurons (ORN) extend into the mucous layer of the olfactory epithelium, while axons of these bipolar neurons extend centrally through the lamina propria and through perforations in the cribriform plate of the ethmoid bone, which separates the nasal and cranial cavities (Fig. 1.07, Box B).[23] The axons of ORNs pass through the subarachnoid space containing CSF and terminate on mitral cells in the olfactory bulbs.

Mechanisms of Intranasal Drug Delivery

The precise mechanisms of intranasal drug delivery from the nose to brain are not entirely understood. Olfactory nerve pathways are thought to be a major component of the mechanism of intranasal delivery. Frey et al. have developed extensive nose to brain mechanism profiles in their studies of intranasal drug delivery. Therapeutics can rapidly gain access to the CNS following intranasal administration along olfactory nerve pathways leading from the nasal cavity directly to the CNS.[23] In order for a drug to reach the brain and CNS from the nasal cavity, it must cross the olfactory membrane and depending on the pathway used after this, also the arachnoid membrane surrounding the arachnoid space containing the cerebrospinal fluid (CSF).[152] Lipophilic drugs typically use a transcellular pathway and are transported by passive diffusion or receptor mediated processes.[152] Polar molecules are believed to follow paracellular pathways, crossing

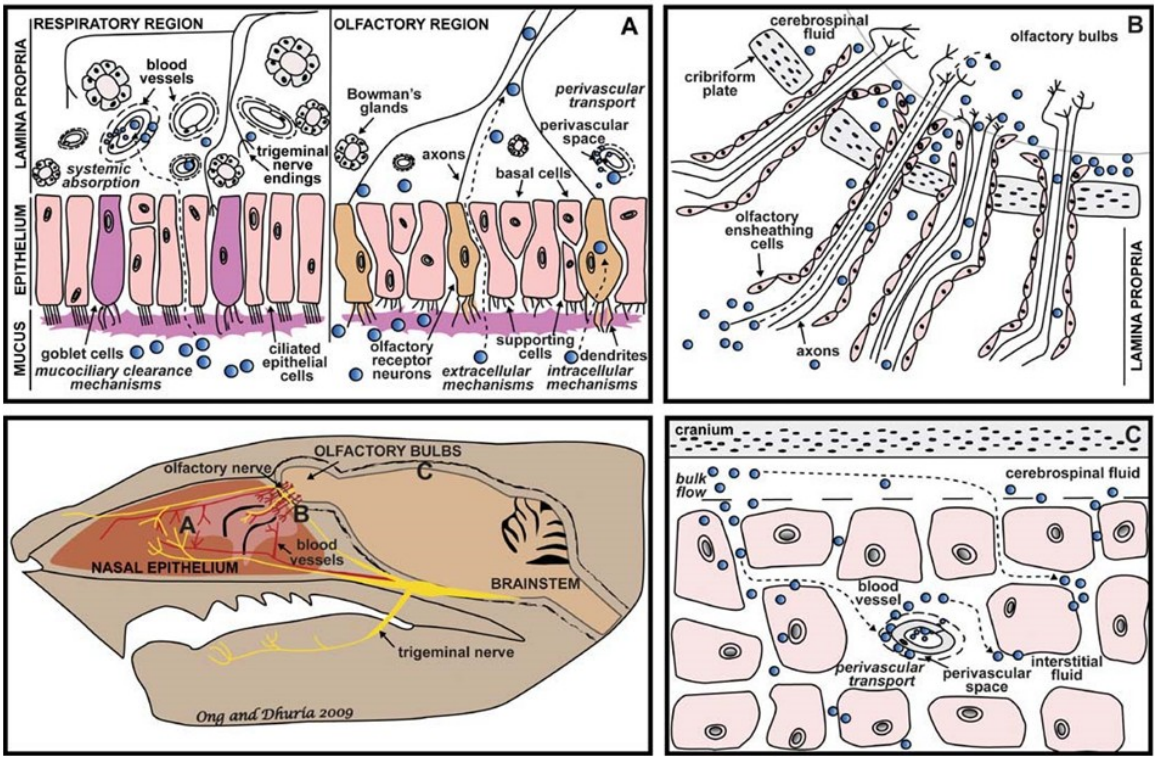

Figure 1.07.[23] Pathways of drug distribution in the nasal cavity and central nervous system. Following intranasal administration, drugs (blue circles) come into contact with the nasal mucosa, which is innervated by olfactory and trigeminal nerves. The nasal mucosa is comprised of the nasal epithelium, which contains various cell types, and the underlying lamina propria, which contains blood vessels, axons, glands, and connective tissue. (A) In the respiratory region, ciliated epithelial cells and mucous secreting goblet cells in the epithelium form the basis of mucociliary clearance mechanisms that remove foreign substances from the mucous layer towards the nasopharynx for elimination. Trigeminal nerve endings residing in the respiratory and olfactory epithelium convey chemosensory information to the CNS. In the olfactory region, olfactory receptor neurons are interspersed among supporting cells and basal cells to form the olfactory epithelium. Drugs can be transported through the nasal mucosa to the CNS by entering perivascular channels (dashed lines surrounding blood vessels) in the lamina propria or via extracellular or intracellular mechanisms involving olfactory and trigeminal nerves (dashed arrows). The blood supply to the respiratory epithelium is relatively greater compared to the olfactory epithelium, making it an ideal site for systemic absorption of nasally applied drugs. (B) After reaching the lamina propria, drugs can enter channels created by olfactory ensheathing cells surrounding the olfactory nerves, where they can access the cerebrospinal fluid (CSF) and olfactory bulbs (dashed arrows). (C) From the CSF, drugs can be distributed via bulk flow mechanisms and mix with brain interstitial fluid throughout the brain (dashed arrows). Drugs can also enter perivascular spaces after reaching the brain to be rapidly distributed throughout the CNS. Drugs that entered perivascular spaces from the nasal mucosa can also exit these spaces in the brain. These same pathways in the reverse direction are involved in the clearance of solutes from the CNS to the periphery.

biological membranes by passing through the tight junctions between cells or open clefts in the membrane.[172] This pathway is especially suited for smaller hydrophilic molecules.

Many substances delivered intranasally at the cribriform plate can enter into the brain via the olfactory nerve endings extending through the cribriform plate, a direct extension of the CNS[173] as evidenced by the fact that fluorescent tracers are associated with olfactory nerves as they traverse the cribriform plate.[174] Drug concentrations in the olfactory bulbs are generally among the highest CNS concentrations observed after intranasal administration[19, 21, 125, 126, 173, 175, 176] and a strong, positive correlation exists between concentrations in the olfactory epithelium and olfactory bulbs.[23, 132]

Intranasal drug delivery into the CNS is thought to involve one of two general mechanisms: 1) internalization of drug into primary neurons of the olfactory epithelium and subsequent intracellular transport into the olfactory bulb, followed by possible distribution of the drug into other CNS areas[1, 27, 177, 178] or 2) absorption of drug across the nasal epithelium to the submucosa, whereupon the drug can either directly access the CSF or undergo extracellular transport within perineuronal[20] channels into the CNS.[17, 20, 27, 124] Extracellular transport mechanisms involve the rapid movement of molecules between cells in the nasal epithelium, requiring only several minutes to 45 min for a drug to reach the olfactory bulbs and other areas of the CNS after i.n. administration.[24] Transport likely involves bulk flow mechanisms[18, 20]within the channels created by the olfactory ensheathing cells (Figure 1.7, Box B).[23, 25] Structural changes that occur during depolarization and axonal propagation of the action potential in adjacent axons may also induce the movement of compounds delivered to the nasal cavity.[179] Intracellular transport mechanisms involve the uptake of molecules into olfactory receptor neurons by passive diffusion, receptor-mediated endocytosis or adsorptive endocytosis, followed by

slower axonal transport, taking several hours to days for a drug to appear in the olfactory bulbs and other brain areas.[178, 180] Due to the large body of evidence indicating rapid intranasal delivery from the nose to CNS, it is more likely that rapid extracellular mechanisms of transport dominate, rather than intracellular mechanisms.[18, 19, 23, 25, 126, 173, 176, 181, 182]

BARRIERS TO NASAL ABSORPTION

Intranasal drug delivery via a nose to brain pathway shows high promise for delivering therapeutically relevant concentrations of drug formulations for the treatment of CNS damage and neurodegenerative diseases such as Alzheimer's. The potential for drug delivery via this pathway however is limited by barrier properties of the olfactory epithelium[183] and the blood brain barrier (BBB). Lipophilic drugs are generally well absorbed into the blood from the nasal cavity with pharmacokinetic profiles often identical to those obtained after an i.v. injection and bioavailabilities approaching 100%.[152] However, most peptide and protein drugs are not well absorbed from the nasal cavity when administered as simple solutions; the bioavailabilities normally achieved being of the order of less than 1%.[167, 184] The permeability of the nasal mucosa is typically low for polar molecules, and large molecular weight peptides and proteins.[152, 185] Small lipophilic drugs can cross the epithelial cell membrane by the transcellular route, along concentration gradients, receptor mediated transport, or vesicular transport mechanisms, or by the paracellular route through tight junctions between the cells. The rapid mucociliary clearance mechanism contributes significantly to low membrane transport. Typical replacement of the CSF (4-5 times daily) will gradually eliminate any

drug from the CSF into the blood.[153] Liquid and powder formulations that are not mucoadhesive can have a half life clearance on the order of 15-20 minutes,[152] limiting the amount of time available for drug absorption in the nasal cavity. Efflux transporters and nasal congestion contribute to decreased efficacy in delivery of drugs to the CNS.[23, 132] Enzymatic and chemical degradation also contributes to the low transport of peptides and proteins across the nasal membrane. This can occur either in the lumen of the nasal cavity, or during passage across the epithelial barrier. Enzymes are present in nasal secretions, in the cytosol of the cells, where they may be free and membrane bound, and in the lamina propria where they are particularly associated with glandular tissue.[168] Exopeptidases, such as mono- and diamino peptidases, are localized in both locations and can cleave peptides at the N and C termini. Endopeptidases such as serine and cysteine can attack internal peptide bonds. Enzymatic and chemical degradation also contributes to the low transport of peptides and proteins across the nasal membrane. Monooxygenase, reductase, transferase, esterase and proteolytic enzymes have been identified in the nasal mucosa.[168] Monooxygenase enzymes such as cytochrome P-450-dependent monooxygenases are thought to be important as a first line defensive mechanism against inhaled xenobiotics, particularly environmental pollutants, volatile chemicals and odorous chemicals, which are bio- transformed into non-toxic compounds which may then be excreted.[170, 186] Despite inter-species variations, the profile of nasal drug metabolizing enzymes in humans is similar to that of rodents.[170]

The blood brain barrier (BBB) is a diffusion barrier between brain blood vasculature and the tissue of the brain itself, formed by tight junctions between capillary

endothelial cells.[4] The brain microvessel wall consists of endothelial cells, whose apposing membranes form tight junctions (TJ), which limit the paracellular passage to water and solutes,[187] exclude almost 100% of large-molecule neurotherapeutics, and more than 98% of all small-molecule drugs.[188] In addition to the brain microvascular endothelial barrier, which forms the BBB, there are other barrier systems within the CNS, including the arachnoid epithelial membrane, which covers the surface of the brain, and the choroid plexus epithelium, which forms the blood-cerebrospinal fluid (CSF) barrier.[165] In humans, there are approximately 400 miles of capillaries perfusing the brain, and the surface area of the brain microvascular endothelium is approximately 20 m^2 [189] which is 1000-fold greater than the surface area of either the blood-CSF barrier or the arachnoid membrane.[164] The BBB maintains ionic concentrations within the brain, and provides protection from potentially toxic molecules that enter the vascular space by ingestion, infection, or other means. The transport of a ligand or substrate in either the brain to blood, or the blood to brain, direction requires movement across the capillary endothelial plasma membranes.[190] Transport pathways across the BBB include both paracellular, transfer of molecules between the epithelial cells, and transcellular pathways,[190] transport molecules through a cell. While large molecules cross the BBB through transcellular pathways, water and small hydrophilic solutes cross the BBB through the paracellular pathway.[191] The paracellular pathway of the BBB is formed by the endothelial tight junction openings, and the openings between adjacent astrocyte foot processes.[187] The surface of the BBB contains transporters for specific target molecules, e.g. glucose, allowing direct transport into the brain CNS region.[4] While the BBB

provides protection, it also creates significant difficulties for the delivery of drugs to the brain. Large, lipid insoluble molecules can be introduced to the brain, but only by transiently disrupting the BBB with hyperosmotic agents like mannitol.[4] The difficulties in transport of large molecules, like peptides and neurotrophins, across the BBB limit available drug therapies that target the CNS for neurological damage and neurodegenerative diseases. Approaches to overcome the BBB limitation include bypassing the BBB entirely, e.g. intranasal drug delivery,[24, 137, 192] or further research into the transporters present in the BBB surface, which can lead to the development of new approaches to brain drug delivery using endogenous brain endothelial transporters.[190]

FLUORESCEIN IN BLOOD BRAIN BARRIER AND INTRANASAL STUDIES

Sodium fluorescein is a hydrophilic and freely soluble salt with a molecular weight of 376.28 Da (Figure 1.08). Fluorescein is a fluorescent molecule commonly used as a cellular marker, approved by the FDA in 1976 as a contrast agent for angiography in ophthalmology practice.[193] It is administered topically to detect epithelial defects of the cornea, and intravenously, for angiography of the retinal vessels and, less frequently, the iris vessels.[194]

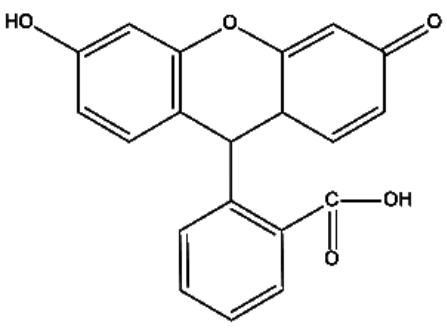

Figure 1.08. Fluorescein

Sodium fluorescein is generally considered safe for use human use, except for an occasional incidence of nausea and vomiting in some patients following intravenous administration.[194] Fluorescein is used extensively in the study of BBB permeability after intravenous administration.[187, 191, 195-198] Recent studies have applied fluorescein and

derivatives of fluorescein intranasally to determine possible mechanisms of delivery to the CNS.[169, 174, 199] Advantages of using fluorescein include its excellent quantum yield, relatively high absorptivity, and good water solubility. It absorbs at an excitation wavelength of around 494 nm, with an emission wavelength of 520 nm, making it easily compatible with argon ion laser and solid state lasers as well. In aqueous solution it occurs in cationic, neutral, anionic and dianionic forms making its absorption and fluorescence properties strongly pH dependent[200] (Figure 1.09). The protolytic constants

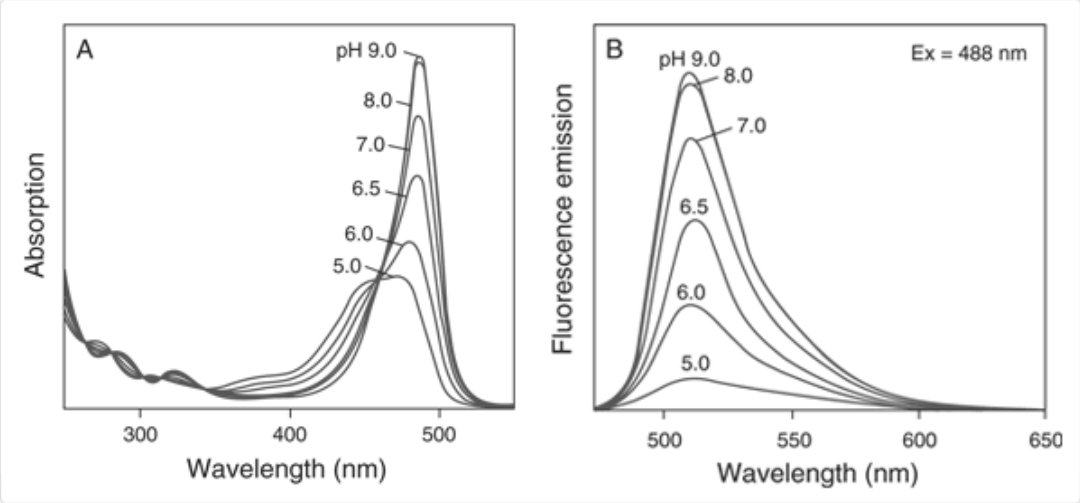

Figure 1.09. Absorption and emission spectra of fluorescein at varied pH in 50 mM phosphate buffer, adapted from Sjoeback et al..[200, 201]

relating the chemical activities (which at low ionic strength equal concentrations) of the cation, neutral form, anion and dianion are $pK_1 = 2.08$, $pK_2 = 4.31$, and $pK_3 = 6.43$. All forms have rather high molar absorptivity being $\varepsilon^{FH_3^+}{}_{,437} = 53\ 000$, $\varepsilon^{FH_2}{}_{,434} = 11\ 000$, $\varepsilon^{FH^-}{}_{,453} = 29\ 000$ ($\varepsilon^{FH^-}{}_{,472} = 29\ 000$) and $\varepsilon^{FH2^-}{}_{,490} = 76\ 900\ M^{-1}\ cm^{-1}$ for the cation, neutral form, anion and dianion, respectively.[200] The dianion has the most intense fluorescence with a quantum yield of 0.93 but the anion shows considerable fluorescence with a quantum yield of 0.37. The pKa of fluorescein is around 6.4, and with its pH

dependence[202-204] a sharp decline in fluorescein is seen at pH below physiological pH of around 7.4. Further issues associated with fluorescein include significant photobleaching.[205] It was commonly held that these properties mean that sodium fluorescein does not easily cross the tightly fenestrated endothelial cells in the blood brain barrier.[206, 207] In addition, it has been reported that sodium fluorescein is a substrate for efflux transporters at the blood brain barrier[196, 208] which could further restrict the access of the substance to the brain from the systemic circulation. At the same time, it is thought that fluorescein should be able to cross epithelial barrier paracellularly to some extent, making the compound suitable for studies of olfactory absorption.

Fluorescein has been used to an increasing extent in the ongoing study of intranasal drug delivery. Bagger et al.[199] evaluated the potential of targeting the central brain by olfactory absorption by use of sodium fluorescein as a hydrophilic model substance with limited permeability across the blood–brain barrier. The intravenous formulation (375 µl) was injected in the tail vein. I.n. administration (15 µl) was given 20 mm into the cavity as a droplet on the mucosa in the right nostril by inserting a soft catheter fitted to a 25 µl Hamilton microsyringe. It was concluded that fluorescein was mainly entering the striatum via passage across the blood brain barrier and only to a minor extent via the olfactory pathway, based on the striatum: plasma dialysate area under the curve (AUC) ratio being approximately 3% regardless of the route of administration. From the microdialysis experiments, the significantly lower elimination rates found in both left and right striatum after nasal administration could be an indication of slowly diffusing sodium fluorescein through the extracellular space of molecules

absorbed via the olfactory pathway and their conclusions were supported by the previously suggested pathway for olfactory absorption of hydrophilic drugs[124] which is via the CSF followed by diffusion through the parenchyma to the striatum. Bagger et al. discovered a higher brain concentration of fluorescein in the right striatum, the side of i.n. dosing in the rat nasal cavity, however, the brain to plasma area under the curve ratios of model substance were low (2–3%) and not significantly different between right and left side of the brain, regardless of the route of administration. The results obtained by microdialysis were supported by findings in whole brain homogenates where concentrations of fluorescein were approximately 40% higher in the right striatum compared with the left side initially after i.n. administration to the right nostril of rats. Despite some indications of olfactory transport to the central rat brain it was concluded that the drug targeting potential of sodium fluorescein and most likely other hydrophilic compounds is limited.[169,199]

This conclusion has been directly refuted by many papers published showing that hydrophilic peptides are targeted to the CNS with i.n. administration,[206,209-211] including some fluorescein derivatives.[169, 174, 199, 212, 213] Successful BBB permeability has been also been described with reference to various small (mostly lipophilic) protein and peptide drugs following intraventricular administration.[166] In addition, it has been stated that in order for a peptide or protein drug to cross the BBB in pharmacologically significant amounts, the molecule must have a molecular weight bellow a threshold of 400–500 Da.[166, 214] Sakane et al.[212] explored the relationship between the direct transport from the rat nasal cavity to the cerebrospinal fluid (CSF) and the molecular weight of the drug

with intranasal administration of fluorescein isothiocyanate-labeled dextran (FD) at various molecular weights. FDs (average molecular weights 4,400 (FD4); 9,400 (FD10); 18,900 (FD20); 40,500 Da (FD40)) were administered nasally or intravenously to rats, and the concentrations in the plasma and the CSF were measured and compared. None of the FDs were detected in the CSF after intravenous administration. However, FD4, FD10 and FD20 were observed to appear in the CSF after nasal administration, whereas the concentration in the plasma was much lower than that after intravenous administration. FD40 was not detected even after nasal administration. In addition, the concentration of these FDs in the CSF decreased with the increase in the molecular weight of FDs. These findings show that drugs with a molecular weight up to at least 20 000 Da can be directly transported from the nasal cavity to the CSF and that the transport of FDs to the CSF is dependent on their molecular weights.[212]

The mechanisms of delivery across the BBB are complex, as indicated by a large body of literature. It is quite clear that the ability of a drug to permeate the BBB is inherent in the physiochemical properties unique to the drug, as well as properties of the nasal olfactory epithelial layer and the BBB, which does not rule out the existence of a direct nose to brain pathway for all compounds. Table 1.04 indicates many of the factors affecting the entry of peptide and protein delivery into the CNS.[166] Early research indicating a lack of BBB permeability to peptides and proteins was likely influenced by the insensitive techniques used as well as by the lack of consideration of the possibility of brain -to-blood passage in these studies.[166]

Characteristics of peptide/protein	Characteristics of BBB	Peripheral Factors
Molecular weight	Lipid composition	Affinity for plasma proteins
Concentration gradient	Membrane charge	Systemic enzymatic stability
Amino acid composition	Presence of transport systems	Cerebral blood flow
Lipid solubility/Hydrogen bonding	Direction of transport systems	Volume of distribution
Charge	Existing pathological conditions	Rates of clearance and cellular sequestration
Aggregation		Bioavailability
3D structure		
Conformation		
Flexibility		
Folding		
Affinity for efflux proteins		
Affinity for receptors or carriers		
Cellular Enzymatic stability		

Table 1.04. Factors affecting the entry of peptide and protein delivery into the CNS.[166]

BBB permeability to sodium fluorescein has been found in mice[215] with the addition of morphine and other opiod agonists, and rats[196] with the co administration of inhibitors, e.g. probenecid, of drug efflux systems related to the multidrug resistance (MRP) family of transport proteins. These results demonstrate that MRPs or MRP-like transport system(s)[196, 208] may play an important role in fluorescein, and other organic anions, distribution across both the BBB and the blood cerebrospinal fluid barrier (BCSFB).

It is important to keep in mind that experimental methodologies play a significant role in the results observed post intranasal delivery. There are a multitude of factors including head position, method of delivery, including surgical interventions (for animal studies), and delivery volume, which can all influence drug deposition in the nasal cavity and the pathway a drug follows to the CNS after intranasal administration.[23] The majority of intranasal research has been carried out in anesthetized mice and rats, with animals positioned in the supine position.[23] Van den Berg et al.[216] found that different head

positions can alter absorption into the blood and CSF following nasal administration to rats when a tube inserted into the nostrils was used to deliver the drug solution. A supine position with the head angle at 70^{o} or $90^{o}$was found to be most suitable for efficient delivery to the CSF using this method of intranasal administration. This head position would also likely favor drainage into the esophagus and trachea, which is why most researchers position animals with the head at 0^{o} (horizontal).[23] In experiments evaluating dye deposition in the nasal passages, Thorne et al.[27] found that nose drops administered to animals lying on their backs resulted in consistent deposition in the olfactory epithelium.[23] Optimal delivery to the CNS along neural pathways required targeting of the drug to the upper third of the nasal cavity.[17] Multiple methods of administration exist for i.n. drug delivery. Several studies administer drops over a period of 10–20 min using a pipettor for delivering drops to alternating nostrils every 1–2 min to allow the solution to be absorbed into the nasal epithelium.[23, 25, 125, 126, 129] This noninvasive method is preferred as it does not involve inserting the pipette tip into the nostril. Instead, drops are placed at the opening of the nostril, allowing the animal to sniff the drop into the nasal cavity. Another method of i.n. administration involves sealing the esophagus and inserting a breathing tube into the trachea to prevent the nasal formulation from being swallowed and to eliminate issues related to respiratory distress.[209, 210] Flexible tubing can also be inserted into the nostrils for localized delivery of a small volumes of the drug solution to the respiratory or olfactory epithelia[23], and the depth of this tubing into the nasal cavity has varied greatly from study to study depending on the length of the tubing.[176, 216-219] While differences in delivery volumes can affect the deposition within

the nasal cavity and distribution to the CNS, no systematic studies have been published that evaluate the effect of solution volume on the efficiency of i.n. delivery to the CNS[23]. Studies involving i.n. administration of drugs should incorporate a delivery technique that repeatedly and reliably delivers the drug to the back of the nasal cavity to ensure the greatest interaction with the olfactory epithelium, e.g. flexible tubing, administer with the animal in a supine position, and minimize sample volume to avoid passage into the trachea and respiratory distress.

NASAL ABSORPTION ENHANCERS

The intranasal delivery of drugs and resultant targeting to the blood, the brain, or both the blood and the brain, can be greatly improved if administered in combination with nasal absorption and membrane permeability promoting agents (Table 1.05). Possible strategies to increase bioavailability in the brain include 1) co-administration with protease inhibitors, 2) the use of membrane permeation enhancers, 3) co-administration with a combination of absorption enhancers and protease inhibitors, 4) modification of peptide structure to improve metabolic stability or membrane permeation, and 5) use of microparticles.[213, 220] Surfactants such as laureth-9, bile salts and bile salt derivatives such as sodium taurodihydrofusidate, fatty acids or fatty acid derivatives, phospholipids, polysaccharides, and various cyclodextrins have all been used in the study of enhancing nasal drug delivery.[152, 153, 172, 183, 221-230] Many lipophilic drugs that have poor solubility in water and large hydrophilic drugs, including peptides and proteins, exhibit poor bioavailability upon i.n. administration.[221] Cyclodextrins, especially methylated beta-cyclodextrins, have improved solubility of these compounds, an

indicated a high applicability as absorption enhancers in nasal drug delivery. Application of absorption and permeability enhancers in intranasal drug delivery should not compromise the essential functions of the nose. Other issues to keep in mind include potential interference with the normal metabolism and function of the mucosal cells, possible metabolism of the enhancer to toxic and carcinogenic substances in the nasal mucosa and the systemic absorption of the enhancer into the blood stream.[213, 231, 232] Absorption enhancers should have an immediate and predictable duration of action, with their effect on the barrier properties of nasal mucosa reversible following absorption of the drug.[233]

Surfactants	Laureth-9 Poloxamer 188 Lysophosphatidylcholine Dodecylmaltoside -2 Sucrose cocoate Soybean-derived sterol Sterol glucoside
Bile Salt and its Derivatives	Trihydroxysalts: cholate Glyco-and taurocholate Dihydroxy salts: deoxycholate Glyco- and taurodeoxycholates
Fusidates	Sodium Taurodihydrofusidate
Phospholipids	L-α-lysophosphatidylcholine
Cyclodextrins	α-, β-, γ-cyclodextrin Dimethyl-β-cyclodextrin Hydroxypropyl-β-cyclodextrin
Chelators	0.5% EDTA-2Na
Cell Penetrating Peptides	L-R8 D-R8 D-penetratin L-penetratin
Cationic Biopolymer	Chitosan N-trimethylchitosan Chitosan Nanoparticles Sperminated gelatin Aminated H-gelatin

Table 1.05. Absorption enhancers used in nasal drug delivery studies.[225, 229, 230, 234]

Bioavailabilities have been enhanced by a variety of mechanisms, typically involving modification of the phospholipid bilayer or the epithelial cell layer, leaching protein from the epithelial membrane, or reducing the viscosity and stripping off the outer layer of the mucosa.[152] In mucus and mucus membranes, enhancers may act by alteration of the mucus layer, opening tight junctions between epithelial cells by interfering with calcium ions in the intercellular spaces, or by increasing membrane fluidity. Increasing membrane fluidity can be a result of creating disorder in the phospholipid domain or by facilitation the leaching of proteins from the membrane.[213] Other mechanisms include an effect on the tight junctions or work as enzymatic inhibitors. Bile salts and bile salt derivatives are thought to increase nasal insulin transport by multiple mechanisms: decreasing viscosity of the mucus layer, solubilization of insulin molecules in mixed micelles with these enhancers, and inhibiting enzymatic degradation during the absorption process.[223] Unfortunately, bile salts, while once assumed to be safe and effective absorption promoters have now found to be particularly toxic to nasal cilia and mucosa and demonstrate particular health concerns with long term application and useage.[172] Potential nasal and systemic toxicity is of great concern with the use of surfactant materials and bile salts.

Absorption enhancing effect versus potential damage to the mucosa is an important consideration during the choice of applied absorption and permeability promoting agents. Any pharmaceutical excipient used as a solubilizer and absorption promoter in nasal drug delivery should have a number of ideal qualifying characteristics. It should be potent at a low concentration, but inert from a pharmacological-toxicological

point of view.[221, 235] This means the promoting agent should 1) have no local or systemic effect, 2) cause no damage to the mucosal integrity, 3) show no severe ciliostatic effect, 4) enhance drug permeation through the nasal epithelium in a transient and reversible way, and 5) be non-irritating and non-allergenic.[221] Toxicity of nasal absorption enhancers has been estimated by measuring their effect on the mucociliary transport rate, nasal morphology and ciliary beat frequency.[224] In the frog palate model, mucociliary transport rate was measured before and after application of an absorption enhancer formulation. It was found immediately after the application of L-α-lysophosphatidylcholine (LPC) (1%), deoxycholate (DC) (1%), laureth-9 (1%), and sodium taurohydrofusidate (STDHF) (1%), that the mucus transport rate was irreversibly halted.[224, 236] Glycocholate (GC) and (1%) and didecanoyl-LPC (1%) however had no effect on the mucociliary transport rate. Enhancers have been studied on the surface morphology of rat nasal mucosa *in vivo* using scanning electron microscopy to characterize structural and cellular changes. Micrographs of nasal tissue were evaluated for surface integrity, ciliary morphology, and mucus/extracellular debris. GC showed morphology similar to a non toxic control buffer, phosphate. Laureth-9, and the dihydroxy bile salts DC and TDC resulted in severe erosion of the nasal mucosa within 5 minutes, indicated a total loss of cellular and ciliary identity as well as prevalence of extracellular debris.[237] Ciliary beat frequency (CBF) is one of the most important parameters in nasal mucociliary clearance. Cyclodextrins have shown a moderate effect on CBF in chicken embryo tracheal tissue and human adenoid tissue.[224] Dimethyl-β-cyclodextrin (DMβCD) and α-CD induced ciliostasis within one hour. This is

comparatively less severe considering STDHF (0.5%), laureth-9 (0.3%), DC (0.3%), GC (1.5%), and taurodeoxycholate (TDC) (1.5%) all caused fast and irreversible ciliostasis. DMβCD CBF however was concentration dependent and reversible after rinsing the tissue with Locke-Ringer solution. These studies were performed in *in vitro* conditions. *In vivo*, cilia are protected by the mucus layer, and nasally administered drugs will undergo dilution in the mucus and elimination by the mucociliary clearance mechanisms. Overall, nasal adsorption enhancers that have a mild effect on nasal tissue morphology also show minor influences on nasal ciliary beat frequency. Compounds that severely damage tissue also exhibit irreversible ciliatoxicity.[222-224, 233]

Increasing brain bioavailability in conjunction with intranasal drug delivery via nasal absorption enhancers and permeability promoters is one method with a high potential for significant improvement in the nasal absorption and rate of transport of drugs from nose to brain. Recent studies observe that co administration of absorption enhancers, e.g. surfactants, cyclodextrins, and polysaccharides, with proteins, peptides, small polar molecules, and vaccine related polysaccharides or DNA plasmids drugs[152] increases delivery of target compounds to the brain. Enhancers work by one or a combination of hypothesized mechanisms. These include a direct effect on nasal mucosa, an inhibitory effect on poteolytic enzymes, and opening of the tight junctions between cells.[221-223, 238] Chitosan, a polysaccharide, has enhanced the brain bioavailability of intranasally administered Nerve Growth Factor (NGF),[183] insulin,[227, 239, 240] the neural dipeptide [D-Arg^2]-Kyotorphin,[241, 242] and 2,3,5,6 Tetramethylpyrazine (TMPP),[242] a drug currently used in China for the treatment of cardiovascular and cerebrovascular

disease.[124, 227, 242, 243] Cyclodextrins, oligosaccharides, are among the most commonly studied membrane permeability agents used in intranasal drug delivery studies. Cyclodextrins have been used to enhance absorption of low molecular weight heparins,[226, 244] insulin,[221, 225, 228, 244] and therapeutic peptides like leucine enkephalin [213] in a variety of species, including dogs, rabbits, humans, and rats.[221] Inadequate nasal adsorption is one of the biggest limitations to nasal drug delivery. Additional disadvantages include toxicity of absorption promoters to nasal absorptive surface and the relative impermeability of prospective drug candidates via nasal mucosa.[244] Promising drug candidates can be eliminated due to poor absorption via nasal mucosa as concentrations necessary for therapeutic application cannot be reached. Due to these limitations, current research focuses on improving the efficacy of the nose to brain method of drug delivery via enhancement of nasal mucosa and/or nasal mucous epithelium permeability and BBB transport while maintaining low systemic toxicity. Use of chitosan and/or cyclodextrins in formulations of pharmaceutical drug therapies may overcome nasal mucosal impermeability and blood brain barrier (BBB) issues.

Chitosan

Chitosan (Figure 1.10) is a polycationic linear polysaccharide (biodegradable) broadly classified as chitosan oligomer composed of about 12 monomer units and chitosan polymer with more than 12 monomer units.[239] It is subdivided into three different types, low molecular weight chitosan of less than 150 kDa, high molecular weight chitosan of 700-1000 kDa, and medium molecular weight chitosan. Chitosan is bioadhesive and interacts strongly with the mucus layer.[183] Chitosan can be found in

fungi, but is typically obtained from the partial deacetylation of chitin, a naturally occurring structural polymer abundant in crab and shrimp shells.[172, 241, 245] The degree of deacetylation of typical commercial chitosan usually ranges between 66% and 95%.[239] Chitosan is also available in salt form, e.g. glutamate, lactate, and chloride. It is currently approved as a food additive in many countries. Owing to the removal of acetyl moieties

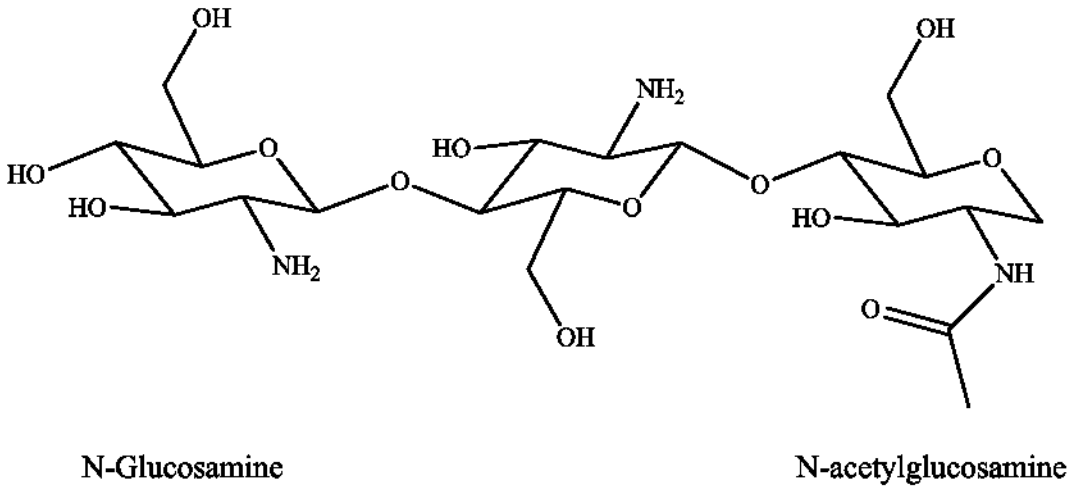

Figure 1.10. Structure of chitosan. Chitosan is a biopolymer consisting of two types of randomly distributed units: N-Glucosamine and N-acetlyglucosamine, with the number of N-Glucosamine units higher than 50%.

that are present in the amine functional groups, chitosan is readily soluble in aqueous acidic solution. It has a low solubility at physiological pH of 7.4 or higher however, as it is a weak base with pKa values ranging from 6.2-7.5.[239] Due to its biocompatibility, biodegradability, and low toxicity, chitosan is an attractive biopolymer for a variety of pharmaceutical applications. Chitosans are potent absorption enhancers for poorly absorbed hydrophilic dugs, with uptake of polypeptides such as atenolol, insulin, and beseriln across nasal and intestinal epithelia.[246] Chitosan is unlike many nasal absorption enhancers in that it is not membrane active or a surfactant, and as far as can be

ascertained in animal models, is not absorbed across mucosal membranes.[172] Mechanisms of chitosan absorption enhancement include increasing paracellular transport of drugs by transiently opening the tight junctions existing between the epithelial cells and suppressing the efflux transporters[183] as has been shown in Caco-2 cell culture studies and in animal models.[247] In Caco-2 cells, chitosan caused a reversible, time and dose-dependent decrease in transepithelial electrical resistance. The effect of chitosan on tight junctions was confirmed by an increased permeability coefficient for mannitol transport when cells were treated with 0.1–0.5% w/v chitosan solution for 60 min compared to control cells. Application of 0.5% chitosan for 60 min did not affect cell viability as shown by Tryptan blue dye exclusion. The data obtained by Dodane et al.[247] suggest that chitosan increases cell permeability by affecting paracellular and intracellular pathways of epithelial cells, in a reversible manner. Chitosan interacts with negatively charged cell surfaces and the negatively charged sialic acid residues in mucus. This mucoadhesion is another likely enhancing mechanism, slowing down mucociliary transport and increasing the residence time of the applied drug in the nasal cavity.[172, 241, 246]

Chitosan has been extensively applied to intranasal drug delivery studies as a potential nasal absorption enhancer. It has shown increased bioavailability when used in conjunction with insulin,[239, 247] salmon calcitonin,[246] opiod dipeptide [D-Arg^2]-Kyotorphin,[241] morphine, and vaccines for pertussis, dyptheria, and influenza.[172, 248] It is important to know the rate and concentration of a drug delivered to the CNS, particularly for therapies that require a known pharmacokinetic profile for treatment within a specified time period for therapeutic effectiveness. Liu et al.[163] found a distinct

therapeutic window of opportunity for up to 6 hours after the onset of ischemia, using intransally administered IGF-I. Intracerebroventricular injection of insulin-like growth factor (IGF)-I has been shown to protect against stroke in rats.[137] However in human beings, it requires an operation with risk of infection and other complications to deliver the drug. Intranasal (IN) drug delivery offers a noninvasive method of bypassing the blood brain barrier to deliver IGF-I to the brain. It is known that neurons continue to die for many hours or even days after ischemia.[163] This delayed evolution of neuronal death provides a potential window of opportunity for neuronal rescue with effective antiapoptotic agents after ischemic injury.[163] Intranasal drug delivery enhancement by absorption promoters is evident in antimigraine studies. The polar antimigraine compound alniditan has been evaluated in phase I and phase II clinical studies. Phase I showed that chitosan was able to enhance nasal absorption of alniditan to a bioavailability of around 60%, a result confirmed earlier in sheep studies.[172] Chitosan administered at two dose levels during a migraine attack indicated an early rise in plasma concentration and the amount of drug in the circulation was found to relate to pain abatement and headache improvement.[172, 249]

Chitosan has shown significantly reduced ciliatoxicity when applied to *in vivo* and *in vitro* studies. Haffejee et al.[250] used human nasal epithelial cells to study the cilia toxicity of selected absorption promoters and compared the toxicity of the promoters with results obtained using histology of the rat nasal mucosa. In both cases lysophatidycholine demonstrated toxic effects and dimethyl-β-cyclodextrin and chitosan showed no toxic effects.

Further *in vivo* preclinical and clinical studies are necessary to assess chitosan as an enhancer in potentially marketable therapies. Chitosan's non toxicity to the local nasal mucosal environment and its absorption promoting abilities has demonstrated that it is an ideal candidate for continued exploration in nasal drug delivery studies presented in this thesis utilizing MD-CE-LIF.

Cyclodextrin

Cyclodextrins are cyclic non-reducing, non-hygroscopic, water soluble oligopolysaccharides (Figure 1.11). These glucose chains form a cone-like cavity into which compounds may enter and form a water-soluble complex and thus change the drugs physical–chemical properties.[251] This can increase the substrate compound's stability against hydrolyses, oxidation, photodecomposition and dehydration. Water solubility of the substrate can increase, as well as its bioavailability.[252, 253] HPβCD forms complexations with the poorly water-soluble flavinoid baicalein (Ba), 6, 5, 7,-trihydroxy

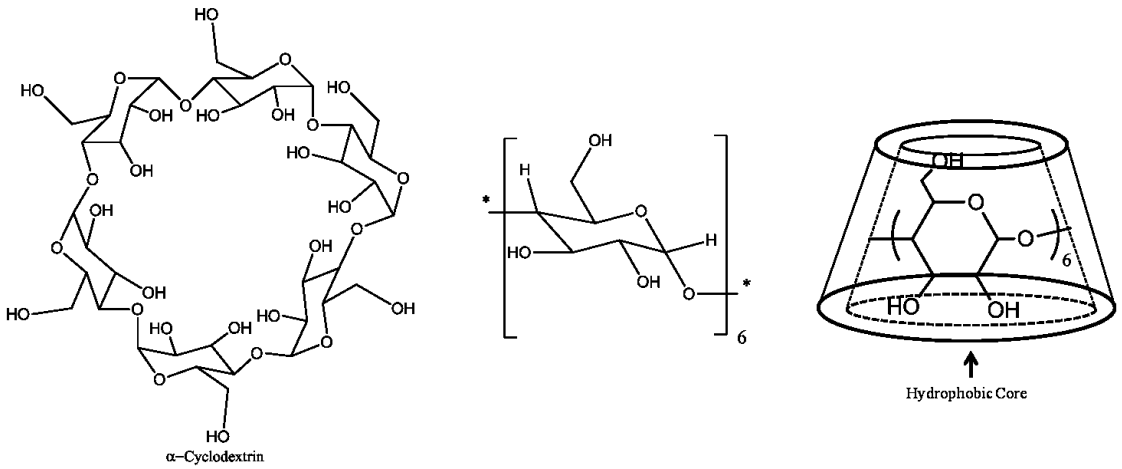

Figure 1.11. α-Cyclodextrin

flavone, resulted in increased bioavailability in intravenous injections in rats. In addition, higher Cmax concentrations of the Ba/HP*β*CD complex were obtained, at a faster time, Tmax, indicating a significant pharmacokinetic advantage over Ba intravenously administered alone.[252]

CDs are available industrially as homogenous (purity >99.5%) crystalline substances. The α-CD consists of 6 (cyclomaltohexaose), the β-CD 7 (cyclomaltoheptaose and the γ-CD 8 (cyclomaltoactaose) glucopyranose units. All secondary OH groups are located on one edge of the torus-like CD molecule, while all primary OH groups are on the other side. The 'lining' of the internal cavity is formed by H atoms, and glucosidic oxygen- bridge atoms, therefore this surface is slightly apolar. [253] In aqueous solution the slightly apolar CD cavity is occupied by water molecules which are energetically unstable (polar-apolar interaction) and can be readily substituted by substrates which are less polar than water molecules. CDs can modify the structure and function of cell membranes, or strongly influence the metabolic activity of the cells. Cyclodextrins and particularly chemically modified CDs can damage the lipoprotein membrane of human erythrocytes at concentrations which strongly depend on the lipophilicity of the molecule.[253] There are CD derivatives which even at high concentrations, are inert toward the erythrocyte membrane. Cyclodextrin has a low aqueous solubility, which led to the synthesis of more soluble derivatives. CDs are available as hydrophilic, hydrophobic, and ionic derivatives.[252] 2-Hydroxypropyl-β-cyclodextrin is a water soluble derivative of β-cyclodextrin. It has been widely studied as a complexing agent for pharmaceuticals as drug substrates complexed to HP*β*CD have

been shown to increase their solubility and stability in aqueous solutions.[252, 254] This is of particular importance in potential intranasal drug delivery studies for peptides and proteins, which may demonstrate solubility issues at physiological pH.[254, 255]

The potential of CDs, especially the methylated CDs, as nasal absorption enhancers has been demonstrated for luteinizing hormone-releasing hormone agonists, insulin, adrenocorticotropic hormone analogue, calcitonin, granulocyte colony-stimulating factor, and insulin like growth factor-I.[256] The safety of the three cyclodextrin derivatives, in order from least to most affect on nasal toxicity can be described in the following order: HPβCD > RMβCD > DMβCD.[257] Hydroxypropyl-β-cyclodextrin at a concentration of (5%, w/v) has significantly promoted the absorption of acyclovir in the nasal cavity of rats and rabbits.[258] ACV is a cyclic analogue of the natural nucleoside 2'-deoxyguanosine. The absorption enhancement was found to be concentration dependent with the order of increasing absorption of ACV by enhancers as HPβCD>sodium deoxycholate> sodium caprate> sodium tauroglycocholate> EDTA. Mechanisms of CD increasing nasal adsorption and permeability are not well understood. Shao et al.[259] analyzed rat nasal perfusate for total protein content upon application of various CDs including α-CD, β-CD, γ-CD, HPβCD, and DMβCD. Perfusing the nasal cavity of the rat with solutions of the CD resulted in a linear increase in protein content of the perfusate over time for all compounds, except for DMβCD, which demonstrated a sharp increase in protein concentration 15 minutes into the perfusion, followed by a linear phase. Among the CDs studied, DMβCD exhibitied a uniquely high activity in removing proteins from the rat nasal mucosa. The authors hypothesized that proteins are shed into the aqueous

phase from the mucous membrane after removal of the surrounding membrane phospholipids. Protein, phospholipid and enzyme assays all indicated the high m embrance solubilizing effect of DMβCD, supporting their hypothesis. More recent studies indicate the CDs enhance nasal aborption of peptides by multiple mechanisms: inhibiting peptide enzymatic degradation, solubilizing nasal mucosa membrane components, and opening cell-cell tight junctions.[226]

Acute histological effects of CDs on the epithelium of the nasal cavity have been investigated in rats with light microscopy, confocal laser scanning microscopy, and scanning electron microscopy.[221] Only minor changes in cilia and apical cell membranes were observed with 2% methylated β-CD or 2% DMβCD. The effects observed were similar to those of the control (physiological saline; 0.9% NaCl). Histological evaluation of γ-cyclodextrin and HPβCD in an *in vivo* rat model, studying intransally administered insulin, showed that 8% HPβCD was only slightly more toxic that the control phosphate buffer. 5% γ CD was comparable to the control. Both CDs were much less toxic than the surfactant laureth-9 at 1%.[221] Zhang et al.[260] surmised that a combination of nasal enhancers could lead to a reduction in toxicity to the nasal cilia while enhancing absorption of intransally administered insulin in rats. Sodium deoxycholate (SDC), typically highly ciliotoxic, was combined with various cyclodextrins including β-cyclodextrin and DMβCD. The formulation of 0.75 % SDC and β-CD at a molar ration of 1:2 lowered the nasal toxicity of SDC and still promoted insulin absorption with a longer inhibitory effect on blood glucose level over time relative to other formulations. Yang et al. reported *in vivo* based reversibility studies with DMβCD, finding the effect of

DMβCD on nasal membrane diminished with time, with increased nasal epithelial permeability returning to restrictive barrier properties after 6 hours. No irreversible nasal mucotoxicity was observed in a concentration ranging from 1%-5%.[226] This data is supported by other studies investigating the effects of CDs on the histological integrity of nasal mucosa. Asai et al. found that less than 10% w/v CD solutions do not induce gross tissue damage and can keep the histological integrity of the nasal mucosa.[257]

Cultured human nasal epithelium was used by Agu et al.[213] as a model to investigate the relationship between the efficacy and cytotoxicity/membrane perturbation or protease inhibitors (bestatin and puromycin) and their combination with absorption enhancers (glycocholate, DMβCD) using Leu-Enk as a model peptide. In addition, transport of sodium fluorescein 1 hour after permeation studies, was performed to assess the epithelial integrity at the end of each experiment. Epithelial integrity was assessed by measuring transepithelial electrical resistance (TEER) using Millicel ERS cell voltammeter, and the paracellular marker sodium fluorescein via a Diode array spectrophotometer at 490 nm. It was determined that transport of Leu-Enk was higher when glycocholate and DMβCD were used in conjunction with the protease inhibitors compared to the protease inhibitors or absorption enhancers alone: 0.5% glycocholate + 1mM puromycin > 2% DMβCD + 1mM puromycein > 0.5% glycocholate + 1mM bestatin > 2% DMβCD + 1mM bestatin.[213] Interestingly, although there was a change in TEER upon application of Leu-Enk and the absorption enhancers, it did not correlate well with transport of sodium fluorescein. Permeation of sodium fluorescein in the presence of combinations of protease inhibitors and absorptions had a better correlation and

appreciable sodium fluorescein transport. The authors concluded that cultured human nasal epithelium may be used to study strategies for enhancing nasal absorption. Permeability of peptides and macromolecules across cultures cells is considered comparatively lower in comparison with intact nasal epithelium.[213] Further studies using *in vivo* nasal models though are required to ascertain whether membrane perturbation and cytotoxicity observed *in vitro* can be extrapolated to *in vivo* conditions.

INTRANASAL MICRODIALYSIS STUDIES WITH NASAL ENHANCERS

Microdialysis is a technique ideally suited for sampling brain cerebrospinal fluid to determine drug concentrations post intranasal delivery. Measuring drug level present in the extracellular fluid can determine the drug activity and toxicity in any tissue. Several studies of nose to brain transport of intranasally administered neurotrophic factor nerve growth factor (NGF) have used the total amount of NGF in the brain tissue homogenate as a measure of successful delivery.[17, 183] As a better predictor of therapeutic effectiveness, adverse effects, and toxicity of neurotrophins it would be highly beneficial to determine concentrations of compounds in the extracellular regions of the brain as opposed to total concentration in the brain tissue.[183] MD is an excellent application to address these issues. When investigating brain pharmacokinetics by microdialysis it is important to ensure that the BBB is not damaged by probe implantation, in particular when a drug with limited access to the CNS is studied. Many BBB studies have studied BBB integrity after implantation of a MD probe and concluded that MD can be performed on the day of implantation.[261]

Analysis systems capable of high temporal resolution are necessary to determine accurate pharmacokinetic profiles. As discussed previously in this document, a common limitation to microdialysis sampling is poor temporal resolution. At present, 5-15 minute sample collection fractions are common for intranasally analysis studies coupling microdialysis to radiochemical and high performance liquid chromatography (HPLC) analysis[78, 199, 261-264] and frequently require sample preparation post MD sampling. These off-line microdialysis analysis systems do not provide the temporal resolution necessary to measure pharmacological events that occur on a rapid time scale.

Microdialysis is currently used to study intranasal administration and drug delivery with nasal absorption enhancers. Vaka et al.[183] explored the ability of chitosan to enhance the permeation of NGF in nose to brain drug delivery and found that chitosan enhanced the transolfactory epithelial transport of NGF by a factor of 14 relative to intranasally administered NGF without chitosan. *In vivo* experiments were performed in male Sprague-Dawley rats (250-300 g), with microdialysis fractions collected at hourly intervals for 6 hours following intranasal administration. The microdialysis probe was inserted into the hippocampal region: A/P: 5.6 mm, M/L: 5.0 mm, D/V: 7.0 mm. Probes were equilibrated by perfusing KRB at 2 µL/min for 1 hour prior to intranasal dose of the NGF solution (100 µg/mL in 100 µL) directly into the posterior segment of the nose using a microsyringe connected with a soft polymer capillary. The brain dialysis was assayed by ELISA. Transolfactory epithelial electrical resistance was measured, and found to decrease significantly in the presence of chitosan (0.25% w/v); an indication of the ability of chitosan to permeabilize the olfactory epithelial membrane.[183] Replacing the

chitosan with KBR saline, the electrical resistance of the membrane was found to recover almost completely within 1-2 hours. This suggests that chitosan acts as an enhancer by a mechanism which permeabilizes the membrane reversibly, and not by a mechanical disruption of the membrane, lending evidence to the theory that chitosan acts as a drug permeation enhancer by opening tight junctions.

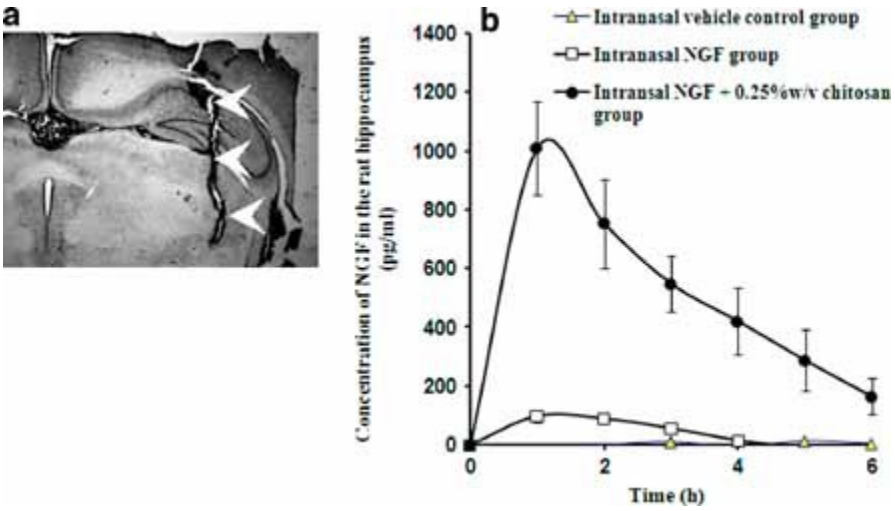

Figure 1.12.[183] Microdialysis Intranasal analysis of NGF in rat hippocampus (a) A representative picture of rat brain showing the location of microdialysis probe (arrowheads) in the hippocampus region. (b) Concentration time profile of NGF in rat hippocampus following intranasal administration. The data points represent baseline adjusted values and are averages of three animals with SEM as error bars.

Vaka et al.[265] have also explored the use of peppermint oil (PO) as an enhancer for intranasal delivery of NGF via microdialysis sampling in the rat hippocampus. Peppermint oil at concentrations of 0.05, 0.1 and 0.5% v/v enhanced the *in vitro* transport of NGF by 5, 7, and 8 fold, respectively. *In vivo* studies employing brain microdialysis in rats demonstrated that intranasal administration of NGF formulation with 0.5% PO enhanced the bioavailability by 8 fold compared to rats administered with NGF alone. The bioavailability of NGF in the brain could be enhanced by intranasal administration of peppermint oil. The temporal resolution of these techniques however is limited.

Li et al.[264] used a dual microdialysis probe technique in awake free-moving rats to determine the contribution of intranasal (i.n.) administration of the centrally acting polypeptide cobrotoxin (NT-I) in addition to the absorption enhancer borneol/menthol eutectic mixture (+BMEM). Pharmacokinetic profiles were developed via collection of NT-I, radio labeled with sodium 125I-Iodide (125I-NT-I), which was administered at the dose of 105 μg/kg intravenously and intranasally. The dialysates sampled simultaneously from olfactory bulb and cerebellar nuclei were measured in a gamma-counter for radioactivity post collection. Data points were obtained every 10 minutes and samples were prepared post sampling, indicating further poor temporal resolution.

The temporal resolution of analytical techniques that require 10 minutes-1 hour for sampling and further time for sample preparation, analysis and detection, up to 40 minutes per sample, is insufficient to determine an accurate time at which intranasally administered compounds reach the brain. The development of online microdialysis has greatly reduced temporal resolution issues associated with off-line analysis systems. Online coupling of microdialysis and capillary electrophoresis with laser induced fluorescence detection in the Bowser lab has become a powerful technique with applications in determining dynamic interactions in the study of neurotransmitters.[28, 32, 33, 78, 97, 99] Temporal resolution on the order of 20-30 seconds is commonly associated with MD-CE-LIF monitoring of amine neurotransmitters and may allow monitoring of rapid changes in the chemical dynamics of intranasal administration of drug mixtures with an absorption enhancer. Coupling microdialysis to the high temporal resolution analytical technique high speed online CE-LIF has the capability to determine whether nasal

absorption enhancers affect pharmacokinetic profiles and enhance brain bioavailability, particularly time to target area and Cmax and Tmax. The time it takes to reach the brain can elucidate the mechanism via which the drug arrived, e.g. axonal transport, diffusion, extracellular bulk flow, or blood to brain, further elucidating the mechanisms involved in intranasal administration and nose to brain transport.

Chapter 2:

Development of High Speed Online MD-CE-LIF Assay for Cyclic Guanosine Monophosphate

INTRODUCTION

Fluorescence derivatization of 3', 5'-cyclic Guanosine Monophosphate (cGMP) will be necessary for detection with the high speed on line MD-CE-LIF system. A large number of fluorophores that may label cGMP are easily excited by UV lasers and allow for detection during online *in vivo* microdialysis. The development of this assay is important to ascertain cGMP's ability to affect the glutamate/NMDA pathway. Initial experiments will need to show conclusive evidence of reaction between the fluorogenic reagent and cGMP, resulting in a fluorescent product. The primary goal is a derivatized product capable of detection by MD-CE-LIF analysis with *in vivo* characterization of the optimized assay in the rat brain.

Important characteristics of an ideal fluorophore include reagents that are nonfluorescent themselves, but react to produce fluorescent products with the compounds of interest. It is also highly desirable, though not always possible, that any side products of the reaction are nonfluorescent, so that excess reagent and side products do not interfere with the detection of the derivatives. Degradation products, if fluorescent, should ideally be easily separated from the derivatized product. Other ideal specifications for a fluorophore include a rapid reaction under mild conditions leading to a single product, stable derivative formation, and reagents that are of low toxicity and high stability. Fluorescence derivatization can introduce both a high degree of sensitivity and selectivity to MD-CE-LIF analysis when the desired fluorogenic reagent has a large molar absorptivity and a large quantum yield of fluorescence.[266] Reaction conditions must be optimized to attain efficient labeling with a specific fluorogenic reagent.

Optimization factors include reaction solvent, pH, concentration of reagents, reaction temperature, and reaction time.[266] The rate of derivatization is a significant factor, as it can strongly influence temporal resolution, an important component of the MD-CE-LIF analysis. Longer reaction times can lead to significant peak broadening and reduced separation times between runs.

There are a number of derivatizing agents available for primary amine analysis. Initial derivatization reactions for cGMP were carried out with 4-fluoro-7-nitrobenz-2-oxa-1,3 diazole (NBD-F). While one of the current high speed MD-CE-LIF instruments available for laboratory use is set up for OPA derivatization, the limit of detection (LOD) for OPA may be too high for the expected 6-9 nM range of basal cGMP levels. NBD-F was therefore used as a starting point for initial cGMP reactions. NBD-F derivatization is known to occur with many aliphatic amines within 5 to 10 minutes of reaction, when heated (60^{o}C).[107] Possible concerns associated with the fluorophore NBD-F include the quenching of cGMP.

Another possible derivatizing agent option is fluorescamine (FA). Fluorescamine is known to react rapidly with primary amines in the presence of potassium cyanide. This reaction occurs in milliseconds, and forms stable fluorescent products. Excess fluorescamine is hydrolyzed in water to form a non-fluorescent product. These characteristics make fluorescamine a desirable option for the derivatization of cGMP. Fluorescamine derivatizations carried out closely below the pH range for typical aliphatic amines will react with many of the primary amines expected to be present *in vivo*. Based

on cGMP's lower pKa, the number of fluorescent analytes present in CE separations will be reduced due to the selectivity of the labeling reaction.

(3-(2-furoyl)) quinoline-2-carboxaldehyde (FQ) forms charged conjugates with primary amines that can easily be analyzed by electrophoresis techniques. Amine detection for capillary zone electrophoresis LIF detection has sensitivity in the subfemtomole range (10^{-15} moles) for FQ.[109] The sensitivity, and temporal resolution needed for a cGMP assay however may not be reached due to longer reaction times. The solubility of FQ in water is low, another potential concern for a cGMP assay.

Due to the wide variety of fluorophores available for amine derivatization, a selection of these compounds known for their previously established sensitive and rapid reactions with primary amines was made. NBD-F, FA, and FQ are fluorogenic probes known to rapidly derivatize primary amines and will be applied first in the development of an assay for cGMP. These exploratory experiments were designed to narrow down possible reagents leading to a successful reaction between cGMP and the fluorogenic reagent. Adjustments to reaction conditions were made to compensate for cGMP specific concerns, e.g. thermal stability and the prevention of the degradation of cGMP to GMP, which can occur at pH > 8.0.

Pharmacological studies incorporating RIA and HPLC analysis have been carried out to further elucidate cGMP's role in the glutamate/NMDA/NO pathway. cGMP is a downstream neuromessenger of the proposed glutamate neuromessenger pathway, as discussed previously in Chapter 1 of this text. Elevated concentrations of glutamate, which occur during ischemia, result in excitotoxic effects, damaging brain tissue and

killing neurons. Unfortunately, pharmacological targets aimed at reducing glutamate levels have resulted in harmful side effects. Modulation of the glutamate pathway, possibly by targeting downstream components like cGMP may result in therapies with less harmful side effects. NMDA applied via reverse microdialysis has been found to induce concentration dependent increases in extracellular cGMP.[8] Elevation of cGMP by NMDA was completely inhibited by the selective receptor channel blocker dizocilpine (MK-801). Ammonia neurotoxicity was studied via infusing ammonia and NMDA into the striatum of rats. The results indicated both ammonia and NMDA promoted extracellular accumulation of cGMP. Taurine has recently been questioned as a neuroprotective agent against oxidative injury due to previous evidence suggesting it forestalls cell damage evoked by glutamate in cultured neurons and brain slices.[267] More research is needed to prove whether Taurine has the same effects *in vivo*.

While RIA analysis is sensitive, a strong limitation is the poor temporal resolution associated with this analysis. HPLC analyses have the same temporal resolution issues. Samples are often collected via microdialysis or tissue extraction, and then transferred for complex sample preparation and analysis. Analytical techniques capable of high throughput and high temporal resolution are necessary to study the rapid changes in pharmacological dynamics associated with the glutamate/NMDA/cGMP pathway. Application of the developed high speed on line MD-CE-LIF assay for cGMP, with low nM limits of detection and a temporal resolution of 25-35 seconds, has the potential measure pharmacokinetics of cGMP in the rat brain, at temporal resolutions higher than any currently applied analytical system for cGMP study.

MATERIALS AND METHODS

Reagents for Fluorimetry and MDQ-CE-LIF Experiments.

Unless otherwise noted, all chemicals were purchased from Sigma-Aldrich (St. Louis, MO). Artificial cerebrospinal fluid (aCSF) contained the following: 145 mM Sodium Chloride (NaCl), 2.7 mM Potassium Chloride (KCl), 1.0 mM Magnesium Sulfate ($MgSO_4$), and 1.2 mM Calcium Chloride ($CaCl_2$) in deionized water. Borate and sodium acetate buffers were prepared in deionized water (Milli-Q, 1.2 MΩ, Millipore Corporation, and Bedford, MA) and were filtered (0.2 μm) prior to use. Fluorophore NBD-F (5 mM) was prepared in acetonitrile (ACN). Fluorophore fluorescamine (FA), concentration 7.19 mM, was prepared in acetone. cGMP was prepared in aCSF. Gamma-aminobutyric acid (GABA), was prepared in deionized water. Potassium cyanide (KCN), concentration 10 mM, was prepared in deionized water. MDQ-CE separation buffer for NBD-F experiments contained the following: 100 mM borate buffer, pH 10.36. Fluorophore NBD-F, concentration 5 mM, was prepared in acetonitrile (ACN). Fluorophore FQ (Molecular Probes, Eugene, OR), concentration 10 mM, was prepared in methanol (MeOH). KCN, concentration 10 mM, was prepared in deionized water. Fluorescamine (FA), concentration 10 mM, was prepared in acetone. Varied reaction buffer experiments contained the following: 50 mM sodium phosphate (pH 8.05, pH 7.05, and pH 6.03), 50 mM sodium citrate (pH 6.08, pH 5.07, and pH 4.00). Fluorophore PGO (Acros Organics, Morris Plains, NJ) was weighed out and added to the reaction mixture. cGMP was prepared in aCSF. NBD-F studies used three buffers: 100 mM borate buffer, pH 10.11, 100 mM borate buffer, pH 8.10, and 100 mM sodium acetate (NaAc)

buffer, pH 4.93, and pH 5.10 respectively. Three buffers were prepared for fluorescamine studies and contained the following: 100 mM borate buffer, pH 10.51, 100 mM borate buffer, pH 7.33, 30 mM sodium acetate buffer, pH 7.20, 30 mM sodium acetate buffer, pH 5.10, respectively.

Reagents for in vivo characterization of cGMP Assay

Unless otherwise noted, all chemicals were obtained from Sigma Aldrich. (St. Luois, MO, USA). Separation and sheath flow buffer was sodium phosphate (50 mM) pH 6.05. All buffers were prepared in deionized water (Milli-Q, 1.2 MΩ, Millipore Corporation, Bedford, MA) and were filtered (0.2 μm) prior to use. Various concentrations of cGMP were prepared in aCSF (preparation described previously). High-K^+ aCSF contained 45 mM NaCl, 102.7 mM KCl, 1.0 mM $MgSO_4$, and 1.2 mM $CaCl_2$. PGO (Acros Organics, Morris Plains, NJ) was weighed out and added to 1.5 mL NaH_2PO_4 (50 mM) pH 6.00-6.05. The mixture was hand vortexed for 1 minute and sonicated for 10 minutes. Glutamate (1 mM) was prepared in aCSF. 3-isobutyl-1-methylxanthine (IBMX) (10 mM) stock solution was prepared in dimethylsulfoxide (DMSO). Desired IBMX concentration was prepared via serial dilution in aCSF and high-K^+ aCSF. IBMX (10 μM) was prepared via serial dilution in 2 x aCSF-Na. 2 x aCSF –Na contained 289 mM NaCl, 105.4 mM KCl, 2.0 mM $MgSO_4$, and 2.4 mM $CaCl_2$ buffered with NaH_2PO_4 (10 mM), adjusted to pH 7.10 with NaOH pellets. Cyclic guanosine monophosphate (cGMP), guanosine monophosphate (GMP), cyclic adenosine monophosphate (cAMP), adenosine monophosphate (AMP), adenosine diphosphate (ADP), adenosine triphosphate (ATP), guanosine diphosphate (GDP), guanosine

triphosphate (GTP), taurine, D and L serine, aspartate, asparagine, glycine, glutamate, threonine, and GABA (all 10 μM) were prepared in aCSF. Adenosine, adenine, guanosine, guanine, and 9-ethylguanine were prepared in aCSF with ≤ 8% dimethylsulfoxide (DMSO).

Fluorimeter

A fluorimeter (Jasco FP-6200 Spectrofluorimeter, Jasco Corp., Tokyo, Japan) was used to determine if an increase in fluorescence output was detected upon combination of cGMP with various fluorogenic reagents. This could indicate the fluorescent labeling and derivatization of cGMP. There is a potential that the chemistry of the derivatized reaction products will cause a variation from predicted excitation and emission wavelengths. The fluorimeter is a useful tool for verification of expected vs. observed wavelengths. pH was varied to determine any discernable difference in fluorescent intensities of derivatized products for potential assay optimization.

MDQ-CE-LIF Experiments

CE (MDQ: Beckman-Coulter, Fullter, CA, USA) separation for NBD-F and FQ was performed in a 50 cm long 360 μm outer diameter, 50 μm inner diameter capillary, with 40 cm to the actual LIF detector. The capillary was rinsed for 1 minute with separation buffer at 20 psi. Sample was then injected for 6 seconds at a pressure of 0.5 psi and a separation voltage of 20 kV was applied. Data was acquired for 20 minutes

Initial experiments on the MDQ CE with phenylglyoxal (PGO) and cGMP were performed to determine the presence or absence of a fluorescent derivatized product. With the confirmation of a derivatized reaction product between cGMP and PGO, it will

be possible to begin optimization of assay parameters, such as injection time and injection voltage, that will be applied to the homebuilt MD-CE-LIF system. Separation was performed in a 50 cm long 360 µm outer diameter, 50 µm inner diameter capillary, with 40 cm to the UV detector, set for absorbance at 200 nm. The capillary was rinsed for 10 minutes with 100 mM NaOH at 20 psi, followed by a rinse of 10 minutes with separation buffer at 20 psi. Pressure injected samples were injected for 5 seconds at 2 psi. Electrokinetic injections were carried out at 7 kV for 5 seconds. Separation was carried out under normal polarity with a voltage ramp of 0.17 minutes. Separation voltage on the commercial CE was applied at 24 kV, achieving a current of 60.1 µA. Run time was 30 minutes. Samples were sonicated upon addition of PGO for 10 minutes prior to addition of cGMP. The reaction mixture was hand vortexed for 1 minute and immediately analyzed.

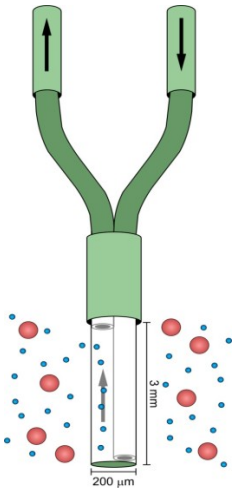

Figure 2.01. Schematic of Side by Side Microdialysis Probe.

Microdialysis

Side-by-side microdialysis probes were constructed in-house (Figure 2.01) and were discussed in Chapter 1 of this text. Briefly, two 40 µm i.d. × 105 µm, o.d. pieces of fused silica capillary (Polymicro Technologies, Phoenix, AZ) were staggered by 3 mm and inserted into a 200 µm diameter piece of hollow fiber, regenerated cellulose, dialysis tubing (18,000 MWCO, Spectrum Laboratories, Rancho Dominquez, CA) and sealed using polyimide (Alltech, Deerfield, IL), leaving a 3 mm sampling region exposed. Probes were perfused with ethanol (60 µL/hr for 50 min) and aCSF (60 µL/hr for 30

minutes) prior to use. The microdialysis probe was perfused with aCSF at 40 μL/hr (0.66 μL/min). Relative recovery of the probe was determined with the online capillary electrophoresis instrument. The MD probe was placed into an aCSF solution containing 100 nM fluorescein and the peak heights were determined. The same solution of aCSF and fluorescein was then pumped directly to the flow gated injection interface and peak height was determined. The ratio of the peak height of fluorescein determined via the MD probe and the peak height of fluorescein directly injected without the MD probe was the relative recovery.

In Vitro Characterization

In vitro recoveries of dialysis probes were measured by comparing the peak area of cGMP collected through the probe with the peak area of cGMP when it is pumped directly into the reaction T. Temporal resolution of the probe was measured by moving the probe from a solution of aCSF to a solution of 10 μM cGMP in aCSF for 4 minutes and then back again. aCSF was used as the perfusate through the probe. Temporal resolution of the valve used in reverse microdialysis was measured by switching the probe perfusate from aCSF to aCSF spiked with 10 μM cGMP for 4 minutes and then back to aCSF. The probe was placed in aCSF throughout all valve switching.

High speed online MD-CE-LIF

A schematic of the online MD-CE-LIF system is shown in Figure 2.02. LIF detection was performed off capillary in a high sensitivity sheath flow cell.[34, 102, 268] CE separations were performed in a 360 μm O.D./10 μm I.D. fused-silica capillary sheath flow cell.[34, 102, 268] CE separations were performed in a 360 μm O.D./10 μm I.D. fused-

silica capillary (Polymicro Technologies, Phoenix, AZ, USA) 7.4 cm long. The tip of the separation capillary was ground to a point using a Dremel tool. Voltage was applied to the outlet end of the separation capillary using a CZE1000R high-voltage power supply (Spellman High Voltage, Hauppauge, NY, USA). LIF detection was performed off-capillary using a sheath flow detector cell. Sheath flow buffer (NaH_2PO_4 (50 mM) pH 6.00-6.07) flows through the cuvette and around the separation capillary. The argon ion laser (Coherent Laser Group, Santa Clara, CA, USA) beam λ_{ex} = 362 nm, unfiltered, was focused by a 1 x fused silica lens onto a spot immediately after the separation capillary for excitation of separated derivatized solution components. Fluorescence was collected at 90^o by a microscope objective, passed through an interference filter (512 nm ± 2 nm; Intor, Inc. Socorro, NM) and focused onto a side-on photomultiplier tube (PMT R1477; Hamamatsu, Bridgewater, NJ, USA). Current from the photomultiplier tube was amplified (10^7 V/A) and filtered (300 ms rise time) using a current amplifier (Keithley Instruments, Cleveland, OH, USA), and recorded on a data acquisition card (PCI-MIO-16XE-50; National Instruments, Austin, TX, USA). Software for data acquisition and data control was written in house using Lab View (National Instruments).[98]

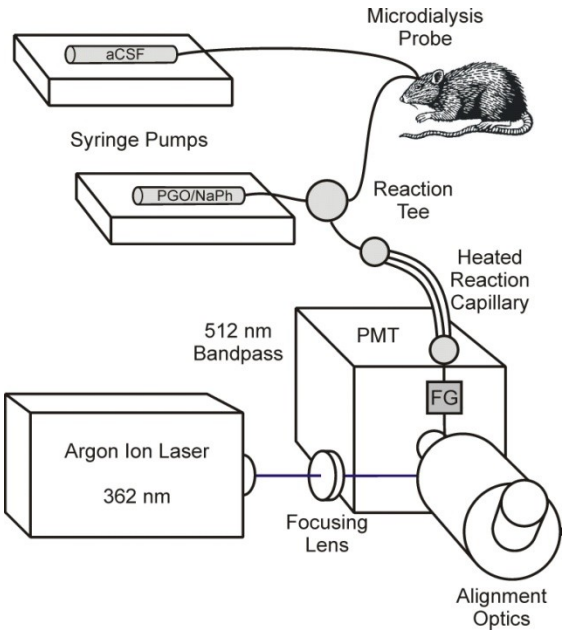

Figure 2.02. Schematic of high speed online microdialysis capillary electrophoresis with laser induced fluorescence detection instrument.

Phenylglyoxal Studies on the MD-CE-LIF Instrument

Optimization of analytical parameters for the cGMP assay was performed on the homebuilt MD-CE-LIF instrument. cGMP was fluorescently derivatized using phenylglyoxal (PGO). cGMP in aCSF was mixed online in a 3 port 0.25 mm stainless steel reaction T (Valco Instruments, Houston, TX, USA) with varying concentrations of PGO. PGO was prepared in NaH_2PO_4 (50 mM) pH 6.00-6.07, sonicated for 10 minutes and hand vortexed. cGMP in aCSF mixed with PGO in NaH_2PO_4 1:1 for optimization studies of PGO concentrations, and 3:1 for the remaining optimization parameters. The reaction occurred in a 360 μm outer diameter (O.D.) 75 μm inner diameter (I.D.) 59-62 cm long fused silica capillary connected to the third port of the reaction tee. In order to increase the rate of derivatization of cGMP, the reaction capillary was heated. The reaction capillary was inserted into one port of a 3 port tee (Valco Instruments Co. Inc., Houston TX), and exited a second port into Teflon® tubing which encapsulated a section of the reaction capillary. The third port of the T contained Teflon® tubing that connected to a heated water circulating system. A second T was setup with one port for the reaction capillary in the Teflon® tube, a second port where the reaction capillary exited the T and entered the flow gate, and a third port with Teflon® tubing connected the water circulator (Neslab EX7 Bath Circulator, Thermo Electron Corp., New Ington, NH). Using this setup, 31 cm of the reaction capillary was heated at temperatures up to 100 ^{o}C. Reaction time was calculated based on the flow rate through the reaction capillary. Derivatization of cGMP was carried out in an online reaction tee (Figure 2.03). Dialysate was mixed online with the derivatization solution in a capillary connected to the reaction T.

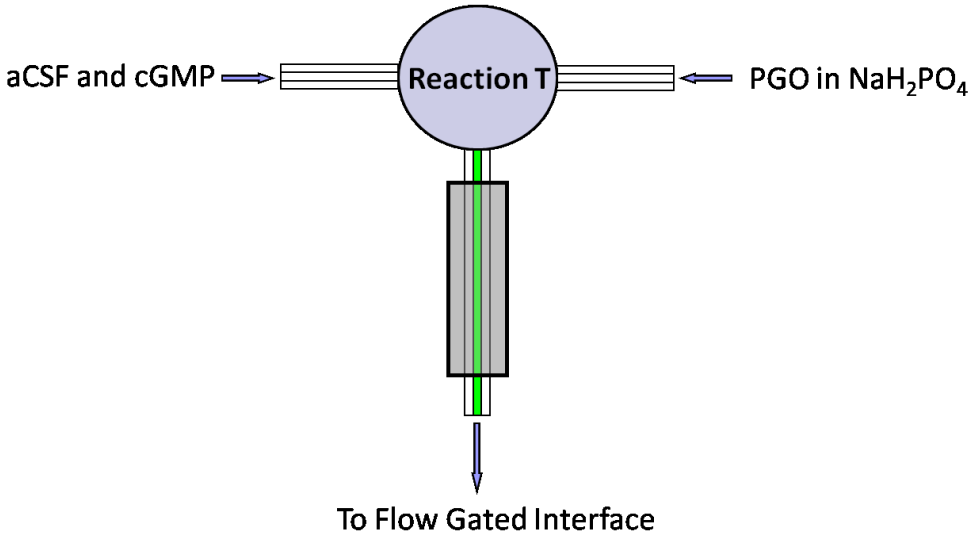

Figure 2.03. Schematic representation of online reaction T. cGMP in aCSF and PGO in buffer enter the reaction T. The derivatization reaction will commence upon mixing and be heated as the reaction mixture exits the reaction T and travels through a heated reaction capillary (360 μm O.D. 75 μm I.D.).

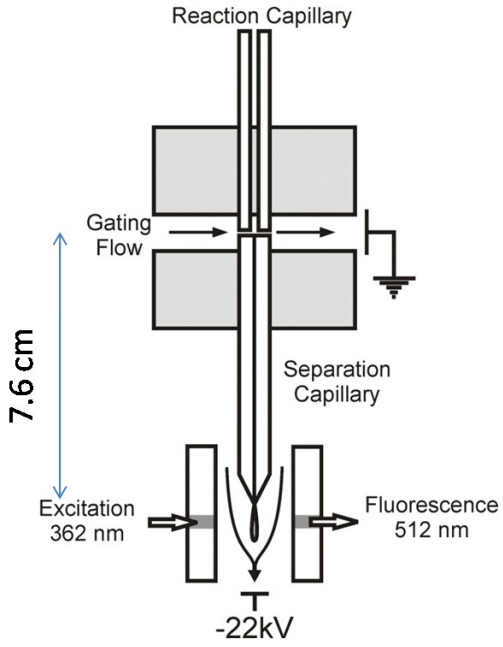

Figure 2.04. Schematic representation of flow gated interface and separation capillary in a sheath flow cuvette cell. Gated flow stops and allows derivatized sample to collect in the gap between the reaction and separation capillary. Voltage is applied to load a sample plug onto the separation capillary. Gating flow resumes, carrying derivatized sample to waste, as the separation voltage is ramped up and separation commences.

Reaction conditions developed off-line were reproduced in the online reaction capillary before injection onto the separation capillary. A flow gated injection interface[28, 30, 33, 34, 88, 92, 95, 96] was used to load the dialysate onto the separation capillary (Figure 2.04). The flow gated injection interface was machined out of a polycarbonate block by the U of MN Machine Shop. The capillary connected to the microdialysis probe outlet was inserted into the top of the flow gate, with a 20-50 μm gap separating it from the separation capillary, which was inserted into the bottom side of the flow gate. Separation buffer flow rate across the flow gated interface was 40 mL/hr. When the separation buffer was flowing, brain dialysate and samples in aCSF were carried to waste. To perform a sample injection, cross flow of the buffer was stopped via a pneumatically actuated valve (Valco Instruments Co. Inc.), for a specified period of time. The injection voltage was applied for specified period of time, and a plug of sample was loaded onto the separation capillary. Derivatized dialysate was flushed to waste while the separation buffer was flowing. Injection occurred when a pneumatically actuated valve stopped the flow of buffer for 500-1000 ms. Dialysate filled the gap between the capillary and the injection voltage was applied to load the plug of dialysate onto the separation capillary. An injection voltage was applied at the outlet of the separation capillary for about 1 second. After injection, the cross flow was resumed and the separation voltage was raised to -20 to -24 kV over 500 ms. CE separation took place in ≈ 7.4-7.8 cm long, 10 μm inner diameter, 360 μm outer diameter fused silica capillary. Anticipated separation time was 10-15 seconds. A sheath flow detection cell was used for detection of derivatized cGMP. Dovichi and co-workers reported that stray light can be minimized through the use of the

sheath-flow cuvette.[104, 269] The outlet of the separation capillary was inserted into a square fused silica cuvette with a 200 μm x 200 μm square inner bore.[78, 98]

In vivo Characterization of the cGMP Assay.

Pharmacological studies were carried out in the rat striatum and cerebellum. A schematic of the online MD-CE-LIF system was shown previously in this chapter (Figure 2.02). Side by side microdialysis probes were fabricated in house (previously described in Chapter 1 and Figure 2.01). Briefly, probes contained a 3 mm long, 200 μm outer diameter regenerated cellulose membrane (18,000 MWCO, Spectrum Laboratories, Inc., Rancho Dominguez, CA) sampling region. The microdialysis probe was perfused with aCSF (30 μL/hr). cGMP/Dialysate was mixed online with PGO in NaH_2PO_4 (10 μL/hr) under conditions previously described in this document in a 0.25 mm inner diameter reaction cross (Valco Instruments Co. Inc., Houston TX). The reaction capillary consisted of a 360 μm O.D./75 μm I.D fused silica capillary (Polymicro Technologies, Phoenix, AZ, USA) 59 cm long. 31 cm of the reaction capillary was heated. Heated derivatization reaction time was determined by the flow rate through the reaction capillary: 2.05 min (40 μL/hr). Post reaction T PGO concentration was 25 mM in sodium phosphate (25 mM post reaction T) pH 6.00-6.05. Separation buffer flow rate across the flow gated interface was 40 mL/hr. Separation of derivatized reaction components was carried out in a 360 μm O.D./10 μm I.D. fused silica capillary (Polymicro Technologies, Phoenix, AZ, USA) 7.4-7.7 cm long. The cross flow of the separation buffer was stopped for 1-2 s, injection of derivatized solution occurred for 350-450 ms at -21 kV. Cross flow was resumed and

separation voltage across the separation capillary was applied at -23 kV. LIF detection was performed in a high sensitivity sheath flow cell.

In vivo Animal Protocols

All animal experiments were performed in strict accordance with protocols approved by the Institutional Animal Care and Use Committee at the University of Minnesota. Monitoring of cGMP was carried out in the rat striatum of male Sprague-Dawley rats (250 to 350 grams). The rats were anesthetized in an induction chamber (Harvard Apparatus, Hollison, MA) in 2.5% isoflurane (Minrad, Inc., Bethlehem, PA) in industrial grade oxygen (1 L/min). The animal was then secured in a stereotaxic frame with an anesthesia mask adapter (David Kopf Instruments, Tujunga, CA). Anesthesia was monitored until the animal no longer exhibited limb reflex to a toe pinch. Ear bars were secured in place and isoflurane was reduced to 1.5% in industrial grade oxygen to maintain surgical anesthesia. Surgery was performed to expose the brain region of interest. The stereotaxic frame was used to implant a microdialysis probe + 0.2 mm AP (anterior/posterior), + 3.0 mm ML (medial/lateral) and - 6.5 mm DV (dorsal/ventral) from bregma, the craniometric point at the junction of the sagittal and coronal sutures at the top of the cranium[270] (Figure 2.05). The probe was slowly inserted to minimize tissue damage over a period of 15 minutes at approximately 500 μm/min. Data collection began one hour after the probe was inserted fully to allow time for the tissue surrounding the probe to recover from the damage caused by probe implantation.

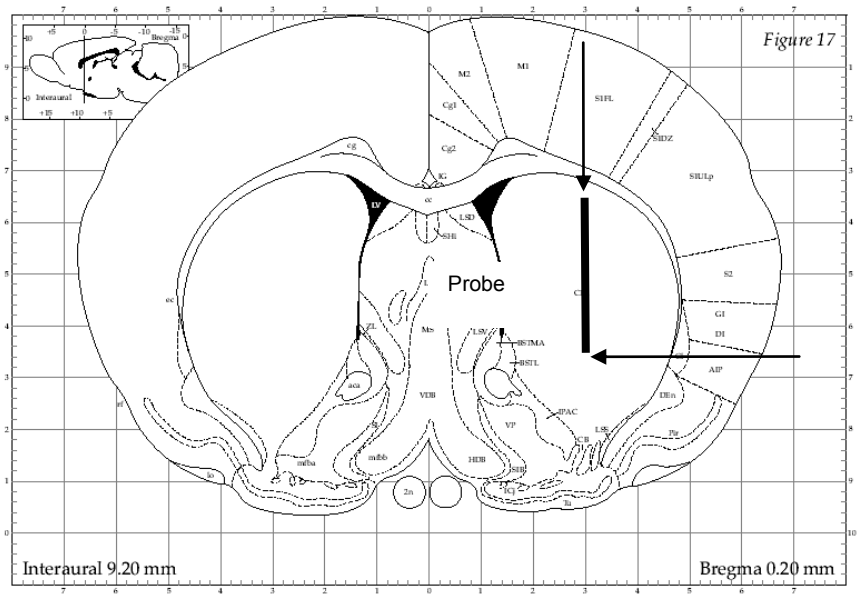

Figure 2.05. MD Probe placement into the rat striatum. Diagram of rat brain coronal section.[270] Depicted slice is 0.2 mm anterior to bregma. The vertical arrow is placed - 3.0 mm in the medial/lateral (ML) plane. The horizontal arrow is placed - 6.5 mm in the dorsal/ventral (DV) plane. Microdialysis probe specifications are 3 mm by 0.2 μm.

Potassium and Glutamate Stimulation

Potassium stimulation was performed immediately following the 1 hour probe equilibration time post insertion in the striatum. A four port manual turn valve was used to switch the microdialysis perfusion solution from aCSF to high potassium aCSF for 3 minutes. A second potassium stimulation was performed 30 minutes after the end of the first potassium stimulation, with application of high potassium aCSF for 15 minutes. Glutamate stimulation was performed 45 minutes after the end of the second potassium stimulation. The four port manual turn valve was used to switch the microdialysis probe perfusion solution from aCSF to Glutamate (1 mM) in aCSF) for 3 minutes. A second

glutamate stimulation was performed 30 minutes after the end of the first glutamate stimulation, with application of glutamate for 10 minutes.

Potassium Stimulation with Phosphodiesterase Inhibitor 3-isobutyl-1-methylxanthine IBMX

Application of IBMX (500 nM) in aCSF was performed immediately following a 45 minute probe equilibration time post insertion in the striatum. A four port manual turn valve was used to switch the microdialysis perfusion solution from aCSF to IBMX (500 nM) in aCSF. aCSF was removed from the micro pump and replaced with IBMX (500 nM) in high-K^+ aCSF. The four port manual valve was switched to apply IBMX in high-K^+ aCSF 30 minutes after application of IBMX in aCSF, with application of IBMX in high-K^+ aCSF for 3 minutes. A second stimulation was performed 30 minutes after the end of the initial IBMX in high-K^+ aCSF stimulation, with application of IBMX in high-K^+ aCSF for 10 minutes. A third stimulation was applied for 15 minutes, 30 minutes after the end of the second IBMX in high-K^+ aCSF stimulation.

Nitric Oxide Donor 2-(N-N-Diethylamino)-diazenolate-2-oxide (DEANO)

Application of IBMX (5 μM) in aCSF was performed immediately following a 1 hour probe equilibration time post insertion in the striatum. A four port manual turn valve was used to switch the microdialysis perfusion solution from aCSF to IBMX in aCSF. aCSF was removed from the micro pump and replaced with IBMX (10 μM) in 2 x aCSF-Na and buffered with NaH_2PO_4 (10 mM), pH 7.10. DEANO (10 μM) in NaOH (1mM) pH 11.0 was placed onto a third micro pump. The capillary exiting the four port manual valve was connected to the first port in a second reaction T throughout the experiment.

During time periods that DEANO was not applied, the second port of the T was plugged closed. Pharmacological agents switched via the manual four port valve exited the third port of the reaction T via a capillary that was connected to the inlet of the microdialysis probe. The four port manual valve was switched to apply IBMX in 2 x aCSF-Na 30 minutes after the application of IBMX in aCSF. Simultaneously, the plug in the second port of the reaction T was removed, and DEANO in NaOH was connected. Flow rates on the micro pumps were adjusted to maintain a total flow rate of 30 μL/hr, allowing DEANO one minute to react and mix with the IBMX (10 μM) in 2 x aCSF-Na (reduced to IBMX (5 μM) in aCSF post the reaction T due to a 1:1 mix with DEANO in NaOH) before reaching the inlet of the microdialysis probe. Application of DEANO occurred for 5 minutes. This process was reversed after the 5 minutes and the valve switched back to IBMX (5 μM) in aCSF. A second DEANO application was performed for 10 minutes 30 minutes after the end of the first DEANO application.

RESULTS

Fluorimeter and MDQ-CE Analysis of Potential Reagents for Fluorescence Derivatization of cGMP

Gamma aminobutyric acid (GABA) is one of many compounds known to be present in brain dialysate. It has been previously established that GABA reacts with NBD-F at a pH of 10.36 resulting in a highly fluorescent product.[107] This sample was prepared as a comparison of a known reaction on the commercial CE to the unknown cGMP. pH was varied in the fluorimeter experiments to accommodate the lower pKa of cGMP and explore the stability of a possible derivatized cGMP product. Samples run in

the buffer sodium acetate (NaAc), pH 4.93 showed a minimal increase in fluorescence for 50 μM GABA over the blank. No concentration dependent increase in fluorescence was indicated for any of the cGMP samples. Samples prepared in borate buffer, pH 10.36, showed no significant increase in fluorescence over the blank for either cGMP or GABA. This was unexpected, as GABA is known to react with NBD-F. The color of the reaction mixtures was an intense yellow, significantly different from the lighter yellow color of reactions run at lower pH. As reaction parameters, e.g. pH, are known to affect the fluorescent yield of derivatized products, a possible conclusion indicates observed hydrolysis products exceeded the upper limitations of the fluorimeter. Results for this experiment are not included here.

Samples prepared in borate buffer, pH 8.10, and sodium acetate buffer, pH 5.10 did indicate a possible concentration dependent increase in fluorescence (Figure 2.06).

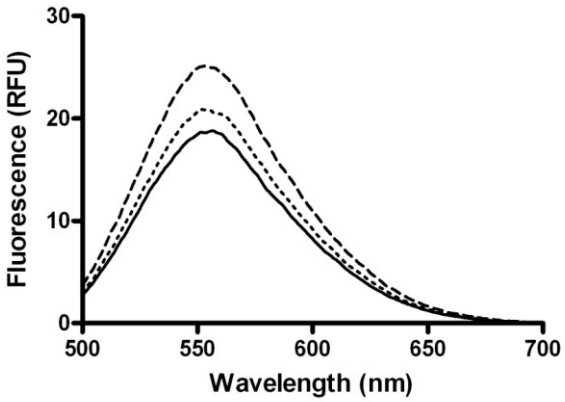

Figure 2.06. NBD-F Fluorimeter Results. NBD-F (5 mM) in ACN with cGMP (10 μM) and GABA (50 μM). Blank ——— , cGMP ····· , GABA – – . NBD-F λex: 470 nm. NBD-F λem: 530 nm Reaction mixture: 400 μL Sodium Acetate (100 mM) pH 5.10 + 80 μL NBD-F (5mM) + (400 μL aCSF – varied μL amine compound (1mM) in aCSF). Reactions were mixed by hand inversion for one minute and placed into a 60°C water bath for 5 minutes. Analysis was performed immediately following on a commercial fluorimeter.

This could suggest the derivatization of cGMP or a concentration dependent increase in fluorescent hydrolysis products. The results do not show conclusive fluorophore reaction with cGMP. The fluorimeter may not be specific enough to determine conclusive derivatization of cGMP. Analyzing the derivatization reactions on the commercial CE with LIF detection was therefore tried.

Due to concerns of the solubility of FA in aqueous solutions, the fluorogenic reagent stock solutions were prepared in three different solvents: acetone, acetonitrile, and methanol. The stock was diluted in the aqueous buffer in the final reaction mixture. FA and 10 μM cGMP reactions did not show any resultant increase in fluorescence over the blank in most experiments. Higher concentrations of cGMP, e.g. 50 μM, did indicate a possible slight increase in fluorescence over the blank, though most experiments showed no significant change in fluorescent output (Figure 2.07). These results were consistent at all experimental pH values. Varying the solvent of the FA stock solution did not affect the reactions in any measurable manner. As repeat measurements on the fluorimeter were not consistent, FA was further explored with cGMP on the commercial MDQ-CE to verify possible product formation or the lack thereof. FA and GABA reactions were run as a reference and indicated concentration dependent increases in resulting product fluorescence (Figure 2.08).

To further determine whether cGMP and NBD-F reacted, derivatization reactions were carried out on the automated commercial CE (MDQ: Beckman-Coulter, Fullerton, CA, USA) with laser induced fluorescence detection. The CE separation provides greater specificity in comparison to fluorimeter analyses. The presence or absence of labeled

target compounds can be determined. Separation of any present hydrolysis side products from derivatized products is also possible.

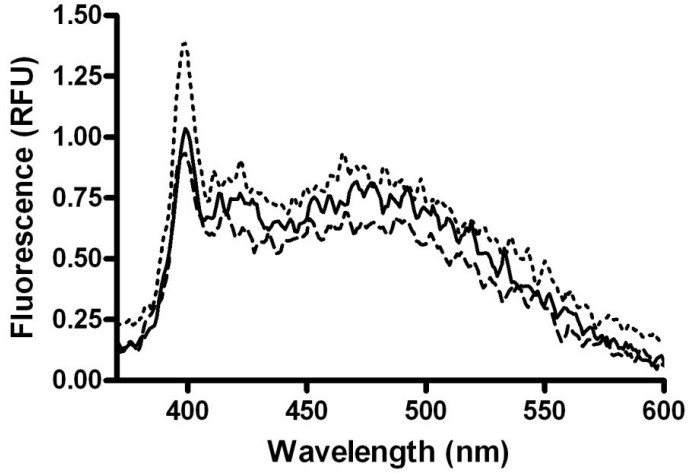

Figure 2.07. FA Fluorimeter Results. FA (7.19 mM) in acetone with cGMP (10 µM) and cGMP (50 µM). Blank ——, cGMP (10 µM) ·····, cGMP (50 µM) – – . FA λex: 380 nm. FA λem: 490 nm. Reaction mixture consisted of 450 µL Borate buffer (100 mM) pH 10.51 + 450 µL Guanine containing compound in aCSF + 100 µL FA (7.19 mM). Heated 60 ^{o}C for 5 minutes.

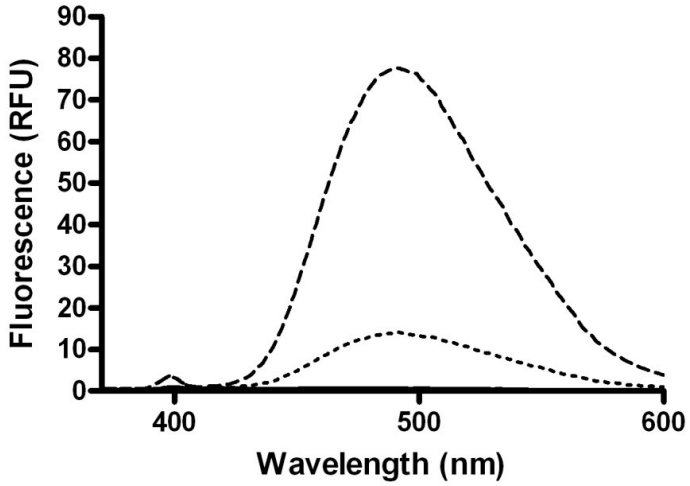

Figure 2.08. FA Fluorimeter Results. FA (7.19 mM) in acetone with GABA (10 µM) and GABA (50 µM). Blank ——, GABA (10 µM) ····· , GABA (50 µM) – – . FA λex: 380 nm. FA λem: 490 nm. Reaction mixture consisted of 450 µL borate buffer (100 mM) pH 10.51 + 450 µL FA + cGMP in aCSF. Heated 60 ^{o}C for 5 minutes.

Results for NBD-F on the MDQ-CE system are shown in Figure 2.09. The pH of the borate buffer, pH 10.36, makes it unlikely that the cyclic nature of cGMP was retained. A peak was visible where the expected GABA derivatization with NBD-F occurred. No peak corresponding to that of cGMP labeling was observed in the electropherogram, though characteristic hydrolysis products were indicated. NBD-F was ruled out as a potential fluorogenic reagent for the derivatization of cGMP.

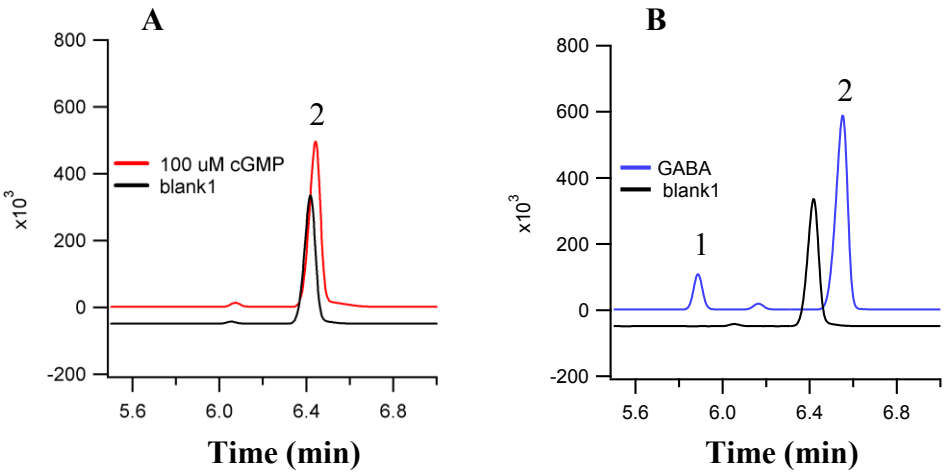

Figure 2.09. cGMP and NBD-F on Commercial CE Instrument. A) 100µM cGMP and B) 50µM GABA Peaks at 2: hydrolysis side products. Peak at 1: 50 µM GABA. Reaction Mixtures: 400 µL pH 10.36 borate buffer (100mM), 400 µL cGMP (100 µM) in ACSF or 400 µL GABA (50 µM), 80 µL NBD-F Reactions were vortexed for one minute and placed into a 60°C water bath for 5 minutes. Analysis was carried out immediately following removal from the bath.

(3-(2-furoyl)) quinoline-2-carboxaldehyde (FQ) was studied as a potential derivatizing agent of cGMP. No indication of derivatization of either GABA or cGMP was found in reactions with FQ. Solubility issues associated with FQ eliminated it as a potential candidate for cGMP derivatization. Initial fluorescamine experiments on the MDQ-CE system were run with sodium acetate buffer at 100 mM, the same concentration as the borate buffer used for previous fluorophore CE runs. The ionic strength for this concentration of sodium acetate (NaAc) was too high for use as a run

buffer to achieve good efficiency and separation within the current and voltage separation parameters. The concentration of NaAc buffer was decreased to 30 mM for subsequent runs. Due to solubility issues associated with FA it was ruled out as a potential derivatizing reagent for cGMP.

Initial attempts at derivatization of cGMP using the fluorophores NBD-F, FQ, and FA were unsuccessful. While these reagents are known to react well with aliphatic primary amines, they did not react with the aromatic primary amine cGMP. The reactivity of amino groups plays an important role in the chemistry of derivatization. Aromatic amines are generally less reactive than aliphatic amines. This is due to the strong resonance delocalization of the lone electron pair of NH_2 onto the aromatic π system. Delocalization also leads to the decreased basicity of aryl amines. Aromatic amines, like cGMP, are weak bases and unprotonated at pH 7. Aliphatic amines are moderately basic and react with most acylating reagents to form carboxamides, sulfonamides, ureas, or thioureas. While most amine acylation reactions are carried out at pH > 8.5, acylation reagents can degrade in the presence of water with the rate of degradation increasing as pH increases. The purine in cGMP will stabilize deprotonation, resulting in a pKa ≈ 4.5. This is significantly lower than most amino acids. pK_1 and pK_2 (pKa) refer respectively to the α-carboxylic acid and α-amino groups in the α-amino acids. Most α-amino groups all have pKa values around 9.4. Below a pH of 8.0, they are in their ammonium form. Many amines become protonated at very high pH and at high pH hydrolysis of the reagent dominates over the fluorogenic reaction.[271] pH is of particular concern for cGMP. cGMP undergoes hydrolysis, losing its cyclic nature, at pH

≥ 7-8, decomposing from cGMP to guanosine monophosphate (GMP). The development of a cGMP assay will most likely result with the reaction and CE run buffer pH < 8.0. Based on the results of these off line experiments, many fluorogenic reagents that react easily with primary amines are not capable of reacting with cGMP. NBD-F, FQ, and FA were ruled out as potential fluorogenic reagents in the development of a cGMP assay.

Fluorescence Derivatization of cGMP by Phenylglyoxal.

Phenylglyoxal (PGO) is a fluorogenic reagent known to react at relatively mild pH and temperature conditions with guanine nucleosides and nucleotides (See previous discussion in Chapter 1 for details). Literature reports an excitation wavelength of 365 nM and an emission wavelength of 515 nm for derivatized products resulting from the reaction of PGO and cGMP.[112] PGO to this point has been used primarily in HPLC based analyses. Initial studies of PGO with guanine containing compounds were performed by Kai et al.[117] Yonekura et al.[114] developed an HPLC method with online post column fluorescence derivatization with PGO. The reaction was carried out under relatively mild conditions and was selective for guanine containing compounds. GDP and GTP were isolated and quantified in human erythrocytes at approximately 17 and 40 nmol/mL. This proposed HPLC method had a sensitivity comparable to HPLC UV methods,[114] but offered the selectivity for the quantification of guanine nucleotides specifically. In order to improve sensitivity and increase the dynamic range a novel chemiluminescence method was developed for the determination of guanine and its nucleosides and nucleotides.[118] GTP, GMP, cGMP, guanosine, and deoxyguanosine were derivatized and analyzed using reversed phase chromatography. The derivatization was carried out with

phenylglyoxal in a phosphate buffer (pH 6.0) at 37 ^{o}C for 20 minutes. Chemiluminescence reaction was then carried out post derivatization with N,N-dimethylformamide in a weakly alkaline medium. The method was selective for guanine and 20-fold more sensitive than any fluorimetric assay at that point. Derivatization conditions with glyoxal reagents for guanine compounds for analysis by HPLC separation have been reported for a phosphate buffer (pH 6.0-7.0)-DMSO,[114] acetate buffer (pH 4.0 and 5.0)-DMSO,[117] and acetic acid.[272] PGO is a likely candidate for cGMP derivatization that may be applied to the development of an assay on the homebuilt MD-CE-LIF instrument.

Reaction mixtures of cGMP and PGO showed the first conclusive evidence of derivatized product formation of all fluorogenic reagents tried to this point (Figure 2.10). The expected emission wavelength of derivatized cGMP by PGO is approximately 515 nm. No indication of fluorescent product was seen in the blank at this wavelength.

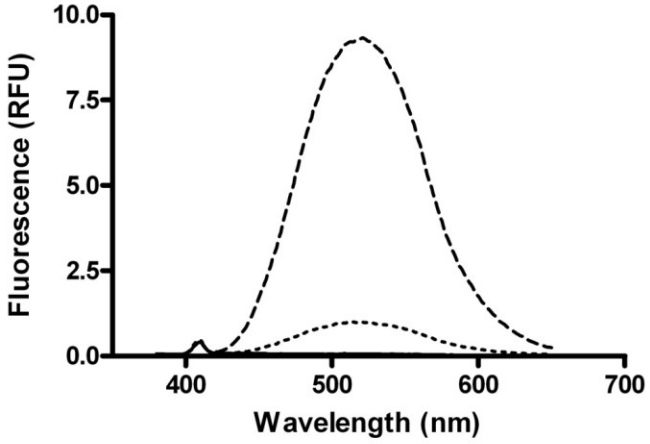

Figure 2.10. Phenylglyoxal (15 mM) and cGMP (100 µM) fluorimeter results. ——Blank, ····· cGMP (10 µM), – – cGMP (100 µM). Reaction mixture: (1 mL Sodium phosphate buffer (50mM) pH 7.05, varied [cGMP] in aCSF + 2.28 mg PGO. Sonicated, then heated 2 minutes, 82 ^{o}C. PGO λex: 365 nm. PGO λem: 515 nm.

Fluorimeter results indicated a concentration dependent increase in fluorescence with the 10 μM cGMP maximum 7 times that of the blank baseline, and the 100 μM cGMP maximum 90 times that of the blank baseline. Optimal emission (Figure 2.11) and excitation wavelengths (Figure 2.12) were determined for products of reaction mixtures containing PGO and cGMP. It was observed that at a fixed λex = 365 nm the λem shifts from ≈ 490 nm at 10 μM cGMP to a longer wavelength ≈ 515 nm, as the concentration of cGMP in the reaction mixture increases. This effect will not greatly alter optimization as the maximum fluorescence signal did not vary significantly between this range of emission wavelengths. pH and reaction buffer were varied to test the effect on the fluorescence output of derivatized reaction products between PGO and cGMP. Fluorimetric fluorescent intensities in reaction mixtures of 10 μM cGMP and PGO from highest to lowest are as follows: Sodium phosphate (pH 6.00), Sodium Citrate (pH 6.08),

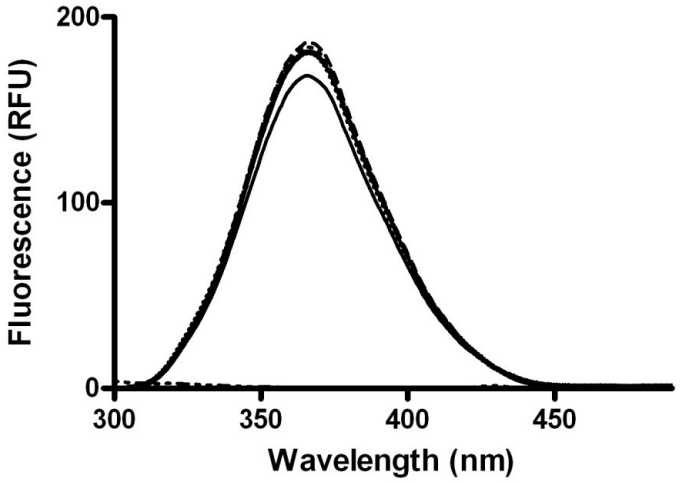

Figure 2.11. Fluorimeter Results: Determination of optimal emission wavelength. PGO (15 mM) and cGMP (100 μM). Reaction Buffer: Sodium phosphate (100 mM) pH 5.97. Reaction Mixture: 900 μL buffer + 100 μL cGMP + 2.3 mg PGO. Sonicated 10 minutes and perfomed fluorimeter analysis immediately afterward. Fixed Emission. Traces from top to bottom: 520 nm, 515 nm, 510 nm, 500 nm, Blank. Ideal λex = 365 nm. Ideal λem = 520 nm.

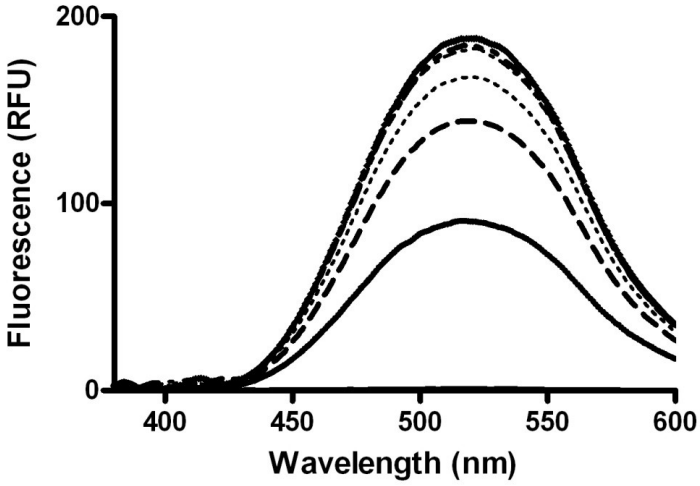

Figure 2.12. Fluorimeter Results: Determination of optimal excitation wavelength. PGO (15 mM) and cGMP (100 μM). Reaction Buffer: Sodium phosphate (100 mM) pH 5.97. Reaction Mixture: 900 μL buffer + 100 μL cGMP + 2.3 mg PGO. Sonicated 10 minutes and perfomed fluorimeter analysis immediately afterward. Fixed Excitation. Traces from top to bottom: 365 nm, 370 nm, 360 nm, 355 nm, 350 nm, 340 nm, Blank. Ideal λex = 365 nm.

Sodium Citrate (pH 5.07), Sodium Phosphate (pH 7.05), Sodium Citrate (pH 4.00), and Sodium Phosphate (pH 8.05). These results were also obtained for reactions of 100 μM cGMP and PGO. Futher optimization of the cGMP reaction will be carried out in a Sodium Phosphate buffer pH ≈ 6.00.

Due to concerns of the solubility of PGO in aqueous solutions, the fluorogenic reagent stock solutions were prepared in buffer with 0% acetonitrile (ACN), 15% acetonitrile (v/v), and 33% acetonitrile (v/v). The % of acetonitrile in the reaction mixture did not appear to affect the resulting fluorescent intensity of derivatized cGMP. However, the baseline of PGO in buffer increased as the % of ACN increased, indicating possible formation of a fluorescent side product. Application of heat to the reaction mixtures containing ACN further increased the baseline of PGO in buffer. As PGO solubility was

not a factor in reaction solutions that were heated, ACN was eliminated from all future sample preparations.

With initial optimization parameters of pH, buffer, and solvent composition established, assay optimization for PGO labeled cGMP was transferred to a commercial MDQ CE instrument. Results obtained from these experiments show derivatized product formation between PGO and cGMP and provide further optimization parameters necessary for the homebuilt MD-CE-LIF system. Sample mixtures for MDQ-CE study of cGMP derivatization were prepared as listed in Table 2.01. The homebuilt MD-CE-LIF instrument requires electrokinetic injection to load the derivatized sample onto the separation capillary. A comparison of pressure injection to electrokinetic injection was therefore carried out concurrently with the experiments designed to determine presence or absence of derivatized cGMP.

Sample Number	1 mM cGMP (uL)	PGO (mM)	50 mM Buffer (uL)	aCSF (uL)
Blank 1 and 1a	-	15	900	100
Blank 2 and 2a	-	-	900	100
Sample 1 and 1a	100	15	900	-
Sample 2 and 2a	100	-	900	-

Table 2.01. MDQ-CE Sample Mixtures. Samples 1 and 2: pressure injection, samples 1a and 2a: electrokinetic injection.

Blank 2 (Figure 2.13, Top Trace) contained aCSF and buffer. No peak appeared in the electropherogram. Blank 1 (Figure 2.13, Middle Trace) consisted of PGO (15 mM) in NaH_2PO_4 buffer (50 mM) pH 6.03. A single peak due to PGO was present at ≈ 4.4 s. Sample 2 (Figure 2.13, Bottom Trace) contained cGMP (100 μM) and NaH_2PO_4 buffer (50 mM) pH 6.03. A single peak for cGMP was present at a migration time of ≈ 11.2 s. Once electropherograms and migration times of the individual components in a reaction

mixture of cGMP and PGO were obtained, a derivatization reaction was analyzed. Reaction 1 (Figure 2.14) contained PGO (15 mM) and cGMP (100 μM). Peaks in the electropherogram were present at migration times of ≈ 4.4 s (PGO) , ≈ 7.9 s (derivatized

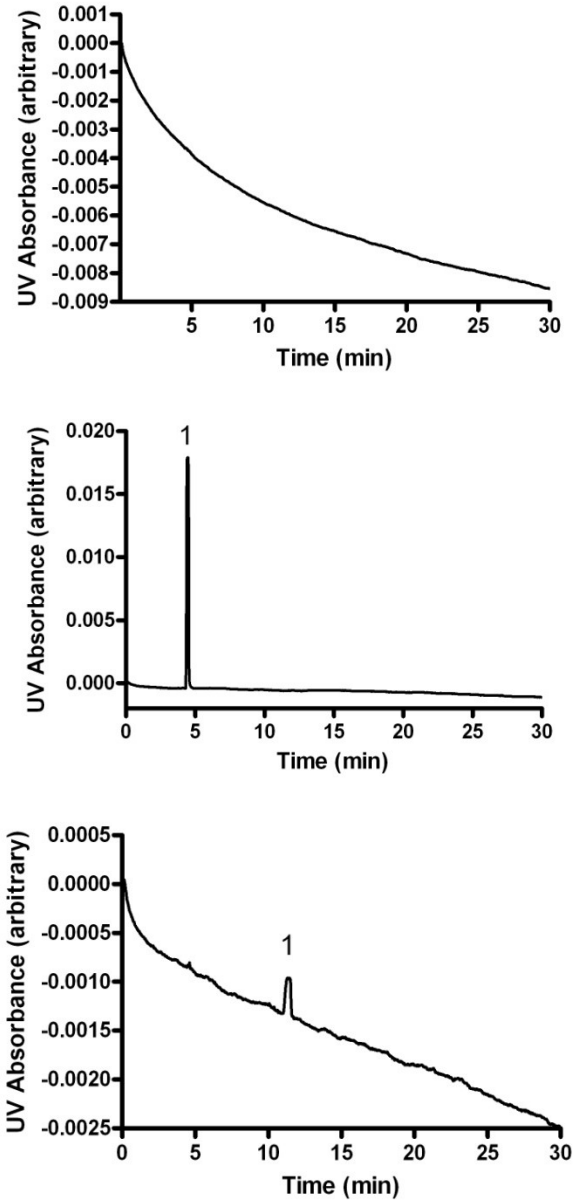

Figure 2.13. MDQ-CE Analysis of cGMP and PGO. Top Trace: aCSF and NaH_2PO_4 (50 mM) pH 6.03. X axis offset -0.009. Middle Trace: PGO (15 mM) and NaH_2PO_4 (50 mM) pH 6.03. Peak at 1) PGO. X axis offset -0.002. Bottom Trace: cGMP (100 mM) and NaH_2PO_4 (50 mM) pH 6.03. Peak at 1) cGMP. X axis offset -0.0025.

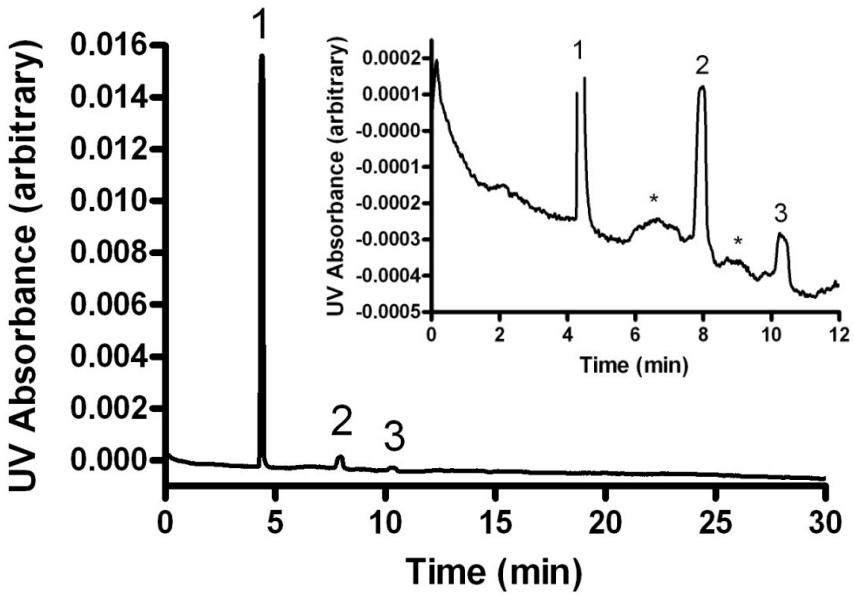

Figure 2.14. MDQ–CE Electropherogram of PGO (15mM) cGMP (100 mM) in NaH_2PO_4 (50 mM) pH 6.03. Peak at 1) PGO. Peak at 2) Derivatized cGMP. Peak at 3) Unreacted cGMP. X axis offset -0.001. Inset graph: Peak at 1) PGO. Peak at 2) Derivatized cGMP. Peak at 3) Unreacted cGMP. Peaks at *) Unidentified. X axis offset -0.0005.

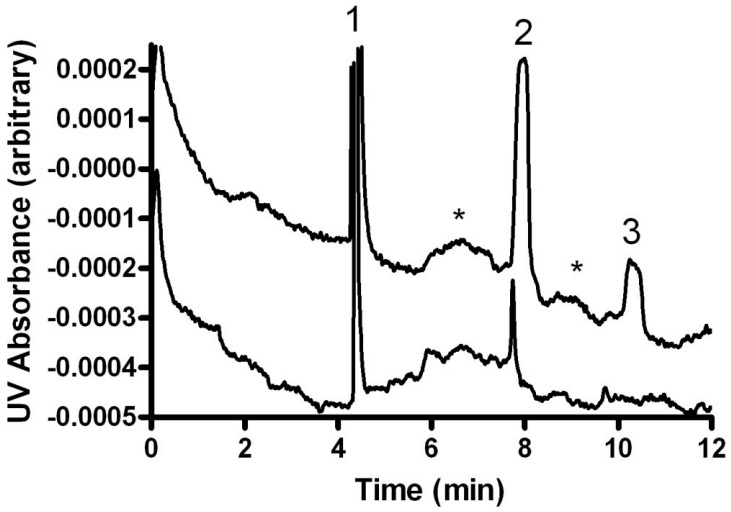

Figure 2.15. MDQ-CE Comparison of Pressure and Electrokinetic Injection. Reaction Mixture: cGMP (100 μM), PGO (15 mM) and NaH_2PO_4 (50 mM) pH 6.03. Upper Trace: Presure Injection. Y o ffset: 0.0001 Lower Trace: Electrokinetic Injection. Y offset: -0.00015. Peaks at 1) PGO. Peaks at 2) Derivatized cGMP. Peaks at 3) Unreacted cGMP. Peaks at *) Unidentified. X Axis offset: -0.0005.

cGMP), and ≈ 10.4 s (unreacted cGMP). The peak at 10.4 s in the PGO and cGMP derivatization reaction is most likely unreacted cGMP in solution. Repeat injections of these samples showed small variability in the migration times of peaks, most likely due to run to run variance on the instrument. These shifts did not prohibit identification of the peaks as changes in migration time could be normalized in comparison to the change in PGO migration time. A comparison of the reaction mixtures containing PGO and cGMP showed higher peak areas with pressure injection than electrokinetic injection (Figure 2.15). The smaller peak area in the electrokinetic injection could be caused by an electrokinetic bias of the negatively charged cGMP while loading onto the separation capillary. Larger voltages may be necessary to increase the amount of sample injected onto the capillary. As the assay will ultimately be injected electrokinetically, this parameter was next explored on the MDQ CE.

Sample mixtures of PGO (15 mM) and cGMP (100 μM) were run on the MDQ CE instrument at injection voltages of 2 kV, 4 kV, 8 kV, and 10 kV. 10 kV is the maximum injection voltage that can be applied with the instrument. Results are shown in (Figure 2.16). Focusing on the section of the electropherogram containing the PGO peak, it is quite clear that increasing voltages are desirable to maximize injection of sample onto the separation capillary. This trend was also visible in the derivatized cGMP product peak areas. Overinjection did not occur at 10 kV, indicating higher injection voltages may be applied. This will be possible to further explore on the homebuilt MD-CE-LIF instrument due to the limitations of the MDQ CE instrument.

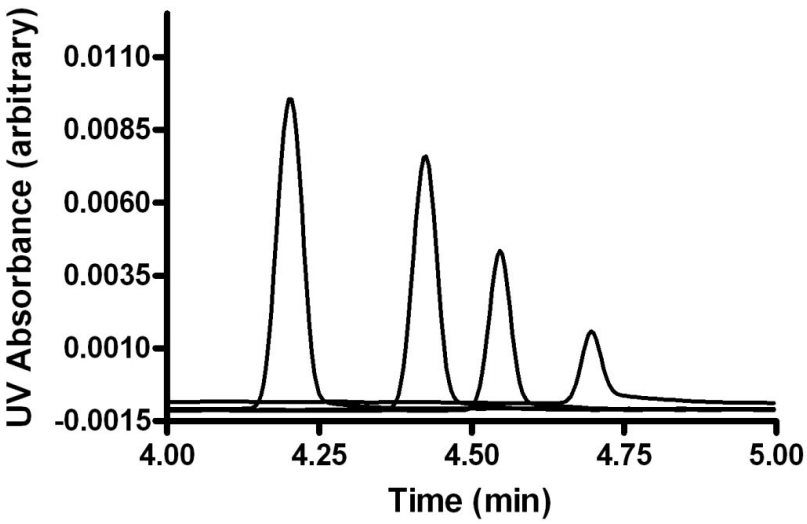

Figure 2.16. MDQ-CE Varying Electrokinetic Injection Voltage. cGMP (100 μM), PGO (15 mM) and NaH_2PO_4 (50 mM) pH 6.03. Peak height from highest to lowest: 10 kV, 8 kV, 4 kV, 2 kV Injection. All peaks in electropherogram are PGO.

The length of injection time onto the separation capillary is also an important parameter to optimize. Over injection of the sample can occur leading to wider baseline peak widths, causing reduced separation efficiency and plate counts. Using the maximum injection voltage of 10 kV, injection time was varied from 10 s – 40 s. (Results not shown here.) it was found that an 18s injection was most ideal on the MDQ-CE instrument. Injection times greater than this caused significant broadening of the derivatized cGMP peak, while injection times less than 18 s did not load as much sample as possible onto the separation capillary. While injection time was optimized for experiments on the commercial CE instrument, injection time will likely be significantly smaller on the homebuilt MD-CE-LIF instrument, as previous injection times for established assays are on the order of milliseconds.[28, 30-33, 99]

Experiments on the commercial MDQ-CE instrument confirmed the presence of a derivatized product between PGO and cGMP. PGO was therefore selected as the fluorogenic reagent to use in optimizing a cGMP assay. Optimal sample injection conditions occurred upon application of the highest injection voltage possible on the MDQ-CE system, 10 kV. Longer injection times were also necessary. With the injection parameters and fluorimeter results for the ideal derivatization reaction buffer, and sodium phosphate pH $\approx$ 6.00, further application and optimization of the cGMP assay was transferred to the commercial MD-CE-LIF instrument.

MD-CE-LIF cGMP Assay Development and Optimization

Optimization of analytical parameters for the cGMP assay was performed on a homebuilt MD-CE-LIF instrument (See the methods and development section previously in this chapter for further details). The maximal reaction yield of the fluorescent derivatization reaction of PGO with cGMP was determined. As was previously discussed, parameters such as temperature, concentration, pH, and reaction time are all significant factors. pH of the separation buffer was varied incrementally to determine maximum fluorescent intensity. Temperature was varied to determine its effect on the fluorescent derivatization yield and the rate at which the reaction occurs. Varying the concentration ratio of PGO to cGMP also narrowed down the reaction parameters leading to the highest derivatization yields. In general, it is important for reproducibility that the fluorescent yield is as close to 100% as possible to reduce any variability present between runs during analysis.

Specific analytical objectives in the development of the cGMP assay on the MD-CE-LIF instrument were as follows. The limit of detection was determined by the concentration of analyte that results in a signal three times the standard deviation of a blank measurement. A goal for the proposed limit of detection for the cGMP assay was 1 nM, as basal levels of 6-9 nM have been determined by previous RIA assays. Temporal resolution is defined as the amount of time required for the signal to change from 10% to 90% in response to a step change in analyte concentration at the microdialysis probe. It is essential for a high temporal resolution of the cGMP assay in order to measure brain dynamics on a fast time scale. The upper calibration range should reach a 10-fold increase in basal (6 nM) cGMP levels. Precision goals in the cGMP assay consisted of a 2-5 % range in error for the standard deviation of measurements in the rat striatum.

Optimal PGO concentration for the online derivatization of cGMP was first explored in the development of the cGMP assay as dicussed previously in this chapter. Reaction mixture concentrations of PGO ranged from 5 mM – 45 mM. The effect of varied reaction time at varied temperature in the derivatization reaction of cGMP with PGO was studied. While cGMP and PGO do react at room temperature to produce fluorescent product, this reaction takes up to an hour to reach maximum fluorescent product yield. This was not acceptable for an online high speed analysis with a goal of high temporal resolution. Heating a reaction can speed up the kinetics of derivatization of cGMP. The temperature and length in time of derivatization was optimized for the online MD-CE-LIF. Separation buffer for varied pH studies (sodium phosphate, 50 mM, pH

5.16, pH 6.04, pH 6.08, pH 6.42, pH 7.06) was prepared. Sodium phosphate concentration was varied from 25-100 mM.

Optimized concentration of the fluorogenic reagent PGO was determined to be 25 mM in the online derivatization reaction of PGO with cGMP (Figure 2.17). This result closely corroborated the off-line results of optimized PGO concentration = 20-25 mM (Results not shown here). Off-line results were obtained by direct injection of a pre mixed solution of cGMP and PGO into the flow gated interface, bypassing the online derivatization occurring in the reaction T. 25 mM PGO demonstrated optimal fluorescence intensity of cGMP derivatized products.

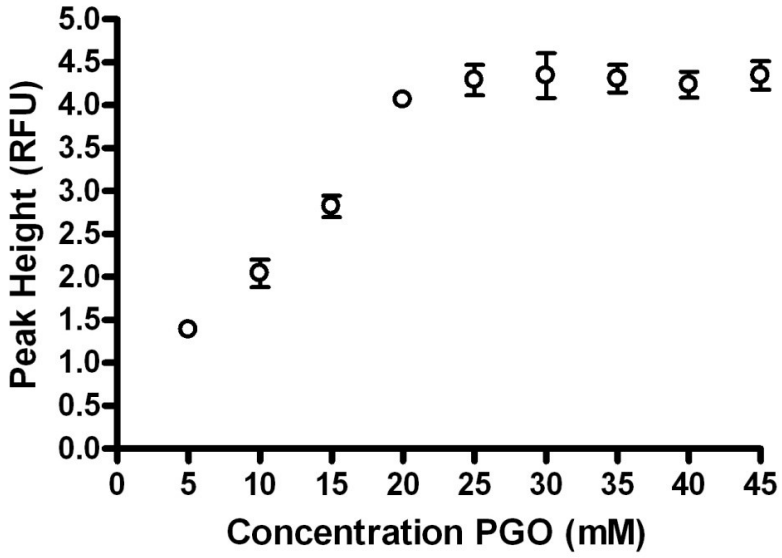

Figure 2.17. Optimization of fluorogenic reagent PGO concentration in online derivatization reaction with cGMP. Reaction mixture: 40 µL cGMP (1 mM) + PGO + 1.460 mL NaH_2PO_4 (50 mM) pH 6.04. Each mixture was sonicated for 10 min and analyzed immediately afterward. Final concentration of cGMP post reaction T = 20 µM. Error bars represent standard deviation of average peak height, $N \geq 3$.

Temperature and time of the derivatization reaction was optimized. Highest fluorescent intensity of derivatized cGMP occurred at an optimal heated reaction time of 1.37 min

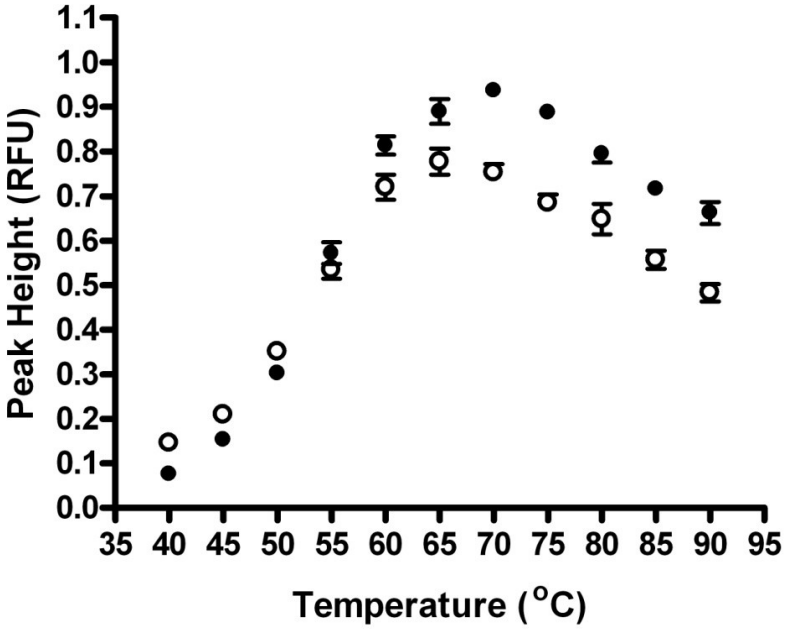

Figure 2.18. Derivatized cGMP at varied temperature and reaction time. Solid circles: Heated reaction time = 1.37 min (60 µL/hr). Open circles = Heated reaction time = 2.05 min (40 µL/hr). Reaction Mixture: PGO (25 mM) in NaH_2PO_4 (50 mM) pH 6.04 + cGMP (10 µM) in aCSF. Data was collected at two derivatization times, 1.37 min and 2.05 min. Error bars represent standard deviations of peak height with N ≥ 3 for each data point.

and a temperature of 65 - 70 ^{o}C (Figure 2.18). Heated reaction times of 1.37 min (60 µL/hr), 2.05 min (40 µL/hr), and 4.11 min (20 µL/hr) were explored at temperatures ranging from 40-90 ^{o}C (Data not shown for 20 µL/hr). Optimal derivatization temperature was determined to be ≈ 65 ^{o}C at all reaction times with maximum peak height at a heated reaction time of 1.37 (60 µL/hr) minutes. At lower temperatures, the rate of derivatization is significantly slower, leading to lower peak height and area counts for the derivatized cGMP peak. While a flow rate of 60 µL/hr through the reaction capillary led to the highest peak area counts for cGMP, this is not an ideal flow rate

through the microdialysis probe that will be incorporated into biological experiments. % recovery through the probe decreases with increasing flow rates. At higher temperatures, structural integrity of the cGMP and PGO becomes a concern, as indicated by the increasingly smaller peak height and area counts at temperatures in excess of 70 ^{o}C. Separations of cGMP and GMP indicate that cGMP does maintain its cyclic nature at higher temperatures (Figure 2.19) and remains resolved from GMP. Further studies were carried out to confirm the optimal reaction time and reaction temperature.

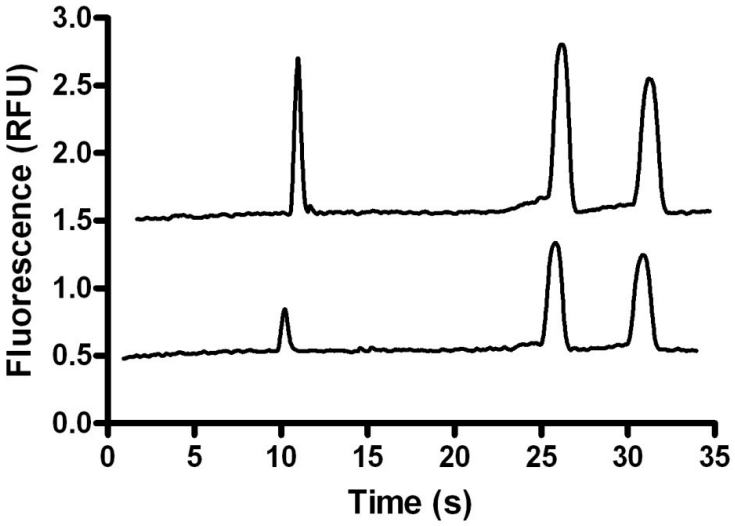

Figure 2.19. Sample electropherogram of separation of cGMP (25.6 s) from GMP (32 s) at varied temperature. Top Trace: T = 60 ^{o}C. Bottom Trace:T = 85 ^{o}C. Y offset: -1.0. Reaction Mixture: PGO (20 mM) in NaH_2PO_4 (50 mM) pH 6.03 + cGMP (20 μM) + GMP (20 μM) in aCSF.

PGO in NaH_2PO_4 was drawn into a 500 μL syringe and connected to one inlet of the reaction T. cGMP in aCSF was drawn into a separate 500 μL syringe and connected to a second inlet of the reaction T. The ratio of PGO in NaH_2PO_4 to cGMP in aCSF in the reaction T was changed to 1:3. This will reduce dilution of dialysate mixing at the reaction T during biological experiments. The length of heated reaction capillary was

changed to 62 cm to study longer reaction times at various flow rates (Data not shown here.). Optimal temperature of derivatization was set to 60 ^{o}C. Heated reaction times were 2.52 min (120 µL/hr) 3.78 min (80 µL/hr) 5.00 min (60 µL/hr) 7.55 min (40 µL/hr) and 15.11 min (20 µL/hr). Maximum fluorescence of derivatized product was achieved at 2.52 min and decreased as reaction time increased. Higher flow rates are not practical and can damage the microdialysis membrane on the sample probe in physiological studies. Lower flow rates would be more ideal in terms of % recovery through the probe. The instrument setup has physical limitations of the length of reaction capillary connected to the instrument that must be considered. Longitudinal diffusion becomes a concern in longer lengths of capillary. The intermediate flow rate of 40 µL/hr at a heated reaction capillary length of 31 cm, 2.05 min, at 65 ^{o}C was therefore chosen for future optimization parameters of the cGMP assay.

The pH and concentration of separation buffer was explored next. Maximum fluorescence for varied separation buffer pH studies was achieved with a sodium phosphate separation buffer pH of approximately 6.00 (Figure 2.20). Fluorescence of derivatized cGMP did not vary in the narrow range of pH 6.00 to 6.4 (Data not shown here.). Separation buffer in further optimization reactions was set to pH ≈ 6.00.

Maximum fluorescence for varied sodium phosphate concentration studies occurred at NaH_2PO_4 50 mM (Figure 2.21). A representative electropherogram at this concentration can be seen in Figure 2.22. The highest signal to noise ratio was achieved at NaH_2PO_4 50 mM. Sodium phosphate (50 mM) pH 6.00 was therefore used as the separation buffer as well. Average plate count of derivatized cGMP at varried sodium

phosphate concentrations in indicated in Table 2.02. High plate counts were achieved at higher separation buffer concentration.

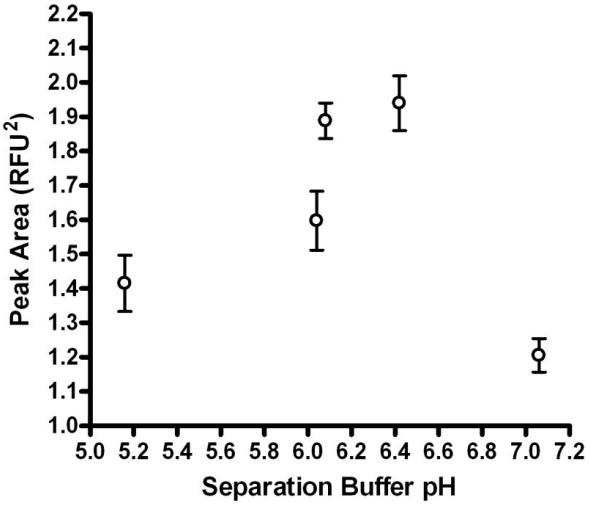

Figure 2.20. Optimization of separation buffer pH**.** cGMP Peak area (open cirlces) with error bars representing standard deviations with N ≥ 3 for each point. Reaction Mixture: PGO (25 mM) in NaH_2PO_4 (50 mM) varied pH + cGMP (10 μM) in aCSF. Derivatization Temperature: 65 ^oC. Heated Reaction Time 2.05 min (40 μL/hr).

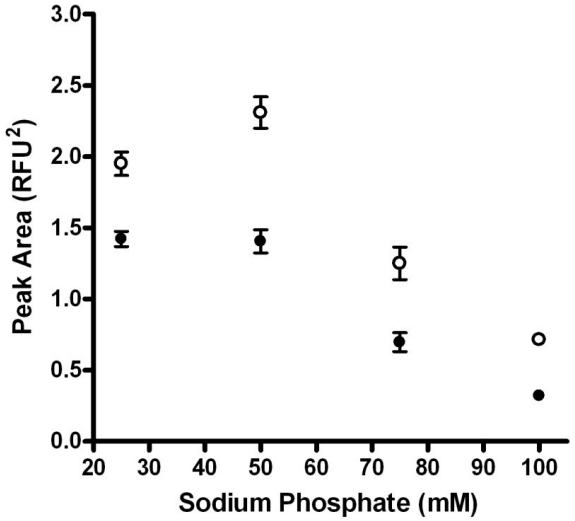

Figure 2.21. Optmization of separation buffer concentration**.** Reaction Mixture: PGO (25 mM) in NaH_2PO_4 (25 mM pH 6.34; closed circles), (50 mM pH 6.23, open circles) + cGMP (10 μM) in aCSF. Derivatization temperature: 65 ^oC. Heated Reaction Time: 2.05 min (40 μL/hr). Error bars represent standard deviation. N ≥ 3 for each point.

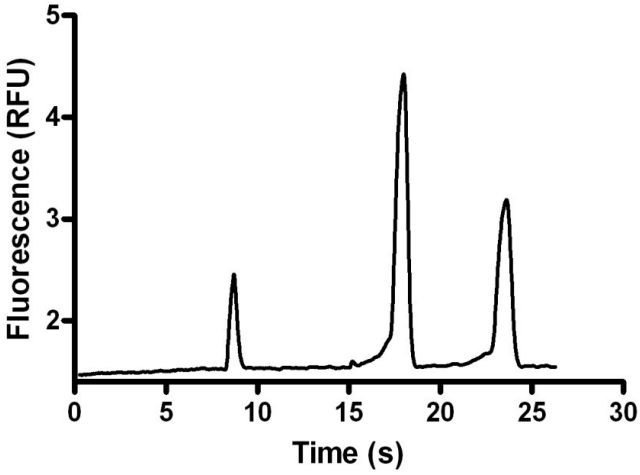

Figure 2.22. CE-LIF Electropherogram. Optmization of separation buffer concentration. Reaction Mixture: PGO (25 mM) in NaH_2PO_4 (50 mM) pH 6.23 + cGMP (10 μM) + GMP (10 μM) in aCSF. Derivatization temperature: 65 ^oC. Heated Reaction Time: 2.05 min (40 μL/hr) Unidentified Peak (8s), cGMP (17s), GMP (23s).

Sodium Phosphate Concentration (mM)	Average Plate Count	N
25	1086 ± 5	9
50	1157 ± 13	10
75	2655 ± 45	8
100	4872 ± 23	3

Table 2.02. Average plate count of derivatized cGMP at varied NaH_2PO_4 buffer concentration.

In Vitro Characterization

As discussed previously, a major advantage of incorporating MD with online CE-LIF analysis is the potential for high temporal resolution and the ability to monitor and measure chemical dynamics in a biological system. Figure 2.23 demonstrates the temporal response of the instrument for the developed cGMP assay. The signal in Figure 2.23 reached a plateau in approximately 2 separations. cGMP migration occurred at 16.84 s. Repeat separations of cGMP were performed every 25.45 s. Dynamics at the surface of the probe fast as 50 s can therefore be measured. Figure 2.24 shows the time profile of the valve used to introduce chemical agents and stimuli into the brain using reverse microdialysis. High temporal resolution is particularly important when performing

pharmacological experiments as it is usually the time course of the drug that determines the shape of the response more than the temporal resolution of the instrument.[97] Many

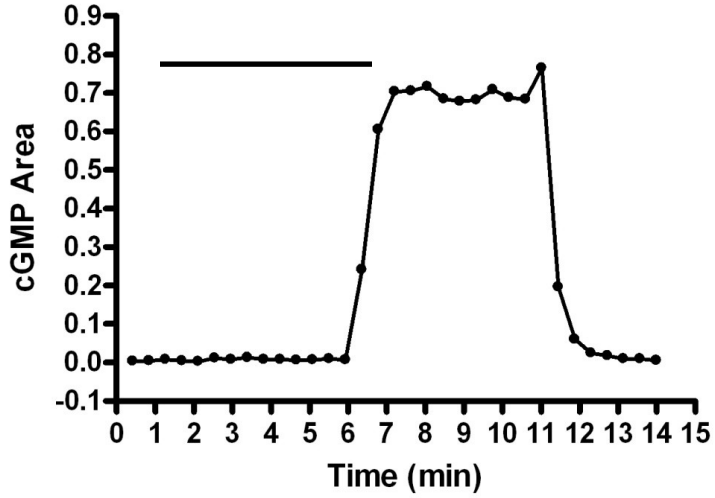

Figure 2.23. Temporal response of the microdialysis probe. The microdialysis probe was moved from aCSF to aCSF spiked with 10 μM cGMP for 4 minutes (denoted by the black bar) and back again. The delay between the insertion of the probe and the observed response is due to the time required for sample in the perfusate to travel from the probe to the CE interface. Timing from the probe to the detector ≈ 5 min. Reaction Mixture: PGO (25 mM) in NaH_2PO_4 (50 mM) pH 6.03 + cGMP (10 μM) in aCSF. Heated reaction time: 2.05 min (40 μL/hr). X Axis offset: -0.1.

experiments focus on application of exogenous compounds via reverse microdialysis, where the microdialysis probe perfusate contains a compound that readily diffuses across the microdialysis membrane into the targeted brain region. Probe perfusate is switched via a 4 port valve (see methods and reagents section) to a spiked perfusate solution to initiate the pharmacological dose application. It is necessary to run control tests to determine whether the switching of the valve introduces any artifacts in the signal, due to pressure differences along the fused silica capillary lines in the instrumental setup. Figure 2.24, Top Graph, demonstrates a control experiment where a probe remained in aCSF and the perfusate was changed from aCSF to aCSF spiked with 10 μM cGMP. Figure 2.24,

Bottom Graph, demonstrates a MD proble placed into a standard solution of 10 μM cGMP and the perfusate through the probe was changed from aCSF to high-K+ aCSF and back, as performed in *in vivo* pharmacological experiments. A small deviation from the baseline was observed, however this was resolved by the time sample from the probe traveled to the detector demonstrating that high-K+ aCSF does not change the recovery of cGMP and switching the four port valve does not generate artifacts in the signal.

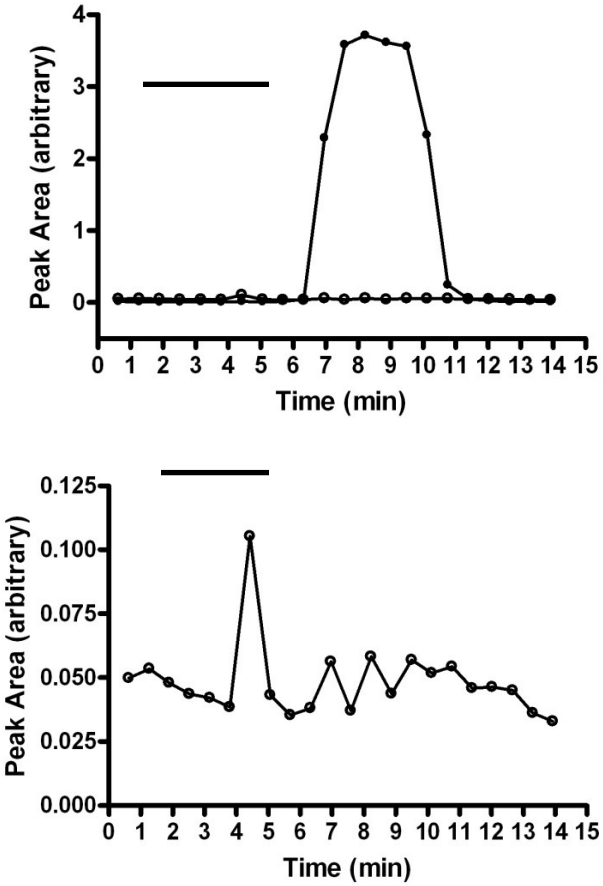

Figure 2.24. Time profile of a 4 minute stimulus introduced by the reverse microdialysis valve. Top Graph: Microdialysis perfusate was switched from aCSF to aCSF spiked with 10 μM cGMP for 4 minutes, (denoted by the black bar) and back to aCSF. The probe was placed in aCSF throughout this experiment. Open Round circle: Unidentified Peak 9.8 s (suspected PGO hydrolysis product). Closed Round Circle: cGMP. Top graph X axis offset: -1.0. Bottom Graph: MD probe was placed in a 10 μM cGMP standard. Perfusate through the probe was switched from aCSF to High K^+-aCSF for four minutes (denoted by the black bar) and back to aCSF. Electropherograms were recorded every 33.4 s.

With reaction and instrumental parameters for the cGMP assay optimized, online determination of the LOD can be performed. Limit of detection is determined by the signal produced at three times the standard deviation of the noise in the baseline. Limits of detection were determined from a daily calibration curve (Figure 2.25). The lowest concentration used in the calibration curve was 100 nM (Table 2.03). Average noise in

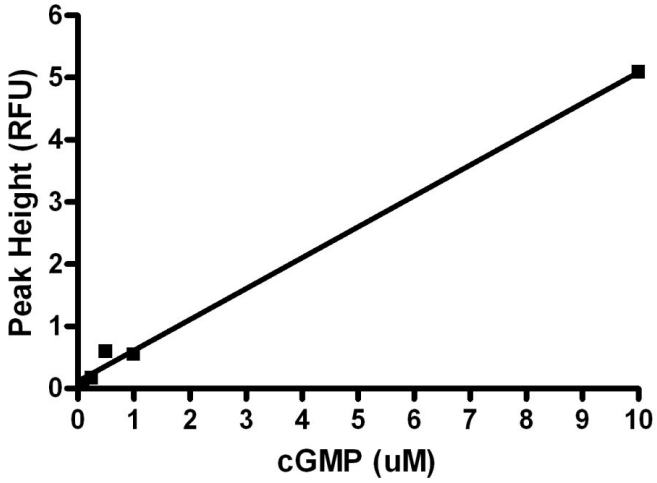

Figure 2.25. cGMP online CE-LIF calibration curve. Slope: 0.49 ± 0.01. Y-intercept**:** 0.15 ± 0.08. X-intercept: -0.23. 95% Confidence Intervals: Slope 0.44 to 0.55. Goodness of Fit: $r^2 = 0.9962$.

cGMP (µM)	Average Peak Height (RFU)	Relative Error	N	Average Plate Count
10	5.09	.02	15	2005 ± 19
1	0.545	.003	14	1539 ± 5
0.5	0.591	.004	9	1411 ± 5
0.25	0.165	.004	9	1597 ± 5
0.10	0.080	.001	9	1276 ± 2

Table 2.03. cGMP Standards for online calibration and determination of LOD.

the baseline = 0.855. Average standard deviation of noise in the baseline = 0.004. LOD was determined to be 22 nM for online direct injection into the reaction T. LOD of cGMP on the CE-LIF system sampled through the microdialysis probe (Figure 2.26) was determined. Concentration of cGMP varied from 100 nM to 10 µM (Table 2.04). Average

standard deviation in the noise of the baseline = 0.004. LOD = 144 nM. % recovery through the probe = 28. This LOD is significantly higher than the expected basal levels of cGMP in the brain, 6-9 nM. Measurement of cGMP at basal levels does not seem likely based on the obtained LOD of cGMP through the microdialysis probe.

cGMP (µM)	Peak Height (RFU)	Relative Error	N	Average Plate Count
10	0.821	.007	10	2215 ± 15
1.0	0.09	.01	31	1739 ± 19
0.50	0.047	.001	21	1876 ± 10
0.25	0.015	.001	20	1888 ± 3
0.10	0.0098	.0006	40	6067 ± 6

Table 2.04. cGMP calibration concentration. Curve obtained through the microdialysis probe.

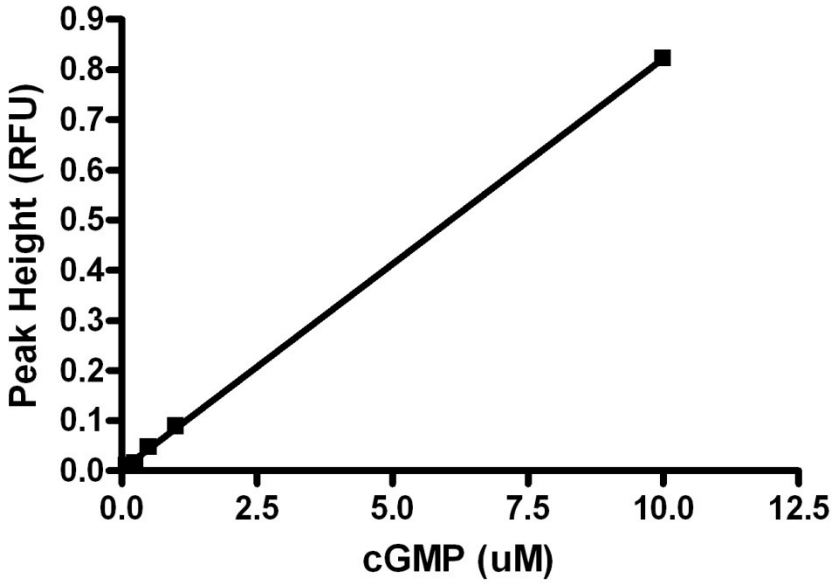

Figure 2.26. cGMP online MD-CE-LIF calibration curve. Slope:0.0819 ± 0.0006 Y-intercept: 0.002 ± 0.003 Goodness of Fit: $r^2 = 0.9998$

A summary of the optimization parameters obtained in the development of the cGMP assay on the CE-LIF instrument can be found in Table 2.05. This is the first high speed online CE-LIF assay for cGMP with high temporal resolution, 45-55 s. Low nanomolar limits of detection for separation via MD-CE-LIF were achieved. The

capability to monitor cGMP in the glutamate/NMDA/NO pathway in the brain at basal levels however is questionsable. Application of the cGMP assay to *in vivo* pharmacological studies has a high potential to elucidate the role and chemical dynamics of cGMP in the glutamate/NMDA/NO pathway, but may need to focus on percent change of baseline in response to pharmacological studies as opposed to changes from basal levels.

Phenylglyoxal (mM)	25
Temperature (^{o}C)	65
Heated Derivatization Time (min)	2.05
Reaction Buffer	Sodium Phosphate
Reaction Buffer (pH)	≈ 6.00
Separation Buffer (pH)	6.00
Separation Buffer (mM)	50
Excitation Wavelength (nm)	365
Emission Wavelength (nm)	522

Table 2.05. Summary of optmization parameters of the cGMP assay.

While the the online LOD, and the *in vitro* LOD, for the developed cGMP assay is higher than basal levels of 6-9 nM as determined by RIA in the rat brain, it may be possible to identify cGMP in other biological samples, such as blood plasma, or tissue. Investigations of plasma levels of cGMP have been performed using radioimmunoassays to study septic shock,[273] heart disease,[274-276] and nitric oxide,[277, 278] to name a few applications.

MD-CE-LIF Characterization of the cGMP Assay in Rat Blood Plasma Samples.

Figure 2.27 demonstrates a representative electropherogram of the application of the cGMP assay in rat blood plasma. cGMP migration time from standards run earlier on the day of experimentation indicated a migration time of 17 s.

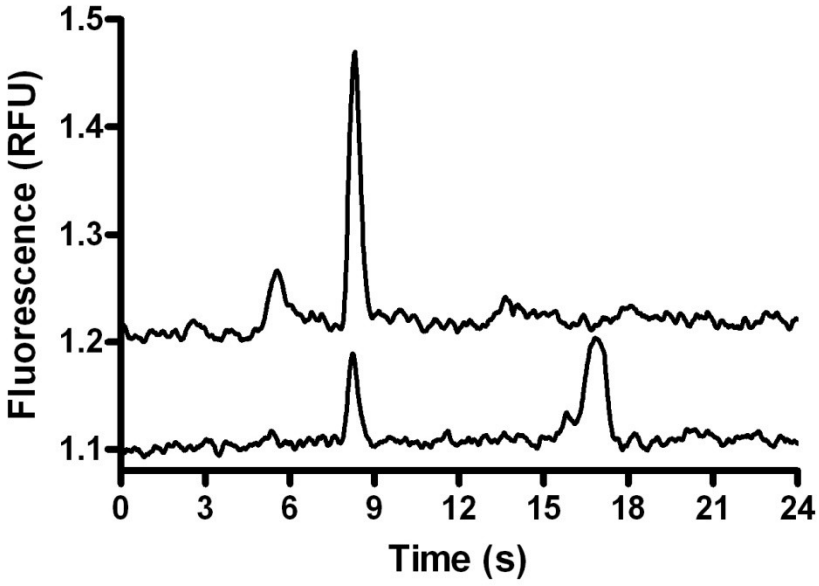

Figure 2.27. Microdialysis sampling of rat blood plasma. Top Trace: Electropherogram from blood plasma. Y offset: 0.11. Bottom Trace: cGMP (1 μM) standard in aCSF. Migration Time: 16.8 s. aCSF was perfused through the microdialysis probe (30 μL/hr) and carried diffused analyte from the blood plasma sample to the reaction T, where upon mixing with PGO in NaH_2PO_4, derivatization commenced. Derivatization Reaction: PGO (25mM) in NaH_2PO_4 (50 mM) pH 6.03 + blood plasma sample in aCSF. Heated reaction time: 2.05 min (40 μL/hr).

Peaks observed in the electropherograms sampled from rat blood plasma are as follows: 5.5 s, 8.4 s, and 12.8 s. The peak present at a migration time of 8.4 s was also present in standard runs of cGMP. Source of this peak was isolated to the PGO in NaH_2PO_4 solution that was directly injected into the reaction T. It is likely a hydrolysis product of PGO, produced upon addition of PGO to the NaH_2PO_4 buffer. Presence of cGMP was not indicated in any of the blood plasma samples. The amount of time for sample to travel from the probe to the detector on the MD-CE-LIF system was measured as approximately 6 min 38 s. The peak at 8.4 s increases 6 min 38s post insertion of the microdialysis probe into the sample as perfusate from the blood plasma sample reaches the detector indicating a possible increase in the compound present in the PGO/NaH_2PO_4 solution, or co-

migration of a compound unique to the blood plasma sample. The temporal response of the cGMP assay to unidentified peaks present in the blood plasma sample is indicated in Figure 2.28. Changes from 10-90% baseline occurred within 1-2 separations, resulting in a temporal resolution on the order of 30-55 seconds.

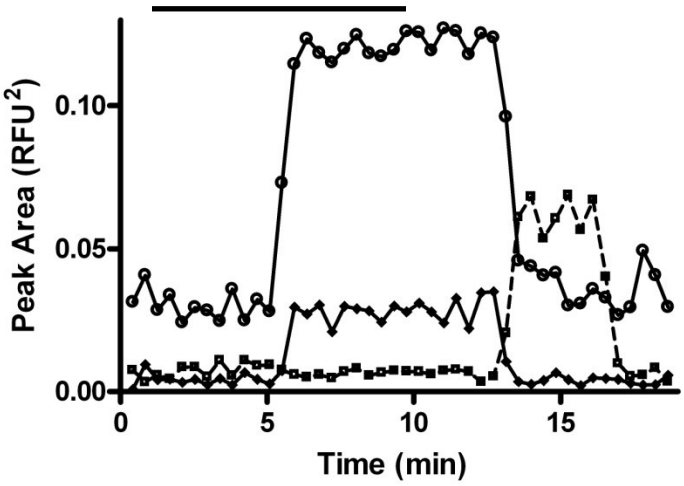

Figure 2.28. Temporal Data for peaks present in blood plasma sample. Solid diamond line: 5.4 s Peak. Open circles line: 8.3 s Peak. Open sqare dashed line: cGMP (1 μM). A microdialysis probe was placed into blood plasma sample for 9 minutes and upon removal, placed into a 1 μM cGMP standard solution for 4 minutes. The probe was removed from the cGMP standard and placed into aCSF for 4 minutes. This cycle was repeated 3 times total. Black bar indicates the time the microdialysis probe was inserted into the blood plasma. The delay between the insertion of the probe and the observed response is due to the time required for sample in the perfusate to travel from the probe to the CE interface. Peak increases at 5.5 s, and 8.4 s were consistent with the time course of sample traveling from the interface of the probe to the detector. Derivatization Reaction: PGO (25mM) in NaH_2PO_4 (50 mM) pH 6.03 + blood plasma sample in aCSF. Heated reaction time: 2.05 min (40 μL/hr).

cGMP was not detected in any rat blood plasma sample. This could be due to the LOD being too high to detect basal blood plasma sample cGMP concentrations, or cGMP is not present in the sample. Altered production of cGMP in biological blood plasma samples is often correlated to a disease state resulting from altered function of glutamate/NMDA/NO pathways. The blood plasma sample history was not known specifically enough to determine whether increased levels of cGMP was likely to be

present in the samples. The cGMP assay did however indicate the presence of 3 other compounds capable of being detected and resolved by the developed cGMP assay.

In vivo Pharmacological Studies of cGMP via MD-CE-LIF

It is expected that in addition to cGMP other compounds may be detected and resolved using the developed cGMP assay.Various guanine and guanosine containing compounds were tested on the MD-CE-LIF system with the PGO assay for cGMP (Table 2.06) Insertion of the microdialysis probe into the rat brain will damage tissue resulting in

Compound	Molar Mass (g/mol)	Migration Time (s)
cGMP	367.20	25.3
Guanosine monophosphate (GMP)	407.18	31.0
Guanosine	283.25	10.1
Guanine	151.13	10.0
9-Ethylguanine	179.20	9.8
Guanosine diphosphate (GDP)	443.20	Not detected
Guanosine triphosphate (GTP)	523.00	Not detected
Adenine	135.13	Not detected
Adenosine	267.25	Not detected
Adenosinemonophosphate (AMP)	391.18	Not detected
cAMP	399.22	Not detected
Adenosinediphosphate (ADP)	471.17	Not detected
Adenosinetriphsophate (ATP)	551.10	Not detected
Taurine	125.14	Not detected
D-Serine	87.08	Not detected
L-Serine	87.08	Not detected
Aspartate	114.11	Not detected
Asparagine	115.09	Not detected
Glycine	57.05	Not detected
Glutamate	129.12	Not detected
Threonine	101.10	Not detected
GABA	103.12	Not detected

Table 2.06. Compounds tested for derivatization by the developed cGMP assay.

the release of neurochemicals into the extracellular environment. To minimize disturbance, the probe is inserted slowly and over a 15 minute period of time at approximately 500 μm/min. A representative electropherogram of the compounds

detected upon insertion of the MD probe can be found in Figure 2.29. After the initial spike in peak area at the beginning of probe insertion into the brain, peak areas decreased (Figure 2.30). cGMP standards run the day of analysis migrated at approximately 19-20 s, in the striatum. Upon equilibration of the probe the peak at 9.5 s (characteristic of the

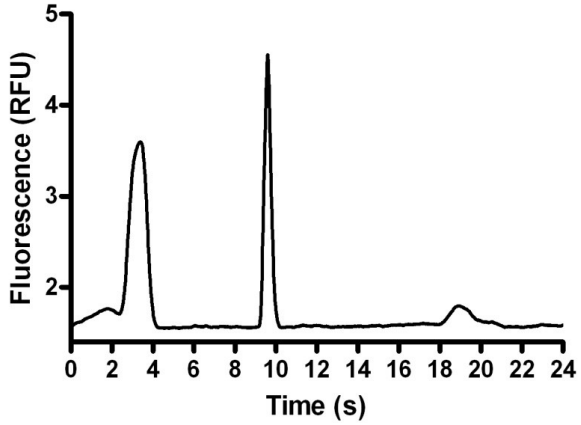

Figure 2.29. Electropherogram of probe insertion into the rat striatum. cGMP is present at a migration time of approximately 19 s. The peak at approximately 3 seconds is overlapped from the previous injection, and coincides with the migration time of GMP. Peaks at 9.5 s correspond to the unidentified peak from the PGO in Na_2PO_4 solution and likely comigrating guanine or guanosine.

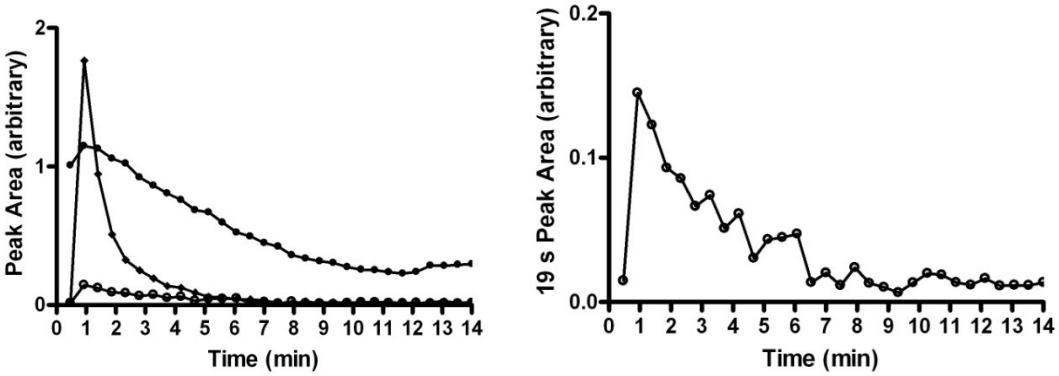

Figure 2.30. Probe insertion into the rat striatum.. Implantation of the probe occurred slowly and over a 15 minute period of time. Increase in peak size at 3 s (diamonds), 9.5 s (closed circles), and 19 s (open circles) was visible upon implantation. Post probe implantation, as equilibration progressed, peak size at 3 s, 9.5 s and 19 s decreased in size until it was no longer detectable while a peak at 13.7 s (not shown on graph) increased to a detectable basal level. Peak at 19 s corresponds to cGMP standards run the day of analysis.

peak present in PGO/NaH_2PO_4, and guanine and guanosine migration times) returned to a basal level. This basal level is higher than the characteristic area of the peak present in the PGO/NaH_2PO_4 solution directly attached to the reaction T, indicating possible co migrating peaks of guanine or guanosine in the brain dialysate sample. Peak size at 9.5 s during cGMP and GMP standard runs also indicated the presence of guanine or guanosine in addition to the unidentified peak inherent in the PGO/NaH_2PO_4 solution. Based on standard separations between cGMP and GMP, the peak present at 3s indicates it is likely GMP. The 3 s peak returned to a non detectable level as the probe equilibrated.

As equilibration of the probe progressed, increases in peak size at 6.8 s and 13.7 s were seen (Figure 2.31). These compounds remain unidentified. Removal of the probe from the striatum occurred at the end of the course of pharamcological experiments (Figure 2.32). Throughout the course of a day, migration time of the peaks shifts. This

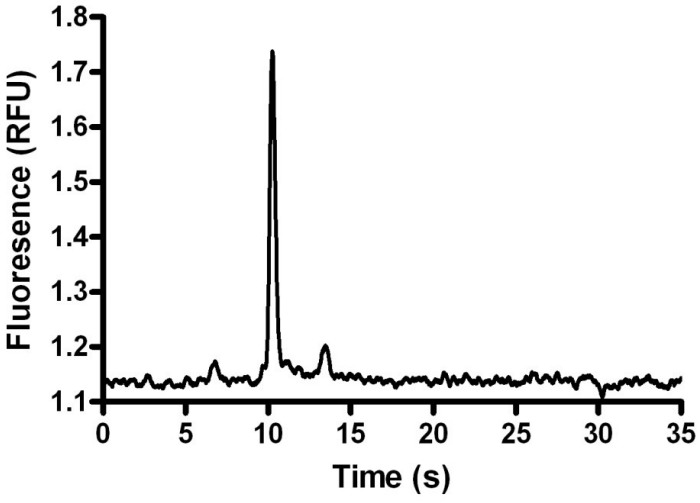

Figure 2.31. Equilibration of MD probe in the rat striatum. Post insertion into the striatum, the microdialysis probe was allowed to equilibrate for 1 hour prior to pharmacological studies. Basal unidentified peaks were present at 6.8 s, 10.8 s (possibly guanine or guanosine), and 13.7 s.

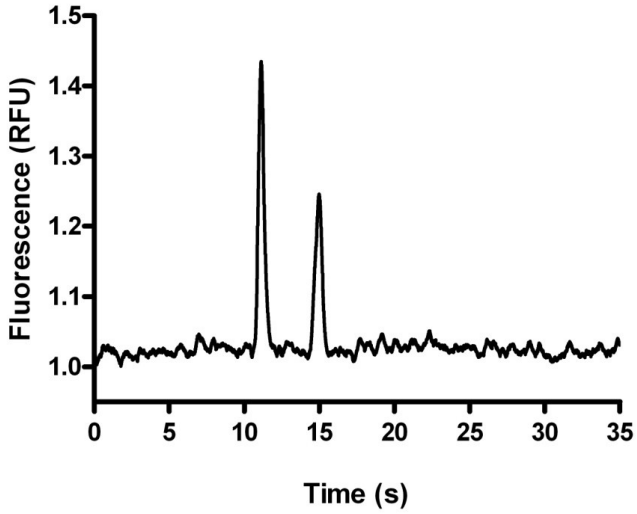

Figure 2.32. Probe removal from the rat striatum. The microdialysis probe was removed slowly and over a 15 minute period of time from the striatum. Characteristic peak present at 10.8 s during equilibrium and basal levels shifted to 11.8 s during the course of the experiment and increased slightly from basal concentration levels. The unidentified peak at 13.7 s during equilibrium shifted to 14.8 s and increased from basal concentration levels as the probe was removed from the brain.

was verified upon insertion of the microdialysis probe into a cGMP (500 nM) standard after it was removed from the striatum. cGMP migrated at 33 s, a 7 s shift from the cGMP standard run (migration = 25 s) prior to probe insertion into the striatum.

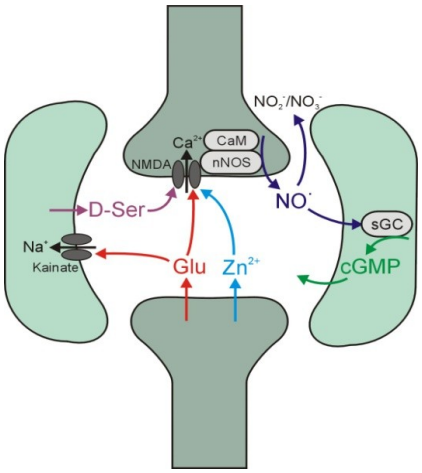

Figure 2.33. Proposed neuromessenger pathway

Perfusion of high-K^+ aCSF through the dialysis probe is expected to depolarize neurons and result in the exocytotic release of high concentrations of neurotransmitters.[97] Current MD-CE-LIF studies have shown a large increase in extracellular glutamate upon application of high-K^+ aCSF in the rat striatum.[78, 97] Release of glutamate will initiate the glutamate/NMDA/NO pathway (Figure 2.33),

resulting in increasing levels of cGMP production and higher concentrations of cGMP in the extracellular environment. Glutamate perfusion into the extracellular environment will directly act on the NMDA receptor, initiating the glutamate/NMDA/NO pathway. This event will lead to the production of cGMP, where it may be detected and resolved in the extracellular environment via MD-CE-LIF.

Potassium Stiumlations in the Rat Striatum

Potassium stimulations were carried out for 3 minutes (Figure 2.34) and 15 minutes (Figure 2.35) in the rat striatum. Data was collected for 30 minutes after the end of the application of high-K^+ aCSF. Basal levels of the unidentified peak present at 9.8 s are higher than the peak areas of suspected PGO hydrolysis product indicating presence of a comigrating peak(s) at 9.8 s in the brain peak did undergo a small increase upon the 3 min high-K^+ aCSF application and a notably larger increase upon the 15 min high-K^+

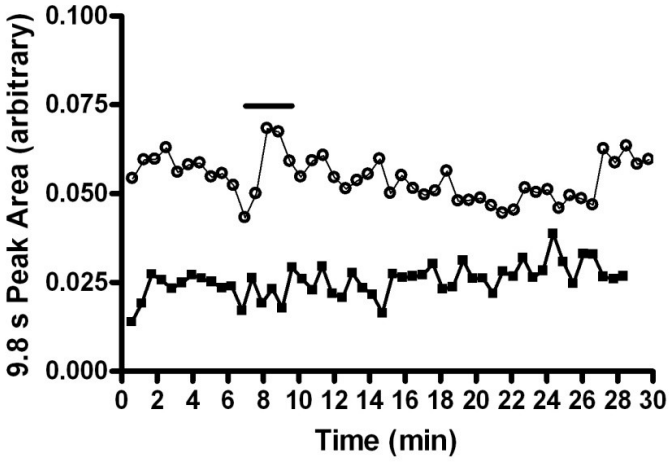

Figure 2.34. Effect of 3 minute potassium stimulation on 9.8 s peak area in the rat striatum. Application of high-K^+ aCSF was performed for 3 min (open circle). Suspected PGO hydrolysis product (solid square) present in PGO / Na_2PO_4 solution in aCSF. MD-CE-LIF was used to analyze dialysate every 33.4 s. Microdialysis probe perfusate aCSF was switched to high-K^+ aCSF for 3 min (denoted by the black bar).

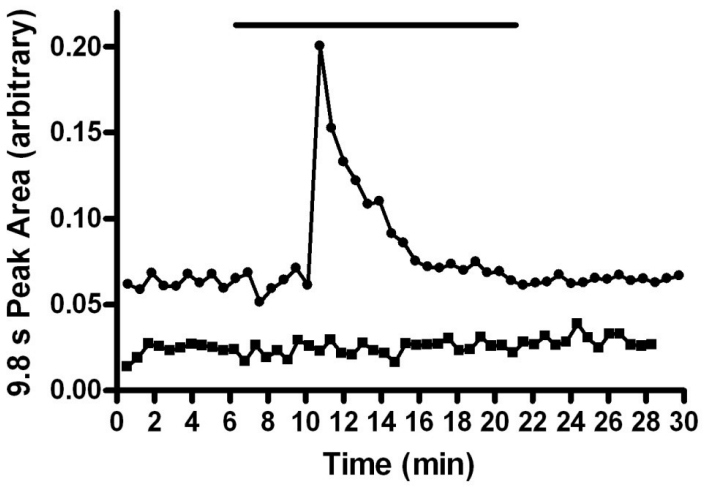

Figure 2.35. Effect of 15 minute potassium stimulation on 9.8 s peak area in the rat striatum. Application of high-K^+ aCSF was performed for 15 min (solid circle). Suspected PGO hydrolysis product (solid square) present in PGO/ NaH_2PO_4 solution in aCSF. MD-CE-LIF was used to analyze dialysate every 33.4 s. Microdialysis probe perfusate aCSF was switched to high-K^+ aCSF for 15 min (denoted by the black bar).

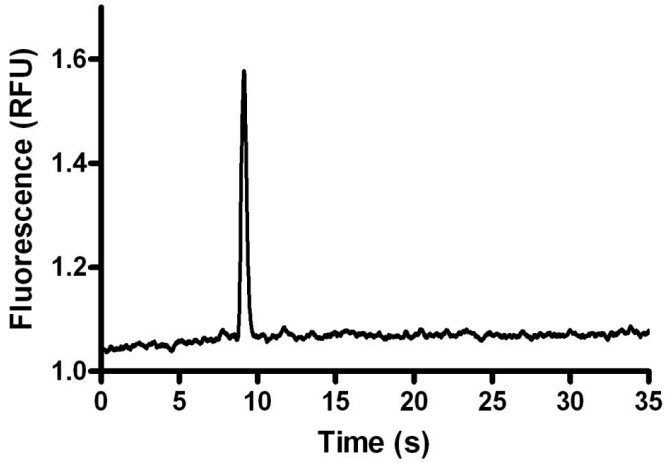

Figure 2.36. Electropherogram of 15 minute potassium stimulation in the rat striatum. Application of high-K^+ aCSF was performed for 15 min**.** Suspected PGO hydrolysis product present in PGO/ NaH_2PO_4 solution in aCSF co migrates with guanosine/guanine at 9.8 s. MD-CE-LIF was used to analyze dialysate every 33.4 s. No cGMP is present, expected migration time = 33 s.

aCSF application. No indication of cGMP was visible in any electropherogram (Figure 2.36).

Glutamate Application in the Rat Striatum

As no indication of cGMP was seen upon application of high-K^+ aCSF, glutamate application was performed (Figure 2.37). Initiation of the proposed neuromessenger pathway begins when the N-methyl-D-aspartate (NMDA) receptor is activated by the binding of glutamate and the activation of the glycine site. Increased glutamate should initiate the proposed neuromessenger pathway, resulting in an increase in cGMP concentrations.[78] No indication of cGMP was seen in any electropherogram. No change in the basal levels of the unidentified peak at 9.8 s upon application of glutamate was seen.

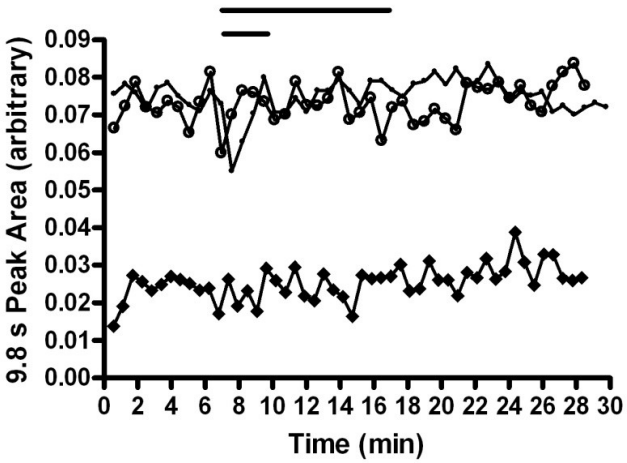

Figure 2.37. Effect of glutamate stimulation on unidentified peak present at a migration time of 9.8 s in the rat striatum. 3 minute application (open circles) and 10 minute application (closed circles). Suspected PGO hydrolysis product (solid square) present in PGO/ NaH_2PO_4 solution in aCSF. MD-CE-LIF was used to analyze dialysate every 33.4 s. Microdialysis probe perfusate aCSF was switched to glutamate (1mM) in aCSF for 3 min (denoted by the short black bar) and 10 min (denoted by the long black bar).

The inability to detect cGMP upon stimulation of the NMDA/NO pathway could be the result of 1) The sensitivity of the MD-CE-LIF cGMP assay is not sufficient to detect the stimulated levels of cGMP in the rat striatum, 2) Applied concentrations of pharmacological agents, high-K^+ aCSF, and glutamate did not diffuse across the

microdialysis membrane at levels sufficient to initiate production of elevated levels of cGMP/ and or did not stimulate production of cGMP or 3) applied anesthesia isoflurane suppressed the response of neurochemicals, including cGMP, in the extracellular regions of the striatum, which has been indicated in a previous study by Galley et al..[279]

Application of Phosphodiesterase Inhibitor IBMX and High Potassium aCSF

As neither basal nor stimulated levels of cGMP were detected in potassium or glutamate applications, the experiment was repeated with the phosphodiesterase inhibitor IBMX. Regulation of cellular concentrations of cGMP is maintained by phosphodiesterases and multidrug resistance proteins. cGMP undergoes degradation by a phosphodiesterase (PDE) or is exported from the cell into the extracellular environment by multidrug resistance proteins (MRP). PDE inhibitors prevent the degradation of cGMP in the cell. Not only will these compounds inhibit the metabolic degradation of cGMP, they may also serve as inhibitors of cyclic nucleotide transporters like MRP5. As a result, greater amounts of cGMP should be seen in the extracellular region. Local perfusion of 3-isobutyl-1-methylxanthine (IBMX) (1mM), a PDE inhibitor, has been found to increase extracellular levels of cGMP by 150% in some experiments.[15, 50] A potential concern of the use of IBMX exists, however. Not only will phosphodiesterase inhibitors inhibit the metabolic degradation of cGMP, they may also serve as inhibitors of cyclic nucleotide transporters like MRP5. If this is true, elevated intracellular levels of cGMP produced from the direct induction or stimulation of the glutamate/NMDA/NO pathway may not significantly increase the extracellular concentration of cGMP. While this is a possibility, scientific evidence has found a direct increase in extracellular concentrations of cGMP

upon application of IBMX.[15, 50] It is hypothesized that with the application of a high potassium stimulation and the PDE inhibitor IBMX, greater amounts of cGMP should be seen in the extracellular region. High potassium aCSF and IBMX were perfused for 3 min (Figure 2.38), 10 min (Figure 2.39), and 15 min (Figure 2.40). Only the peak at 9.9 s

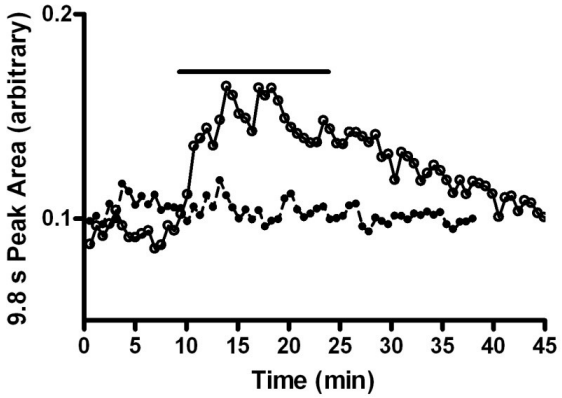

Figure 2.38. Effect of IBMX (500 nM) in high-K^+ aCSF on the unidentified peak at 9.9 s in the rat striatum. Application of IBMX in high-K^+ aCSF was performed for 3 min (open circle). Microdialysis probe perfusate IBMX in aCSF was switched to high-K^+ aCSF for 3 min (denoted by the black bar).Control experiment (solid circles): Microdialysis probe perfusate aCSF was switched to IBMX in aCSF 1 minute after start of data collection, and collected data for 30 min. MD-CE-LIF was used to analyze dialysate every 37.9 s.

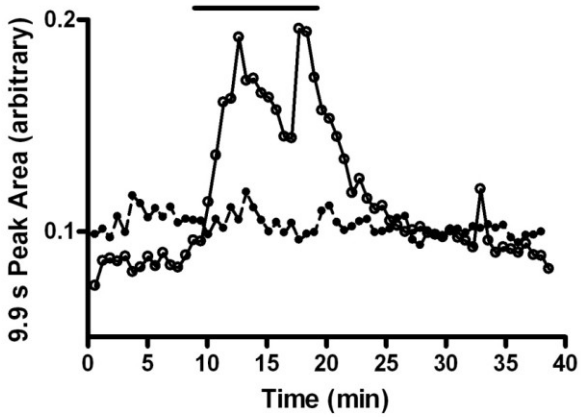

Figure 2.39. Effect of IBMX (500 nM) in high-K^+ aCSF on the unidentified peak at 9.9 s in the rat striatum. Application of IBMX in high-K^+ aCSF was performed for 10 min (open circle). Microdialysis probe perfusate IBMX in aCSF was switched to high-K^+ aCSF for 10 min (denoted by the black bar). Control experiment (solid circles): Microdialysis probe perfusate aCSF was switched to IBMX in aCSF 1minute after start of data collection, and collected data for 30 min. MD-CE-LIF was used to analyze dialysate every 37.9 s.

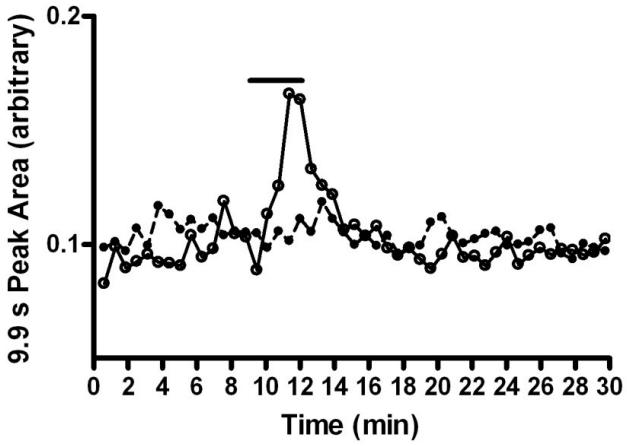

Figure 2.40. Effect of IBMX (500 nM) in high-K^+ aCSF on the unidentified peak at 9.9 s in the rat striatum. Application of IBMX in high-K^+ aCSF was performed for 15 min (open circle). Microdialysis probe perfusate IBMX in aCSF was switched to high-K^+ aCSF for 15 min (denoted by the black bar). Control experiment (solid circles): Microdialysis probe perfusate aCSF was switched to IBMX in aCSF 1 minute after start of data collection, and collected data for 30 min. MD-CE-LIF was used to analyze dialysate every 37.9 s.

was seen to increase in response to the high-K^+ aCSF/IBMX application. No indication of the presence of cGMP in the rat striatum was seen in any electropherogram.

To address the possibility that the concentration of IBMX (500 nM) did not diffuse across the microdialysis membrane at a level sufficient to inhibit the degradation of cGMP a second experiment was performed with a higher concentration of IBMX (5 μM). Application of the high-K^+ aCSF/IBMX (5 μM) was performed for 6 minutes (data not included here) and 10 minutes (Figure 2.41). Surprisingly, no change in the peak at 9.8 seconds was seen, indicating the possible inhibition of this compound by the higher concentration of IBMX present. Another possibility to consider, though one less likely, is that the response of the rat to the pharmacological agents was different in each rat. A slight increase in peak size was seen for the unidentified peak at 7.5 s and 15.7 s. The possible increase in peak size at 33.9 s, which corresponds to the presence of cGMP, is

difficult to verify as the peak size is difficult to discern from the noise in the baseline though data analysis programs indicate the possible presence of cGMP at the LOD.

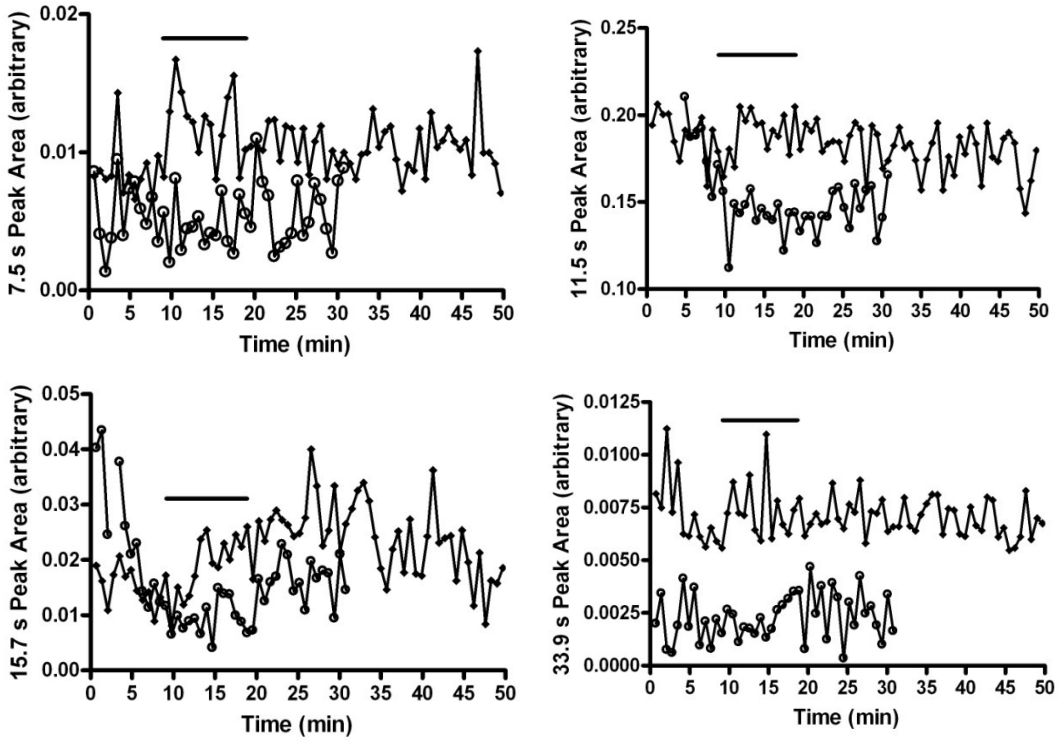

Figure 2.41. Effect of IBMX (5 μM) in high-K^+ aCSF in the rat striatum. Application of IBMX in high-K^+ aCSF was performed for 10 min (closed circles). Microdialysis probe perfusate IBMX in aCSF was switched to high-K^+ aCSF for 10 min (denoted by the black bar). Control experiment (open circles): Microdialysis probe perfusate aCSF was switched to IBMX in aCSF 1 minute after start of data collection, and collected data for 30 min. MD-CE-LIF was used to analyze dialysate every 38.4 s. Data offset for clarity of IBMX in high-K^+ aCSF graphs.

The inability to definitively detect cGMP upon stimulation of the NMDA/NO pathway could be the result of similar possibilities as listed in conclusion to high-K+ aCSF stimulation without IBMX: 1) experimental complications e.g. an unknown crack in the microdialysis probe, preventing adequate detectable levels of cGMP from reaching the reaction T, 2) The sensitivity of the cGMP assay is not sufficient to detect the stimulated levels of cGMP in the rat striatum, 3) Applied concentrations of

pharmacological agents IBMX in aCSF, and high-K+ aCSF did not diffuse across the microdialysis membrane at levels sufficient to inhibit degradation of cGMP by PDE, initiate production of elevated levels of cGMP, and/or did not stimulate production of cGMP, 4) applied anesthesia isoflurane suppressed the response of neurochemicals, including cGMP, in the extracellular regions of the striatum.

Application of NO Donating Compound DEANO

Further pharmacological experiments were explored with the nitric oxide donating compound DEANO. The NO/cGMP signaling cascade involves NO endogenously produced by NO synthases or released from exogenously applied NO donors. This activates NO-sensitive sGC and leads to increased synthesis of cGMP. cGMP modulates the activity of cGMP-dependent kinases, cGMP-gated ion channels, and cGMP-regulated phosphodiesterases.[39] Application of NO compounds is expected to increase extracellular levels of cGMP. NO is not stored in vesicles, rather it is produced when needed upon induction of the glutamate NMDA pathway in response to an increase in intracellular calcium.[40]

Previous experiments have been designed to study the effect of NO supply on cGMP and involve perfusion of the NO generator S-nitroso-N-penicillamine (SNAP) (1 mM) or sodium nitroprusside (SNP) (1 mM).[15, 50] Studies have found a 200% increase in cGMP, with a return to basal levels soon after SNAP was removed from infusing medium. Another commonly used nitric oxide donor is DEANO. Current studies show a direct correlation between application of DEANO and subsequent increases on intracellular cGMP levels.[280] DEANO is a NO donor with a half life of 2-4 minutes. It

most closely models endogenous NO production and is therefore an ideal candidate for NO donation into the rat striatum. Application of NO more closely stimulates the direct synthesis of cGMP in the glutamate/NMDA/NO pathway. Production of endogenously applied NO activates NO-sensitive sGC and leads to increased synthesis of cGMP. Extracellular concentrations of cGMP are expected to increase.

Two separate applications of DEANO at 5 minutes and 10 minutes (Figure 2.42) utlizing reverse microdialysis were carried out during this experiment. Unidentified peaks were visible prior to the application of DEANO at 7.5 s, 11 s, and 14.5 s. cGMP standard

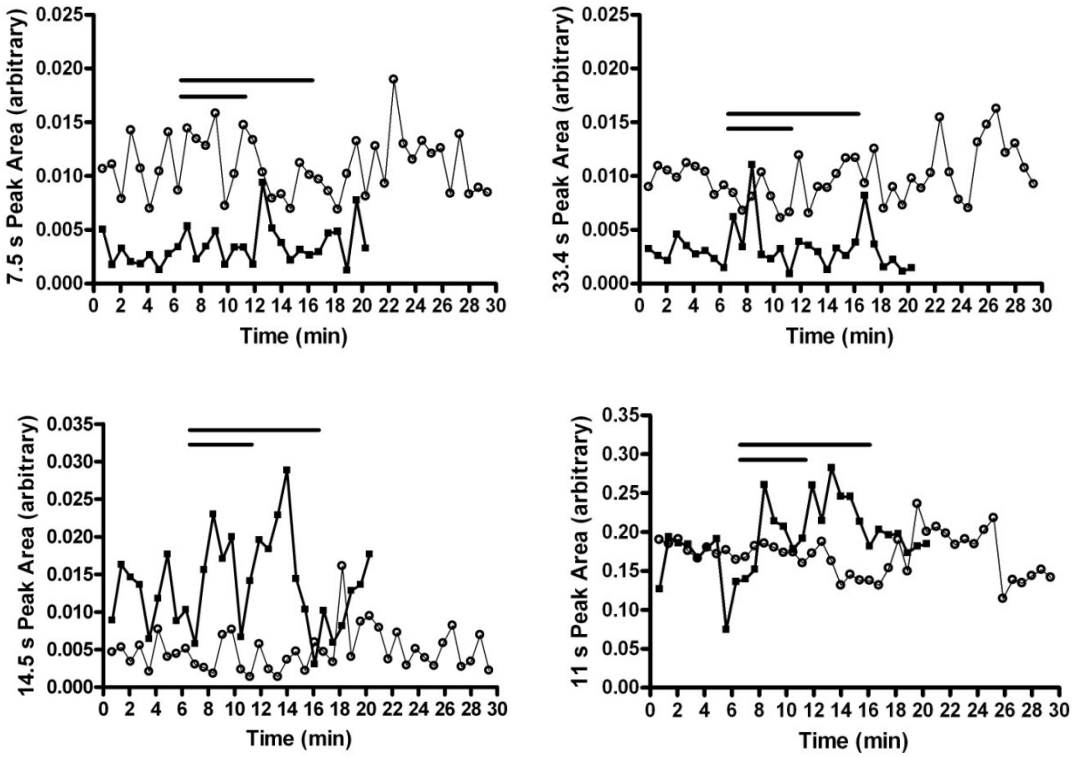

Figure 2.42. Effect of 10 min DEANO (circles) and 5 min DEANO (squares) application on the rat striatum Microdialysis probe perfusate IBMX (5 μM) in aCSF was switched to IBMX (5 μM) in aCSF and DEANO (5 μM) in NaOH (1 mM) for 3 min (denoted by the short black bar) and 10 min (denoted by the long black bar). MD-CE-LIF was used to analyze dialysate every 38.4 s. Data offset for clarity of IBMX in high-K^+ aCSF graphs.

prepared the day of analysis migrated at 25.7s at the beginning of the day and 33.4 s at the end. DEANO perfused for 5 minutes resulted in detectable peak increasses occuring at the migration times of 11 s and 14.5 s. Peak size at 7.5 s remained consistent, and no visible change in the baseline, other than noise, was determined at the cGMP standard migration time of 33.4s No change in peak size was visible for DEANO perfusion of 10 minutes. No indication of cGMP was detected in any electropherogram.

MD-CE-LIF Monitoring of Global Brain Ischemia (Anoxic Depolarization)

Sacrifice of the animal by sodium pentobarbital injection occurs at the end of the pharmacological experimental studies. With the onset of cardiac arrest, decreased levels of oxygen are delivered to the rat brain with subsequent end of cerebral blood flow. The result is complete global brain ischemia (stroke). Within the first 2 minutes of global brain ischemia, massive K^+ efflux and Na^+ influx result in increased extracellular K^+(> 60 mM) and decreased Na^+ (50 mM) concentrations. This phenomenon is known as anoxic depolarization (AD).[281] Anoxic depolarization is closely linked to the pathology of brain ischemia. With widespread tissue depolarization, voltage dependent neural ion channels open, resulting in large scale neurotransmitter release into the extracellular region of the brain.[282] Extracellular glutamate concentrations are significantly elevated during ischemia[283] resulting in excitotoxic damage to surrounding neuronal and glial tissue. Current studies are trying to elucidate the physiological role glutamate plays specifically in ischemia and AD with the intent to mediate damage caused by stroke and elevated glutamate.[284-287] Extracellular concentrations of cGMP are expected to increase

with the resultant release of high concentrations of glutamate and other neurotransmitters upon AD.

MD-CE-LIF was used to monitor changes in the striatum induced by global ischemia. The ischemic event triggered a significant increase in GMP at 7-8 s, and guanine/guanosine at 11.5 s as well as increases in the unidentified peak at 15.7 s, and the cGMP migration time of 34.7 s (Figure 2.43, Figure 2.44 A, and 2.44 B). These responses occurred temporally fast with maximum peak heights reached within 1-2 separations. The cGMP standard peak shifted significantly over the 9 hours of the experiment from 28 s to a migration time of 34-35 s. GMP initially present upon probe implantation at 34.2 s shifted to 43.4 s and overlapped at 7-8 s with a 35 s separation window. Based on these results, it can be concluded that global ischemia does result in increased extracellular levels of GMP, guanine/guanosine, and other unidentified peaks, however the increase for cGMP was not statistically significant over the baseline.

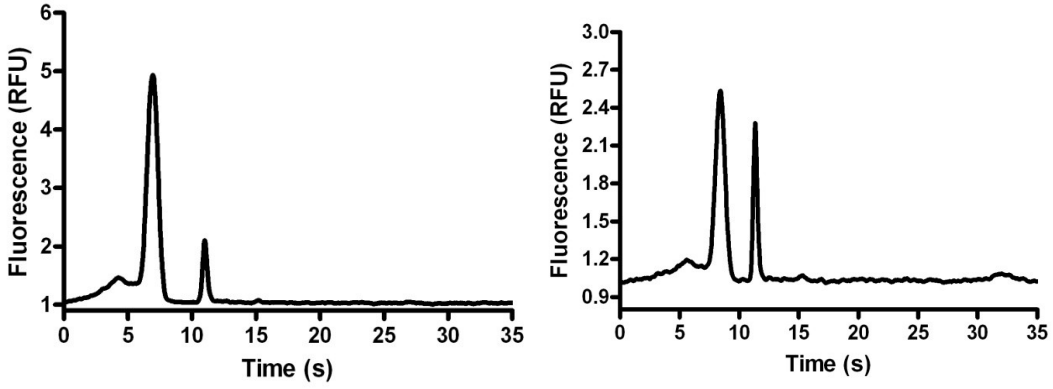

Figure 2.43. Representative electropherograms of global ischemic event in the rat striatum. Unidentified peaks present at migration times of: 7-8 s (likely GMP, overlapped injection), 11.5 s (likely guanine or guanosine), 15.7 s, and likely cGMP (33-34 s). Microdialysis probe perfusate consisted of IBMX (5 μM) in aCSF.). MD-CE-LIF was used to analyze dialysate every 38.4 s.

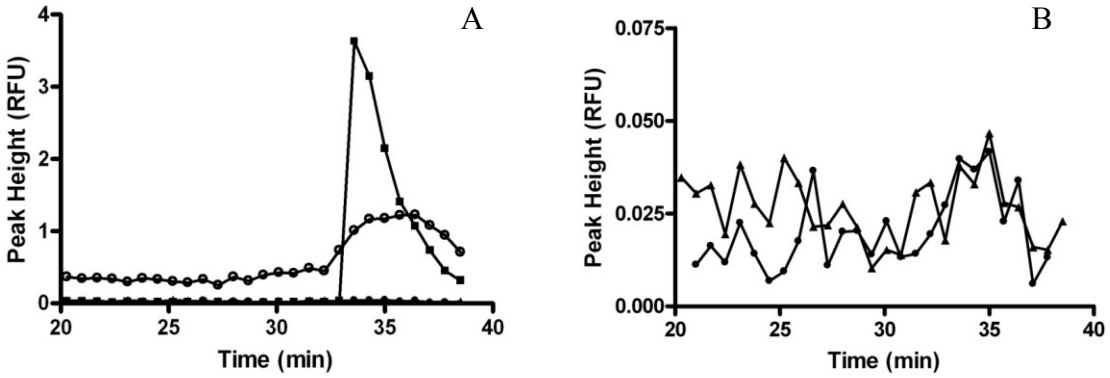

Figure 2.44 A and B. Effect of global ischemic event in the rat striatum. Representative peak height over time for unidentified peaks at A: 7-8 s (squares), and 11.5 s (open circles) and B: Unidentified peak at 15.7 s (triangles) and likely cGMP (34.7 s) (closed circles). Microdialysis probe perfusate consisted of IBMX (5 μM) in aCSF. MD-CE-LIF was used to analyze dialysate every 38.4 s.

cGMP was not detected during any pharmacological stimulations in the rat striatum. While the LOD of the assay is higher than the reported basal levels of cGMP in the brain, it is important to keep in mind that many of the reported studies utilized brain homogenates via RIA analysis to determine cGMP concentrations. This includes intracellular levels of cGMP, whereas MD analysis samples cGMP levels in the extracellular region where it is likely to be present at much lower concentrations than in intracellular regions. This consideration leads to the conclusion that the LOD for the developed cGMP assay requires further improvement to detect extracellular cGMP brain pharmacokinetics in the rat striatum.

Reoptimization of the High Speed Online MD-CE-LIF cGMP Assay

To address the LOD of the cGMP assay, 110-140 nM, physical components of the MD-CE-LIF instrument were modified to determine whether an improvement in the LOD of cGMP could be attained. It was found that lowering the sheath flow reservoir height

and modifying the sheath flow cuvette holder to produce slower sheath flow through the cuvette improved the LOD of derivatized cGMP by approximately a factor of 5-6. Figure 2.45 shows a representative calibration curve of peak heights determined for cGMP concentrations ranging from 100 nM to 1 μM. LOD for this curve was determined to be 7 ± 2 nM. A resulting average LOD of 17 ± 3 nM for the cGMP assay was achieved.

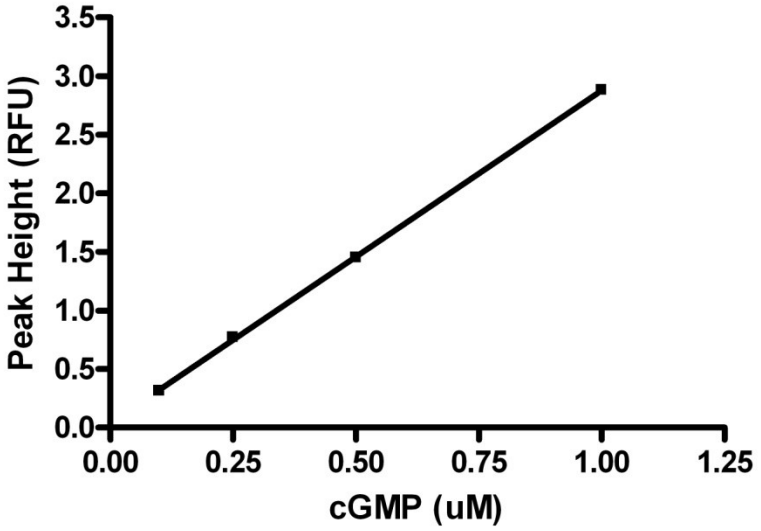

Figure 2.45. Determination of online LOD of cGMP assay. Slope: 2.84 ± 0.03. Y-intercept**:** 0.04 ± 0.02. Goodness of Fit: $r^2 = 0.999$.

IBMX Application and Pharmacological Studies of cGMP in the Rat Cerebellum

In vivo characterization of the improved cGMP assay was performed in the left cerebellum of the rat, where cGMP is known to be present at low nM levels, as determined by RIA (see Chapter 1 Background). The MD probe was placed -1.23 mm AP (anterior/posterior), 0.1 mm ML (medial/lateral) -0.4 mm DV (dorsal/ventral). Figure 2.46 shows a representative electropherogram taken during the MD probe insertion into the cerebellum. 1 mM IBMX in aCSF (discussed previously in this chapter and Chapter 1

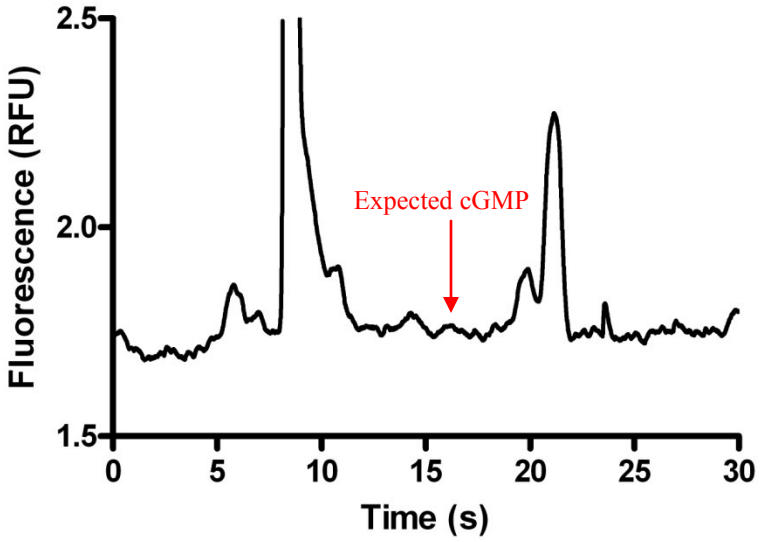

Figure 2.46. Dialysate in the left cerebellum sampled via MD-CE-LIF with PGO derivatization. The MD probe was placed -1.23 mm AP (anterior/posterior), 0.1 mm ML (medial/lateral) -0.4 mm DV (dorsal/ventral). Expected cGMP based on migration time during standard calibration is indicated on the graph at about 16 seconds.

Introduction), was continuously applied via reverse microdialysis to the left cerebellum. Application of IBMX should result in an increase in extracellular cGMP levels. Figure 2.47 demonstrates representative electropherograms taken prior to IBMX application (black bar – 1), and 17, 27 and 54 minutes post exogenous application of IBMX in aCSF. Over time, a number of peaks increased from baseline, including a peak at around 16 seconds, indicative of possible cGMP, and corresponding to the migration time of cGMP standards run the day of the *in vivo* experiment. To confirm presence or absence of cGMP, the probe was removed at the end of the *in vivo* experiment from the cerebellum and placed into a standard solution of 1 µM cGMP (Figure 2.48). A corresponding increase in fluorescence was indicated at a migration time of about 23 seconds, the migration time of the cGMP standard in aCSF post *in vivo* monitoring.

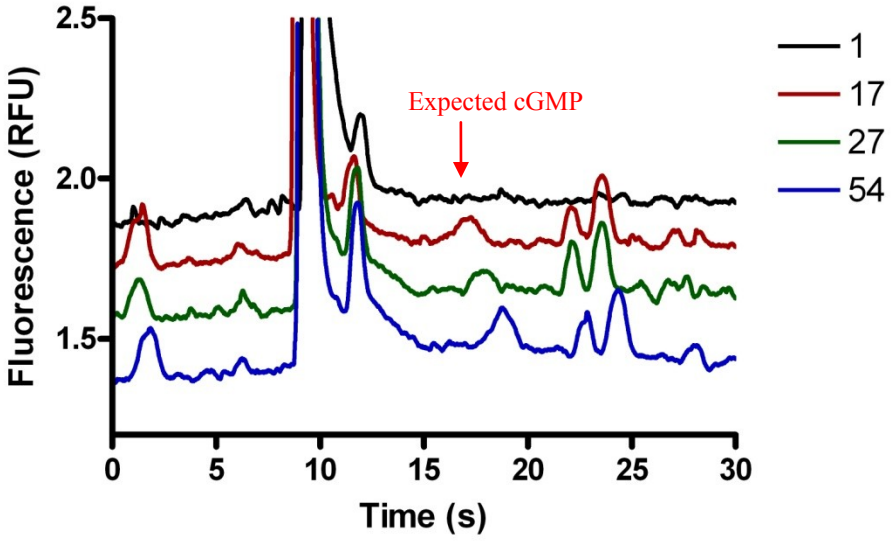

Figure 2.47. Application of IBMX (1mM) in high K^+ via reverse microdialysis in the left rat cerebellum. Separations were complete in 30 seconds. From top to bottom traces are: -1, prior to IBMX application, -17, 17 minutes of IBMX application, -27, 27 minutes of IBMX application, -54, 54 minutes of IBMX application. Electropherograms are offset for clarity.

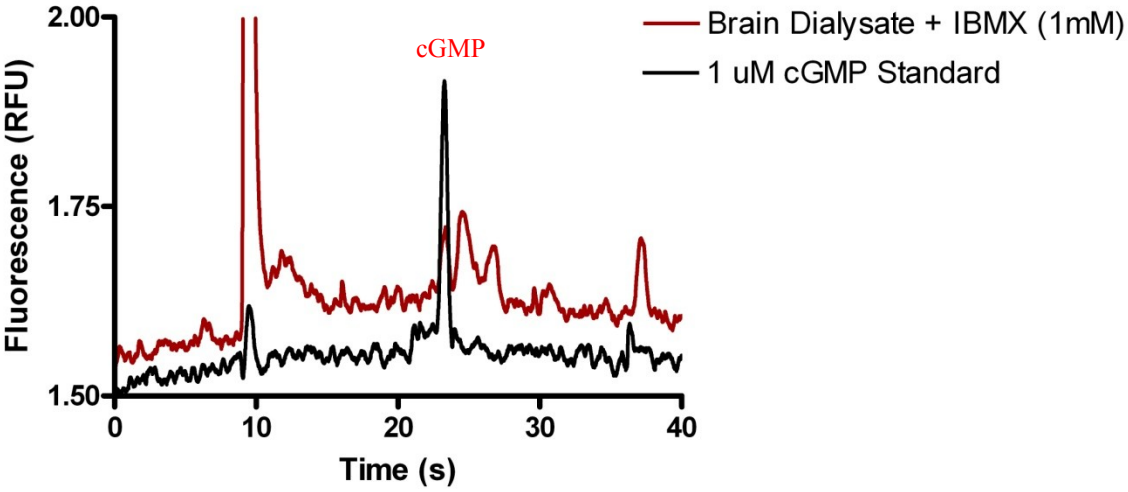

Figure 2.48. MD probe removal from the left striatum and insertion into cGMP (1 µM) standard.

Development and optimization of an online high speed MD-CE-LIF assay for 3', 5' cyclic Guanosine Monophosphate achieved low nanomolar limits of detection, ≈ 17 nM, with a high temporal resolution on the order of 25-50 seconds. This assay was characterized in *in vivo* conditions with extensive pharmacokinetic studies performed in

the rat striatum. cGMP was detected only upon insertion of the MD probe and during anoxic depolarization in the striatum, with a cGMP assay LOD of 110-140 nM. The sensitivity of the early cGMP assay was limiting and likely insufficient to detect stimulated levels of cGMP in the rat striatum. Structural modifications to the sheath flow cuvette holder of the MD-CE-LIF system resulted in a 5-6 fold improvement in LOD of the cGMP assay. cGMP was likely detected in the rat cerebellum after application of the PDE inhibitor IBMX in conjunction with high-K^+ aCSF. Because cyclic nucleotide concentrations change rapidly within minutes during anoxia produced by decapitation, it is difficult to obtain accurate estimates of their concentrations in many brain regions.[288] Several techniques have been described, such as microwave irradiation, freezing in liquid nitrogen and living brain slices, to allow rapid inactivation of brain enzymes involved in cAMP and cGMP homeostasis.[288] Another factor to consider is that RIA studies involving analysis for cGMP analyze total brain homogenate samples. If cGMP is present at higher concentrations in intracellular regions, extracellular concentrations of cGMP are likely significantly lower than the previously reported 6-9 nM. Basal levels of subpicomolar are more likely in the CSF, which is where MD sampling occurs. The current assay is therefore limited by its LOD, and would need to undergo reoptimization with a different fluorogenic reagent, or continue to focus on elevating basal cGMP levels via application of exogenous compounds like IBMX to observe % changes of baseline. Initial study indicates presence of cGMP in this *in vivo* experiment, with increasing fluorescence over time of exposure to IBMX. Further study is necessary to conclusively determine the presence of cGMP in cerebellum dialysate samples.

CONCLUSIONS

Research involving the study of cGMP is essential in the effort to understand the pathogenesis of human diseases and the treatment of neurologically related disorders. As a downstream indicator of glutamate and nitric oxide (NO) activity, the study of cGMP may also lead to a greater understanding of the steps involved in reduction of oxidative stress and excitotoxic effects associated with the glutamate/NMDA/NO pathway. Greater knowledge of the steps involved in this signaling pathway, will lead to more effective potential targeted drug therapies.

Optimization and characterization of the cGMP assay was carried out to achieve maximum sensitivity, selectivity, resolution, and speed of analysis. Detection limits capable of resolving cGMP at nanomolar levels with a temporal resolution on the order of seconds have been achieved. Temporal resolution on the order of 25-50 s offers a significant improvement over previous cGMP *in vivo* microdialysis. Most microdialysis probe recoveries tested to date range from 17-25 %. The LOD range through the probe is 14-20 nM. While cGMP was detected in the rat brain during insertion of the microdialysis probe and during anoxic depolarization, it was not possible to see basal or pharmacologically stimulated levels of cGMP in the striatum. cGMP was likely detected in the rat cerebellum after application of the PDE inhibitor IBMX in conjunction with high-K^+ aCSF. Possible improvements to the cGMP assay could be made utilizing a different derivatizing reagent, e.g. dimethyl phenylglyoxal, and a different laser for excitation of the generated fluorophores in the derivatization reaction, specific to the derivatizing reagent.

The developed cGMP assay is the first assay for cGMP with high temporal resolution and has potential application to the study of brain pharmacokinetics where stimulated cGMP levels are in excess of 14-20 nM. A more definitive picture of cGMP's role as a secondary messenger in the glutamate NMDA pathway can be elucidated through the use of high speed online MD-CE-LIF.

The author would like to thank Galila Agam for the plasma samples. Funding for this research was generously provided by the University of Minnesota and the National Institutes of Health (Grant NS043304) and is greatly appreciated.

Chapter 3:

Development of High Speed Online MD-CE-LIF Assay for Fluorescein and Monitoring Pharmacokinetics of Intranasal Drug Delivery in the Mammalian Brain

INTRODUCTION

It is currently estimated that as many as 1.5 billion people worldwide are suffering at any given time from some type of central nervous system (CNS) disorder.[166] Due to an increasing number of elderly people in the general population, these numbers will substantially increase over the next decades. If treatments fail to emerge, the number of people with CNS disorders will be approximately 1.9 billion by 2020.[188, 190] Despite the immense network of the cerebral vasculature, systemic delivery of therapeutics to the central nervous system (CNS) is not effective for greater than 98% of small molecules and for nearly 100% of large molecules.[23, 188] Drug therapy is limited by the barrier properties of the blood brain barrier (BBB). The BBB is comprised in part of tight junctions between the capillary endothelial cells in the brain microvasculature; this prevents free diffusion of molecules across the BBB and prevents most molecules from reaching the central nervous system (CNS) from the bloodstream.[125]The need for drug therapies that can bypass the BBB and target the CNS for treatment of neurological damage and disease are essential. Intranasal delivery is an attractive alternative to invasive delivery methods to bypass the BBB and rapidly target therapeutics directly to the CNS utilizing pathways along olfactory and trigeminal nerves innervating the nasal passages.[18, 23, 24] Currently, the mechanisms behind nose to brain transfer are not well understood. Further study of nose to brain transport is necessary to aid in the development of clinical therapies designed to target the CNS directly. The study of the mechanisms of absorption and distribution of an administered drug, the rate at which a drug action begins and the duration of the effect, the chemical changes of the substance in

the body, and the effects and routes of excretion of the metabolites of the drug are all implicit in the study of pharmacokinetics. Dynamics in the brain occur on an extremely fast time scale, with neurotransmission along a myelinated axon moving at a rate of 150 m/s^3.[4] Analytical techniques capable of high temporal resolution are critical in the development of pharmacokinetic profiles, or much of the information involved in a drugs movement into and out of the brain will be lost. When using microdialysis sampling, temporal resolution is usually limited by mass sensitivity of the analytical method coupled to the probe, i.e. how long a sample must be collected long enough to obtain a detectable quantity. The temporal resolution of current microdialysis intranasal studies is poor, with 10-20 minutes frequently required to collect enough sample for transfer to systems like HPLC,[196, 198, 199, 262, 263] or radio labeled gamma counting,[264] where the sample then undergoes another 10-20 minutes for separation. Microdialysis coupled to high speed online capillary electrophoresis with laser induced fluorescence detection is capable of monitoring brain dynamics with a temporal resolution on the order of seconds.[28, 29, 31-33, 97, 99]

The work presented in this chapter is part of a collaborative project with the Alzheimer's Research Center at Regions Hospital in St. Paul, MN to determine whether a homebuilt MD-CE-LIF system is compatible with research involving *in vivo* analysis of intranasally administered drug therapies. Frey, Hanson, Thorne, and coworkers have developed a careful characterization of nose to brain transport, indicating the existence of a direct nose to brain pathway post intranasal administration.[17-27] High speed online MD-CE-LIF analysis was used to develop a fluorescein assay with high temporal resolution,

on the order of 50 seconds, and then applied to monitor pharmacokinetics in the rat olfactory bulb post intranasal administration of fluorescein. The results are a high temporal resolution pharmacokinetic profile, with electrophoretic separations of fluorescein occurring every 20-30 seconds. This research indicates an excellent application of high speed online MD-CE-LIF to the intranasal study of future potential drug and protein candidates for treatment of CNS diseases.

MATERIALS AND METHODS

Chemicals and Reagents

Unless otherwise noted, all chemicals were obtained from Sigma Aldrich. (St. Luois, MO, USA) or the University of Minnesota Boynton Health Services Pharmacy (Minneapolis, MN). Separation and sheath flow buffer was Sodium Borate (100 mM) pH 10.50. All buffers were prepared in deionized water (Milli-Q, 1.2 MΩ, Millipore Corporation, Bedford, MA) and were filtered (0.2 μm) prior to use. Artificial cerebral spinal fluid (aCSF) consisted of NaCl (145 mM), KCl (2.7 mM), $MgSO_4$ (1.0 mM) and $CaCl_2$ (1.2 mM).Various concentrations of fluorescein were prepared in aCSF. Various concentrations of rhodamine 123 and rhodamine 110 were prepared in buffered aCSF, sodium phosphate (2 mM), pH 7.3. Ketamine cocktail consisted of: Ketamine HCl (100 mg/mL), Xylazine HCl (100 mg/mL), and Acepromazine (10 mg/mL) administered at a final concentration of ketamine (30 mg/kg), xylazine (6 mg.kg), and acepromazine (1 mg/kg) with a dose of 0.7 mL/kg by subcutaneous injection.

In Vivo Monitoring of Intranasal Administration of Fluorescein

All animal experiments were performed in strict accordance with protocols approved by the Institutional Animal Care and Use Committee at the University of Minnesota. Animals were housed under a 12 h light/dark cycle with food and water provided ad libitum. Monitoring of fluorescein post i.n. administration was carried out in the rat olfactory bulb of male Sprague-Dawley rats (250 to 380 grams). Pharmacokinetic monitoring was carried out via a high speed online microdialysis (MD) capillary electrophoresis (CE) with laser induced fluorescence (LIF) detection method. In an attempt to deliver drug directly to the brain using an i.n. drug delivery method, fluorescein was delivered intranasally to the right nasal cavity of an anesthetized rat, MD sampling was carried out in the right olfactory bulb. A single intranasal (i.n.) dose of Fluorescein (1 mM, 50 nanomoles), in aCSF, volume = 50 μL, was administered to the right nasal cavity. Rats were anesthetized via a subcutaneous injection of ketamine cocktail (up to two full doses, ½ at a time), then maintained anesthesia with straight ketamine at ½ doses as needed. Anesthesia was monitored until the animal no longer exhibited limb reflex to a toe pinch. A lab constructed intranasal pipette tip apparatus consisted of approximately 25 mm of a gel loading pipette tip inserted into approximately 25 mm of tygon tubing. The pipette tip apparatus was inserted 15 mm into the right nasal cavity approximately 20-30 minutes post initial anesthesia application (animal no longer exhibited limb reflex to toe pinch) and prior to placement of the animal into the stereotaxic frame. After placement of the pipette tip apparatus, the animal was transferred to a stereotaxic frame. Ear bars were secured in place. Surgery was performed to expose

the brain region of interest. The stereotaxic frame was used to implant a microdialysis probe into the right olfactory bulb: + 7.0 mm AP (anterior/posterior), -0.9 mm ML (medial/lateral) and -5.5 mm DV (dorsal/ventral) from bregma, the craniometric point at the junction of the sagittal and coronal sutures at the top of the cranium (Figure 3.01 and Figure 3.02).[270] D/V was measured from the surface of the brain post surgical exposure of the probe implantation site. The probe was inserted slowly to minimize tissue damage over a period of 15 minutes at approximately 500 μm/min. Data collection began one hour after the probe was inserted fully to allow time for the tissue surrounding the probe to recover from the damage caused by probe implantation. 30 minutes post MD probe placement into the olfactory bulb, the animal was placed in a supine position by inversion of the stereotaxic frame. The corners of the inverted stereotaxic frame were placed onto the supporting pillars of a home built machined platform table, inverted onto the surface of the experiment station, with supporting pillars extending approximately 12 inches upward. The animal was secured to the stereotaxic frame via a self designed supportive sling. The dorsal position of the animal's head was facing the bench counter top, with the surface of the skull and nasal cavities parallel to the bench top throughout all *in vivo* experiments. The microdialysis probe was continuously perfused with aCSF throughout the inversion process. The probe outlet remained directly connected to the CE-LIF instrument to reduce introduction of air bubbles into capillary lines, capillary connections, and the MD probe itself. Body temperature of 37 ^{o}C was maintained and monitored via a self adjusting rectal temperature probe, and heating pad (Fine Science Tools Inc. Foster City, CA) I.n. administration of fluorescein in aCSF was performed 1

hour post probe placement via a blunt tipped 1 cc microsyringe upon insertion into the pipette tip apparatus. With approximately 10-15 µL of dead volume at the end of the pipette tip apparatus, total volume of fluorescein in delivery syringe was 60-65 µL. After the i.n. dose, the pipette tip apparatus was removed from the nasal cavity. Prior to MD-CE-LIF monitoring of i.n. administered fluorescein *in vivo* studies the i.n. delivery experimental method was recreated and tested with methylene blue dye at the Alzheimer's Research Center at Region's Hospital in St. Paul, MN. 50 µL of methylene blue was administered via the pipette tip apparatus into the right nasal cavity of the rat, which was in a supine position, dorsal position of the head facing the bench top surface with head and nasal cavities parallel to the surface of the bench top. All i.n. applications of methylene blue dye resulted in delivery of the dye to the rat olfactory bulb, confirmed via visual inspection upon dissection of the rat brain cavity post mortem.

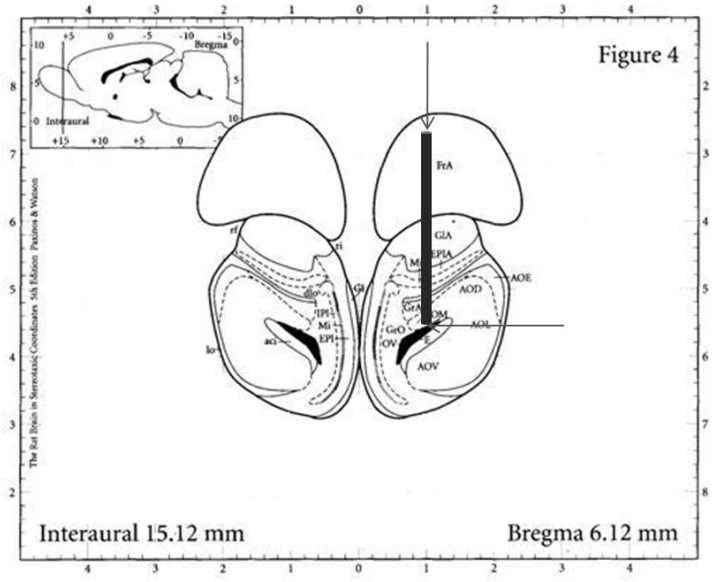

Figure 3.01. Diagram of rat brain olfactory bulb section.[270] Depicted slice is 6.12 mm anterior to bregma. The vertical arrow is placed 0.90 mm in the medial/lateral (ML) plane. The horizontal arrow is placed -5.5 mm in the dorsal/ventral (DV) plane. Microdialysis probe specifications are 3mm by 0.2 µm.

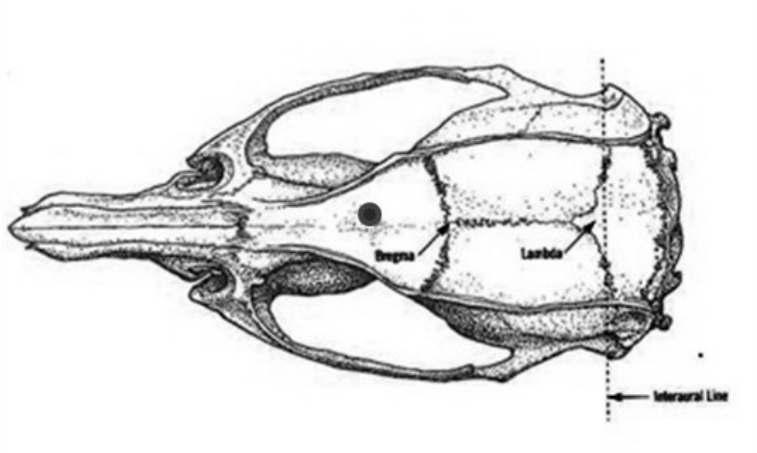

F**igure 3.02.** Diagram of dorsal view of surface of rat skull.[270] Solid circle depicted on the surface of the rat skull is the location of surgery on the skull for implantation of microdialysis probe. The anterior/posterior A/P distance from bregma is 7.0 mm. Microdialysis probe specifications are 3mm by 0.2 μm.

Analysis of Fluorescein in Whole Blood Post Intranasal Administration

Whole blood samples were drawn prior (as a control) and during the *in vivo* analysis of the i.n. administration of fluorescein to quantify fluorescein in the blood. This analysis was done to determine how much drug measured in the brain was due to direct nose-to-brain delivery and how much was from the blood when drug was delivered. Post the i.n. fluorescein dose 80 μL aliquots of whole blood were collected at 4 time points: 5, 10, 20, and 40 minutes. Blood was drawn from the tail of the anesthetized rat using a distal tail slice method. This procedure was carried out by using a 5.5 mm "Goldenrod" animal lancet or alternately an 18-16 gauge needle to centrally bisect the most distal 2-3 mm portion of the tail vein. It was easy to open the incision for blood collection (via a finger flick to the incision site), and easy to close with compression (via tying a gauze strip over the incision site) between blood collections. Other methods of blood collection were considered, however the experimental setup was prohibitive to many traditional

blood sample collection methods. Cheek puncture was not a viable option. First, the rat's head was secured in a stereotaxic device, and the precise location of the microdialysis probe in the brain could be compromised by pressure against the head during the blood draw. Second, the drug concentrations in the head region may not accurately represent those in the rest of the body because it was so close to the nose following intranasal drug delivery. Orbital sinus was not possible because the rat's head is in a stereotaxic frame. Cardiac puncture was not ideal for multiple aliquots sampling and the high risk of animal death during the procedure. Axillary bleed was also inaccessible due to the stereotaxic frame. Total drawn blood volume ranged from 300-750 µL, and the rats weighed 250-380 g. Percent of body weight drawn was approximately 0.1%-0.3% eliminating any fluid replacement concerns. All whole blood samples were placed in cool storage (2-8 ^{o}C) for analysis via microdialysis (MD) capillary electrophoresis (CE) with laser induced fluorescence detection (LIF). Analysis of whole blood samples was carried out within 12 hours of sample collection. The microdialysis probe, coupled to the high speed online CE-LIF system, was perfused at 40 µL/hr with artificial cerebrospinal fluid (aCSF) and placed directly into the whole blood samples.

Intranasal Whole Blood Standard Curve

Prior to the i.n. fluorescein dose, approximately 560 µL of whole blood was collected from the anesthetized rat for a standard blood curve in a CAPIJECT 500 µL Lithium Heparin Gel Barrier collection tube (12.5 I.U., mint green cap). 80 µL aliquots of whole blood were distributed into six 600 µL microcentrifuge vials. At the time of analysis via MD-CE-LIF, each 80 µL aliquot of whole blood was spiked with 20 µL of

fluorescein in aCSF standard stock solution (varied concentration) for a final standard concentration range of 300 pM to 100 nM Fluorescein. One 80 µL aliquot was spiked with 20 µL of aCSF without fluorescein as a blank control. The MD probe was placed into fresh aCSF in between the sampling of each whole blood standard vial. At the time of analysis via MD-CE-LIF, the spiked blood standard curve was run first, followed by the whole blood samples taken post i.n. fluorescein administration.

In vivo Monitoring of Intravenous Administration of Fluorescein

All animal experiments were performed in strict accordance with protocols approved by the Institutional Animal Care and Use Committee at the University of Minnesota. Monitoring of fluorescein was carried out in the rat olfactory bulb of male Sprague-Dawley rats (250 to 380 grams). Studies were carried out to measure the delivery and pharmacokinetics of fluorescein in the brain via a high speed online microdialysis (MD) capillary electrophoresis (CE) with laser induced fluorescence (LIF) detection method. In an attempt to discern what percent of fluorescein in the brain was due to a direct nose to brain pathway post i.n. administration, intravenous administration of fluorescein studies were performed. A single intravenous (i.v.) dose of fluorescein (160 µM, 8 nanomoles), volume = 50 µL was administered mid tail directly into the tail vein via a 1 cc Kendall Monoject Ultra Comfort syringe (28 gauge x ½ inch length). The microdialysis probe was placed into the right olfactory bulb at stereotaxic coordinates + 0.7 A/P, +0.09 M/L, – 0.55 D/V, and allowed one hour for equilibration prior to i.v. dosing. The rats were anesthetized via a subcutaneous injection of ketamine cocktail (up to two full doses), then maintained anesthesia with straight ketamine. Anesthesia was

monitored until the animal no longer exhibited limb reflex to a toe pinch. The animal was then transferred to the stereotaxic frame. Ear bars were secured in place. Surgery was performed to expose the brain region of interest (Figure 3.02, earlier in text). The probe was inserted slowly to minimize tissue damage over a period of 15 minutes at approximately 500 μm/min. Data collection began one hour after the probe was inserted fully to allow time for the tissue surrounding the probe to recover from the damage caused by probe implantation. 30 minutes post MD probe placement into the olfactory bulb, the animal was placed in a supine position by inversion of the stereotaxic frame. The corners of the inverted stereotaxic frame were placed onto the supporting pillars of a home built machined platform table, inverted onto the surface of the experiment station, with supporting pillars extending approximately 12 inches upward. The animal was secured to the stereotaxic frame via a self designed supportive sling. The dorsal position of the animal's head was facing the bench counter top, with the surface of the skull and nasal cavities parallel to the bench top throughout all *in vivo* experiments. The microdialysis probe was continuously perfused with aCSF throughout the inversion process. The probe outlet remained directly connected to the CE-LIF instrument to reduce introduction of air bubbles into capillary lines, capillary connections, and the microdialysis probe itself. Body temperature of 37 ^{o}C was maintained and monitored via a self adjusting rectal temperature probe, and heating pad (Fine Science Tools Inc. Foster City, CA) The intravenous dose of fluorescein was performed 1 hour to 1 hour and 10 minutes post probe placement After the i.v. dose, the delivery syringe was immediately

removed from the tail vein, and pressure applied to the i.v administration site via a tied gauze strip.

Analysis of Fluorescein in Whole Blood Post Intravenous Administration

Whole blood samples were drawn prior (as a control) and during the *in vivo* analysis of the i.v. administration of fluorescein to quantify fluorescein in the blood. This analysis was done to determine how much drug measured in the brain was due to direct nose-to-brain delivery and how much was from the blood when drug was delivered. Post the i.n. fluorescein dose 80 μL aliquots of whole blood were collected at 4 time points: 5, 10, 20, and 40 minutes. Blood was drawn from the tail of the anesthetized rat using a distal tail slice method. This procedure was carried out by using a 5.5 mm "Goldenrod" animal lancet or alternately an 18-16 gauge needle to centrally bisect the most distal 2-3 mm portion of the tail vein. It was easy to open the incision for blood collection (via a finger flick to the incision site), and easy to close with compression (via tying a gauze strip over the incision site) between blood collections. All whole blood samples were placed in cool storage (2-8 ^{o}C) for analysis via microdialysis (MD) capillary electrophoresis (CE) with laser induced fluorescence detection (LIF). Analysis of whole blood samples was carried out within 12 hours of sample collection. The microdialysis probe, coupled to the high speed online CE-LIF system, was perfused at 40 μL/hr with artificial cerebrospinal fluid (aCSF) and placed directly into the whole blood samples.

Intravenous Whole Blood Standard Curve

Prior to the i.v. fluorescein dose, approximately 560 µL of whole blood was collected from the anesthetized rat for a standard blood curve in a CAPIJECT 500 µL Lithium Heparin Gel Barrier collection tube (12.5 I.U., mint green cap). 80 µL aliquots of whole blood were distributed into six 600 µL microcentrifuge vials. At the time of analysis via MD-CE-LIF, each 80 µL aliquot of whole blood was spiked with 20 µL of fluorescein standard stock solution (varied concentration) for a final standard concentration range of 300 pM to 100 nM Fluorescein. One 80 µL aliquot was spiked with 20 µL of aCSF without fluorescein as a blank control. The MD probe was placed into fresh aCSF in between the sampling of each whole blood standard vial. At the time of analysis via MD-CE-LIF, the spiked blood standard curve was run first, followed by the whole blood samples taken post i.v. fluorescein administration.

In vivo Monitoring of Intravenous and Intranasal Administration of artificial Cerebrospinal Fluid (aCSF)

All animal experiments were performed in strict accordance with protocols approved by the Institutional Animal Care and Use Committee at the University of Minnesota. MD-CE-LIF monitoring of aCSF was carried out in the rat olfactory bulb of male Sprague-Dawley rats (250 to 380 grams) post intranasal, and post intravenous dosing of aCSF. These experiments were performed as a control. For intranasal control, a single i.n. dose of aCSF, volume = 50 µL was administered. As an intravenous control, a single i.v. dose of aCSF, volume = 50 µL was administered mid tail directly into the tail vein via a 1 cc Kendall Monoject Ultra Comfort syringe (28 gauge x ½ inch Length). The

doses were administered 1 hour to 1 hour and 10 minutes post MD probe placement into the olfactory bulb. Animals were anesthetized via a subcutaneous injection of ketamine cocktail (up to two full doses, ½ at a time), then maintained anesthesia with straight ketamine at ½ doses as needed. Anesthesia was monitored until the animal no longer exhibited limb reflex to a toe pinch. A lab constructed intranasal pipette tip apparatus consisted of approximately 25 mm of a gel loading pipette tip inserted into approximately 25 mm of tygon tubing. The pipette tip apparatus was inserted 15 mm into the right nasal cavity approximately 20-30 minutes post initial anesthesia application (animal no longer exhibited limb reflex to toe pinch) and prior to placement of the animal into the stereotaxic frame. After placement of the pipette tip apparatus into the right nasal cavity, the animal was transferred to a stereotaxic frame. Ear bars were secured in place. Surgery was performed to expose the brain region of interest. The stereotaxic frame was used to implant a microdialysis probe into the right olfactory bulb: +7.0 mm AP (anterior/posterior), -0.9 mm ML (medial/lateral) and -5.5 mm DV (dorsal/ventral) from bregma, the craniometric point at the junction of the sagittal and coronal sutures at the top of the cranium[270] (Figure 3.01 and Figure 3.02). D/V was measured from the surface of the brain post surgical exposure of the probe implantation site. The probe was inserted slowly to minimize tissue damage over a period of 15 minutes at approximately 500 μm/min. Data collection began one hour after the probe was inserted fully to allow time for the tissue surrounding the probe to recover from the damage caused by probe implantation. 30 minutes post MD probe placement into the olfactory bulb, the animal was placed in a supine position by inversion of the stereotaxic frame. The corners of the

inverted stereotaxic frame were placed onto the supporting pillars of a home built machined platform table, inverted onto the surface of the experiment station, with supporting pillars extending approximately 12 inches upward. The animal was secured to the stereotaxic frame via a self designed supportive sling. The dorsal position of the animal's head was facing the bench counter top, with the surface of the skull and nasal cavities parallel to the bench top throughout all *in vivo* experiments. The microdialysis probe was continuously perfused with aCSF throughout the inversion process. The probe outlet remained directly connected to the CE-LIF instrument to reduce introduction of air bubbles into capillary lines, capillary connections, and the microdialysis probe itself. Body temperature of 37 ^{o}C was maintained and monitored via a self adjusting rectal temperature probe, and heating pad (Fine Science Tools Inc. Foster City, CA) The pipette tip apparatus was immediately removed after intranasal administration of aCSF. No pipette tip apparatus was inserted into the nasal cavity for i.v. control studies. After the i.v. dose, the delivery syringe was immediately removed from the tail vein, and pressure applied to the i.v \administration site via a tied gauze strip.

Whole Blood Analysis Post I.N. and I.V. Control Experiments

Whole blood samples were drawn prior (as a control) and during the *in vivo* analysis of the i.n. administration of aCSF to acquire a baseline control for direct comparison to whole blood samples drawn post i.n. fluorescein and i.v. fluorescein administration. Post the i.n. and i.v. aCSF dose, 80 μL aliquots of whole blood were collected at 4 time points: 5, 10, 20, and 40 minutes. Blood was drawn from the tail of the anesthetized rat using a distal tail slice method. This procedure was carried out by using a

5.5 mm “Goldenrod” animal lancet or alternately an 18-16 gauge needle to centrally bisect the most distal 2-3 mm portion of the tail vein. It was easy to open the incision for blood collection (via a finger flick to the incision site), and easy to close with compression (via tying a gauze strip over the incision site) between blood collections. All whole blood samples were placed in cool storage (2-8 ^{o}C) for analysis via microdialysis (MD) capillary electrophoresis (CE) with laser induced fluorescence detection (LIF). Analysis of whole blood samples was carried out within 12 hours of sample collection. The microdialysis probe, coupled to the high speed online CE-LIF system, was perfused at 40 μL/hr with artificial cerebrospinal fluid (aCSF) and placed directly into the whole blood samples.

I.N. and I.V. aCSF Control Whole Blood Standard Curve

Prior to the i.n. and i.v. aCSF dose, approximately 560 μL of whole blood was collected from the anesthetized rat for a standard blood curve in a CAPIJECT 500 μL Lithium Heparin Gel Barrier collection tube (12.5 I.U., mint green cap). 80 μL aliquots of whole blood were distributed into six 600 μL microcentrifuge vials. At the time of analysis via MD-CE-LIF, each 80 μL aliquot of whole blood was spiked with 20 μL of fluorescein standard stock solution (varied concentration) for a final standard concentration range of 300 pM to 100 nM Fluorescein. One 80 μL aliquot was spiked with 20 μL of aCSF without fluorescein as a blank control. The MD probe was placed into fresh aCSF in between the sampling of each whole blood standard vial. At the time of analysis via MD-CE-LIF, the spiked blood standard curve was run first, followed by the whole blood samples taken post i.v. fluorescein administration.

In vivo Monitoring of Intranasal Administration of Rhodamine 123, Rhodamine 110, and Fluorescein

All animal experiments were performed in strict accordance with protocols approved by the Institutional Animal Care and Use Committee at the University of Minnesota. Monitoring of rhodamine 123, rhodamine 110, and fluorescein was carried out in the rat olfactory bulb of male Sprague-Dawley rats (250 to 380 grams). Studies were carried out to measure the delivery and pharmacokinetics of a mixture of variously charged drugs in the brain via a high speed online microdialysis (MD) capillary electrophoresis (CE) with laser induced fluorescence (LIF) detection method. The microdialysis probe was placed into the right olfactory bulb at stereotaxic coordinates + 0.6 A/P, -0.09 M/L, – 0.55 D/V, and allowed one hour for equilibration prior to i.n. dosing. The rats were anesthetized via a subcutaneous injection of ketamine cocktail (up to two full doses), then maintained anesthesia with straight ketamine. Anesthesia was monitored until the animal no longer exhibited limb reflex to a toe pinch. The animal was then transferred to the stereotaxic frame. Ear bars were secured in place. Surgery was performed to expose the brain region of interest (Figure 3.02, earlier in text). The probe was inserted slowly to minimize tissue damage over a period of 15 minutes at approximately 500 μm/min. Data collection began one hour after the probe was inserted fully to allow time for the tissue surrounding the probe to recover from the damage caused by probe implantation. 30 minutes post MD probe placement into the olfactory bulb, the animal was placed in a supine position by inversion of the stereotaxic frame. The corners of the inverted stereotaxic frame were placed onto the supporting pillars of a

home built machined platform table, inverted onto the surface of the experiment station, with supporting pillars extending approximately 12 inches upward. The animal was secured to the stereotaxic frame via a self designed supportive sling. The dorsal position of the animal's head was facing the bench counter top, with the surface of the skull and nasal cavities parallel to the bench top throughout all *in vivo* experiments. The microdialysis probe was continuously perfused with aCSF throughout the inversion process. The probe outlet remained directly connected to the CE-LIF instrument to reduce introduction of air bubbles into capillary lines, capillary connections, and the microdialysis probe itself. Body temperature of 37 ^{o}C was maintained and monitored via a self adjusting rectal temperature probe, and heating pad (Fine Science Tools Inc. Foster City, CA). Multiple i.n. doses of a mixture of rhodamine 110 (333 μM), rhodamine 123 (333 μM) and fluorescein (333 μM), in buffered aCSF (2 mM Sodium Phosphate), volume = 35 μL, were administered to the right nasal cavity. The intranasal doses were administered 1 hour to 3 hours and 40 minutes post probe placement.

Microdialysis

Side-by-side microdialysis probes were constructed in-house (Figure 3.03) and were discussed in Chapter 1 of this text. Briefly, two 40 μm i.d. × 105 μm, o.d. pieces of fused silica capillary (Polymicro Technologies, Phoenix, AZ) were staggered by 3 mm and inserted into a 200 μm diameter piece of hollow fiber, regenerated cellulose, dialysis tubing (18,000 MWCO, Spectrum Laboratories, Rancho Dominquez, CA) and sealed using polyimide (Alltech, Deerfield, IL), leaving a 3 mm sampling region exposed. Probes were perfused with ethanol (60 μL/hr for 50 min) and aCSF (60 μL/hr for 30

minutes) prior to use. The microdialysis probe was perfused with aCSF at 40 µL/hr (0.66 µL/min). Relative recovery of the probe was determined with the online capillary electrophoresis instrument. The MD probe was placed into an aCSF solution containing 100 nM fluorescein and the peak heights were determined. The same solution of aCSF and fluorescein was then pumped directly to the flow gated injection interface and peak height was determined. The ratio of the peak height of fluorescein determined via the MD probe and the peak height of fluorescein directly injected without the MD probe was the relative recovery.

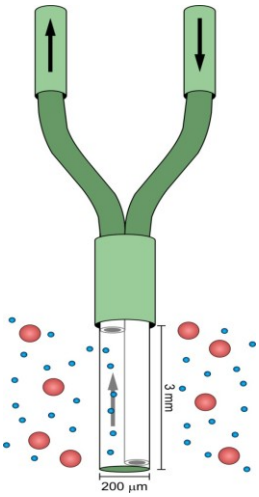

Figure 3.03. Schematic of Side by Side Microdialysis Probe.

In Vitro Characterization

Recovery of the dialysis probes was measured by comparing the peak area resulting from analyte sampled through the probe to the peak area that results when the same analyte solution is pumped directly into the reaction cross. Temporal resolution was determined by moving the microdialysis probe from aCSF to a solution containing 100 nM Fluorescein in aCSF for 3 minutes and then returning the probe to aCSF.

Flow gated injection interface

The dialysate was sampled for the online MD-CE-LIF system by a flow gated injection interface.[28, 30, 33, 34, 88, 92, 95, 96] The flow gated injection interface was machined out of a polycarbonate block by the U of MN Machine Shop. The capillary connected to the microdialysis probe outlet was inserted into the top of the flow gate, with a 20-50 µm

gap separating it from the separation capillary, which was inserted into the bottom side of the flow gate. (Figure 3.4) Separation buffer flow rate across the flow gated interface was 40 mL/hr. When the separation buffer was flowing, brain dialysate and samples in aCSF were carried to waste. To perform a sample injection, cross flow of the buffer was stopped via a pneumatically actuated valve (Valco Instruments Co. Inc.), for a specified period of time. The injection voltage was applied for a specified period of time, and a plug of sample was loaded onto the separation capillary. The cross flow of the separation buffer was stopped for 0.8-2 s, injection of brain dialysate occurred for 800-900 ms at -22 kV. Cross flow was resumed and separation voltage across the separation capillary was applied at -23 kV.

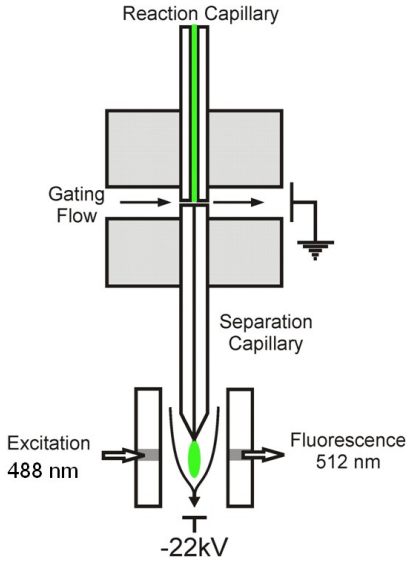

Figure 3.04. Schematic of Flow Gate Injection Interface and Sheath Flow Cuvette

High speed Online Capillary Electrophoresis with Laser Induced Fluorescence Detection

A schematic of the online MD-CE-LIF system is shown in (Figure 3.05). LIF detection was performed off capillary. in a high sensitivity sheath flow cell.[34, 102, 268] Separation of fluorescein was carried out in a 360 µm O.D./5 µm I.D. fused silica capillary (Polymicro Technologies, Phoenix, AZ, USA) 7.4-7.7 cm long. The separation capillary was inserted into a 200 x 200 µm square fused silica cuvette (NSG Precision Cells, Inc, Farmindale, NY, USA). Sheath flow buffer (Borate, 100 mM, pH 10.5)flows through the cuvette, and around the separation capillary. This flow induces a laminar flow profile of the sample exiting the separation capillary. The exiting end of the

separation capillary was ground to a fine tip using a dremel tool. The 488 nm line (20 mW) from a diode pumped solid state laser (Sapphire, Coherent, Santa Clara, CA) was used for excitation. The laser beam was expanded with a 10 × beam expander (Edmund Optics, Barrington, NJ) and passed through a 1 × focusing lens. The beam was focused off of the end of the separation capillary inside of the sheath flow cuvette. Fluorescence was collected at 90° through a 60 ×, 0.7 NA long working distance objective (Universe Kogaku, Oyster Bay, NY), passed through spatial and band-pass filters (510 ± 10 nm) (Melles Griot, Irvine, CA USA) and collected on a photomultiplier tube (PMT R1477, Hamamatsu Corp., Bridgewater, NJ). Current from the PMT was amplified, filtered (300 ms rise time), and recorded using a data acquisition card (National Instruments Corp., Austin, TX). Data analysis was performed using Cutter Analysis 7.0.

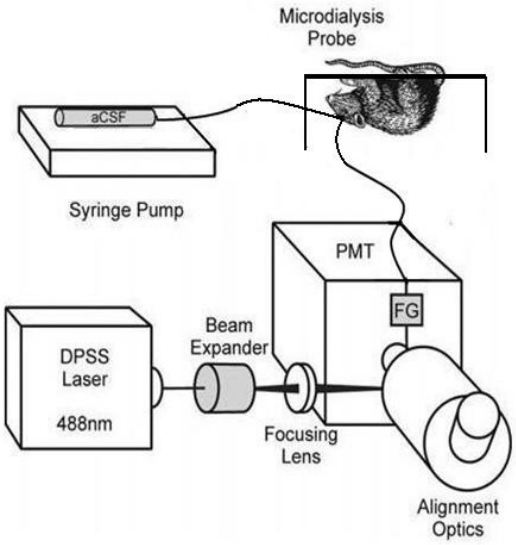

Figure 3.05. Schematic of the online microdialysis-CE-LIF detection system. A microdialysis probe is inserted into the rat olfactory bulb and perfused with artificial cerebrospinal fluid (aCSF). Dialysate is carried from the probe outlet to the online high speed capillary electrophoresis with high sensitivity laser induced fluorescence detection system where it is analyzed for fluorescein.

Data Analysis

Dose normalized concentrations in the olfactory bulb and whole blood samples from intranasal and intravenous experiments at 5, 10, 20, and 40 minutes were calculated and expressed in nmol/L (assuming a density of 1g/mL) as mean ± S.D. Unpaired two-sample t-tests were performed on concentrations in the rat olfactory bulb and whole

blood samples to compare intranasal and intravenous groups at each time point using GraphPad Prism software (version 4.0, GraphPad Software, Inc., San Diego, CA). Differences between groups were significant if $p < 0.05$.

The area under the concentration time curve (AUC) was generated from mean concentration time pharmacokinetic profiles from 0-120 minutes (AUC→120min) for olfactory bulb and blood fluorescein concentrations, without extrapolation to infinity, using the trapezoidal method. AUC→40 min was also calculated for comparison of intranasal and intravenous studies to whole blood samples, without extrapolation to infinity.

Intranasal drug targeting of fluorescein to the rat olfactory bulb was assessed by 3 approaches: 1) normalizing intravenous fluorescein concentrations in the olfactory bulb and blood to dose, 2) normalizing intravenous and intranasal fluorescein concentration in the olfactory bulb and blood to AUC→40,and 3) by determining the drug targeting index (DTI),[209] a measure of the difference in targeting between intranasal and intravenous delivery.[25] The DTI was calculated as the ratio of brain AUC/blood AUC after intranasal administration to that after intravenous administration, after being corrected for dose.[25]

RESULTS AND DISCUSSION

In vitro Characterization of Fluorescein Assay Development.

In order to assess whether high speed online MD-CE-LIF was a viable technique for the study of intranasal administration, a fluorescein assay needed to be developed for proof of concept. Fluorescein is an excellent choice for *in vivo* monitoring, due to its high fluorescence quantum yield, solubility in aqueous solutions, high molar absorptivity, and

good fluorescence profiles at physiological pH (See Chapter 1 for discussion). The limit of detection, probe recovery, and temporal resolution of the fluorescein assay were all determined. Validation of the assay, and the goal of the initial step in the study of pharmacokinetics, post assay development, was whether fluorescein could be observed or not in *in vivo* environments post intranasal dosing. If so, what did the pharmacokinetics of fluorescein indicate? If MD-CE-LIF was capable of monitoring pharmacokinetics, the next step of expansion to intranasal delivery of therapeutic agents is possible. In addition to the olfactory bulb, other areas of the brain can also be targeted.

Extensive method development was carried out to develop the MD-CE-LIF assay. Key results include the limit of detection (LOD), probe recovery, and temporal resolution of the assay. Figure 3.06 shows a typical electropherogram of a fluorescein standard (100 nM) in aCSF and Figure 3.07 shows a typical electropherogram of a 300 pM fluorescein standard in aCSF. Peak shapes are excellent, achieving efficiencies of 28,000 theoretical plates. Peak widths as narrow as 0.74 s (300 pM fluorescein), up to 0.84 s were observed. Electrophoretic migration of fluorescein occurred in less than 20 seconds.

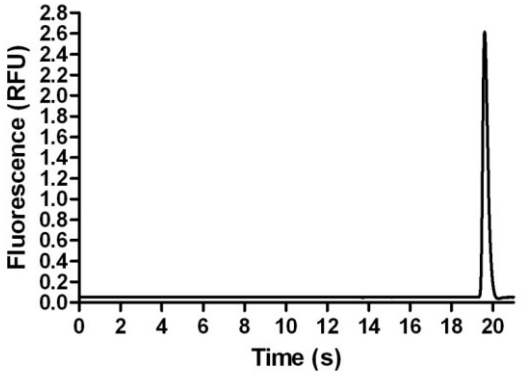

Figure 3.06. Electrophoretic separation of fluorescein (100 nM) standard in aCSF. Migration time: 19.6 s. Injection: 1 s. Delay: 1 s. Separation kV: 21. Injection kV: 20.0. Theoretical Plate Count, N: 28,142. Peak width: 0.85 s.

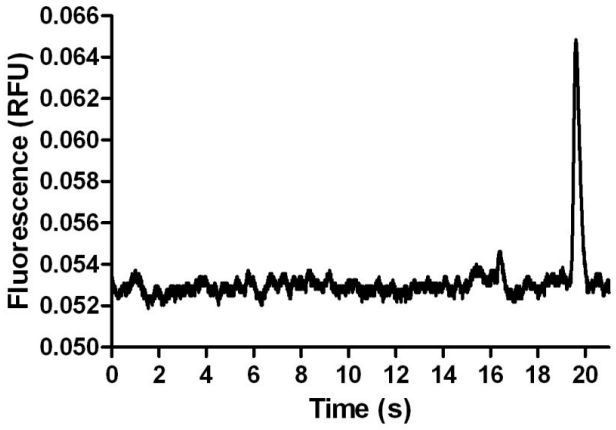

Figure 3.07. Electrophoretic separation of fluorescein (300 pM) standard in aCSF. Migration time: 19.6 s. Injection: 1 s. Delay: 1 s. Separation kV: 21. Injection kV: 20. Theoretical Plate Count, N: 8,822. Peak Width, 0.74 s.

Typical linear regression analysis (Table 3.01) of a fluorescein standard curve in aCSF can be found in Figure 3.08 (300 pM – 100 nM), and Figure 3.09 (300 pM to 10 nM). LOD of the developed fluorescein assay was determined to be 34 ± 4 pM. High precision from run to run resulted in low standard deviations of standards and an $R^2 = 0.999$.

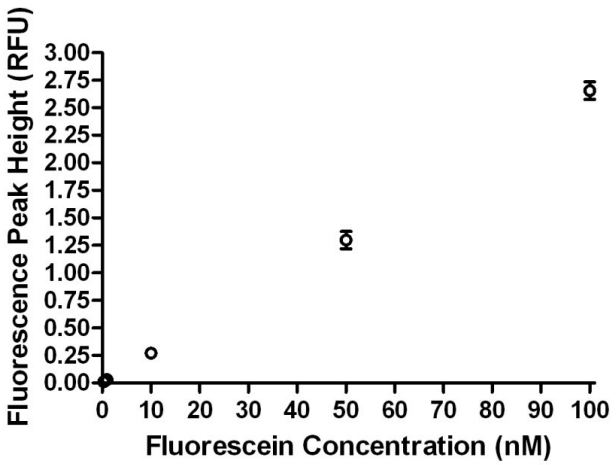

Figure 3.08. Fluorescein Calibration Curve. Fluorescein standards 300 pM – 100 nM in aCSF. Fluorescence peak height of fluorescein (round circles). Standard deviation represented by error bars for each point. N≥ 4.

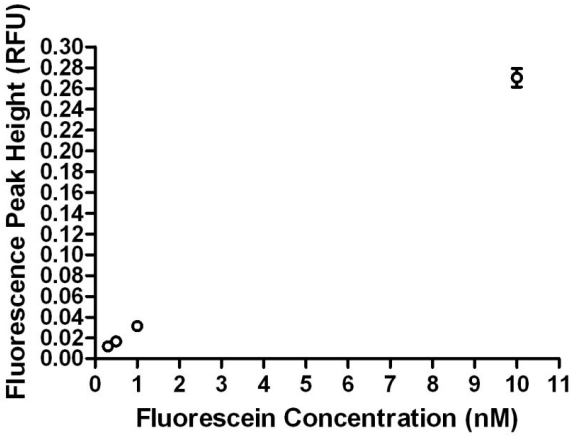

Figure 3.09. Fluorescein Calibration Curve. Fluorescein standards 300 pM – 10 nM in aCSF. Fluorescence peak height of fluorescein (round circles). Standard deviation represented by error bars for each point, $N \geq 4$.

	Coefficients	*Standard Error*	*t Stat*	*P-value*	*Lower 95%*	*Upper 95%*
Intercept	0.0039	0.0004	9.5	0.01	0.002	0.006
X Variable 1	0.02664	8.1-05	326.5	9.38E-06	0.03	0.03
LOD (pM)	33.6	3.5				
R^2	0.999					

Table 3.01. Linear Regression of Typical Fluorescein Calibration Curve

Reaction Optimization

A schematic showing the setup of the online sampling of fluorescein via microdialysis in the rat olfactory bulb was shown in Figure 3.05 of this text. Considerations to keep in mind during the setup of the online MD-CE-LIF system and assay optimization include minimizing the length of capillary connecting the microdialysis probe to the flow gated injection interface during *in vivo* experiments. This is important to reduce longitudinal diffusion which can contribute to poor temporal resolution. While it is ideal for sample to reach the flow gate in as short a time as possible, probe percent recovery issues arise at high perfusion rates. In addition to this,

the physical robustness of the probe must considered, at flow rates > 40 µL/hr, the regenerated cellulose microdialysis membrane burst, or leaked. The length of capillary (360 µm o.d./75 µm i.d.) from the flow gate to the probe outlet was optimized to ~ 90 cm. At these specifications, time from the probe outlet to the detector was around 2.46 minutes. Time from probe outlet to detector includes the time it takes for dialysate to travel from the probe outlet through the connecting capillary to the flow gate, load onto the separation capillary, then undergo separation and exit the separation capillary where it is detected in the sheath flow cuvette. Figure 3.10 shows the effect of varied injection time (A) pH of separation buffer (B) separation buffer concentration (C) injection time

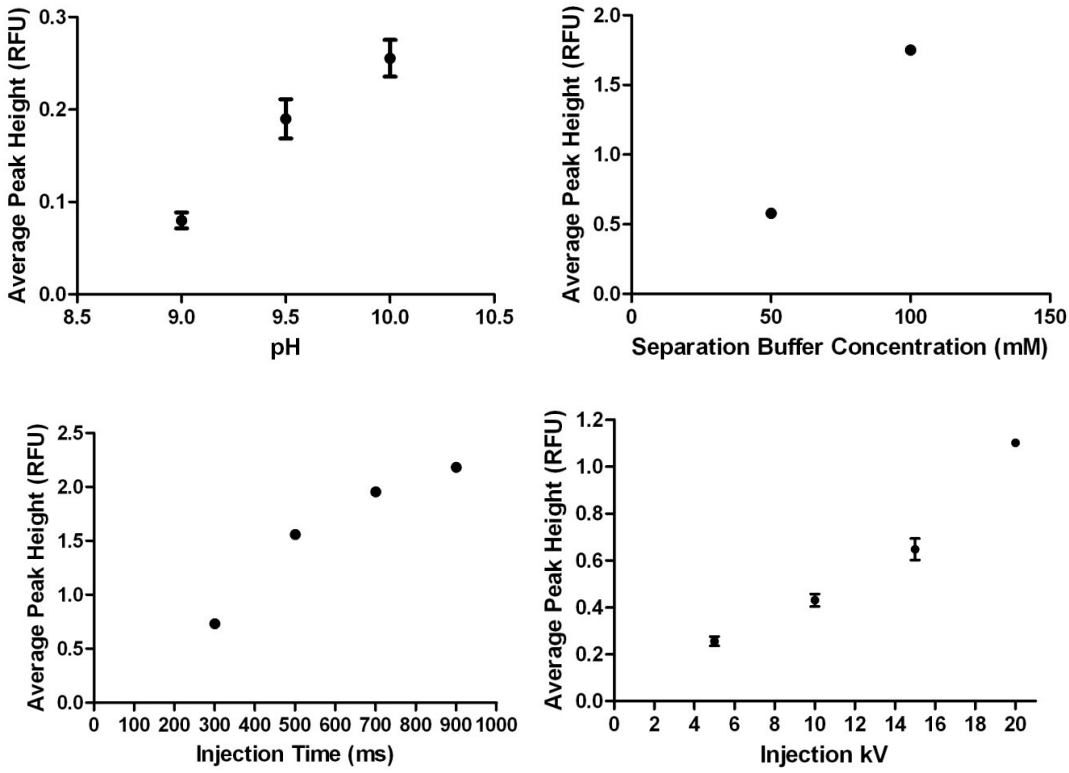

Figure 3.10. Optimization of fluorescein (100 mM) on the high speed online MD-CE-LIF system. A) Varied pH of the separation buffer. B) Varied concentration (mM) of the separation buffer. C) Varied injection time of fluorescein in Borate Buffer (100 mM) pH 10.5 D) Varied injection voltage (kV) to load fluorescein onto the separation capillary.

(ms) and (D) injection kV on the average peak height of fluorescein. Injection time was varied from 300 ms to 900 ms, with fluorescein peak height increasing with longer injection times. This is likely due to the double anionic nature of fluorescein in the separation buffer, Sodium Borate (100 mM), at pH 10.5. The application of a negative voltage at the outlet of the separation capillary makes it relatively more difficult to inject doubly negatively charged anions, like fluorescein. This electrokinetic bias against fluorescein understandably results in longer injection times. Injection time can be increased until fluorescein peak profile indicates excessive band broadening due to over injection of sample. Injection voltage improved the fluorescein peak height as it increased, in part due to the same electrokinetic bias. An injection voltage 1 kV less than the separation voltage was therefore selected for the day of analysis. Separation buffer of Sodium Tetraborate was varied from 25 mM to 150 mM, with optimal fluorescein peak height averages at 150 mM. pH of the separation buffer was varied from 25 mM to 150 mM, with the best fluorescein peak heights obtained at a pH of 10.5. A summary of fluorescein assay optimization parameters can be found in Table 3.02.

Separation Buffer	Sodium Borate
Separation Buffer (pH)	10.5
Separation Buffer (Concentration)	100 mM
aCSF Perfusate (µL/hr)	60
Excitation Wavelength (nm)	488
Emission Wavelength (nm)	520
Injection Time (ms)	900-1000

Table 3.02. Summary of MD-CE-LIF fluorescein assay development optimization parameters

Temporal resolution of the fluorescein assay is indicated in Figure 3.11 as a plot of fluorescein peak area (grey circles) vs. time. To test the temporal resolution of the MD-CE-LIF system for the fluorescein assay, the microdialysis probe was moved from aCSF, to aCSF spiked with a fluorescein standard (final concentration 500 pM), for 3 minutes, and then returned to aCSF. The MD probe was then transferred from the aCSF solution to fluorescein (300 pM) in aCSF, for three minutes, and back again to aCSF. Each electrophoretic separation was completed in 25 seconds, with a total separation time (including delay for sample collection between the capillaries in the flow gated injection

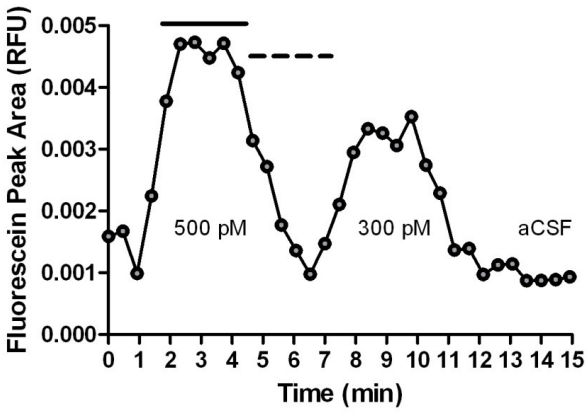

Figure 3.11. Temporal Response of MD Probe and MD-CE-LIF system to developed fluorescein assay. Each point represents fluorescein peak area (gray circles). Electrophoretic separation was completed in 28 s. Solid bar represents the time the MD probe spent in a 300 pM fluorescein solution (3 minutes). The probe was then transferred to an aCSF solution, represented by and the dashed bar represents the time the MD probe was placed into aCSF. The lag time from the solid bar's end to 300 pM peak area increase is equivalent to the time it takes for dialysate to travel from the probe outlet to the detector.

interface, time sample was injected, and ramp down voltage between each separation) of 28 seconds between each point on the graph. The black bar denotes time the MD probe was in a 300 pM fluorescein solution. Delay from the end of the bar to first peak increase for 300 pM is equivalent to the time it takes for dialysate/sample in aCSF to travel from the probe outlet to the detector, 4.61 minutes this day of analysis. The dashed line on the

graph indicates the time the MD probe was in the aCSF solution alone. There was some initial concern during the experimental design process regarding the length of capillary from the probe outlet to the detector. Incorporating the animal in a supine position while remaining connected to the MD-CE-LIF system could have required long capillary lines, contributing to the longitudinal diffusion process as fluorescein traveled from the brain to the MD-DE-LIF system. Longitudinal diffusion along the axis of the capillary lines from the probe outlet to the detector is the main detrimental contributing factor to temporal resolution. Optimized capillary length of 90 cm was determined. This minimized length of capillary lines, while providing enough maneuverability to invert the animal and stereotaxic frame, while maintaining the MD probe's connection to the MD-CE-LIF system. As evidenced in Figure 3.11, a step change from 10% to 90% of the baseline occurs in 2 separations, indicating a fast temporal response of the MD probe and analytical system to the fluorescein assay of around 56 seconds. This suggests that chemical dynamics that occur in the brain on a time scale of 56 seconds can be measured.

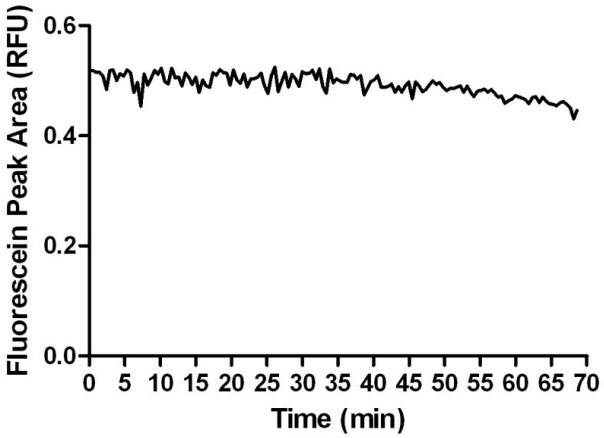

Figure 3.12. Long term stability of the online MD-CE-LIF assay. The microdialysis probe was inserted into a solution of fluorescein (100 nM) in aCSF. Electropherograms were recorded every 29 seconds over

Long term stability of the instrument was monitored. Intranasal drug delivery studies are often carried out over a period of several hours. Figure 3.12 indicates microdialysis sampled fluorescein (100 nM in aCSF) peak area over a period of 70 minutes.

Electropherograms were recorded every 29 seconds. Peak areas were not normalized, and remained very constant over the 70 minute period. A slight drift is indicated in the results, likely due to a small decrease in sheath flow buffer flow rate over time, however it is well within acceptable tolerances and will likely not interfere with pharmacokinetic data obtained in *in vivo* studies.

In Vivo Characterization of Fluorescein Assay: Intranasal Drug Delivery to the Rat Olfactory Bulb and Pharmacokinetic Monitoring via MD-CE-LIF

After development of the fluorescein assay, *in vivo* characterization was carried out to determine whether fluorescein could be detected by MD-CE-LIF in the olfactory bulb, post intranasal administration in the rat's right nasal cavity. The MD probe was placed into the right olfactory bulb, on the same side as the dose (See Methods and Development section earlier in this text for further details). Figure 3.13 shows a typical electropherogram of an online MD-CE-LIF analysis of dialysate collected from the rat olfactory bulb after intranasal administration of sodium fluorescein (1 mM, 50 nano-

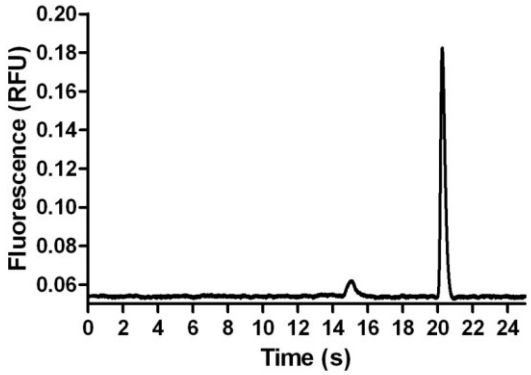

Figure 3.13. Electrophoretic separation of fluorescein sampled in the rat olfactory bulb, 96.1 minutes post intranasal administration of fluorescein via online high speed microdialysis capillary electrophoresis with laser induced fluorescence detection. Intranasal Dose: F (1mM, 50 nanomoles), 50 µL, 15 mm into the right nasal cavity.

moles, 50 μL). Electrophoretic separations were carried out every 25 seconds, with a total separation time of 28 seconds, including all injection and separation parameters. This electrophoretic separation was performed 96.1 minutes post i.n. dose of fluorescein (1 mM, 50 nanomoles, and 50 μL). Excellent peak shape is apparent, and the biological matrix is uncomplicated, clearly indicating a fully resolved fluorescein, present at a migration time of 20.3 s. A theoretical plate count, N = 9,876, was achieved, with peak width = 0.85 s. Identity of the fluorescein peak was verified by transfer of the probe from the brain to a standard solution containing fluorescein, after the i.n. *in vivo* experiment was complete, with consistent migration time, and increase in fluorescein peak height comparisons. I.n. administration of fluorescein was compared to a control dose of i.n. administered aCSF, the matrix for the i.n. dose experiments to determine possible matrix effects or other peaks present at the migration time of fluorescein. Further identification of fluorescein was confirmed via a Maestro In-Vivo Fluorescence Imaging system (University of Minnesota Biomedical Imaging Processing Lab, Minneapolis, MN). Maestro *in vivo* imaging allows high spectral accuracy and improved signal separation via multispectral acquisition and analysis. Reducing and subtracting auto fluorescence signals from the background, the Maestro system can provide dramatically improved sensitivity, multicolor flexibility and quantitative accuracy for both visible and near-infrared labels. Fluorescein standards were analyzed via the Maestro system, and used to determine presence or absence of fluorescein in the OB samples obtained post i.n. administration of fluorescein. An excitation filter of λ: 445 – 490 nm was inserted into the instrument, with a 515 nm long pass emission filter. Olfactory bulb samples were

dissected post mortem and scanned via the Maestro in-vivo imaging system over a wavelength range of 500-700 nm. Fluorescence signal at approximately 520 nm was extracted and all background wavelengths were subtracted, leaving the signal due to fluorescein alone. Fluorescein was clearly visible in the olfactory epithelium and olfactory bulb post intranasal administration (Figure 3.14). Fluorescein was also present in the frontal cortex of the rat brain and to a lesser extent in the cerebellum, in addition to other unidentified regions brain (Figure 3.15).

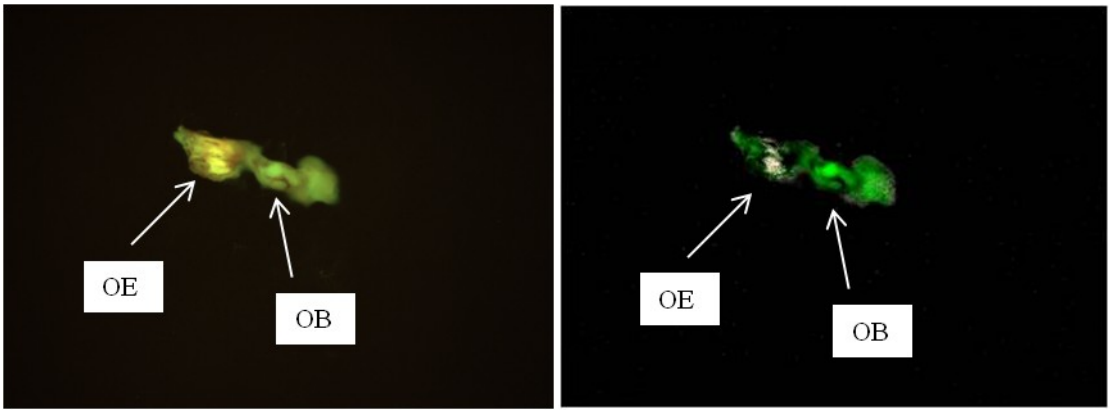

Figure 3.14. Maestro *in vivo* fluorescence images of the right rat olfactory epithelium (OE) and right olfactory bulb (OB). Left image consists of multispectral scans, λ = 500-700 nm. The right image subtracted the background wavelengths out, and extracted the wavelength assigned to fluorescein standards the day of analysis. Fluorescein is represented by the light green color.

Figure 3.15. Maestro *in vivo* fluorescence images of the rat brain. Left image consists of multispectral scans, λ = 500-700 nm. The right image subtracted the background wavelengths out, and extracted the wavelength assigned to fluorescein standards the day of analysis. Fluorescein is represented by the light green color.

Pharmacokinetic sampling in the brain is currently limited by techniques that require long sampling times to collect enough sample for analysis, and transfer of brain dialysate to an analysis method for quantification and identification. The developed fluorescein assay and pharmacokinetic monitoring with high speed online MD-CE-LIF in produced the first high temporal resolution pharmacokinetic profile of fluorescein in the rat olfactory bulb. MD Sampling, and analysis occurred in a complete online system, and achieved a temporal resolution on the order of 50 seconds. An example of a high temporal resolution pharmacokinetic profile of fluorescein in the rat olfactory bulb is shown in Figure 3.16. Fluorescein peak height (closed circles) was calculated for each electrophoretic separation during the experiment and plotted as fluorescein peak height over time. Complete separations were performed every 34.2 seconds. Included in the graph is the average 500 pM fluorescein standard (purple, long dashed line), measured the day of the experiment during calibration of the MD-CE-LIF instrument. The average baseline at fluorescein's migration time in aCSF at the start of the i.n. experiment is indicated by the orange short dashed line. Intranasal dose (green triangle) was administered 1.00 minute into the data collection. The time taken for brain dialysate to travel from the probe outlet to the detector is indicated by the blue diamond, in this case, 2.85 minutes. Sodium pentobarbital (red asterisk) was used as the euthanizing agent and was injected directly into the heart approximately 176 minutes post i.n. dose. Figure 3.16A focuses on the first 40 minutes of the i.n. experiment, and indicates the first fluorescein peak in the olfactory bulb at T = 2.38 minutes after the i.n. dose. This time point is determined by the first peak that is higher than the S.D. of the average baseline,

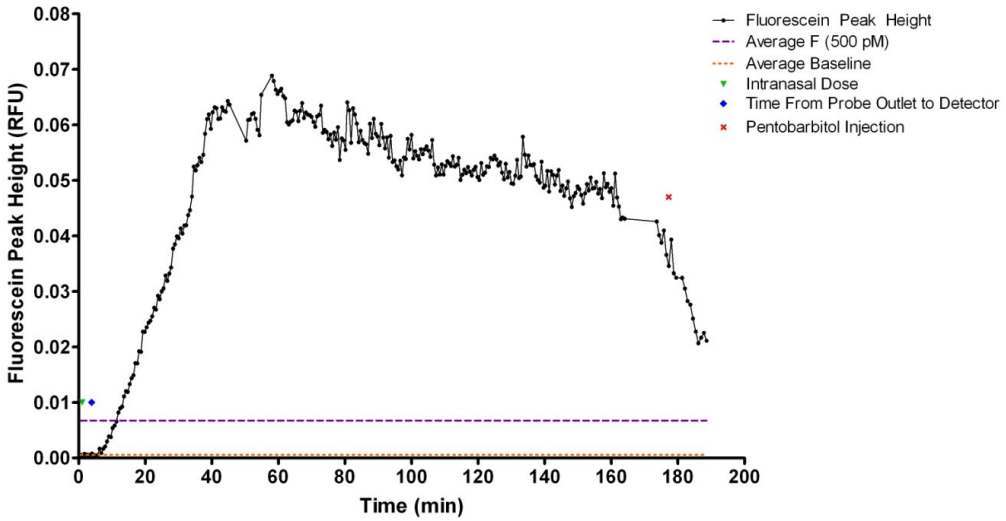

Figure 3.16. Pharmacokinetic profile of fluorescein peak height (black round circles) in the rat olfactory bulb (OB), measured with online high speed microdialysis capillary electrophoresis with laser induced fluorescence detection. Intranasal Dose to the right nostril: F (1mM, 50 nanomoles), 50 µL. Each circle represents fluorescein peak height in a single electrophoretic separation. Electropherograms were recorded every 34.2 s. The intranasal dose was performed at 1.00 minutes into data collection. The amount of time for dialysate to travel from the probe outlet to the detector is indicated by the blue diamond = 2.85 min. The 500 pM fluorescein standard is indicated by the purple long-dashed line. Average baseline at the fluorescein migration time, is indicated by the orange short-dashed lines. The first fluorescein peak in the olfactory bulb was detected 2.38 minutes post the intranasal dose.

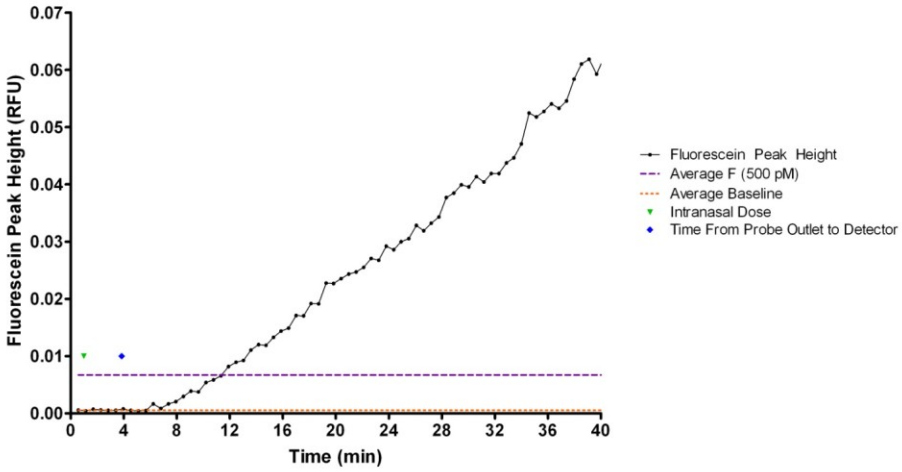

Figure 3.16A. First 40 minutes of pharmacokinetic profile of fluorescein peak height (black round circles) in the rat olfactory bulb (OB), measured with online high speed microdialysis capillary electrophoresis with laser induced fluorescence detection. Intranasal Dose to the right nostril: F (1mM, 50 nanomoles), 50 µL. Each circle represents fluorescein peak height in a single electrophoretic separation. Electropherograms were recorded every 34.2 s. The intranasal dose was performed at 1.00 minute into data collection. The amount of time for dialysate to travel from the probe outlet to the detector is indicated by the blue diamond = 2.85 min. The 500 pM fluorescein standard is indicated by the purple long-dashed line. Average baseline at the fluorescein migration time, is indicated by the orange short-dashed lines. The first fluorescein peak in the olfactory bulb was detected 2.38 minutes post the intranasal dose.

and by visual confirmation of a peak present in the separation at that time point in the experiment, in addition to data analysis confirmation of peaks present via Cutter 7 software. The time of the i.n. dose, and time it takes to travel from the probe outlet to the detector is subtracted from the time point of the first fluorescein peak detected in the olfactory bulb, indicating the time it takes for fluorescein to reach the olfactory bulb after intranasal administration. Rigorous pharmacokinetic analysis was not performed, however a gradually increasing rate of fluorescein, relatively linear, in the OB can be seen over the first 36 minutes post i.n. dose. From 40 to 160 minutes there is a slow decline, possibly indicating clearance of fluorescein from the OB. At the time of sacrifice, about 176 minutes in, a sharp decline in fluorescein measured in the OB is apparent. This decrease in fluorescein measured in the OB after the sacrifice of the animal and cessation of the heartbeat was consistent across every i.n. experiment performed in this study. It is possible that fluorescein is undergoing an energy dependent active transport into the OB, or is in the blood and ceases absorption into the OB upon cessation of the heart beat with a stoppage of the blood flow in the vasculatory system. There was variability between the i.n. pharmacokinetic profiles of fluorescein in the OB from animal to animal. On the majority, sampling during the first 2 hours did not result in significant decreases in fluorescein concentrations in the OB at any point in time. In fact, fluorescein tended to increase continuously over the time monitored. It can be supposed that if sampling were carried out even longer, a continuous rise in fluorescein concentration would be seen, until some point at which clearance from the OB was

apparent. It is not possible to calculate the half life, $t_{1/2}$ of fluorescein's residency in the OB, without an apparent decline from maximum peak levels.

The average pharmacokinetic profile of intranasally administered fluorescein (1mM, 50 nanomoles, and 50 µL, in aCSF) in the rat olfactory bulb is indicated in Figure 3.17. Fluorescein peak height was calculated at time points T = 0 min, prior to the i.n. dose, and T = 2 minutes, plus a point every 2 subsequent minutes for 120 minutes of the *in vivo* experiments, N = 5 animals. Complete separations for all of the *in vivo* i.n. experiments were performed every 25-30 seconds. Intranasal delivery resulted in a steadily increasing absorption rate of fluorescein in the OB throughout the *in vivo* experiments. This rate was higher over the first 30 minutes post i.n. dose until fluorescein (nM) reached about 2.8 nM, followed by a more gradual increase to 6 nM that continued

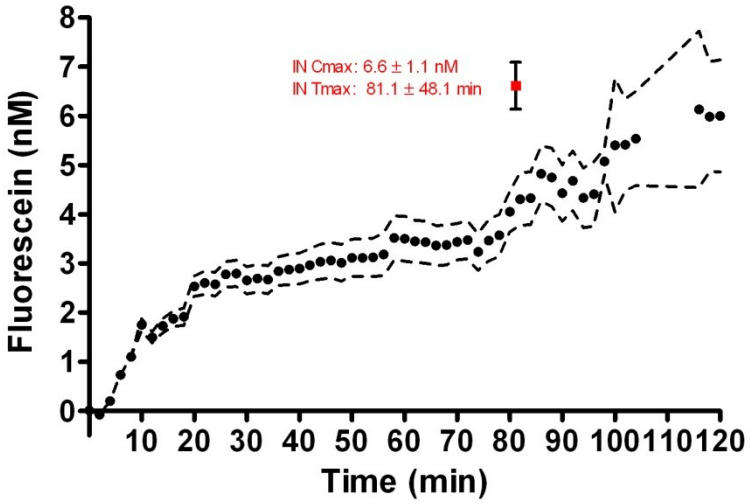

Figure 3.17. Average pharmacokinetic profile of intranasally administered fluorescein (nM) in the rat olfactory bulb (OB), measured via online high speed microdialysis capillary electrophoresis with laser induced fluorescence detection. Intranasal Dose (closed circles): F (1mM, 50 nanomoles) in aCSF, 50 µL, N = 5 animals. Each point represents fluorescein in the OB averaged at the initial time point T = 0 (prior to i.n. dose), and every 2 subsequent minutes (post i.n. dose) with the dashed line above and below representing standard deviation. Maximum average fluorescein concentration, Cmax, and Tmax, time to Cmax, is indicated on the graph. Electropherograms were recorded every 25-30 seconds.

to the end of the experiment. Peak concentration (Cmax) of 6.6 ±1.1 nM was reached at a time to peak concentration (Tmax) of 81.1 ± 48.1 minutes, with time to the OB post i.n. dose of 2.8 ± 0.5 minutes. Regardless of the route of fluorescein transport to the OB, either directly from nose to brain or indirectly e.g. nose to blood to brain, this determination indicates the fast temporal response of the online MD-CE-LIF system to the fluorescein assay. It is a time point in a pharmacological profile not seen in previously reported intranasal studies in the brain, which typically report the first data point at 5-30 minutes, with subsequent data points collected once every 5-30 minutes.

Prior to and during the *in vivo* analysis, whole blood samples were collected at T = 0 (prior to i.n. dose) and T = 5, 10, 20, and 40 minutes post i.n. fluorescein administration for comparison of fluorescein levels in blood to those observed in the brain. Figure 3.18 A reports average fluorescein (nM) in whole blood. Data points were normalized based on rat blood volume = 6.86 ± 0.53 mL per/100 g^2 to correct for

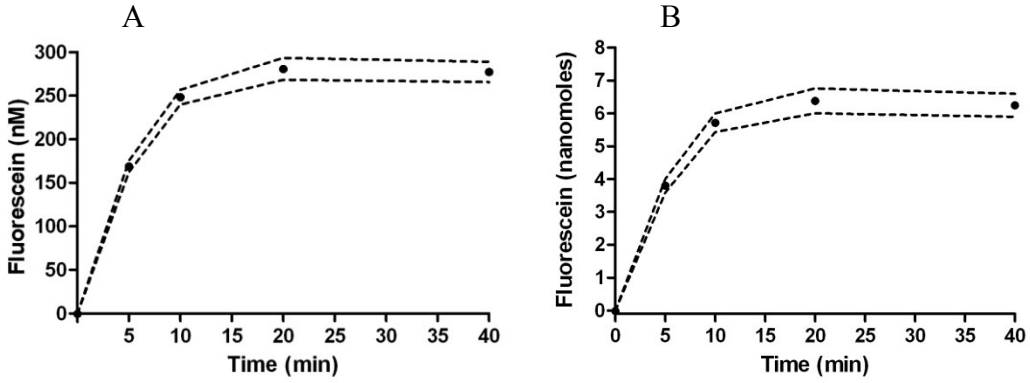

Figure 3.18 A and B. Average fluorescein (nM in A, nanomoles in B) in whole blood post intranasal administration, measured with online high speed microdialysis capillary electrophoresis with laser induced fluorescence detection. Intranasal Dose (closed circles): F (1 mM, 50 nanomoles) in aCSF, 50 µL, N = 5 animals. Each point represents average fluorescein in whole blood sampled via distal tail slice at T = 0 (prior to i.n. dose) and T = 5, 10, 20, and 40 min (post i.n. dose animals, with the dashed line representing standard deviation, N ≥ 3. Data points in B were normalized based on rat blood volume = 6.86 ± 0.53 mL per/100 g.[2] Electropherograms were recorded every 23 seconds

differences in rat size (Figure 3.16 B). Fluorescein blood levels (nM) were significantly higher than those observed in the olfactory bulb, indicating fluorescein transfer from the nose to the blood, either directly or through an intermediary pathway. A steep increase in rate was observed over the first 10 minutes, followed by a steadying of fluorescein concentration in the blood from 15 to 40 minutes. Cmax = 248 ± 8 nM was reached in a time to maximum concentration, Tmax = 10 minutes. Fluorescein (nanomoles) present in the blood leveled off at Tmax to approximately 6 nanomoles.

In Vivo Characterization of Fluorescein Assay: Intravenous Drug Delivery to the Rat Olfactory Bulb and Pharmacokinetic Monitoring via MD-CE-LIF

Fluorescein (160 μM, 8 nanomoles, and 50 μL) in aCSF was administered intravenously, to further elucidate the pathways and contributing mechanisms of fluorescein transport to the OB. Blood volume normalized fluorescein (nanomoles) appeared to remain steady at around 6 nanomoles post intranasal administration which determined the i.v. dosage for the next step of experiments. A 1.3 fold higher dose was chosen, 8 nanomoles of fluorescein, for further intravenous *in vivo* studies to determine if the resulting pharmacokinetic profile in the olfactory bulb was the same as that observed after intranasal administration. Based on previously published studies, it was hypothesized that fluorescein did not easily cross the blood brain barrier. Absence of fluorescein detection in the brain post i.v. dose would lend support to fluorescein reaching the OB via a direct nose to brain pathway, or indicate whether alternative mechanisms of transport into the OB occur for fluorescein.

Average fluorescein (nM) in the OB post i.v. dose is indicated in Figure 3.19. Fluorescein concentration over time was monitored with online high speed microdialysis capillary electrophoresis with laser induced fluorescence detection. The intravenous dose (triangles): F (160 µM, 8 nanomoles) in aCSF, 50 µL, was determined for N = 3 animals. Each point in the graph represents fluorescein in the OB averaged at the initial time point

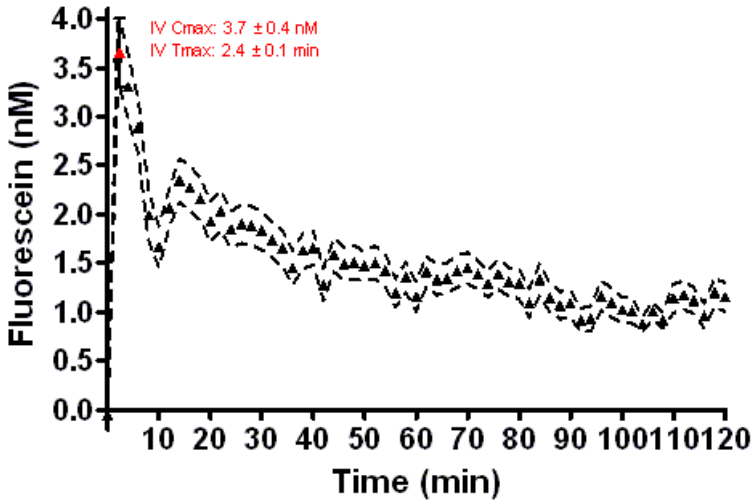

Figure 3.19. Average pharmacokinetic profile of intravenously administered fluorescein (nM) in the rat olfactory bulb (OB), measured via online high speed microdialysis capillary electrophoresis with laser induced fluorescence detection. intravenous Dose (closed triangles): F (160 µM, 8 nanomoles) in aCSF, 50 µL, N = 3 animals. Each point represents fluorescein in the OB averaged at the initial time point T = 0 (prior to i.n. dose), and every 2 subsequent minutes (post i.n. dose) with the dashed line above and below representing standard deviation. Maximum average fluorescein concentration, Cmax, and Tmax, time to Cmax, is indicated on the graph. Electropherograms were recorded every 25-30 seconds.

T = 0 (prior to i.n. dose), and every 2 subsequent minutes (post i.n. dose) with the dashed lines representing standard deviation. Electropherograms were recorded every 25-30 seconds. Intravenous administration of fluorescein resulted in fluorescein detection in the olfactory bulb. Fluorescein reached the olfactory bulb quickly, with an average time to OB of 0.81 ± 0.18 minutes. This is significantly faster than the intranasal average time to OB of 2.8 ± 0.5 minutes. A fast rate of transport led to a peak concentration of

fluorescein in the OB, Cmax, of 3.7 ± 0.4 nM. Time to peak concentration, Tmax, was 2.4 ± 0.1 minutes. The pharmacological results in the OB indicate a possibly biphasic decrease in fluorescein concentrations. The initial sharp rise in absorption rate to the Cmax, quickly declined until around 10 minutes, where a small increase in fluorescein to 2.4 nM was followed by a gradual decrease in fluorescein concentration over time. Prior to and during the *in vivo* analysis, whole blood samples were collected at T = 0 (prior to

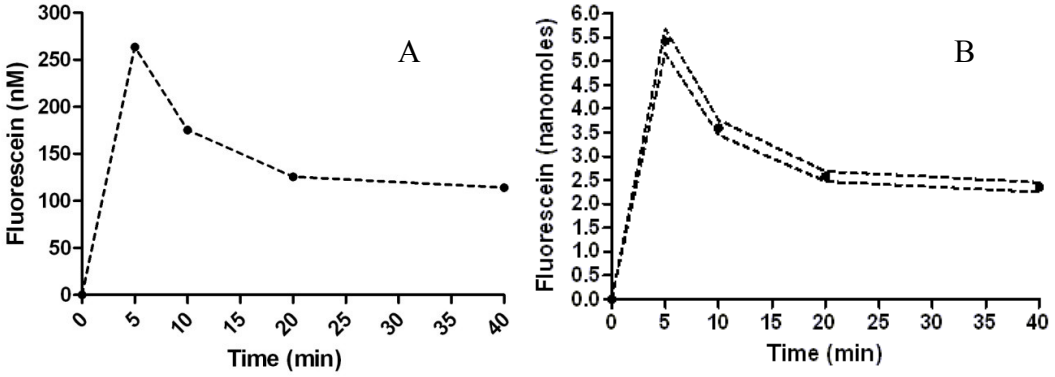

Figure 3.20 A and B. Whole blood analysis of intravenously administered fluorescein (nM in A and nanomoles in B) in the rat olfactory bulb (OB), measured with online high speed microdialysis capillary electrophoresis with laser induced fluorescence detection. Intravenous Dose (solid circles): F (160 µM, 8 nanomoles) in aCSF, 50 µL, N = 3 animals. Each point represents average fluorescein in whole blood sampled via distal tail slice at T = 0 (prior to i.n. dose) and T = 5, 10, 20, and 40 min (post i.n. dose), with the dashed line representing standard deviation, N ≥ 3. Data points were normalized based on rat blood volume = 6.86 ± 0.53 mL per/100 g.[2] Electropherograms were recorded every 23 seconds

i.v. dose) and T = 5, 10, 20, and 40 minutes post dose for comparison of fluorescein in blood levels to those observed in the brain. Figure 3.20 A reports average fluorescein (nM) in whole blood (round circles) with dashed lines representing the standard deviation. Data points were normalized based on rat blood volume =6.86 ± 0.53 mL per/100 g^2 to correct for differences in rat size (Figure 3.20 B). Cmax (nM) = 264 ± 4 nM was reached at Tmax = 5 minutes I.v. administered fluorescein levels rose quickly over the first 5 minutes, decreased at a similar rate from 5 to 15 minutes, and then slowed

down considerably from 20 to 40, leveling off at a concentration of 114 ± 2 nM. Nanomoles of fluorescein reached a Cmax = 5.4 ±0.2 at Tmax = 5 minutes and decreased over 40 minutes to 2.4 ± 0.1 nanomoles, indicating significant clearance of fluorescein from the blood over time.

Fluorescein was detected in the OB after both intranasal and intravenous dosing (Figure 3.21). Intranasal administration of fluorescein resulted in an approximate 1.6 fold increase in F (nM) over i.v. concentrations in the olfactory bulb at T = 40 minutes (Figure 3.22), and a 4.6 fold increase in i.n. vs. i.v. fluorescein concentrations at T = 120 minutes. Interestingly, i.v. administered fluorescein was cleared rapidly from the olfactory bulb, whereas i.n. administration demonstrated a continuous increase in fluorescein levels in the OB.

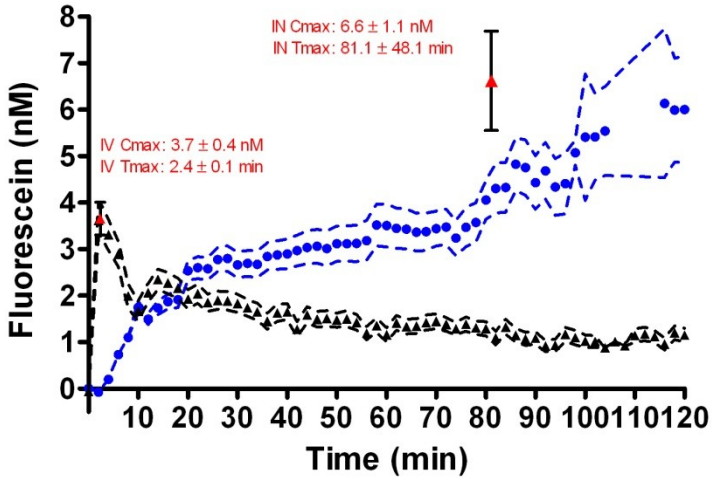

Figure 3.21. Average pharmacokinetic profile comparisons of i.n. and i.v. fluorescein (nM) in the rat olfactory bulb (OB), measured with online high speed microdialysis capillary electrophoresis with laser induced fluorescence detection. Intranasal Dose (closed circles): F (1mM, 50 nanomoles) in aCSF, 50 µL, N = 5. Intravenous Dose (closed triangles): F (160 µM, 8 nanomoles) in aCSF, 50 µL, N = 3animals. Each point represents fluorescein in the OB averaged at the initial time point T = 0 (pre dose), and every 2 subsequent minutes (post dose) with the dashed line representing standard deviation. Maximum average fluorescein concentration, Cmax, and time to Cmax, Tmax, is indicated on the graph for each set of data. Electropherograms were recorded every 25-30 seconds.

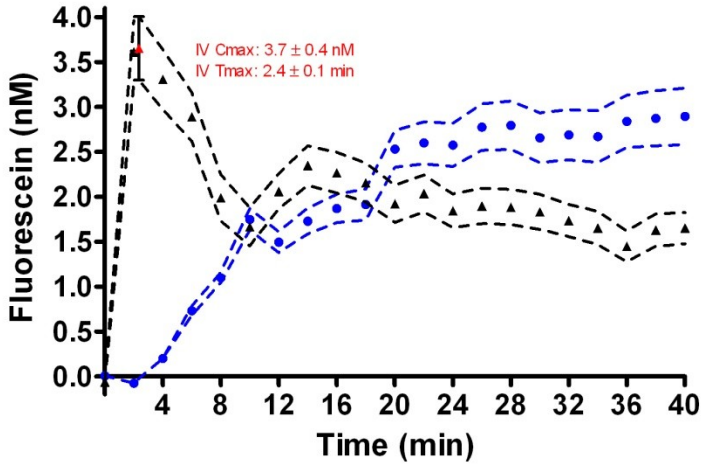

Figure 3.22. First 40 minutes of average pharmacokinetic profile comparisons of i.n. and i.v. fluorescein (nM) in the rat olfactory bulb (OB), measured with online high speed microdialysis capillary electrophoresis with laser induced fluorescence detection. Intranasal Dose (closed circles): F (1mM, 50 nanomoles) in aCSF, 50 µL, N = 5. Intravenous Dose (closed triangles): F (160 µM, 8 nanomoles) in aCSF, 50 µL, N = 3animals. Each point represents fluorescein in the OB averaged at the initial time point T = 0 (pre dose), and every 2 subsequent minutes (post dose) with the dashed line representing standard deviation. Maximum average fluorescein concentration, Cmax, and time to Cmax, Tmax, is indicated on the graph for each set of data. Electropherograms were recorded every 25-30 seconds.

Intranasal administration of fluorescein resulted in sustained levels of fluorescein in the blood over 40 minutes, relative to a more rapid clearance of fluorescein in the blood after intravenous administration (Figure 3.23). This result indicates a significant advantage in the application of drugs applied intranasally over intravenously regardless of the specific route to the brain. There are multiple clearance mechanisms associated with oral and intravenous dosing, including enzymatic degradation and clearance through the liver and kidney, resulting in lower bioavailabilities for brain targeted therapies. Intranasally applied drug therapies have not only the potential for direct nose to brain transport, but bypass first hepatic pass clearance and elimination from the blood, potentially resulting in an overall higher drug exposure over time. The slow increase in nasal absorption of fluorescein post i.n. dosing may be due to the use of anesthetics, which inhibit the nasal

mucociliary clearance and thereby prolong the residence time of the administered formulation in the nasal cavity.

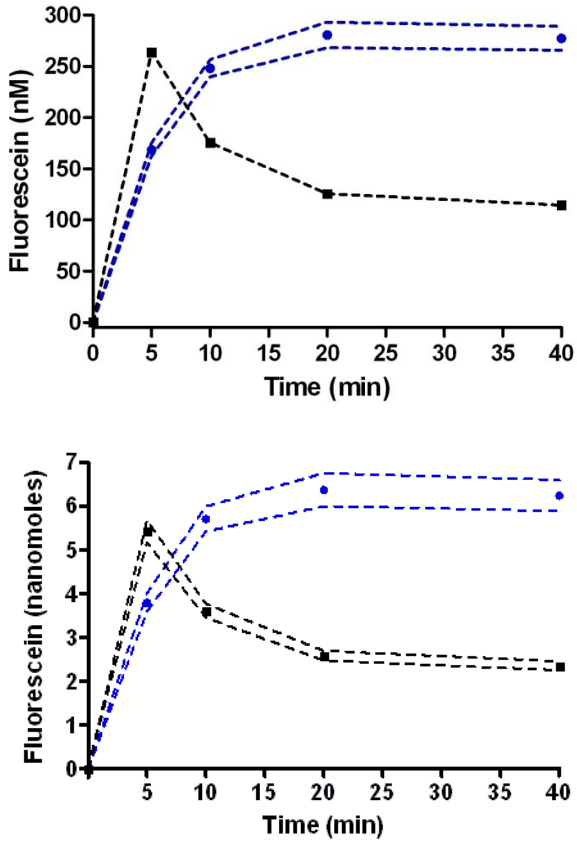

Figure 3.23 Whole blood analysis comparisons of i.n. (blue circles) and i.v. (black circles) administered fluorescein in the rat olfactory bulb (OB), measured with online high speed microdialysis capillary electrophoresis with laser induced fluorescence detection. Top Graph: fluorescein (nM) in whole blood. Bottom Graph: Fluorescein (nanomoles) in whole blood. Intranasal Dose: F (1mM, 50 nanomoles) in aCSF, 50 µL, N = 5 animals. Intravenous Dose F (160 µM, 8 nanomoles) in aCSF, 50 µL, N = 3 animals. Each point represents average fluorescein in whole blood sampled via distal tail slice at T = 0 (prior to i.n. dose) and T = 5, 10, 20, and 40 min (post i.n. dose), with the dashed line representing standard deviation, N ≥ 3. Data points were normalized based on rat blood volume = 6.86 ± 0.53 mL per/100 g.[2] Electropherograms were recorded every 23 seconds

While i.n. administration indicated an advantage over i.v. dosing based on the pharmacokinetic clearance profile, these results are not corrected for the i.n. and i.v. dose differences. I.n. dose of 50 nanomoles of fluorescein, is 6.25 time higher than that of the

i.v. fluorescein dose of 8 nanomoles. Dose correction was therefore performed and used for future comparisons of pharmacokinetic parameters between i.n. and i.v. experiments. Intravenous fluorescein concentrations were normalized to the intranasal dose by multiplying the concentrations of fluorescein (nM) after i.v. administration by a factor of 6.25 (Figure 3.24, and Figure 3.25), under the assumption that concentration of fluorescein is a linear function of the applied dose. After this correction, it is clear that

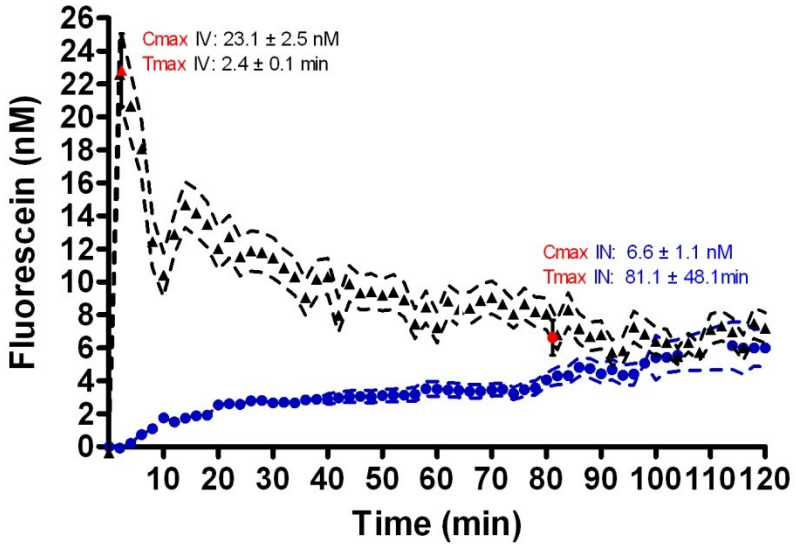

Figure 3.24. DOSE CORRECTED Average pharmacokinetic profile comparisons of i.n. and i.v. fluorescein (nM) in the rat olfactory bulb (OB), measured with online high speed microdialysis capillary electrophoresis with laser induced fluorescence detection. Intranasal Dose (closed circles): F (1mM, 50 nanomoles) in aCSF, 50 µL, N = 5 animals. Intravenous Dose, corrected (closed triangles): F (1mM, 50 nanomoles) in aCSF, 50 µL, N = 3 animals. Each point represents fluorescein in the OB averaged at the initial time point T = 0 (pre dose), and every 2 subsequent minutes (post dose) with the dashed line representing standard deviation. Maximum average fluorescein concentration, Cmax, and time to Cmax, Tmax, is indicated on the graph for each set of data. Electropherograms were recorded every 25-30 seconds. I.v. dose was corrected by the i.n./i.v. dose ratio = 6.25.

intravenous fluorescein results initially in significantly higher concentrations in the OB compared to intranasal. Corrected i.v. maximum concentration, Cmax of 23.1 ± 2.5 nM was achieved. This experiment is limited however by length, in time, of the experiment,

and there is a possibility that concentrations of fluorescein in the OB would continue to rise, while i.v. levels continued to decline, indicating the potential for greater drug delivery over time with i.n. administration. Longer *in vivo* sampling and analysis by MD-CE-LIF would address some of these questions.

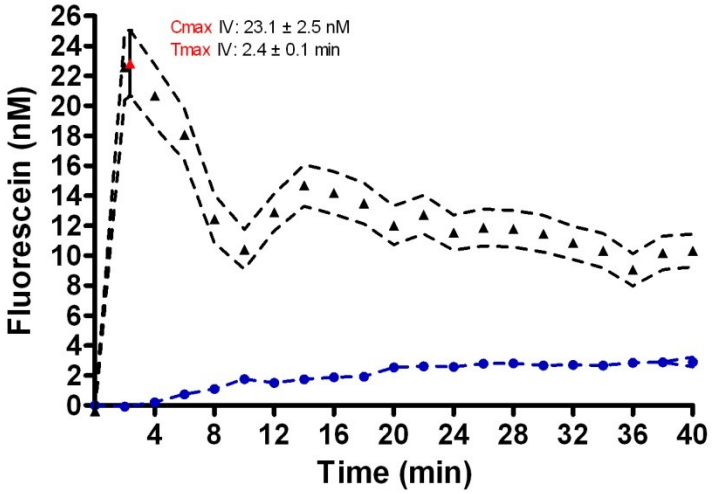

Figure 3.25. First 40 minutes of **DOSE CORRECTED** average pharmacokinetic profile comparisons of i.n. and i.v. fluorescein (nM) in the rat olfactory bulb (OB), measured with online high speed microdialysis capillary electrophoresis with laser induced fluorescence detection. Intranasal Dose (closed circles): F (1mM, 50 nanomoles) in aCSF, 50 µL, N = 5 animals. Intravenous Dose, corrected (closed triangles): F (1mM, 50 nanomoles) in aCSF, 50 µL, N = 3 animals. Each point represents fluorescein in the OB averaged at the initial time point T = 0 (pre dose), and every 2 subsequent minutes (post dose) with the dashed line representing standard deviation. Maximum average fluorescein concentration, Cmax, and time to Cmax, Tmax, is indicated on the graph for each set of data. Electropherograms were recorded every 25-30 seconds. I.v. dose was corrected by the i.n./i.v. dose ratio = 6.25.
.

Intranasal and Intravenous aCSF Administration

In order to further verify fluorescein identification in the olfactory bulb after intranasal administration, and to explore the potential matrix of aCSF, MD-CE-LIF sampling was carried out in the rat olfactory bulb. The intranasal control consisted of 50 µL of aCSF delivered to the right nasal cavity of a rat with MD probe placement in the

right olfactory bulb. Intranasal administration methodologies were carried out for the intranasal aCSF control experiment (see the methods and development section for further details). A representative electropherogram of dialysate sampled 130 minutes post i.n. administration of aCSF dosing can be found in Figure 3.26. The lower black trace of the dialysate from the OB was compared to an electropherogram of aCSF (grey upper trace) sampled prior to insertion in the olfactory bulb, with the microdialysis probe placed directly into a solution of aCSF. Unidentified peaks were evident in the OB dialysate sample at migration times of 13.5 s, 16.5 s, and 25 s. These peaks were not apparent in the *in vitro* aCSF sample. No adverse matrix effects on the separation were evident after i.n. application of aCSF. The peak present at 24.5 seconds coincided with the migration time of fluorescein standards run that day on the MD-CE-LIF system. No fluorescein peak was detected prior to insertion of the MD probe into the olfactory bulb. Possible sources of the unidentified peak at 24.5 s are trace fluorescein from the analytical system,

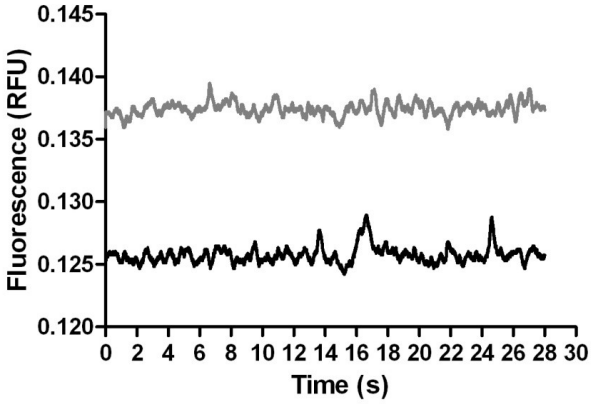

Figure 3.26. Electropherogram of brain dialysate sampled in the OB, 130 min post i.n. dose of aCSF control (black trace). Electropherogram of aCSF (grey trace), sampled via MD-CE-LIF immediately prior to insertion of probe into the OB. Separations were performed every 23.4 s.

or an unidentified peak present in the brain with the same migration time as fluorescein. The peak was not detected at significant levels relative to fluorescein detected in the OB post i.n. administration and did not interfere in any way with *in vivo* experiments. The peak height at fluorescein's known migration time was analyzed throughout the entire 145 minutes of the control experiment (Figure 3.27). Fluorescein (nM) in the olfactory bulb was calculated and plotted over time based on the calibration curve run the day of analysis (Figure 3.28). Fluorescein concentration was below the LOD of fluorescein for the entire intranasal control experiment.

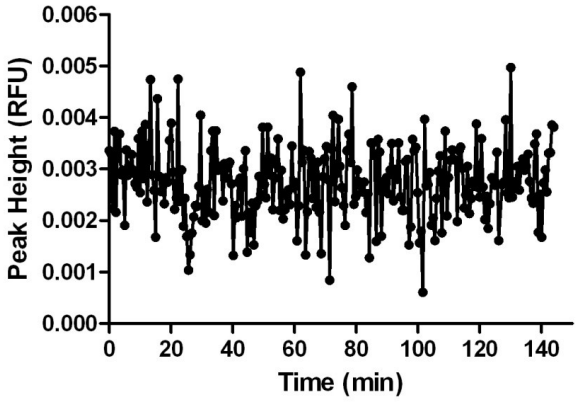

Figure 3.27. Intranasal control: aCSF. Peak height (RFU) at known migration time of fluorescein standard was plotted over the time of the control experiment. Separations were carried out every 23.4 s.

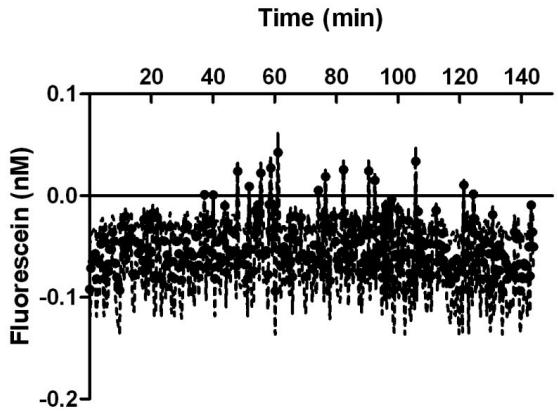

Figure 3.28. Intranasal control: aCSF. Fluorescein (nM) (closed circles) calculated from the analyzed peak height at fluorescein's migration time throughout course of the i.n. experiment. Error bars in the form of standard deviation are depicted by a dashed line above and below.

An intravenous control was carried out via a single injection, mid tail vein, of 50 µL aCSF. Sample delivery was carried out following the same methodologies as i.v. fluorescein injection. A representative electropherogram, taken 30 minutes post i.v. aCSF in the OB (black trace) is shown in Figure 3.29. One small peak at about 6 seconds is

present in the OB dialysate sample. It is not close to the migration time of fluorescein. Fluorescence peak height at the migration time of fluorescein was reported (Figure 3.30).

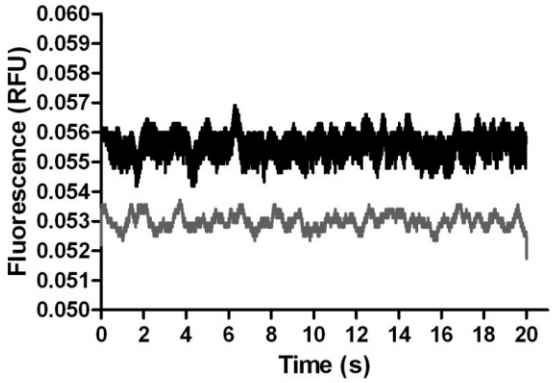

Figure 3.29. Electropherogram of intravenous aCSF control. Brain dialysate sampled via MD-CE-LIF 30 min post i.v. dose of aCSF. Complete separations were performed every 33.4 s

Separations were performed every 33.4 seconds. Fluorescein (nM) was determined based on the peak height at fluorescein's migration time the day of analysis (Figure 3.31). No adverse matrix effects on the electrophoretic separation via MD-CE-LIF were apparent in the i.v. control. No peak at the migration time of the fluorescein standard was apparent.

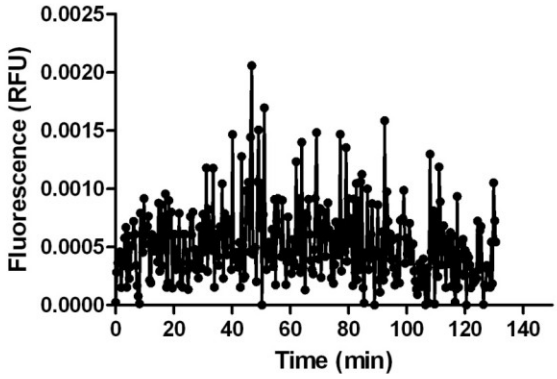

Figure 3.30. Intravenous control: aCSF. Peak height (RFU) at known migration time of fluorescein standard was plotted over the time of the control experiment. Separations were carried out every 33.4 s.

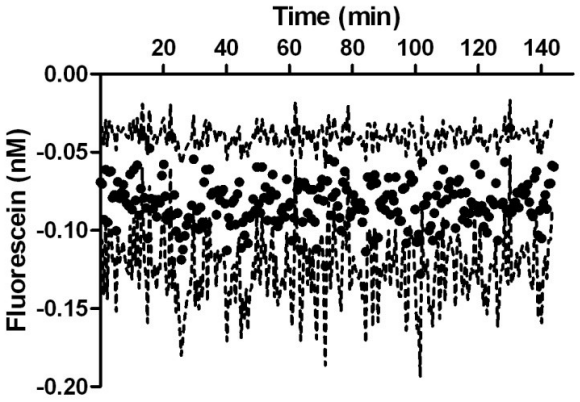

Figure 3.31. Intravenous Control: aCSF. Fluorescein (nM) (closed circles) calculated from peak height at fluorescein standard migration time. Separations were performed every 33.4 s. Standard deviation is represented by dashed line above and below.

Whole blood sample analysis of intravenous and intranasal controls was also performed via MD-CE-LIF, with no matrix interferences indicated, and no peaks present at the migration time of fluorescein (Data not shown).

Intranasal Drug Delivery of Co-Administered Rhodamine 123, Rhodamine, 110, and Fluorescein

Initial MD-CE-LIF assay development and exploratory intranasal drug delivery studies involved co administration of Rhodamine 123 (333 μM), Rhodamine 110 (333 μM), and Fluorescein (333 μM). This approach was designed to study the possible effect charge may have on nose to brain transport, in addition to aiding in the selection of an appropriate compound for intranasal drug delivery studies Rhodamine 110 (Figure of 3.32). has a MW of 366.8 and λex: 496 nm λem:530 nm.

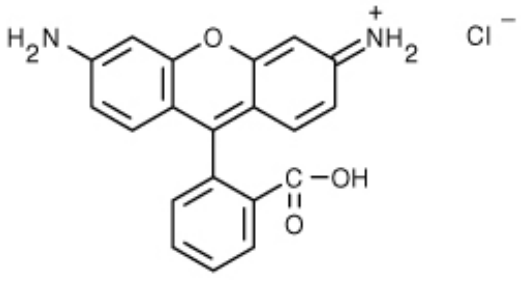

Figure 3.32. Structure of Rhodamine 110

R110 has a low pKa of around 4.3 and is zwitterionic; simultaneously bearing a positive charge on the xanthenes ring and a negative charge on the carboxyl group on the isolated benzene ring.[289] At physiological pH only 1/1000 of R110 molecules in the protonated acidic form bear a positive charge in extracellular medium.[289] The higher the pH the more the negative zwitterionic form of R110 is present. Rhodamine 123 (Figure 3.33) is a green fluorescent cationic dye with a MW of 380.83 and λex: 496 nm and λem:530 nm. Extensive assay development was performed, resulting in baseline resolution of R123, R110, and fluorescein (Figure 3.34). R110, R123, and fluorescein stock solutions (final concentration = 1 μM) were mixed in aCSF, buffered with sodium phosphate (2 mM), pH 7.3, and directly injected onto the MD-CE-LIF

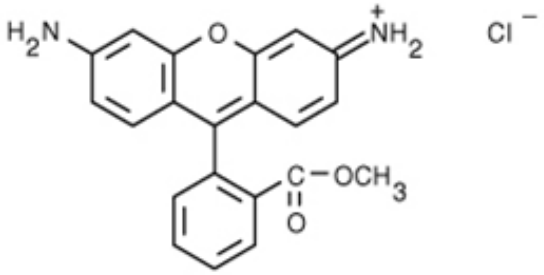

3.33. Structure of Rhodamine 123

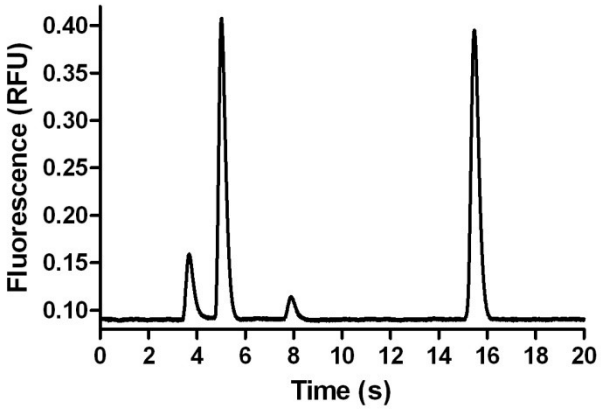

Figure 3.34. MD-CE-LIF electrophoretic separation of 1 μM mixture of Rhodamine 123 (3.7 s), Rhodamine 110 (5.0 s), R110 Impurity (7.9 s), and Fluorescein (15.5 s). Sample was directly injected onto the MD-CE-LIF system. Injection: 100 ms, Delay: 5 s, Separation kV: 23, Injection kV: 21.

system. All separation buffer conditions were equivalent to the final optimized fluorescein assay (see earlier text in the chapter for details). Separation buffer consisted of sodium phosphate (100 mM), pH 10.5, with the same parameters for the sheath flow buffer. Rhodamine 123 exited the separation capillary first with a migration time of 3.7 s, followed by Rhodamine 110 at 5.9 s, an impurity associated with R110 at 7.9 s, and fluorescein at 15.5 s. Achieved peak widths for R123, R110, and fluorescein were 0.9 seconds, 0.4 s, and 0.4 s respectively with theoretical plate counts for R123, R110, and fluorescein of 251, 502, and 3,690 respectively. The cationic fluorescent dye R123 was difficult to work with due to its high adsorption to most instrumental surfaces, particularly fused silica capillary lines, including the microdialysis probe. With its high fluorescence quantum yield, trace R123 was frequently present in electrophoretic separations of aCSF alone. R123 standard was therefore eliminated from mixtures analyzed via MD-CE-LIF prior to intranasal administration experiments. R123 standard migration times were verified post vivo. A representative electropherogram of 10 nM

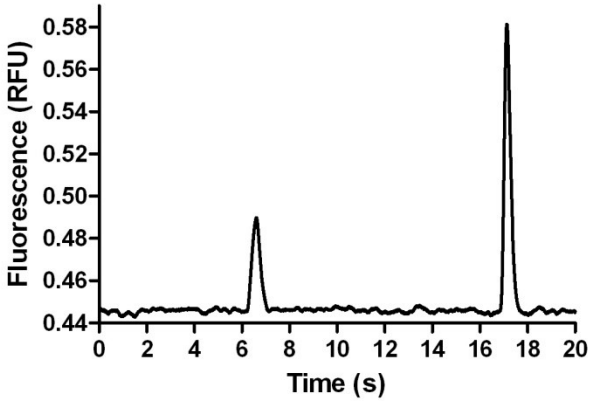

Figure 3.35. Representative electrophoretic separation of 10 nM R110 (6.7 s), and fluorescein (17.2 s). Sampled through MD probe and analyzed via MD-CE-LIF.

R110 and fluorescein in buffered aCSF, pH 7.3, sampled through a MD probe, is shown in Figure 3.35. 10 nM R110 migrated at 6.7 s with a migration time for fluorescein of 17.2 s. Of the three compounds administered intranasally, rhodamine 123 was not detected in the rat olfactory bulb. Rhodamine 110 and fluorescein were detected in the OB approximately 4.2 and 3.1 minutes post i.n. dose, respectively. A representative pharmacokinetic profile of intransally administered R110, co administered with R123 and fluorescein (each 333 µM) is shown in Figure 3.36. A representative pharmacokinetic

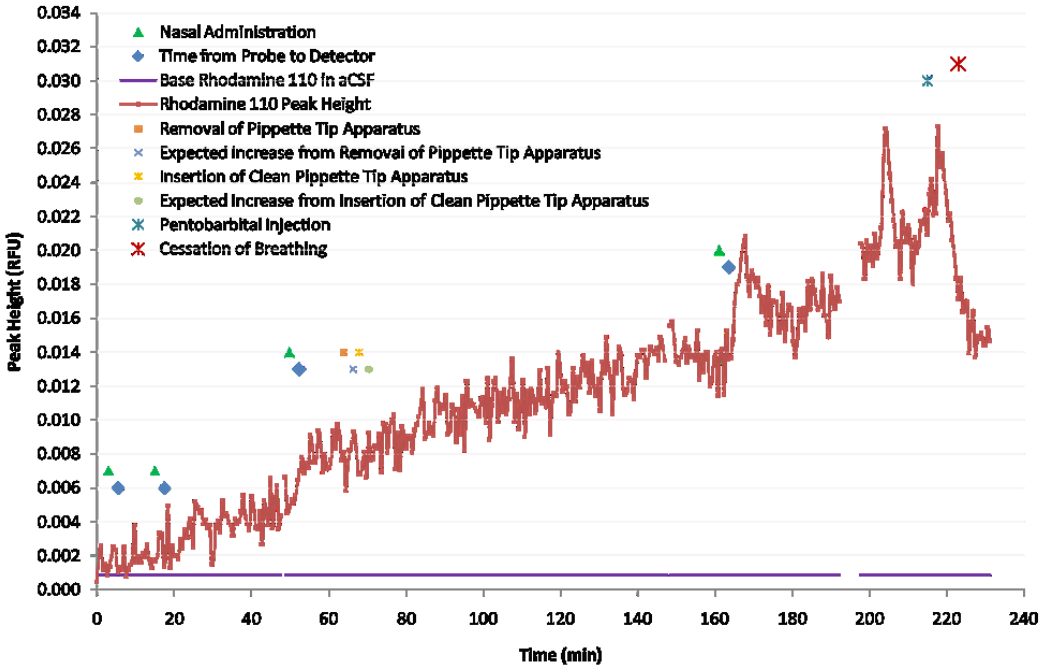

Figure 3.36. Pharmacokinetic profile of rhodamine 110 peak height (red round circles) in the rat olfactory bulb (OB), measured via online high speed microdialysis capillary electrophoresis with laser induced fluorescence detection. Intranasal Dose to the right nostril consisted of a mixture: R123 (333 µM), R110 (333 µM), and F (333 µM), 35 µL. Each circle represents R110 peak height in a single electrophoretic separation. Electropherograms were recorded every 32.4 s. Intranasal doses were administered 3.00, 15.0, 49.8, and 158.8 minutes into data collection (green triangles) and 212 min (dose not indicated on graph). The amount of time for dialysate to travel from the probe outlet to the detector is indicated by the blue diamonds = 2.50 min. Average baseline at the rhodamine 110 migration time in aCSF, is indicated by the purple line. The first fluorescein peak in the olfactory bulb was detected 2.38 minutes post the intranasal dose.

profile of fluorescein in the OB post i.n. dosing of rhodamine/fluorescein mixture is presented in Figure 3.37. Initial intranasal administration of a mixture of 333 µM R123, R110, and fluorescein was carried out 3 minutes into data collection, with repeat i.n. doses at 15.0, 49.8, and 158.8 and 212 minutes into the *in vivo* experiment. Gaps present in data represent the time the instrument was stopped to refill sheath flow or separation

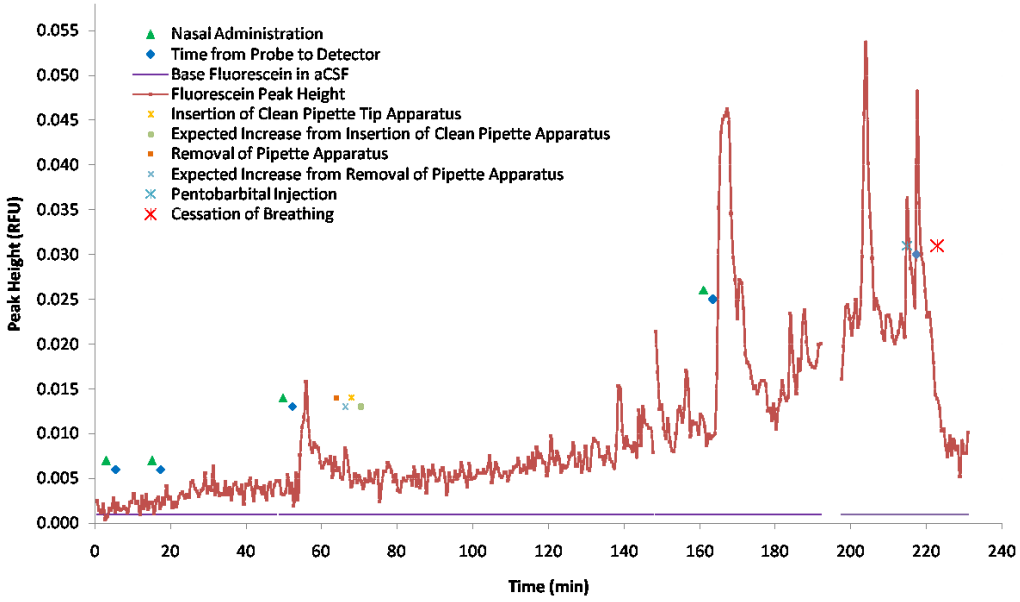

Figure 3.37. Pharmacokinetic profile of fluorescein peak height (red round circles) in the rat olfactory bulb (OB), measured via online high speed microdialysis capillary electrophoresis with laser induced fluorescence detection. Intranasal Dose to the right nostril consisted of a mixture: R123 (333 µM), R110 (333 µM), and F (333 µM), 35 µL. Each circle represents R110 peak height in a single electrophoretic separation. Electropherograms were recorded every 32.4 s. Intranasal doses were administered 3.00, 15.0, 49.8, and 158.8 minutes into data collection (green triangles) and 212 min (dose not indicated on graph). The amount of time for dialysate to travel from the probe outlet to the detector is indicated by the blue diamonds = 2.50 min. Average baseline at the rhodamine 110 migration time in aCSF, is indicated by the purple line. The first fluorescein peak in the olfactory bulb was detected 2.38 minutes post the intranasal dose.

buffer reservoirs. Blue triangles represent the amount of time it takes for dialysate to travel from the probe outlet to the detector, 2.5 minutes this day of analysis. The

intranasal dosing pipette tip apparatus was removed from the nasal cavity at T = 64 minutes, and insertion of a clean pipette tip apparatus occurred at T = 68 minutes. A representative electropherogram of brain dialysate sampled 218 minutes post intranasal administration of R123, R110, and fluorescein (all 333 μM) via MD-CE-LIF is indicated in Figure 3.38.

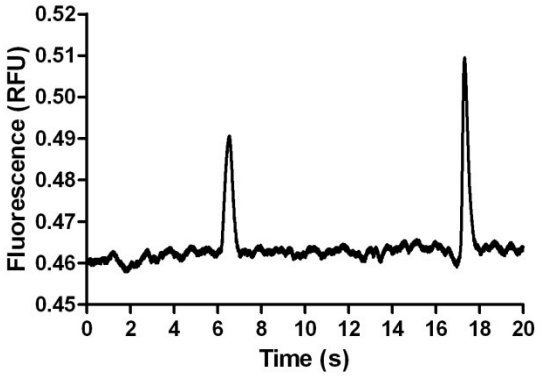

Figure 3.38. Representative electrophoretic separation of brain dialysate 218 minutes post i.n. administration of 333 μM R123 (not detected), R110 (6.7 s), and fluorescein (17.2 s). Sampled through MD probe and analyzed via MD-CE-LIF. Each electrophoretic separation was completed in 32.4 s.

Of interesting significance is the rapid spike in R110 peak height occurring within a single separation (32.4 seconds) after the i.n. dose. This is particularly apparent for i.n. doses administered as the experiment progressed. In addition to the detected spikes in fluorescence peak height for R110, a continuously increasing level of R110 was apparent, possibly indicating multiple mechanisms of transport of R110 from the nose to the olfactory bulb. Fluorescein was also detected in the olfactory bulb post intranasal administration of the R123, R110, and fluorescein mixture. The pharmacokinetic profile obtained for fluorescein was similar to that obtained for R110, with a steadily increasing level of fluorescein in the OB, and spikes in fluorescence signal one separation (32.4 s)

after the intranasal dose. LOD for R110 and fluorescein were determined from calibration curves run the day of analysis. LOD R110 = 963 pM, LOD fluorescein = 237 pM. Approximate Cmax for R110 and fluorescein were reached at the same Tmax = 204 min. Cmax for R110 was approximately 6 nM and Cmax for fluorescein was approximately 4 nM.

As no precedence existed regarding MD-CE-LIF monitoring of nose to brain transport of co administered drugs of various charge, there was concern regarding possible interactions the compounds may have with each other in *in vivo* environments in addition to interactions with the *in vivo* matrix. The intranasal drug formulation was simplified to include fluorescein alone for all future *in vivo* studies. Use of sodium phosphate (2 mM) buffered aCSF solution, pH 7.3, resulted in the formation of a white particulate in the flow gated injection interface, likely due to insolubility of precipitates formed between sodium phosphate and aCSF at the pH of Borate Buffer (100 mM, pH 10.5). This particulate occluded the openings of the separation capillary and the capillary extending from the probe outlet into the flow gated injection interface, and caused blockages within the separation capillary during electrophoretic separations. aCSF was not buffered for future studies to eliminate the possibility that particulate adversely effected the amount of sample injected onto the separation capillary, with could falsely indicate decreasing levels in pharmacokinetic profiles. MD-CE-LIF demonstrated the first high temporal resolution pharmacokinetic profile of rhodamine 110, and fluorescein in the olfactory bulb, indicating the high applicability of the MD-CE-LIF system for intranasal drug delivery studies.

Pharmacokinetic Analysis of Intranasal and Intravenous Fluorescein Studies

Area under the curve (AUC) analyses were performed on the intranasal fluorescein and whole blood fluorescein mean concentration over time profiles from 0 - 120 minutes (AUC→120 and from 0-40 minutes (AUC→40) for both i.n. and i.v. studies. in the brain. It is apparent from these calculations that dose corrected intravenous administration of fluorescein (50 nanomoles) demonstrates significantly more delivery of fluorescein to the olfactory bulb at both AUC→40 and AUC→120, with a 6.5 fold, and 2.7 fold increase over i.n. AUC in the brain, respectively. A summary of pharmacokinetic analysis of i.n. and i.v. *in vivo* administration of fluorescein in the brain can be found in Table 3.03. Intravenous administration demonstrated a higher maximum concentration,

Parameter	Intranasal	Intravenous	Dose Corrected Intravenous
Cmax (nM)	6.6 ± 1.1	3.7 ± 0.4	23.1 ± 2.5
Tmax (min)	81.1 ± 48.1	2.4 ± 0.1	2.4 ± 0.1
Time Post Dose Fluorescein Detected in OB (min)	2.8 ± 0.5	0.8 ± 0.2	2.8 ± 0.5
AUC→120 (nmol x min/L)	418.3	180.5	1128.0
AUC→40 (nmol x min/L)	78.6	82.1	512.9

Table 3.03. Summary of pharmacokinetic analysis in the OB for intranasal and intravenous studies

Cmax i.v. = 23.1 ± 2.5 nM vs. Cmax i.n. = 6.6 ± 1.1 nM, and faster time to maximum concentration, Tmax i.v. = 2.4 ± 0.1 min vs. Tmax i.n. = 81.1 ± 48.1 min. The calculated time for fluorescein to reach the olfactory bulb post i.n. administration was determined to be 2.8 ± 0.5 min vs. i.v. 0.8 ± 0.2 min. Drug targeting to the OB of fluorescein after intranasal and intravenous delivery was calculated by comparing olfactory bulb to blood concentration ratios (Figure 3.39). While intravenous fluorescein resulted in higher area under the curve profiles in the brain, and brain olfactory bulb to blood concentration

ratios were increased for i.v. vs. i.n., there was no statistically significant advantage of intravenous over intranasal dosing (Table 3.04).

Unpaired t test	
P value	0.1943
P value summary	ns
Are means signif. different? (P < 0.05)	No
One- or two-tailed P value?	Two-tailed

Table 3.04 Statistics for brain olfactory bulb to blood concentration ratios.

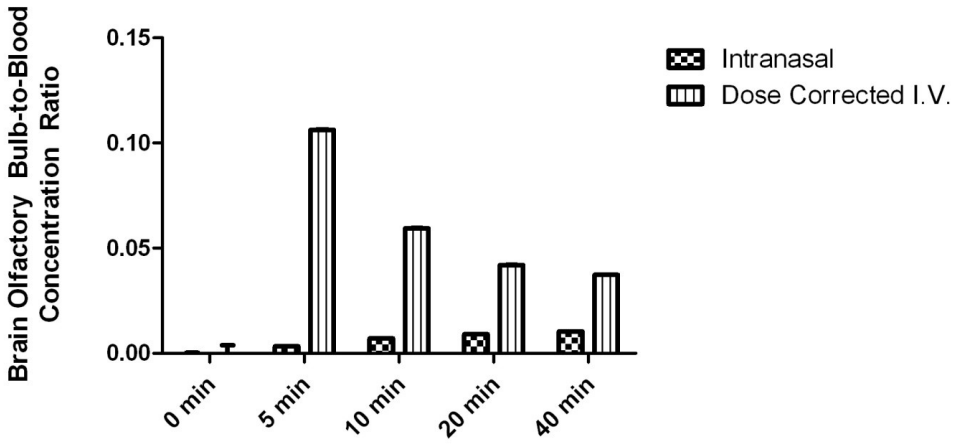

Figure 3.39. Brain olfactory bulb to corrected blood concentration ratios following intranasal and intravenous delivery to anesthetized rats (mean ratio ± SD, n = 3-5 for each time point). Ratios were greater in the OB following intravenous compared to intranasal delivery at all time points post dosing, though not statistically different from those determined for intranasal experiments.

Normalizing the area under the curve (AUC→40) to concentration in the brain was carried out to discern any appreciable differences in intranasal vs. intravenous fluorescein delivery (Figure 3.40). Statistically significant results (Table 3.05) indicate a higher fluorescein exposure over the first 40 minutes for intravenous vs. intranasal administration. Blood samples were not collected past 40 min, due to fluid replenishing restrictions during *in vivo* analysis. The time period used to calculate these numbers is therefore heavily weighted toward the intravenous method of delivery, as it reached Cmax within 2-3 minutes after i.v. dosing and i.n. did not reach Cmax until over an hour

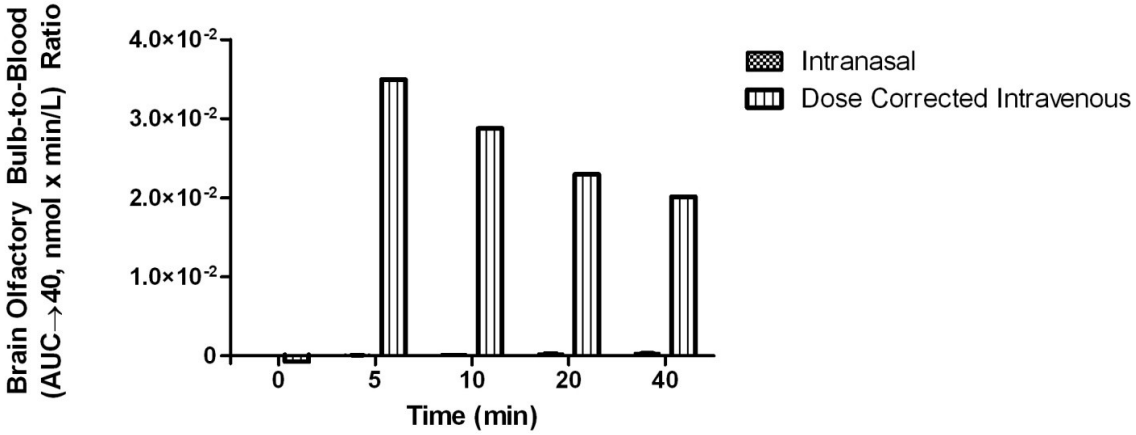

Figure 3.40. Brain concentration to blood AUC dose corrected brain olfactory bulb to blood AUC →40 ratios following intranasal and intravenous delivery to anesthetized rats (mean ratio ± SD, n ≥ 3 for each time point). Ratios were statistically greater in the OB following intravenous compared to intranasal delivery at all time points.

Unpaired t test	
P value	0.0083
P value summary	**
Are means signif. different? (P < 0.05)	Yes
One- or two-tailed P value?	Two-tailed
t, df	t=3.478 df=8

Table 3.05. Statistical analysis of brain concentration to blood AUC→40 (Dose Corrected) ratios.

later. Experimental modifications incorporating fluid replacement would allow collection of more blood samples, and provide a more accurate picture of the pharmacokinetics of fluorescein in the OB over time. This is especially significant as the AUCi.n. increases over time, which is demonstrated over the 120 minutes of analysis for these experiments.

In order to discern the contribution of fluorescein in the OB resulting from intranasal delivery vs. the contribution of fluorescein in the OB resulting from intravenous delivery, the drug targeting index was calculated (DTI). DTI is determined as the ratio of brain AUC/blood AUC after intranasal administration to that after intravenous administration, after being corrected for dose.[25] Intranasal delivery of fluorescein alone

resulted in a 0.56 fold increase in overall drug targeting to the brain compared to intravenous delivery as determined by the DTI (Table 3.06).

DTI t = 40 min	DTP%	Bx using nM in Whole Blood
0.56	-78.43	140.16

Olfactory Bulb and Whole Blood AUC Values (AUC Fluorescein (nM x min/L)	**Intranasal**	**Intravenous**
AUC Brain → 120	418.3	180.5
AUC Brain → 40	78.55	82.07
Dose Corrected AUC Brain → 120	418.3	1128
Dose Corrected Brain AUC Brain → 40	78.55	512.9
AUC Whole Blood (nM) → 40	9682	5660
AUC Whole Blood (nanomoles) → 40	219.8	116.4
AUC Dose Corrected Whole Blood (nM) → 40	9682	35431
AUC Dose Corrected Whole Blood (nanomoles) → 40	219.8	728.9

Table 3.06. Area Under the Curve and Intranasal Drug Targeting Index and Direct Transport Percentage to the Olfactory Bulb

DTI of less than 1 is not significant. This implies that there is no overall statistical difference in targeting to the OB between i.n. and i.v. delivery. Direct transport percentage (DTP%), which can be derived from the DTI is a measure of the direct transport from the nose to the brain.[25, 290] The DTP% (Figure 3.41) subtracts the fraction levels over the first 40 minutes, DTP% is not a useful tool for calculating what %, if any, of the fluorescein observed in the brain is due to direct nose to brain transport.

$$\frac{(AUC_{brain})_{i.v.}}{(AUC_{blood})_{i.v.}} = \frac{Bx}{(AUC_{blood})_{i.n.}}$$

$$DTP\% = \frac{(AUC_{brain})_{i.n.} - Bx}{(AUC_{brain})_{i.n.}} \times 100\%$$

Figure 3.41. Calculation of direct transport percent.

There is currently a debate in literature regarding whether fluorescein and its derivatives can cross from the nose into the CSF and the brain post intranasal administration. It must be noted that significant differences exist between experimental methodologies and play a significant role in the results observed post intranasal delivery, making it sometimes difficult to compare between different studies. There are a multitude of factors including head position, method of delivery, surgical interventions (for animal studies), and delivery volume, which can all influence drug deposition in the nasal cavity and the pathway a drug follows to the CNS after intranasal administration.[23] Concentrations reported with microdialysis intranasal studies are considerably lower than that of brain homogenates, which is to be expected if the fluorescein is taken up into cells easily, and it is expected to do so as fluorescein is used as a viable cell marker in numerous studies. Based on the fast Cmax and time to the olfactory bulb results, it is likely that a small hydrophilic molecule, like fluorescein enters the blood after intranasal administration and then travels to the brain. The rate of decay of fluorescein in the olfactory bulb in intravenous studies could be due to clearance from the brain, or clearance from the blood, decreasing the bioavailability of fluorescein and hence decreasing the absorption dynamics of fluorescein entering the OB from the blood. If the latter is true, it can be theorized that i.n. administration is the more advantageous method of delivery, as it will avoid enzymatic degradation and clearance by the liver and kidneys. Based on preliminary data involving co administration of rhodamine compounds with fluorescein, future i.n. and i.v. studies could incorporate multiple fluorescent compounds of varying charge. Interestingly, the cationic R123 was not detected in the brain post i.n.

administration, however the zwitterionic R110 and doubly anionic fluorescein were detected. Possible barriers to positively charged compounds could exist, specifically related to the negatively charged nasal mucosal layer. Intravenous studies would further clarify whether R123 entered predominantly into the blood, or was cleared via other mechanisms. MD-CE-LIF monitoring of intranasally administered charged fluorescent compounds may elucidate the effect of charge on possible transport mechanisms involving nose to brain transport.

CONCLUSIONS

High speed online microdialysis capillary electrophoresis with laser induced fluorescence detection was used to develop a fluorescein assay with excellent limits of detection, around 35 pM, and high temporal resolution, on the order of 50 seconds. Validation of the developed fluorescein assay in *in vivo* studies achieved the first high temporal resolution pharmacokinetic profiles of fluorescein transport into the olfactory bulb. Time from dose to first detected fluorescein peak in the olfactory bulb was less than 3 minutes in intranasal studies, and less than 1 minute for intravenous studies. Pharmacokinetic profiles of rhodamine 110 in the OB were also obtained, with a time from i.n. dose to detection in the OB of around 3 minutes. Drug therapies capable of directly targeting the CNS and brain are essential for the treatment of neurologically related disease and injury. Bypassing the BBB and nasal mucosa epithelial membrane barriers however is not trivial. Extensive research indicates that direct nose to brain transport is capable of bypassing the BBB and targets the CNS directly, however the

understanding of what occurs to a drug once it reaches the CNS is limited due to poor temporal resolution analytical sampling and analysis methods.

This chapter concludes that intranasally administered sodium fluorescein studies are not ideal in addressing the questions of mechanisms involved in direct nose to brain transport. Fluorescein was found to target the olfactory bulb in both intranasal, and intravenous administration without any statistical advantage of one method of delivery over the other. Of interest, however is the pharmacokinetic profile demonstrated by fluorescein in the olfactory bulb after intranasal administration: it continues to increase over time, without being adversely effected by clearance mechanisms in the brain and vascular system. This result is particularly significant considering the mucosal clearance time in rats is typically on the order of 5 minutes. A resultant higher overall exposure of the brain to fluorescein could occur after intranasal administration vs. intravenous over an extended period of time, a concept with high applicability in ensuring drugs remain in the CNS at therapeutically relevant concentrations. Transfer of fluorescein across the BBB does appear likely with detection of fluorescein in the OB post i.v. dose, and the fast rate at which fluorescein reached the O.B. Future studies should ideally incorporate a fluorescent compound that can cross into the brain intranasally, but not undergo transport into the brain after intravenous administration, e.g. small peptide drugs or Fluorescein isothiocyanate labeled dextran of mid molecular weight (<20,000 Da).

In conclusion the developed fluorescein assay demonstrates the high applicability and potential of utilizing high speed online microdialysis capillary electrophoresis with laser induced fluorescence detection in the study of brain pharmacokinetics in

conjunction with intranasal drug delivery studies. The first high temporal resolution pharmacokinetic profiles of fluorescein in the rat olfactory bulb were achieved.

This work was a collaborative project with Dr. William H. Frey II, Dr. Leah Hanson, and Dr. Jared Fine at the Alzheimer's Research Center at Regions Hospital in St. Paul, MN. The author would like to thank Aleta Svitak at the Alzheimer's Research Center for performing all intravenous fluorescein dose injections. The author would also like to thank Dr. Shyeilla Dhuria for her time and correspondence regarding pharmaceutical data analysis. Financial support for this research was provided by the University of Minnesota, the Alzheimer's Research Center, and National Institutes of Health (Grants GM063533 and NS043304) and is greatly appreciated.

Chapter 4:

Intranasal Administration of Fluorescein with Nasal Absorption Enhancers

INTRODUCTION

Intranasal delivery of peptides and proteins demonstrate significant promise in the development of drug therapies directly targeting central nervous system (CNS) damage and neurodegenerative diseases such as Alzheimer's disease. Cyclodextrins (CD) have been commonly studied as intranasal absorption enhancers due to their low nasal and systemic toxicity. While the mechanisms of the enhancing effect of CD are not completely understood, extensive literature indicates that methylated CDs significantly enhance nasal absorption for intranasal drug delivery. Hydroxypropyl-*β*-cyclodextrin (HPβCD) has demonstrated little damage when administered to nasal cilia and mucosa and has been found to be well tolerated in numerous animal species (rats, mice and dogs).[251] In addition to the good membrane and cell safety profile, HP*β*CD is soluble in water (as high as 50%) and can be used as a carrier to increase the solubility of poorly soluble drugs.[225] Chitosan studies indicate non toxicity to the local nasal mucosal environment and its absorption promoting abilities have demonstrated that it is also an ideal candidate for continued exploration in nasal drug delivery studies. Chitosan and HP*β*CD were therefore selected in this study as nasal absorption enhancers for intranasal administration of fluorescein.

Chapter 3 of this thesis has proven that high temporal resolution pharmacokinetic profiles of fluorescein can be obtained with high speed online microdialysis (MD) capillary electrophoresis (CE) with laser induced fluorescence detection (LIF) after intranasal and intravenous administration of fluorescein. This chapter will focus on fluorescein combined with two separate absorption enhancers, chitosan and HP*β*CD, with

brain pharmacokinetics measured in the rat olfactory bulb. *In vivo* measurements of fluorescein were made in the rat olfactory bulb to demonstrate the effectiveness of chitosan and HPβCD as enhancers of intransally delivered fluorescein. Whole blood samples were drawn and analyzed via microdialysis to elucidate fluorescein's likely nose to brain delivery pathways. Pharmacokinetic profiles of fluorescein in the olfactory bulb were attained with temporal resolution not demonstrated previously published in any intranasal drug delivery study. A single chitosan experiment did not indicate increased absorption and detection of fluorescein in the rat olfactory bulb. HPβCD demonstrated statistically significant fluorescein enhancement in the rat olfactory bulb relative to intransally administered fluorescein without an absorption enhancer.

The work presented in this chapter is part of a collaborative project with the Alzheimer's Research Center at Regions Hospital in St. Paul, MN to determine whether the MD-CE-LIF system is compatible with research involving *in vivo* analysis of intranasally administered drug therapies. Frey, Hanson, Thorne, Liu, Dhuria, et al. have developed a careful characterization of nose to brain transport, indicating the existence of a direct nose to brain pathway post intranasal administration.[17-27] The rate at which a drug reaches the brain is indicative of the transport mechanisms involved the drugs path to the brain post intranasal administration. The rate of decline of a drug can indicate possible clearance mechanisms. Application of nasal absorption enhancement compounds to intranasally administered drugs may increase the bioavailability of the drug in target regions of the CNS at therapeutically relevant levels and increase the rate at which a drug can reach the CNS.

High speed online MD-CE-LIF analysis was used to study and develop fluorescein pharmacokinetics in the rat olfactory bulb in response to fluorescein co administered with two separate nasal absorption and permeation promoters: HPβCD and Chitosan, delivered intranasally. In contrast to the poor temporal resolution and 15-20 minute HPLC, and radioimmunoassay analysis of intransally administered compounds, our instrument is capable of 20-30 second electrophoretic separations. This dramatic improvement in temporal resolution will demonstrate the importance of high speed separations for the monitoring of *in vivo* pharmacokinetic dynamics and the high potential application of MD-CE-LIF to high throughput analysis and development of pharmacokinetic drug profiles with the best temporal resolution, precision, and long term stability available to current drug therapy research.

MATERIALS AND METHODS

Chemicals and Reagents

Unless otherwise noted, all chemicals were obtained from Sigma Aldrich. (St. Luois, MO, USA) or the University of Minnesota Boynton Health Services Pharmacy (Minneapolis, MN). Separation and sheath flow buffer was Sodium Borate (100 mM) pH 10.50. All buffers were prepared in deionized water (Milli-Q, 1.2 MΩ, Millipore Corporation, Bedford, MA) and were filtered (0.2 μm) prior to use. Artificial cerebral spinal fluid (aCSF) consisted of NaCl (145 mM), KCl (2.7 mM), $MgSO_4$ (1.0 mM) and $CaCl_2$ (1.2 mM).Various concentrations of fluorescein were prepared in aCSF. Ketamine cocktail consisted of: Ketamine HCl (100 mg/mL), Xylazine HCl (100 mg/mL), and Acepromazine (10 mg/mL) administered at a final concentration of ketamine (30 mg/kg),

xylazine (6 mg.kg), and acepromazine (1 mg/kg) and dose of 0.7 mL/kg by subcutaneous injection. Chitosan (0.5% w/v) was prepared in an aCSF and 1% (v/v) glacial acetic acid solution. Hydroxypropyl-β-cyclodextrin (9.9% w/v) was prepared in aCSF.

In Vivo Monitoring-Intranasal Administration of Fluorescein and Nasal Absorption Promoters Chitosan and Hydroxypropyl-β-cyclodextrin

All animal experiments were performed in strict accordance with protocols approved by the Institutional Animal Care and Use Committee at the University of Minnesota. Monitoring of fluorescein was carried out in the rat olfactory bulb of male Sprague-Dawley rats (250 to 380 grams). Two studies were carried out to determine effect of nasal absorption enhancers on brain uptake of i.n. administered fluorescein: 1) a single intranasal (i.n.) dose of Fluorescein (1 mM, 150 nanomoles) and Chitosan (0.5%, in aCSF and glacial acetic acid (1%), volume = 50 μL) was administered to the right nasal cavity and 2) a single intranasal (i.n.) dose of Fluorescein (1 mM, 50 nanomoles) and HPβCD (9.9% w/v in aCSF), volume = 50 μL, was administered to the right nasal cavity. Rats were anesthetized via a subcutaneous injection of ketamine cocktail (up to two full doses, ½ at a time), then maintained anesthesia with straight ketamine at ½ doses as needed. Anesthesia was monitored until the animal no longer exhibited limb reflex to a toe pinch. A lab constructed intranasal pipette tip apparatus consisted of approximately 25 mm of a gel loading pipette tip inserted into approximately 25 mm of tygon tubing. The pipette tip apparatus was inserted 15 mm into the right nasal cavity approximately 20-30 minutes post initial anesthesia application (animal no longer exhibited limb reflex to toe pinch) and prior to placement of the animal into the stereotaxic frame. After

placement of the pipette tip apparatus into the right nasal cavity, the animal was transferred to a stereotaxic frame. Ear bars were secured in place. Surgery was performed to expose the brain region of interest. The stereotaxic frame was used to implant a microdialysis probe into the right olfactory bulb: +7.0 mm AP (anterior/posterior), - 0.9 mm ML (medial/lateral) and -5.5 mm DV (dorsal/ventral) from bregma, the craniometric point at the junction of the sagittal and coronal sutures at the top of the cranium[270] (Figure 4.01 and Figure 4.02). D/V was measured from the surface of the brain post surgical exposure of the probe implantation site. The probe was inserted slowly to minimize tissue damage over a period of 15 minutes at approximately 500 μm/min. Data collection began one hour after the probe was inserted fully to allow time for the tissue surrounding the probe to recover from the damage caused by probe implantation. 30 minutes post MD probe placement into the olfactory bulb, the animal was placed in a supine position by inversion of the stereotaxic frame. The corners of the inverted stereotaxic frame were placed onto the supporting pillars of a home built machined platform table, inverted onto the surface of the experiment station, with supporting pillars extending approximately 12 inches upward. The animal was secured to the stereotaxic frame via a self designed supportive sling. The dorsal position of the animal's head was facing the bench counter top, with the surface of the skull and nasal cavities parallel to the bench top throughout all *in vivo* experiments. The microdialysis probe was continuously perfused with aCSF throughout the inversion process. The probe outlet remained directly connected to the CE-LIF instrument to reduce introduction of air bubbles into capillary lines, capillary connections, and the microdialysis probe itself. Body temperature of 37 ^{o}C was

maintained and monitored via a self adjusting rectal temperature probe, and heating pad (Fine Science Tools Inc. Foster City, CA) The intranasal dose of fluorescein in aCSF was performed 1 hour post probe placement via a blunt tipped 1 cc microsyringe upon insertion into the pipette tip apparatus. With approximately 10-15 µL of dead volume at the end of the pipette tip apparatus, total volume of fluorescein in delivery syringe was 60-65 µL. After the i.n. dose, the pipette tip apparatus was removed from the nasal cavity.

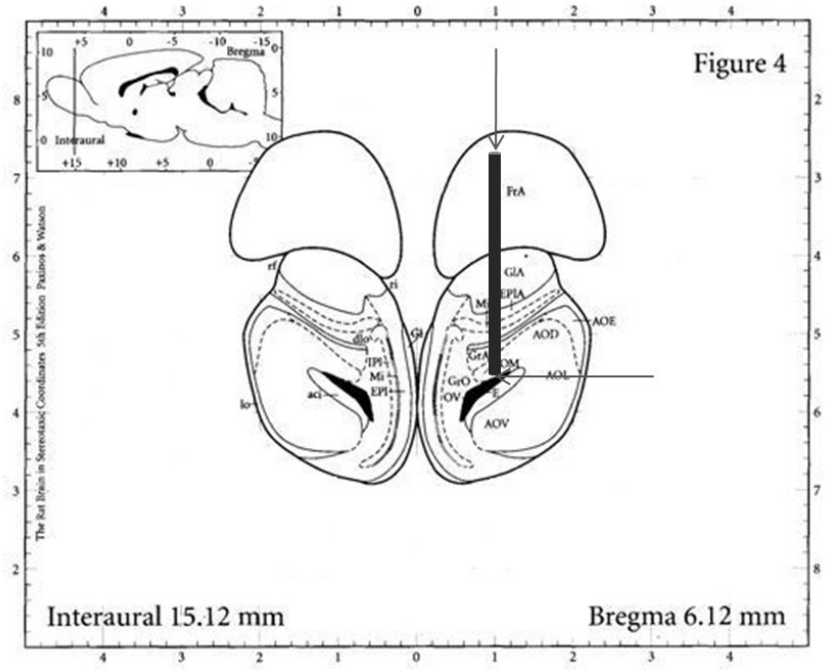

Figure 4.01. Diagram of rat brain olfactory bulb section.[270] Depicted slice is 6.12 mm anterior to bregma. The vertical arrow is placed 0.90 mm in the medial/lateral (ML) plane. The horizontal arrow is placed -5.5 mm in the dorsal/ventral (DV) plane. Microdialysis probe specifications are 3mm by 0.2 µm.

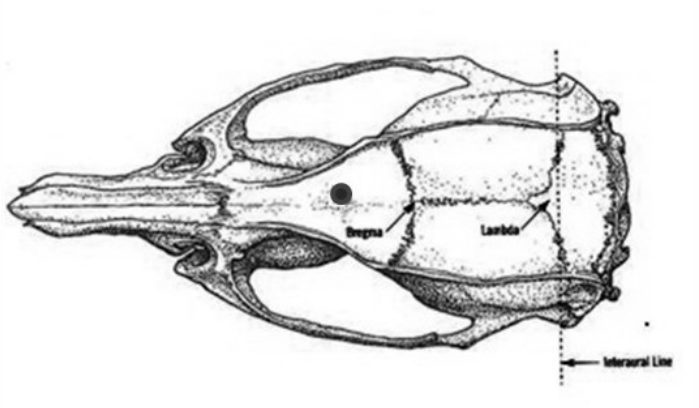

Figure 4.02 Diagram of dorsal view of surface of rat skull.[270] Solid circle depicted on the surface of the rat skull is the location of surgery on the skull for implantation of microdialysis probe. The anterior/posterior A/P distance from bregma is 7.0 mm. Microdialysis probe specifications are 3mm by 0.2 μm.

Analysis of Fluorescein in Whole Blood Post Intranasal Administration

Whole blood samples were drawn prior (as a control) and during the *in vivo* analysis of the i.n. administration of fluorescein to quantify fluorescein in the blood. This analysis was done to determine how much drug measured in the brain was due to direct nose-to-brain delivery and how much was from the blood when drug was delivered. Post the i.n. fluorescein dose 80 μL aliquots of whole blood were collected at 4 time points: 5, 10, 20, and 40 minutes. Blood was drawn from the tail of the anesthetized rat using a distal tail slice method. This procedure was carried out by using a 5.5 mm "Goldenrod" animal lancet or alternately an 18-16 gauge needle to centrally bisect the most distal 2-3 mm portion of the tail vein. It was easy to open the incision for blood collection (via a finger flick to the incision site), and easy to close with compression (via tying a gauze strip over the incision site) between blood collections. Other methods of blood collection were considered, however the experimental setup was prohibitive to many traditional blood sample collection methods. Cheek puncture was not a viable option. First, the rat's

head was secured in a stereotaxic device, and the precise location of the microdialysis probe in the brain could be compromised by pressure against the head during the blood draw. Second, the drug concentrations in the head region may not accurately represent those in the rest of the body because it was so close to the nose following intranasal drug delivery. Orbital sinus was not possible because the rat's head is in a stereotaxic frame. Cardiac puncture was not ideal for multiple aliquots sampling and the high risk of animal death during the procedure. Axillary bleed was also inaccessible due to the stereotaxic frame. Total drawn blood volume ranged from 300-750 µL, and the rats weighed 250-380 g. Percent of body weight drawn was approximately 0.1%-0.3% eliminating any fluid replacement concerns. All whole blood samples were placed in cool storage (2-8 ^{o}C) for analysis via microdialysis (MD) capillary electrophoresis (CE) with laser induced fluorescence detection (LIF). Analysis of whole blood samples was carried out within 12 hours of sample collection. The microdialysis probe, coupled to the high speed online CE-LIF system, was perfused at 40 µL/hr with artificial cerebrospinal fluid (aCSF) and placed directly into the whole blood samples.

Intranasal Whole Blood Standard Curve

Prior to the i.n. fluorescein + nasal absorption enhancer dose, approximately 560 µL of whole blood was collected from the anesthetized rat for a standard blood curve in a CAPIJECT 500 µL Lithium Heparin Gel Barrier collection tube (12.5 I.U., mint green cap). 80 µL aliquots of whole blood were distributed into six 600 µL microcentrifuge vials. At the time of analysis via MD-CE-LIF, each 80 µL aliquot of whole blood was spiked with 20 µL of fluorescein standard stock solution (varied concentration) for a final

standard concentration range of 300 pM to 100 nM Fluorescein. One 80 µL aliquot was spiked with 20 µL of aCSF without fluorescein as a blank control. The MD probe was placed into fresh aCSF in between the sampling of each whole blood standard vial. At the time of analysis via MD-CE-LIF, the spiked blood standard curve was run first, followed by the whole blood samples taken post i.n. fluorescein administration.

In Vivo Monitoring of Intravenous Administration of Fluorescein

All animal experiments were performed in strict accordance with protocols approved by the Institutional Animal Care and Use Committee at the University of Minnesota. Monitoring of fluorescein was carried out in the rat olfactory bulb of male Sprague-Dawley rats (250 to 380 grams). Studies were carried out to measure the delivery and pharmacokinetics of fluorescein in the brain via a high speed online microdialysis (MD) capillary electrophoresis (CE) with laser induced fluorescence (LIF) detection method. In an attempt to discern what percent of fluorescein in the brain was due to a direct nose to brain pathway post i.n. administration, intravenous administration of fluorescein studies were performed. A single intravenous (i.v.) dose of fluorescein (160 µM, 8 nanomoles), volume = 50 µL was administered mid tail directly into the tail vein via a 1 cc Kendall Monoject Ultra Comfort syringe (28 gauge x ½ inch Length). The microdialysis probe was placed into the right olfactory bulb at stereotaxic coordinates + 0.7 A/P, +0.09 M/L, – 0.55 D/V, and allowed one hour for equilibration prior to i.v. dosing. The rats were anesthetized via a subcutaneous injection of ketamine cocktail (up to two full doses), then maintained anesthesia with straight ketamine. Anesthesia was monitored until the animal no longer exhibited limb reflex to a toe pinch. The animal was

then transferred to the stereotaxic frame. Ear bars were secured in place. Surgery was performed to expose the brain region of interest (Figure 3.02, earlier in text). The probe was inserted slowly to minimize tissue damage over a period of 15 minutes at approximately 500 μm/min. Data collection began one hour after the probe was inserted fully to allow time for the tissue surrounding the probe to recover from the damage caused by probe implantation. 30 minutes post MD probe placement into the olfactory bulb, the animal was placed in a supine position by inversion of the stereotaxic frame. The corners of the inverted stereotaxic frame were placed onto the supporting pillars of a home built machined platform table, inverted onto the surface of the experiment station, with supporting pillars extending approximately 12 inches upward. The animal was secured to the stereotaxic frame via a self designed supportive sling. The dorsal position of the animal's head was facing the bench counter top, with the surface of the skull and nasal cavities parallel to the bench top throughout all *in vivo* experiments. The microdialysis probe was continuously perfused with aCSF throughout the inversion process. The probe outlet remained directly connected to the CE-LIF instrument to reduce introduction of air bubbles into capillary lines, capillary connections, and the microdialysis probe itself. Body temperature of 37 ^{o}C was maintained and monitored via a self adjusting rectal temperature probe, and heating pad (Fine Science Tools Inc. Foster City, CA) The intravenous dose of fluorescein was performed 1 hour to 1 hour and 10 minutes post probe placement After the i.v. dose, the delivery syringe was immediately removed from the tail vein, and pressure applied to the i.v administration site via a tied gauze strip.

Analysis of Fluorescein in Whole Blood Post Intravenous Administration

Whole blood samples were drawn prior (as a control) and during the *in vivo* analysis of the i.v. administration of fluorescein to quantify fluorescein in the blood. This analysis was done to determine how much drug measured in the brain was due to direct nose-to-brain delivery and how much was from the blood when drug was delivered. Post the i.n. fluorescein dose 80 µL aliquots of whole blood were collected at 4 time points: 5, 10, 20, and 40 minutes. Blood was drawn from the tail of the anesthetized rat using a distal tail slice method. This procedure was carried out by using a 5.5 mm "Goldenrod" animal lancet or alternately an 18-16 gauge needle to centrally bisect the most distal 2-3 mm portion of the tail vein. It was easy to open the incision for blood collection (via a finger flick to the incision site), and easy to close with compression (via tying a gauze strip over the incision site) between blood collections. All whole blood samples were placed in cool storage (2-8 ^{o}C) for analysis via microdialysis (MD) capillary electrophoresis (CE) with laser induced fluorescence detection (LIF). Analysis of whole blood samples was carried out within 12 hours of sample collection. The microdialysis probe, coupled to the high speed online CE-LIF system, was perfused at 40 µL/hr with artificial cerebrospinal fluid (aCSF) and placed directly into the whole blood samples.

Intravenous Whole Blood Standard Curve

Prior to the i.v. fluorescein dose, approximately 560 µL of whole blood was collected from the anesthetized rat for a standard blood curve in a CAPIJECT 500 µL Lithium Heparin Gel Barrier collection tube (12.5 I.U., mint green cap). 80 µL aliquots of whole blood were distributed into six 600 µL microcentrifuge vials. At the time of

analysis via MD-CE-LIF, each 80 µL aliquot of whole blood was spiked with 20 µL of fluorescein standard stock solution (varied concentration) for a final standard concentration range of 300 pM to 100 nM Fluorescein. One 80 µL aliquot was spiked with 20 µL of aCSF without fluorescein as a blank control. The MD probe was placed into fresh aCSF in between the sampling of each whole blood standard vial. At the time of analysis via MD-CE-LIF, the spiked blood standard curve was run first, followed by the whole blood samples taken post i.v. fluorescein administration.

Microdialysis

Side-by-side microdialysis probes were constructed in-house (Figure 4.03). Briefly, two 40 µm i.d. × 105 µm, o.d. pieces of fused silica capillary (Polymicro Technologies, Phoenix, AZ) were staggered by 3 mm and inserted into a 200 µm diameter piece of hollow fiber, regenerated cellulose, dialysis tubing (18,000 MWCO, Spectrum Laboratories, Rancho Dominquez, CA) and sealed using polyimide (Alltech, Deerfield, IL), leaving a 3 mm sampling region exposed. Probes were perfused with ethanol (60 µL/hr for 50 min) and aCSF (60 µL/hr for 30 minutes) prior to use. The microdialysis probe was perfused with aCSF at 40 µL/hr (0.66 µL/min). Relative recovery of the probe was determined with the online capillary electrophoresis instrument. The MD probe was placed into an aCSF solution containing 100 nM fluorescein and the peak heights were determined. The same solution of aCSF and fluorescein was then pumped directly to the flow gated injection interface and peak

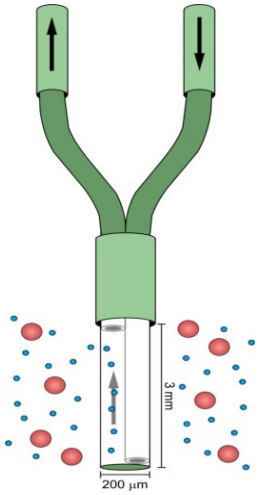

Figure 4.03. Schematic of Side by Side Microdialysis Probe.

height was determined. The ratio of the peak height of fluorescein determined via the MD probe and the peak height of fluorescein directly injected without the MD probe was the relative recovery.

In Vitro Characterization

Recovery of the dialysis probes was measured by comparing the peak area resulting from analyte sampled through the probe to the peak area that results when the same analyte solution is pumped directly into the reaction cross. Temporal resolution was determined by moving the microdialysis probe from aCSF to a solution containing 100 nM Fluorescein in aCSF for 3 minutes and then returning the probe to aCSF.

Flow gated injection interface

The dialysate was sampled for the online MD-CE-LIF system by a flow gated injection interface[28, 30, 33, 34, 88, 92, 95, 96]. The flow gated injection interface was machined out of a polycarbonate block by the U of MN Machine Shop. The capillary connected to the microdialysis probe outlet was inserted into the top of the flow gate, with a 20-50 μm gap separating it from the separation capillary, which was inserted into the bottom side of the flow gate (Figure 4.04). Separation buffer flow rate across the flow gated interface was 40 mL/hr. When the separation buffer was flowing, brain dialysate and samples in aCSF were carried to waste. To perform a sample injection, cross flow of the buffer was

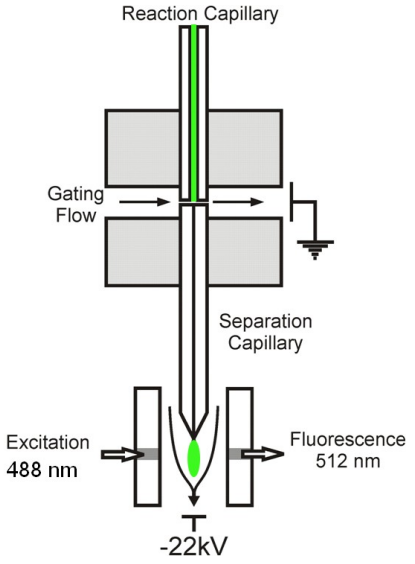

Figure 4.04. Schematic of flow gated injection interface and sheath flow cuvette cell.

stopped via a pneumatically actuated valve (Valco Instruments Co. Inc.),for a specified period of time. The injection voltage was applied for specified period of time, and a plug of sample in loaded onto the separation capillary. The cross flow of the separation buffer was stopped for 0.8-2 s, injection of brain dialysate occurred for 800-900 ms at -22 kV. Cross flow was resumed and separation voltage across the separation capillary was applied at -23 kV.

High speed Online Capillary Electrophoresis with Laser Induced Fluorescence Detection

A schematic of the online MD-CE-LIF system is shown in (Figure 4.05). LIF detection was performed off capillary in a high sensitivity sheath flow cell.[34, 102, 268] Separation of fluorescein was carried out in a 360 μm O.D./5 μm I.D. fused silica capillary (Polymicro Technologies, Phoenix, AZ, USA) 7.4-7.7 cm long. The separation capillary was inserted into a 200 x 200 μm square fused silica cuvette (NSG Precision Cells, Inc, Farmindale, NY, USA). Sheath flow buffer (Borate, 100 mM, pH 10.5) flowed through the cuvette, and around the separation capillary. This flow induced a laminar flow profile of the sample exiting the separation capillary. The exiting end of the separation capillary was ground to a fine tip using a

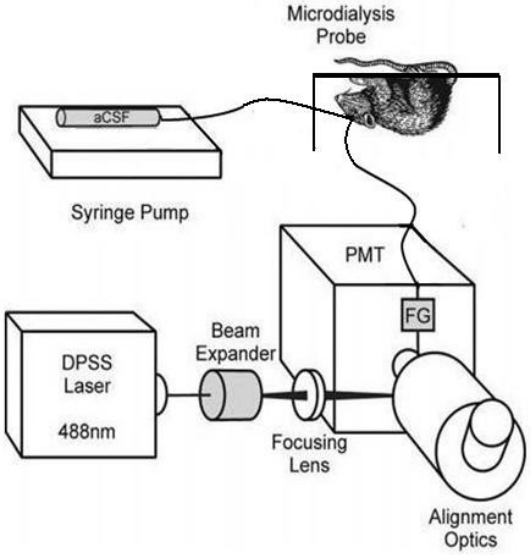

Figure 4.05. Schematic of the online microdialysis CE LIF detection system. A microdialysis probe is inserted into the rat olfactory bulb and perfused with artificial cerebrospinal fluid (aCSF). Dialysate is carried from the probe outlet to the online high speed capillary electrophoresis with high sensitivity laser induced fluorescence detection system where it is analvzed for fluorescein.

dremel tool. The 488 nm line (20 mW) from a diode pumped solid state laser (Sapphire, Coherent, Santa Clara, CA) was used for excitation. The laser beam was expanded with a 10 × beam expander (Edmund Optics, Barrington, NJ) and passed through a 1× focusing lens. The beam was focused off of the end of the separation capillary inside of the sheath flow cuvette. Fluorescence was collected at 90° through a 60 ×, 0.7 NA long working distance objective (Universe Kogaku, Oyster Bay, NY), passed through spatial and band-pass filters (510 ± 10 nm) (Melles Griot, Irvine, CA USA) and collected on a photomultiplier tube (PMT R1477, Hamamatsu Corp., Bridgewater, NJ). Current from the PMT was amplified, filtered (300 ms rise time), and recorded using a data acquisition card (National Instruments Corp., Austin, TX). Data analysis was performed using Cutter Analysis 7.0.

Data Analysis

Dose normalized concentrations in the olfactory bulb and whole blood samples from intranasal and intravenous experiments at 5, 10, 20, and 40 minutes were calculated and expressed in nmol/L (assuming a density of 1g/mL) as mean ± S.D. Unpaired two-sample t-tests were performed on concentrations in the rat olfactory bulb and whole blood samples to compare intranasal and intravenous groups at each time point using GraphPad Prism software (version 4.0, GraphPad Software, Inc., San Diego, CA). Differences between groups were significant if $p < 0.05$.

The area under the concentration time curve (AUC) was generated from mean concentration time pharmacokinetic profiles from 0-120 minutes (AUC→120min) for olfactory bulb and blood fluorescein concentrations, without extrapolation to infinity,

using the trapezoidal method. AUC→40 min was also calculated for comparison of intranasal and intravenous studies to whole blood samples, without extrapolation to infinity.

Intranasal drug targeting of fluorescein to the rat olfactory bulb was assessed by 3 approaches: 1) normalizing intravenous fluorescein concentrations in the olfactory bulb and blood to dose, 2) normalizing intravenous and intranasal fluorescein concentration in the olfactory bulb and blood to AUC→40,and 3) by determining the drug targeting index (DTI),[209] a measure of the difference in targeting between intranasal and intravenous delivery.[25] The DTI was calculated as the ratio of brain AUC/blood AUC after intranasal administration to that after intravenous administration, after being corrected for dose.[25]

RESULTS AND DISCUSSION

In vitro Characterization of MD-CE-LIF system in aCSF and Whole Blood

Online microdialysis CE-LIF offers significant advantages over traditional intranasal analytical techniques due to its ability to monitor chemical dynamics over time with high temporal resolution. Figure 4.06 illustrates the instrument response to the introduction of a step change in fluorescein concentration at the surface of the microdialysis probe. The probe was moved from a solution of aCSF to a 300 pM fluorescein spiked aCSF standard solution for 3 minutes and back to aCSF again for 2 minutes, then moved to a solution of 500 pM fluorescein for 3 minutes and back to aCSF again for two minutes. The signal reached a plateau in approximately 2 separations. Separations were performed every 25.4 seconds, indicating a temporal resolution of 50.8

seconds. Figure 4.07 and Figure 4.07A illustrate the temporal response of the instrument while the microdialysis probe is inserted into rat whole blood samples, spiked with

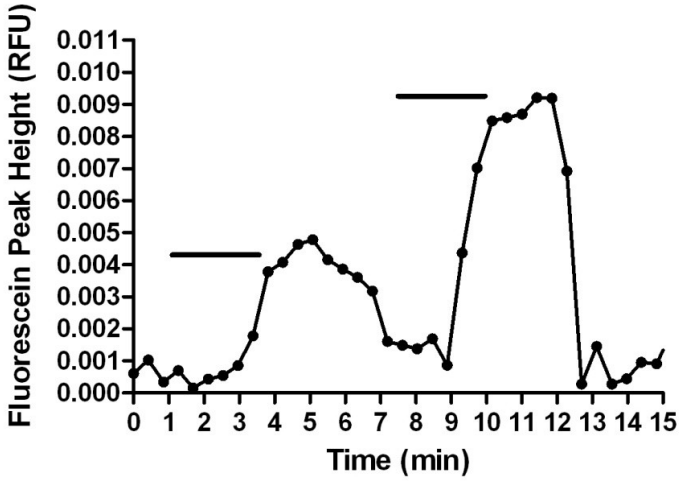

Figure 4.06. Temporal response of the MD-CE-LIF System. The microdialysis probe was moved from aCSF to aCSF spiked with 300 pM fluorescein for 3 minutes (denoted by the black bar) and back again to aCSF, then inserted into aCSF spiked with 500 pM fluorescein for 3 minutes and back again to aCSF.

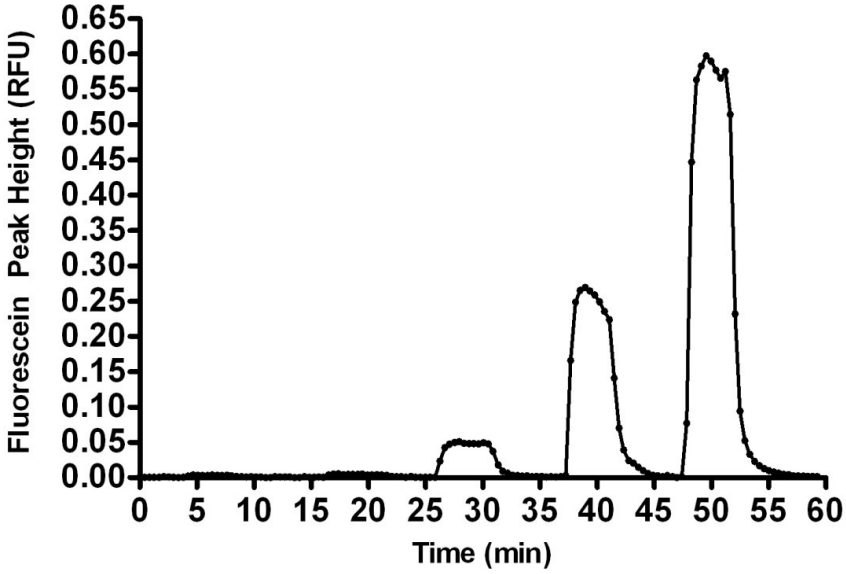

Figure 4.07. In vitro characterization: temporal response of microdialysis probe to whole blood spiked with fluorescein standard solution in aCSF. Microdialysis probe was place in aCSF, transferred to a whole blood standard spiked with varying concentrations of fluorescein, at equal volumes. Response of MD-CE-LIF instrument from 300 pM F (4-8 minutes) to 100 nM F (48-52 minutes) in whole blood. Each electrophoretic separation was 25.4 seconds. A 10-90% change in baseline occurs within about 2 separations, indicating a temporal resolution on the order of 50.8 seconds.

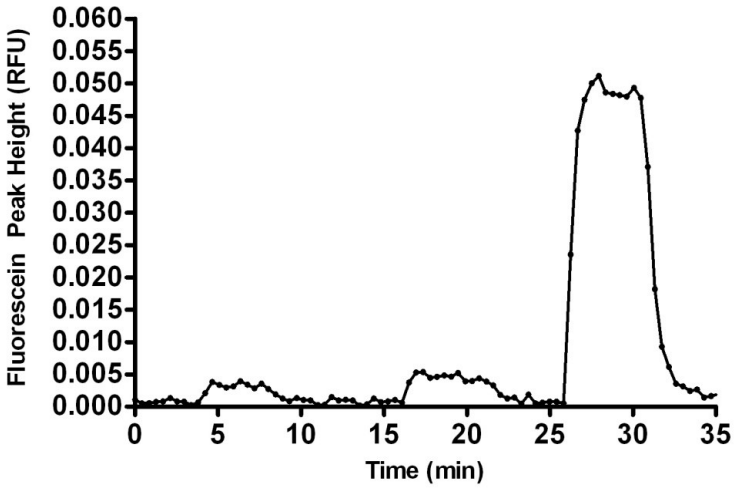

Figure 4.07A. In vitro Characterization: Temporal Response of Microdialysis Probe to Whole Blood Spiked with Fluorescein Standard Solution in aCSF. Microdialysis probe was place in aCSF, transferred to a whole blood standard spiked with varying concentrations of fluorescein, at equal volumes, and back into clean aCSF. Response of MD-CE-LIF instrument to 300 pM F (4-8 minutes), 500 pM F (17-21 minutes), and 1 nM F (27-32 minutes) in whole blood. Each electrophoretic separation was 25.4 seconds. A 10-90% change in baseline occurs within about 2 separations, indicating a temporal resolution on the order of 50.8 seconds.

varying concentrations of fluorescein standard for the whole blood standard curve. The microdialysis probe was inserted into aCSF for 1 minute, then transferred to a whole blood sample spiked with to 300 pM F (4-8 minutes) to 100 nM F (48-52 minutes) in whole blood. Each electrophoretic separation was 25.4 seconds. A 10-90% change in baseline occurs within about 2 separations, indicating a temporal resolution on the order of 50.8 seconds.

Whole blood standard curve analysis was performed to determine the limit of detection of fluorescein in whole blood samples and for analysis of fluorescein blood concentrations (Table 4.01) during *in vivo* pharmacokinetic analysis of intranasally administered fluorescein and fluorescein with nasal permeation enhancers. Linear regression analysis was carried out to determine best fit for the whole blood standard

curve (Figure 4.08 and Table 4.02). The LOD achieved in whole blood (Table 4.03) was 74 ± 1 pM. The percent recovery of the probe for fluorescein in whole blood was 6.1 ±0.7%, with aCSF perfusing through the probe at a flow rate of 40 µL/hour.

Fluorescein Concentration (nM)	Fluorescence Peak Height (RFU)	Standard Deviation	N
0.5	0.0034	0.0005	6
1	0.0049	0.0004	4
10	0.049	0.006	5
50	0.2665	0.0004	4
100	0.58	0.01	9

Table 4.01. Whole blood standard curve spiked with fluorescein standards

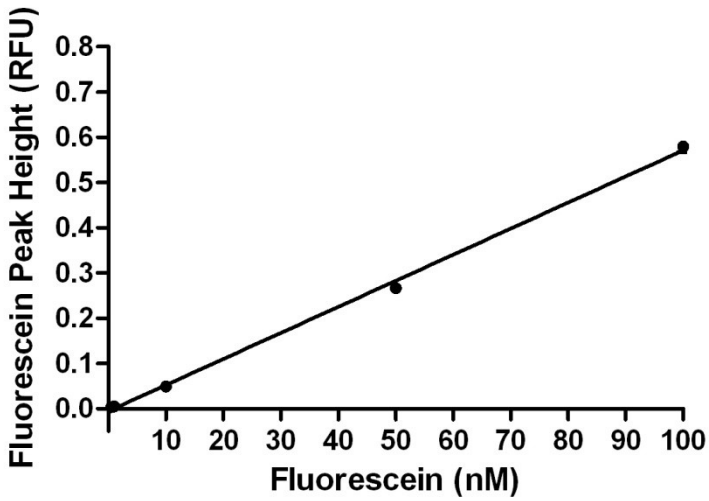

Figure 4.08. Linear regression of fluorescein spiked whole blood standard curve

Slope	0.0058 ± 0.0001
Y-intercept when X=0.0	-0.006 ± 0.007
X-intercept when Y=0.0	0.976
1/slope	174
Goodness of Fit r^2	0.9984

Table 4.02. Linear regression analysis of fluorescein spike whole blood standard curve

Limit of Detection	Percent Recovery of Probe
74 ± 1 pM	6.1 ± 0.7

Table 4.03. Limit of detection of fluorescein in whole blood and microdialysis probe percent recovery

Figure 4.09 illustrates an electrophoretic separation of fluorescein spiked in whole blood samples, final fluorescein concentration = 50 nM. The migration time of fluorescein is 17.97 s, with a plate count, N, of 13,278.

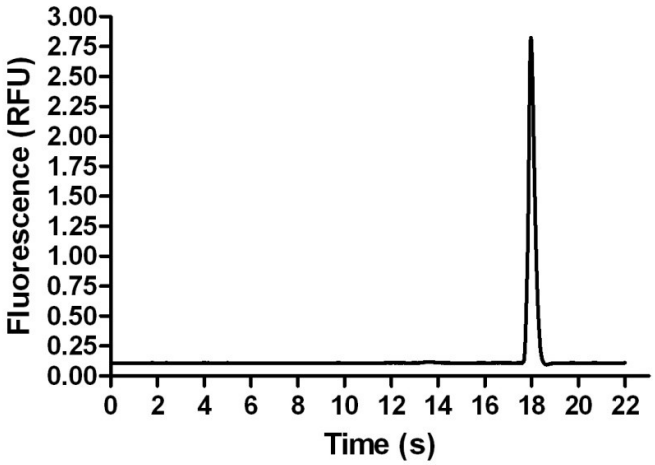

Figure 4.09. Fluorescein (50 nM) in whole blood standard curve analysis. Electrophoretic separation occurred in 22 seconds, with a fluorescein migration time of 17.967 seconds.

Intranasal Administration of Fluorescein and Hydroxypropyl-β-Cyclodextrin

A typical pharmacokinetic profile of an *in vivo* experiment with intranasal administration of fluorescein and the nasal absorption enhancer HPβCD is indicated in Figure 4.10 with a focused inset of the first 40 min of the experiment in Figure 4.10A. Electrophoretic separations were performed every 24.7 seconds. The fluorescein peak height was determined and graphed as fluorescence peak height (RFU) vs. time. The intranasal dose was administered at 1.02 minutes into data collection, and is represented by the green triangle on the graph. The amount of time for dialysate to travel from the probe outlet to the detector is indicated by the blue diamond, and is calculated prior to the *in vivo* experiment during fluorescein standard calibration run the day of *in vivo* analysis. If fluorescein were to reach the olfactory bulb immediately after the i.n. dose, expected

increase in fluorescein peak height, as measured in the olfactory bulb, would occur at the time point equivalent to the amount of time it takes for the dialysate to travel from the outlet of the microdialysis probe to the detector. Average peak height in the baseline of aCSF at the migration time of fluorescein was determined and plotted on the pharmacokinetic graph. The time point at which fluorescein peak height was greater than the S.D. of the average baseline was assigned as the first detected fluorescein peak in the olfactory bulb. This was confirmed with data analysis via Cutter Software. Subtracting the time from probe outlet to detector from the time fluorescein is first detected in the olfactory bulb results in the amount of time it took for fluorescein to reach the olfactory bulb after the i.n. dose.

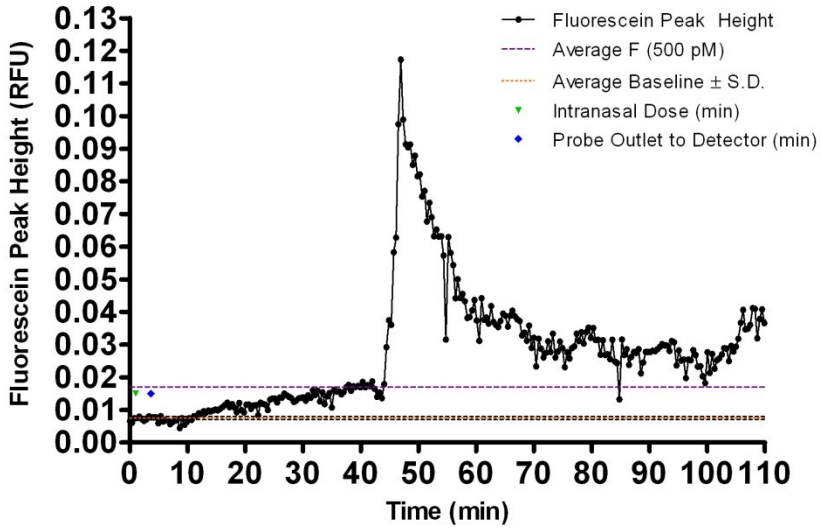

Figure 4.10. Pharmacokinetic profile of Fluorescein (nM) in the rat olfactory bulb (OB), measured with online high speed microdialysis capillary electrophoresis with laser induced fluorescence detection. Intranasal Dose (round circles) with Absorption Promoter: F (1mM, 50 nanomoles) + HPβCD (9.9% w/v), 50 µL. Each circle represents fluorescein peak height in a single electrophoretic separation. Electropherograms were recorded every 24.7 s. The intranasal dose was performed at 1.02 minutes into data collection. The amount of time for dialysate to travel from the probe outlet to the detector is indicated by the blue diamond. The 500 pM fluorescein standard is indicated by the purple long-dashed line. Average baseline at the fluorescein migration time, ± S.D. is indicated by the orange short-dashed lines.

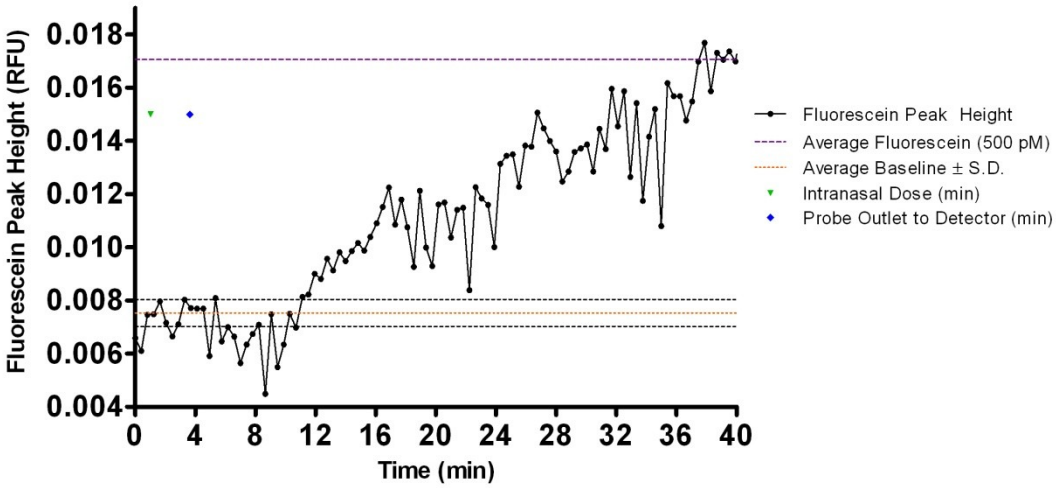

Figure 4.10A. Inset, first 40 minutes of pharmacokinetic profile of fluorescein (nM) in the rat olfactory bulb (OB), measured with online high speed microdialysis capillary electrophoresis with laser induced fluorescence detection. Intranasal Dose (round circles) with Absorption Promoter: F (1mM, 50 nanomoles) + HPβCD (9.9% w/v), 50 µL. Each circle represents fluorescein peak height in a single electrophoretic separation. Electropherograms were recorded every 24.7 s. The intranasal dose was performed at 1.02 minutes into data collection. The amount of time for dialysate to travel from the probe outlet to the detector is indicated by the blue diamond. The 500 pM fluorescein standard is indicated by the purple long-dashed line. Average baseline at the fluorescein migration time, ± S.D. is indicated by the orange short-dashed lines.

A representative electropherogram of fluorescein detected in the rat olfactory bulb 16.09 minutes post intranasal administration of fluorescein (1mM, 50 nanomoles) in conjunction with the nasal absorption permeation enhancer Hydroxypropyl-β-cyclodextrin (9.9% w/v) is indicated in Figure 4.11. The separation was carried out in 22 seconds, with a fluorescein migration time of 16.3 seconds. Two unidentified peaks are apparent at 11 and 12 seconds. Fluorescein peak heights obtained during the intranasal delivery of fluorescein with the nasal absorption enhancer HPβCD were averaged at T=0 minutes, prior to intranasal dose, and T=2 min post intranasal dose, and every 2 subsequent minutes up to 120 minutes post intranasal dose. The resulting average fluorescein pharmacokinetic profile in the rat olfactory bulb is indicated in figure 4.12.

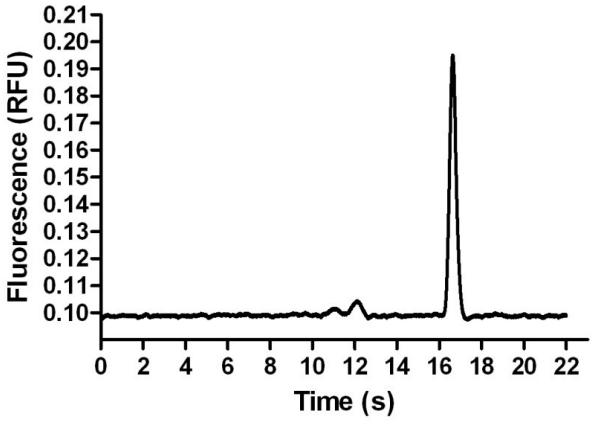

Figure 4.11. Electrophoretic separation of fluorescein in the olfactory bulb measured with online high speed microdialysis capillary electrophoresis with laser induced fluorescence detection. Intranasal Dose with Absorption Promoter: F (1mM, 50 nanomoles) + HPβCD (9.9% w/v), 50 µL.

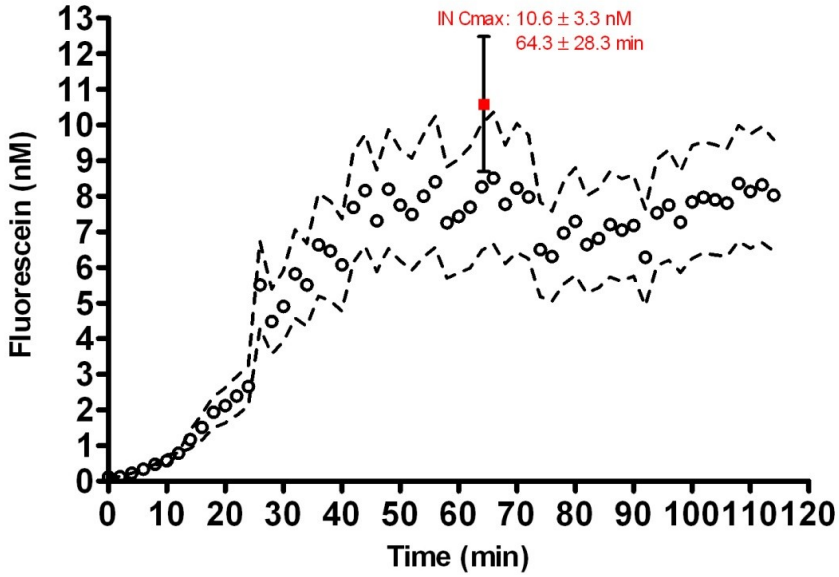

Figure 4.12. Average pharmacokinetic profile of fluorescein (nM) in the rat olfactory bulb (OB), measured with online high speed microdialysis capillary electrophoresis with laser induced fluorescence detection. Intranasal Dose (open circles) with Absorption Promoter: F (1mM, 50 nanomoles) + HPβCD (9.9% w/v), 50 µL. Each circle represents fluorescein averaged at the initial time point T = 0 (pre i.n. dose), and every 2 subsequent minutes (post i.n. dose) over N=3 animals, with the dashed line representing standard deviation. Maximum average fluorescein concentration, Cmax (red solid square) and time post i.n. dose to reach Cmax, Tmax, is indicated on the graph. Electropherograms were recorded every 25-30 seconds.

Initially, fluorescein increased slowly over the first 10 - 15 minutes. From 15 - 25 minutes the rate of fluorescein in the olfactory bulb increased, until a statistically

significant sharp increase in fluorescein concentration occurred from approximately 25 - 35 minutes. Fluorescein levels in the OB leveled off at this point for the remainder of the *in vivo* experiments. Pharmacokinetics of fluorescein in the OB post i.n. fluorescein + HPβCD were calculated (Table 4.04). The maximum concentration, Cmax of fluorescein in the OB was determined to be 10.6 ± 3.3 nM and occurred at a time, Tmax, of 64.3 ± 28.3 minutes across N = 3 animals. Area under the concentration-time curve was generated from mean concentration-time profiles from 0-120 min (AUC→120) and 0-40 minutes (AUC→40).

Parameter	Intranasal Fluorescein with HPβCD
Cmax (nM)	10.6 ± 3.3
Tmax (min)	64.3 ± 28.3
Time Post Dose Fluorescein Detected in OB (min)	6.5 ± 3.8
AUC→120 (nmol x min/L)	660.0
AUC→40 (nmol x min/L)	126.8

Table 4.04. Pharmacokinetics of fluorescein in the rat OB post in administration with nasal absorption enhancer HPβCD.

Pharmacokinetics in the blood were determined from whole blood samples collected in conjunction with *in vivo* monitoring of fluorescein in the rat olfactory bulb. Whole blood samples were collected at T = 0 min (prior to i.n. dose), and T = 5, 10, 20, and 40 minutes (post i.n. dose) Figure 4.13. Fluorescein was sampled and analyzed via MD-CE-LIF directly in the whole blood samples. Intranasal delivery of fluorescein with the nasal absorption enhancer HPβCD resulted in a gradual increase in fluorescein blood concentrations over the first 5 minutes, with the peak concentration (Cmax), of 505.5 ± 8.7 nM obtained at the last collected whole blood sample, T = 40 minutes. A faster rate of increase occurred from 5-10 minutes, which then decreased slightly and maintained a

relatively linear increase in rate from 10-40 minutes. A correction for the blood volume of individual rats was made in the determination of blood pharmacokinetics plot of fluorescein (nanomoles) vs. time. Animals ranged in size from 250 g – 380 g, and a blood correction of 6.86 ±0.53 mL/100 g was made.[2] The pharmacokinetic profile of fluorescein (nanomoles) in whole blood post in administration was similar to that obtained for fluorescein (nM) in whole blood. Area under the concentration-time curve was generated for fluorescein(nM) and blood volume corrected fluorescein (nanomoles) (Table 4.05 and Table 4.06).

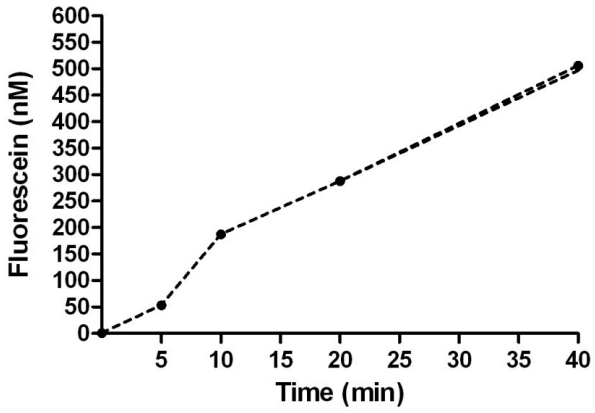

Figure 4.13. Average fluorescein (nanomoles) in whole blood measured with online high speed microdialysis capillary electrophoresis with laser induced fluorescence detection. Intranasal Dose (round circles) with Absorption Promoter: F (1mM, 50 nanomoles) + HPβCD (9.9% w/v), 50 µL. Each point represents average fluorescein in whole blood sampled via distal tail slice at T = 0 (prior to i.n. dose) and T = 5, 10, 20, and 40 min (post i.n. dose animals, with the dashed line above and below representing standard deviation, N = 3 animals. Data points (N ≥ 3) were normalized based on rat blood volume = 6.86 ± 0.53 mL per/100 g.[2] Electropherograms were recorded every 23 seconds.

Parameter	Intranasal Fluorescein and HPβCD
Cmax (nM)	506 ± 9
Tmax (min)	40
Time Post Dose Fluorescein Detected in OB (min)	7 ± 4
AUC→40 (nM x min/L)	11,031.0

Table 4.05. Pharmacokinetics of fluorescein (nM) in rat whole blood post in administration with nasal absorption enhancer HPβCD.

Parameter	Intranasal Fluorescein and HPβCD
Cmax (nanomoles)	12 ± 1
Tmax (min)	40
Time Post Dose Fluorescein Detected in OB (min)	7 ± 4
AUC→40 (nmol x min/L)	267.4

Table 4.06. Pharmacokinetics of fluorescein (nanomoles) in rat whole blood post in administration with nasal absorption enhancer HPβCD.

In order to determine whether the combination of fluorescein with HPβCD resulted in significantly increased concentrations of fluorescein in the olfactory bulb post intranasal administration, the results were compared to the pharmacokinetic profile of fluorescein in the olfactory bulb obtained post i.n. administration of fluorescein without nasal absorption enhancer (Figure 4.14). An inset of the first 40 minutes of Figure 4.14 can be found in Figure 4.14A.

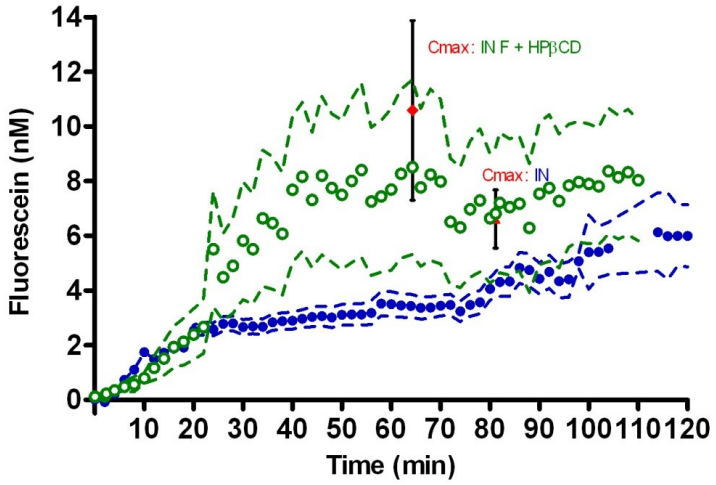

Figure 4.14. Average pharmacokinetic profile comparisons of fluorescein (nM) in the rat olfactory bulb (OB), measured with online high speed microdialysis capillary electrophoresis with laser induced fluorescence detection. Intranasal Dose with Nasal Absorption Promoter (open circles): F (1mM, 50 nanomoles) + HPβCD (9.9% w/v) in aCSF, 50 µL, N = 3 animals. Intranasal Dose (closed circles): F (1mM, 50 nanomoles) in aCSF, 50 µL, N = 5 animals. Each point represents fluorescein in the OB averaged at the initial time point T = 0 (prior to i.n. dose), and every 2 subsequent minutes (post i.n. dose) with the dashed line representing standard deviation. Maximum average fluorescein concentration, Cmax, is indicated on the graph for each set of data. Electropherograms were recorded every 25-30 seconds.

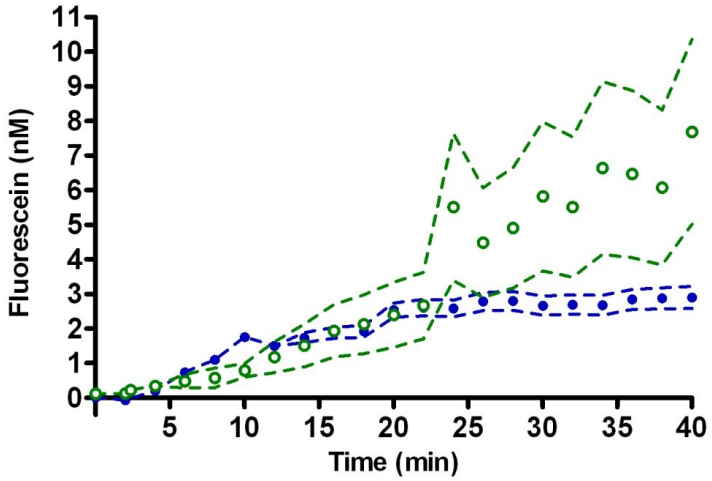

Figure 4.14A. First 40 minutes of average pharmacokinetic profile comparisons of fluorescein (nM) in the rat olfactory bulb (OB), measured with online high speed microdialysis capillary electrophoresis with laser induced fluorescence detection. Intranasal Dose with Nasal Absorption Promoter (open circles): F (1mM, 50 nanomoles) + HPβCD (9.9% w/v) in aCSF, 50 µL, N = 3 animals. Intranasal Dose (closed circles): F (1mM, 50 nanomoles) in aCSF, 50 µL, N = 5 animals. Each point represents fluorescein in the OB averaged at the initial time point T = 0 (prior to i.n. dose), and every 2 subsequent minutes (post i.n. dose) with the dashed line representing standard deviation. Electropherograms were recorded every 25-30 seconds.

The greatest concentration of fluorescein in the olfactory bulb was found to occur after i.n. administration of fluorescein with the absorption enhancer (Table 4.07). A 1.6 fold increase in Cmax was determined when HPβCD (9.9% w/v) was added to the fluorescein (1 mM), 50 nanomoles) in aCSF. AUC analysis for both 120 min and 40 min indicated a statistically significant difference between i.n. and i.n. with a nasal absorption enhancer (Table 4.08). Unpaired t-test was performed, with statistical significance at a $p<0.05$.

Parameter	Intranasal	Intranasal Fluorescein and HPβCD
Cmax (nM)	6.6 ± 1.1	10.6 ± 3.3
Tmax (min)	81.1 ± 48.1	64.3 ± 28.3
Time Post Dose Fluorescein Detected in OB (min)	2.8 ± 0.5	6.5 ± 3.8
AUC→120 (nmol x min/L)	418.3	660.0
AUC→40 (nmol x min/L)	78.6	126.8

Table 4.07. Pharmacokinetics comparison of fluorescein (nM) in rat olfactory bulb post in administration of fluorescein with nasal absorption enhancer HPβCD and fluorescein alone.

Unpaired t test	T→120 min	T→40 min
P value	P<0.0001	P<0.0001
P value summary	***	***
Are means signif. different? (P < 0.05)	Yes	Yes
One- or two-tailed P value?	Two-tailed	Two-tailed
t, df	t=6.236 df=113	t=6.236 df=113

Table 4.08. AUC comparison of fluorescein in the rat olfactory bulb between intranasally administered fluorescein and intranasally administered fluorescein with HPβCD.

These results indicate that increased concentrations of fluorescein do reach the olfactory bulb with the addition of HPβCD. Differences between i.n. fluorescein administered with and without HPβCD were found in the rate of absorbance of fluorescein in the OB. Intranasal dosing indicated a gradual absorption of fluorescein over time, demonstrating an independence from possible clearance mechanisms occurring in the nasal cavity and the blood. Intranasal administration of fluorescein with HPβCD indicated a leveling of fluorescein concentration in the OB with a faster time, Tmax, to Cmax, and a slower initial rate of absorption in fluorescein relative to i.n. dose without HPβCD. It would be interesting to see if the rate of fluorescein absorption in the OB remained stable over a longer sampling time, greater than 120 min, and whether i.n. pharmacokinetics would indicate a continuous increase in fluorescein absorption over time. Interestingly, no statistical difference was found when comparing the AUC→40 of fluorescein in whole blood with and without addition of a nasal absorption enhancer to the i.n. formulation (Table 4.09), indicating a similar systemic total blood exposure over T = 40 min. A comparison of the in pharmacokinetics of fluorescein (nM) and fluorescein (nanomoles) in whole blood over time can be found in figure 4.15 and figure 4.16.

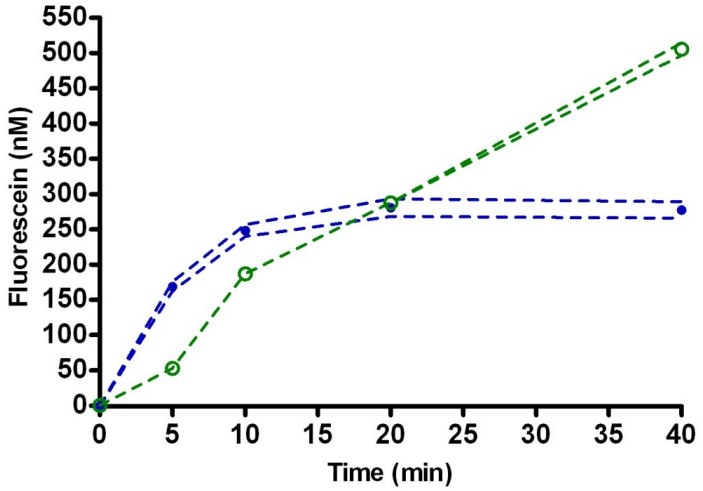

Figure 4.15. Average fluorescein (nM) comparisons in whole blood measured with online high speed microdialysis capillary electrophoresis with laser induced fluorescence detection. Intranasal Dose with Nasal Absorption Enhancer (open circles): F (1mM, 50 nanomoles) + HPβCD (9.9% w/v) in aCSF, 50 µL, N = 3. Intranasal Dose (closed circles): F (1mM, 50 nanomoles) in aCSF, 50 µL, N = 5 animals. Each point represents average fluorescein in whole blood sampled via distal tail slice at T = 0 (prior to i.n. dose) and T = 5, 10, 20, and 40 min (post i.n. dose), with the dashed lines above and below representing standard deviation, N ≥ 3. Electropherograms were recorded every 23 seconds.

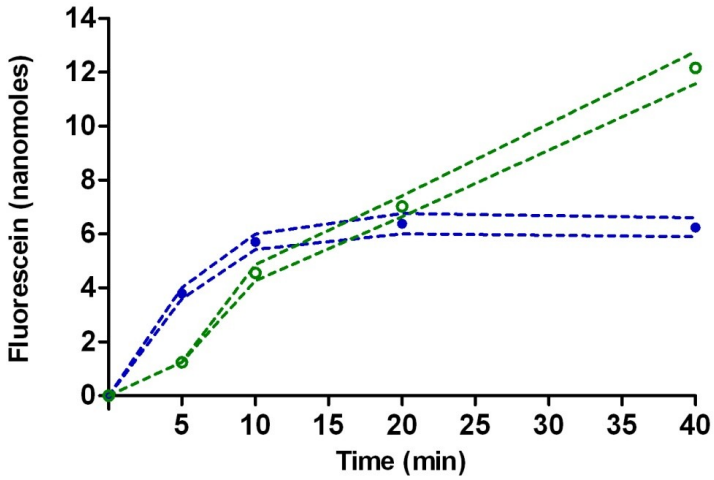

Figure 4.16. Average fluorescein (nanomoles) comparisons in whole blood measured with online high speed microdialysis capillary electrophoresis with laser induced fluorescence detection. Intranasal Dose with Nasal Absorption Enhancer (open circles): F (1mM, 50 nanomoles) + HPβCD (9.9% w/v) in aCSF, 50 µL, N = 3. Intranasal Dose (closed circles): F (1mM, 50 nanomoles) in aCSF, 50 µL, N = 5 animals. Each point represents average fluorescein in whole blood sampled via distal tail slice at T = 0 (prior to i.n. dose) and T = 5, 10, 20, and 40 min (post i.n. dose), with the dashed lines above and below representing standard deviation, N ≥ 3. Data points (N ≥ 3) were normalized based on rat blood volume = 6.86 ± 0.53 mL per/100 g.[2] Electropherograms were recorded every 23 seconds.

A pharmacokinetic comparison of fluorescein in whole blood samples can be found in Table 4.09. A Cmax (nM) of 506 ± 9 was achieved with the use of HPβCD in the intranasal dose composition, and a Cmax (nM) of 277 ±12 was obtained with an i.n. dose of fluorescein alone. Tmax of 20 minutes in the blood was reached at a faster rate in intranasal studies than the Tmax of 40 minutes in whole blood samples from i.n. experiments with nasal absorption enhancer HPβCD. AUC→40 (nM x min/L) at 11,031 for i.n. with absorption enhancer was higher than the AUC→40 (nM x min/L) of 9,682 for i.n. alone, however this was not found to be a statistically significant difference (Table 4.10).

Parameter	Intranasal with HPβCD	Intranasal
Cmax (nM)	506 ± 9	277 ±12
Tmax (min)	40	20
Time Post Dose Fluorescein Detected in OB (min)	6.5 ± 3.8	2.8 ± 0.5
AUC→40 (nanomoles x min/L)	11031	9682

Table 4.09. Pharmacokinetics comparison of fluorescein (nM) in rat whole blood post i.n. administration with nasal absorption enhancer HPβCD to i.n. administration of fluorescein alone.

Unpaired t test	T→40 min
P value	0.9131
P value summary	ns
Are means signif. different? (P < 0.05)	No
One- or two-tailed P value?	Two-tailed
t, df	t=0.1126 df=8

Table 4.10. Correlation of fluorescein (nM) intranasal and intranasal with HPβCD in rat whole blood samples.

Mass of animals within the study varied from 250-380 g. Blood volumes were normalized based on rat blood volume = 6.86 ± 0.53 mL per/100 g.[2] Correction for blood volume values of fluorescein in whole blood samples is indicated in the pharmacokinetic results for AUC (nmoles x time) in Table 4.11 and Table 4.12.

Parameter	Intranasal with HPβCD	Intranasal
Cmax (nanomoles)	12.2 ±0.6	6.2 ± 0.4
Tmax (min)	40	20
Time Post Dose Fluorescein Detected in OB (min)	6.5 ± 3.8	2.8 ± 0.5
AUC→40 (nanomoles x min)	267.4	219.8

Table 4.11. Pharmacokinetics comparison of fluorescein (nanomoles) in rat whole blood post in administration of fluorescein and post i.n. administration of fluorescein with HPβCD.

Unpaired t test	T→40 min
P value	0.822
P value summary	ns
Are means signif. different? (P < 0.05)	No
One- or two-tailed P value?	Two-tailed
t, df	t=0.232 df=8

Table 4.12. Correlation of blood volume corrected (nanomoles) AUC→40 for Intranasal and Intranasal with HPβCD in rat whole blood samples.

Intranasal delivery resulted in significantly greater olfactory bulb-to-blood concentration ratios the first 40 minutes of analysis. This is possibly misleading over the course of the 120 minutes samples however, as the concentration of fluorescein in the OB post i.n. with nasal enhancer did not increase significantly over the i.n. levels until 40 minutes after dosing. Sampling for a longer period of time in the blood may give a more accurate picture of olfactory bulb to blood concentration ration comparison between the i.n. and i.n. plus enhancer formulations.

Effectiveness of the addition of the nasal absorption enhancer HPβCD to fluorescein i.n. formulations was evaluated. Fluorescein levels in the OB due to intranasal administration of fluorescein and i.n. administration of fluorescein with the nasal absorption enhancer HPβCD were analyzed via normalization ratios of fluorescein brain concentration to blood concentration (Figure 4.17 and Table 4.13) and normalization ratios of fluorescein brain concentration to total blood exposure over the first forty minutes of analysis post i.n. dose (AUC→40 values) (Figure 4.18 and Table 4.14).

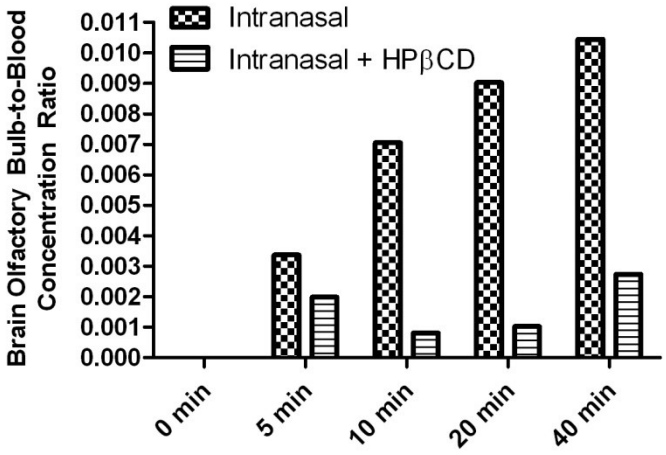

Figure 4.17. Olfactory bulb-to-blood fluorescein (nM) concentration ratios following intranasal and intranasal with permeation enhancer delivery of fluorescein to anesthetized rats (mean ratio ± S.E., n =3-5 for each time point). Ratios were significantly greater in the olfactory bulb following intranasal fluorescein delivery. $p < 0.5$, unpaired t test comparing intranasal result with intranasal plus absorption enhancer result at each respective time point.

Unpaired t test	F (nM)
P value	0.0451
P value summary	*
Are means signif. different? (P < 0.05)	Yes
One- or two-tailed P value?	Two-tailed
t, df	t=2.372 df=8

Table 4.13. Comparison of olfactory bulb to whole blood fluorescein (nM) concentration ratios.

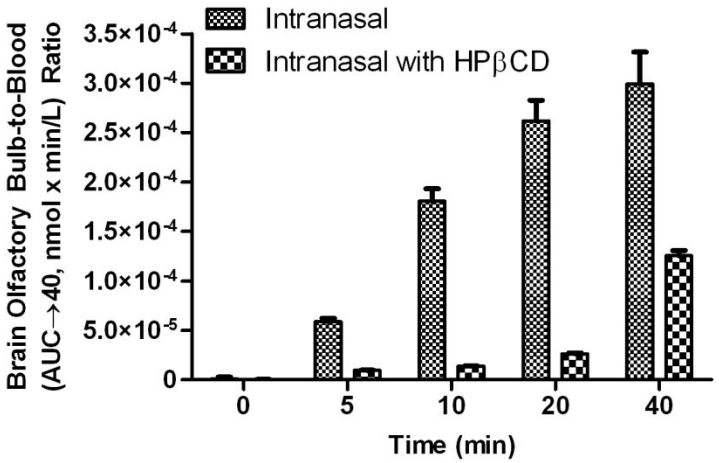

Figure 4.18. Olfactory bulb-to-blood AUC→40 concentration ratios following intranasal and intranasal with permeation enhancer delivery of fluorescein to anesthetized rats (mean ratio ± S.E., n =3-5 for each time point). Ratios were not found to be statistically different from each other. $p > 0.05$, unpaired t test comparing intranasal result with intranasal plus absorption enhancer result at each respective time point.

Unpaired t test	AUC→40 (nanomoles x min/L)
P value	0.0775
P value summary	ns
Are means signif. different? (P < 0.05)	No
One- or two-tailed P value?	Two-tailed
t, df	t=2.025 df=8

Table 4.14. Comparison of brain olfactory bulb concentration to whole blood AUC→40 (nanomoles x min/L) ratio.

Normalizing fluorescein brain concentration to fluorescein blood concentration results indicated intranasal administration of fluorescein alone resulted in statistically significant higher brain-to-blood concentration ratios. This result however is weighted due to the limited sampling time of whole blood, the first 40 minutes post i.n. dose. Fluorescein concentrations in the OB and the blood due to addition of HPβCD increased significantly after the 30-40 minutes post i.n. dose. While the total blood exposure is not statistically different between i.n. fluorescein and i.n. fluorescein + HPβCD, over the entire 2 hours of the *in vivo* experiment, addition of HPβCD did result in higher total fluorescein (nM) exposure in the brain throughout the course of the experiment. A comparison of intranasal drug delivery with nasal enhancer HPβCD to i.n. fluorescein, and i.v fluorescein is represented in Figure 4.19. Fluorescein i.v. dose however is not corrected for the difference in nanomoles of fluorescein administered. Dose corrected comparisons of fluorescein (nM) in the OB (Figure 4.20), and whole blood analysis (Figures 4.21 and 4.22) indicate that while HPβCD results in higher fluorescein absorption in the OB relative to i.n., the dose corrected i.v. indicates the most likely pathway of the highest fluorescein (nM) delivery to the OB occurs from the blood to the brain.

A comparison of intranasal drug delivery with the nasal enhancer HPβCD to i.n. and i.v. administered fluorescein is represented in Figure 4.19. The fluorescein i.v. dose

is not corrected for the difference in dose (nanomoles) administered between i.v and i.n. studies. I.n. dose of 50 nanomoles of fluorescein, is 6.25 time higher than that of the i.v. fluorescein dose of 8 nanomoles. Intravenous fluorescein concentrations were normalized to the intranasal dose by multiplying the concentrations of fluorescein (nM) after i.v. administration by a factor of 6.25, under the assumption that concentration of fluorescein is a linear function of the applied dose. Intravenous dose corrected comparisons of fluorescein (nM) in the OB (Figure 4.20), and whole blood analysis (Figures 4.21 and 4.22) indicate that while HPβCD results in higher fluorescein absorption in the OB relative to i.n. fluorescein without HPβCD, the dose corrected i.v. fluorescein administration results in the highest fluorescein delivery to the O.B. This suggests that

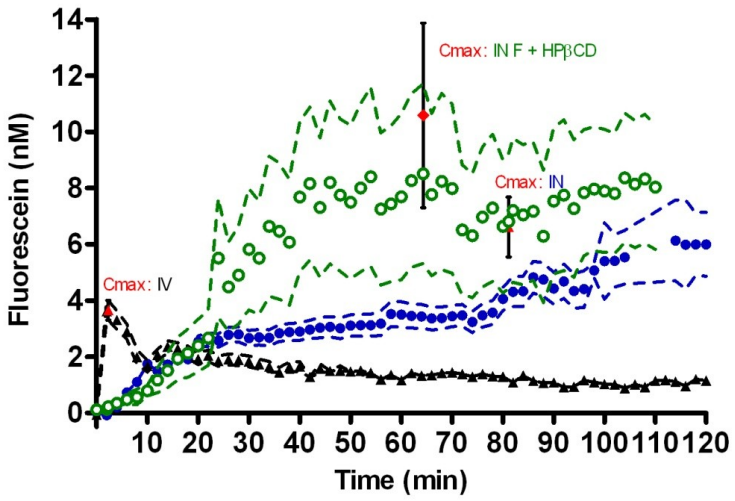

Figure 4.19. Average pharmacokinetic profile comparisons of Fluorescein (nM) in the rat olfactory bulb (OB), measured with online high speed microdialysis capillary electrophoresis with laser induced fluorescence detection. Intranasal Dose with Nasal Absorption Promoter (green open circles): F (1mM, 50 nanomoles) + HPβCD (9.9% w/v) in aCSF, 50 µL, N = 3 animals. Intranasal Dose (blue closed circles): F (1mM, 50 nanomoles) in aCSF, 50 µL, N = 5 animals. Intravenous Dose (black closed triangles): F (160 µM, 8 nanomoles) in aCSF, 50 µL, N = 3 animals. Each point represents fluorescein in the OB averaged at the initial time point T = 0 (pre dose), and every 2 subsequent minutes (post dose) with the dashed lines above and below representing standard deviation. Maximum average fluorescein concentration, Cmax, is indicated on the graph for each set of data. Electropherograms were recorded every 25-30 seconds.

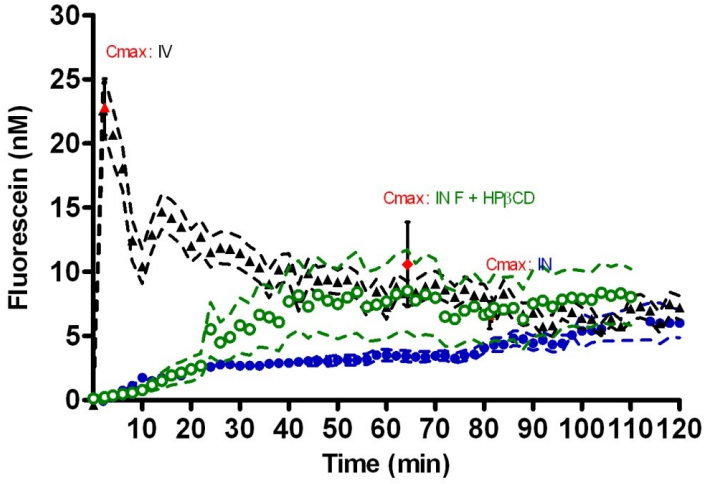

Figure 4.20. DOSE CORRECTED Average pharmacokinetic profile comparisons of Fluorescein (nM) in the rat olfactory bulb (OB), measured with online high speed microdialysis capillary electrophoresis with laser induced fluorescence detection. Intranasal Dose with Nasal Absorption Promoter (green open circles): F (1mM, 50 nanomoles) + HPβCD (9.9% w/v) in aCSF, 50 µL, N = 3 animals. Intranasal Dose (blue closed circles): F (1mM, 50 nanomoles) in aCSF, 50 µL, N = 5 animals. Dose Corrected Intravenous Dose (black closed triangles): F (1 mM, 150 nanomoles) in aCSF, 50 µL, N = 3 animals. Each point represents fluorescein in the OB averaged at the initial time point T = 0 (pre dose), and every 2 subsequent minutes (post dose) with the dashed lines above and below representing standard deviation. Maximum average fluorescein concentration, Cmax, is indicated on the graph for each set of data. Electropherograms were recorded every 25-30 seconds.

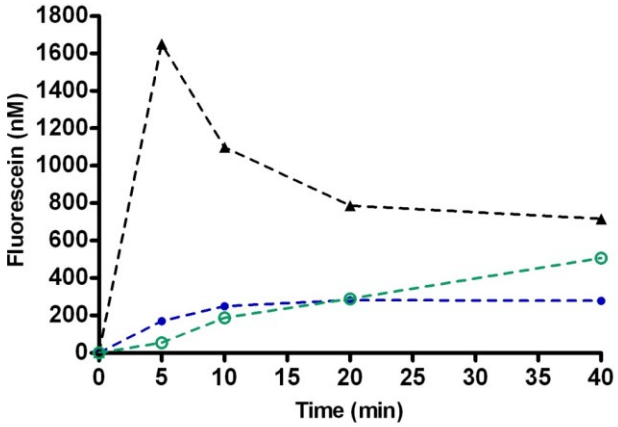

Figure 4.21. (**DOSE CORRECTED**) Average fluorescein (nM) comparisons in whole blood measured with online high speed microdialysis capillary electrophoresis with laser induced fluorescence detection. Intranasal Dose with Nasal Absorption Promoter (green open circles): F (1mM, 50 nanomoles) + HPβCD (9.9% w/v) in aCSF, 50 µL, N = 3 animals. Intranasal Dose (blue closed circles): F (1mM, 50 nanomoles) in aCSF, 50 µL, N = 5 animals. Dose Corrected Intravenous Dose (black closed triangles): F (1 mM, 150 nanomoles) in aCSF, 50 µL, N = 3 animals. Each point represents average fluorescein in whole blood sampled via distal tail slice at T = 0 (prior to i.n. dose) and T = 5, 10, 20, and 40 min (post i.n. dose animals, with the dashed line above and below representing standard deviation, N ≥ 3. Electropherograms were recorded every 23 seconds.

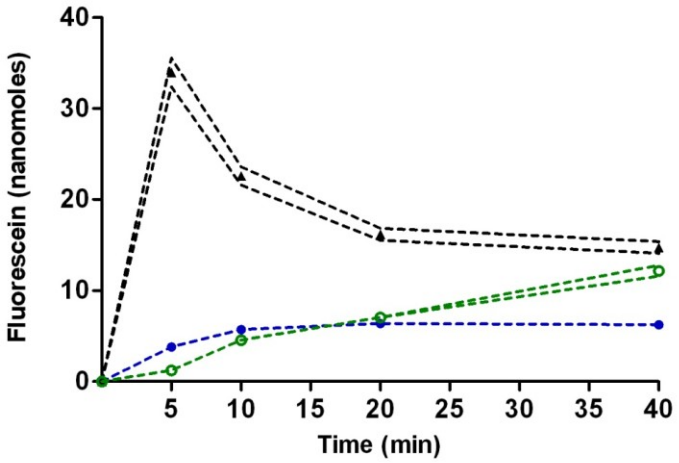

Figure 4.22. (**DOSE CORRECTED**) Average fluorescein (nanomoles) comparisons in whole blood measured with online high speed microdialysis capillary electrophoresis with laser induced fluorescence detection. Intranasal Dose with Nasal Absorption Promoter (green open circles): F (1mM, 50 nanomoles) + HPβCD (9.9% w/v) in aCSF, 50 µL, N = 3 animals. Intranasal Dose (blue closed circles): F (1mM, 50 nanomoles) in aCSF, 50 µL, N = 5 animals. Dose Corrected Intravenous Dose (black closed triangles): F (1 mM, 150 nanomoles) in aCSF, 50 µL, N = 3 animals. Each point represents average fluorescein in whole blood sampled via distal tail slice at T = 0 (prior to i.n. dose) and T = 5, 10, 20, and 40 min (post i.n. dose animals, with the dashed line above and below representing standard deviation. Data points ($N \geq 3$) were normalized based on rat blood volume = 6.86 ± 0.53 mL per/100 g.[2] Electropherograms were recorded every 23 seconds.

while some fluorescein could reach the OB via a blood independent pathway, nose to blood to brain likely remains the most significant transport pathway of fluorescein delivery to the OB.

A single intranasal studiey with the nasal absorption enhancer chitosan was performed to determine whether the nasal permeation enhancer resulted in increased concentration in the olfactory bulb, relative to i.n. administration of fluorescein without any nasal enhancer. Comparisons were made between chitosan and HPβCD to evaluate whether inclusion of a nasal absorption enhancer with an intranasally administered drug is applicable to future MD-CE-LIF intranasal studies. Intranasal Fluorescein (1 mM in aCSF) + Chitosan (0.5% w/v) was administered to the right rat nasal cavity. Fluorescein peak height (RFU) was determined (Figure 4.23). Each point (black circle) on the graph

represents fluorescein peak height in a single electrophoretic separation. Electropherograms were recorded every 24.7 s. The intranasal dose was performed at 1.02 minutes into data collection. The amount of time for dialysate to travel from the probe outlet to the detector is indicated by the blue diamond = 3.93 minutes. The 500 pM fluorescein standard is indicated by the purple long-dashed line. Average baseline at the fluorescein migration time, ± S.D. is indicated by the orange short-dashed lines.

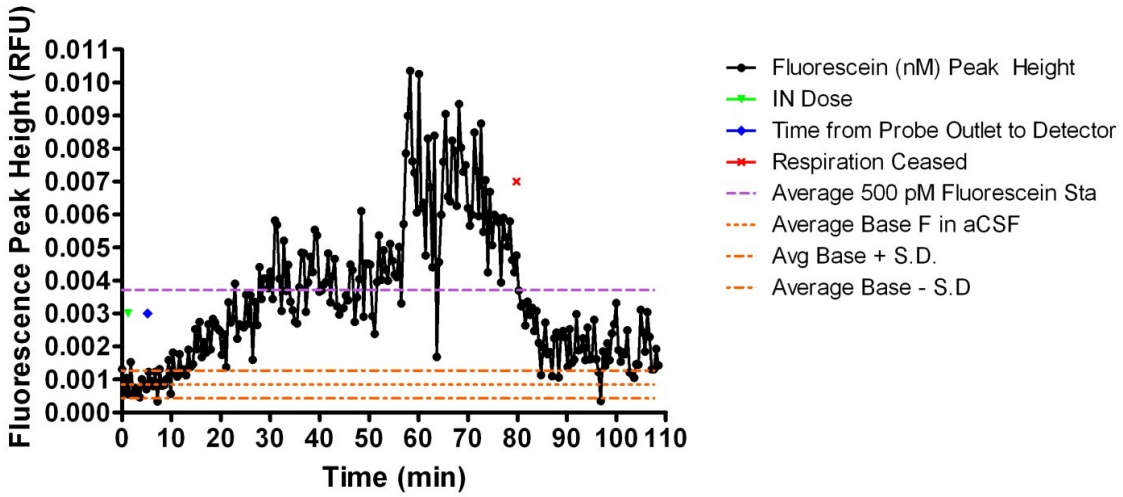

Figure 4.23. Intranasal fluorescein (1 mM) + chitosan (0.5% w/v). Pharmacokinetic profile of fluorescein peak height (RFU) in the rat olfactory bulb (OB), measured with online high speed microdialysis capillary electrophoresis with laser induced fluorescence detection. Intranasal Dose with Absorption Promoter (black round circles): F (1mM, 50 nanomoles) + Chitosan (0.5% w/v), 50 µL. Each circle represents fluorescein peak height in a single electrophoretic separation. Electropherograms were recorded every 24.7 s. The intranasal dose was performed at 1.02 minutes into data collection. The amount of time for dialysate to travel from the probe outlet to the detector is indicated by the blue diamond. The 500 pM fluorescein standard is indicated by the purple long-dashed line. Average baseline at the fluorescein migration time, ± S.D. is indicated by the orange short-dashed lines.

The pharmacokinetic profile for fluorescein (nM) in the olfactory after intranasal co administration of fluorescein with the nasal enhancer chitosan was determined in Figure 4.24. Cmax of chitosan = 1.2 ± 0.9 nM at a time to maximum concentration, Tmax, of 58.28 minutes. Fluorescein concentration increased slowly over first 30 minutes

of the experiment, where it then steadied for another 30 minutes. Around T = 60 minutes post i.n. dose, there was an increase in fluorescein (nM) for 10 minutes, followed by a sharp decline at T = 80 minutes, where respiration of the animal suddenly ceased.

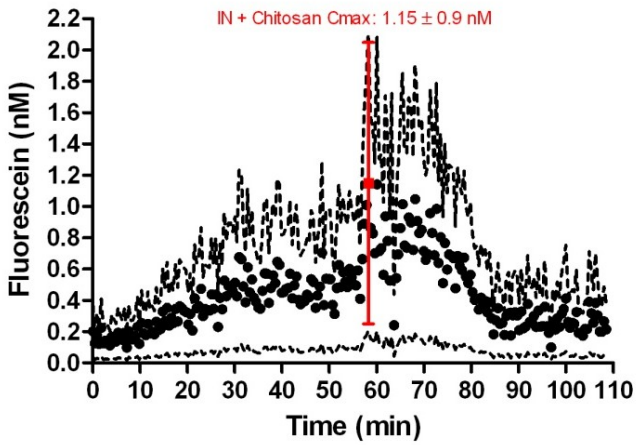

Figure 4.24. Fluorescein (nM) pharmacokinetic profile post i.n. dose of fluorescein with the nasal enhancer chitosan, measured with online high speed microdialysis capillary electrophoresis with laser induced fluorescence detection Intranasal Dose with Absorption Promoter (black round circles): F (1mM, 50 nanomoles) + Chitosan (0.5% w/v), 50 µL, N = 1 animal. Each point represents fluorescein (nM) in the OB over the time course of the experiment with the dashed lines above and below representing standard deviation. Maximum average fluorescein concentration, Cmax, is indicated on the graph. Electropherograms were recorded every 24.7 seconds.

Concentration of fluorescein in the OB, measured via MD-CE-LIF, after intranasal administration of fluorescein + chitosan was significantly less than that achieved with the nasal enhancer Hydroxypropyl-β-cyclodextrin (Figure 4.25 and Table 4.15). Intranasal fluorescein formulations with HPβCD resulted in statistically significant higher fluorescein delivery to the olfactory bulb.

Unpaired t test	F (nM) in the OB: HPβCD vs. Chitosan
P value	P<0.0001
P value summary	***
Are means signif. different? (P < 0.05)	Yes
One- or two-tailed P value?	Two-tailed
t, df	t=14.57 df=111

Table 4.15. Statistical comparison of chitosan and HPβCD.

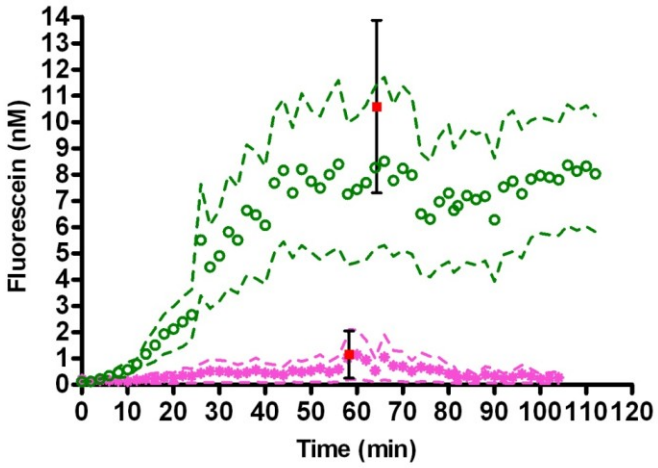

Figure 4.25. Average fluorescein pharmacokinetic profile comparisons of nasal absorption enhancers HPβCD and chitosan. Fluorescein (nM) in the rat olfactory bulb (OB), was measured with online high speed microdialysis capillary electrophoresis with laser induced fluorescence detection. Intranasal Dose with Nasal Absorption Promoter HPβCD (green open circles): F (1mM, 50 nanomoles) + HPβCD (9.9% w/v) in aCSF, 50 µL, N = 3 animals. Intranasal Dose with Nasal Absorption Promoter Chitosan (rose closed circles): F (1mM, 50 nanomoles) in aCSF with Chitosan (0.5% w/v), 50 µL, N = 1 animal. Each point represents fluorescein in the OB averaged at the initial time point T = 0 (pre dose), and every 2 subsequent minutes (post dose) with the dashed lines above and below representing standard deviation. Maximum average fluorescein concentration, Cmax, is indicated on the graph for each set of data. Electropherograms were recorded every 25-30 seconds.

Figure 4.26 demonstrates fluorescein (nM) concentration in the OB over time relative to the pharmacokinetic profile developed for intranasal fluorescein administered without a nasal absorption enhancer. HPβCD indicates significant improvement in fluorescein delivery to the OB. Chitosan did not indicate any advantage over intranasal fluorescein alone. In addition to this, the animal did not survive more than 80 minutes past the dosage. This was unexpected, as literature reports relatively safe toxicity profiles in rats. As n=1, not enough data is available to make a statistically significant conclusion. Chitosan's use as a nasal absorption promoter does not indicate strong potential in i.n. fluorescein formulations. It is unknown how fluorescein interacts with chitosan in *in vivo* conditions. The strong pH dependence of fluorescein, solubility issues of chitosan at physiological pH, possible quenching upon addition of fluorescein to the biopolymer

chitosan, and likely strong interactions of positively charged chitosan with the negatively charged nasal mucosa, or some combination of these hypotheses may have contributed to decreased fluorescein (nM) in the OB. With a single exploratory chitosan experiment performed, it is difficult to make any definitive conclusion.

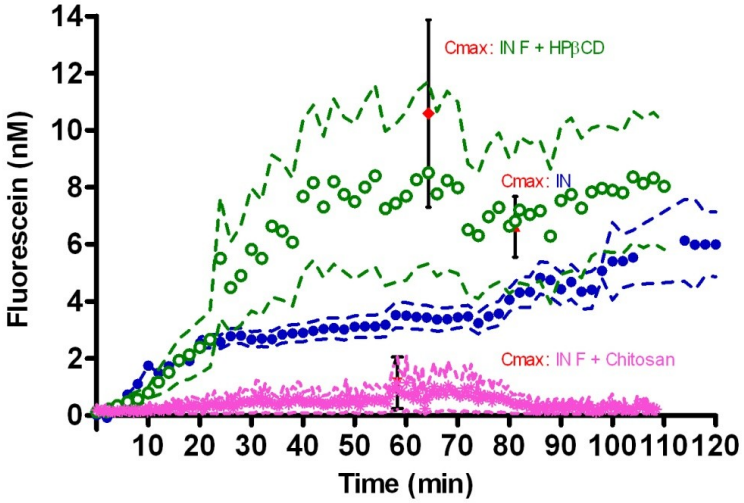

Figure 4.26. Average fluorescein pharmacokinetic profile comparisons of nasal absorption enhancers HPβCD and chitosan. Fluorescein (nM) in the rat olfactory bulb (OB), was measured with online high speed microdialysis capillary electrophoresis with laser induced fluorescence detection. Intranasal Dose with Nasal Absorption Promoter HPβCD (green open circles): F (1mM, 50 nanomoles) + HPβCD (9.9% w/v) in aCSF, 50 µL, N = 3 animals. Intranasal Dose with Nasal Absorption Promoter Chitosan (rose closed circles): F (1mM, 50 nanomoles) in aCSF with Chitosan (0.5% w/v), 50 µL, N = 1 animal. Intranasal Dose (blue, closed circles): F (1mM, 50 nanomoles) in aCSF, 50 µL, N = 5 animals. Each point represents fluorescein in the OB averaged at the initial time point T = 0 (prior to i.n. dose), and every 2 subsequent minutes (post i.n. dose) with the dashed lines above and below representing standard deviation. Maximum average fluorescein concentration, Cmax, is indicated on the graph for each set of data. Electropherograms were recorded every 25-30 seconds.

In order to compare distribution of fluorescein in the olfactory bulb and the blood, whole blood samples were collected prior to the i.n. dose, T=0, and T=5, 10, 20, and 40 min post dosing. Fluorescein concentration in whole blood samples post i.n. dose with chitosan increased quickly from 5-10 minutes, and then began a slow increase up to 40 minutes (Figure 4.27). Cmax (nanomoles) was reached at T= 40 minutes, and was

determined to be 19.2 ± 1.4 nanomoles (Figure 4.28). Fluorescein in whole blood (nM) (Table 4.28) Tmax was reached at 40 minutes, with a Cmax of 801 ± 36 nM.

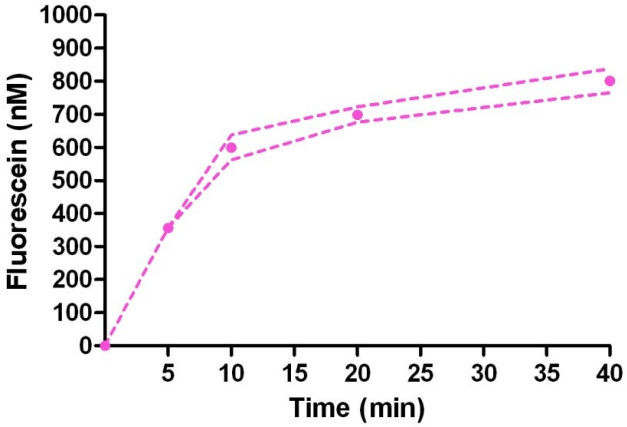

Figure 4.27. Average fluorescein (nanomoles) in whole blood post i.n. fluorescein + chitosan, measured with online high speed microdialysis capillary electrophoresis with laser induced fluorescence detection. Intranasal Dose with Absorption Promoter (rose circles): F (1mM, 50 nanomoles) + Chitosan (0.5% w/v), 50 µL. Each point represents average fluorescein in whole blood sampled via distal tail slice at T = 0 (prior to i.n. dose) and T = 5, 10, 20, and 40 min (post i.n. dose), with the dashed lines above and below representing standard deviation, N=1animal. Electropherograms were recorded every 23.4 seconds.

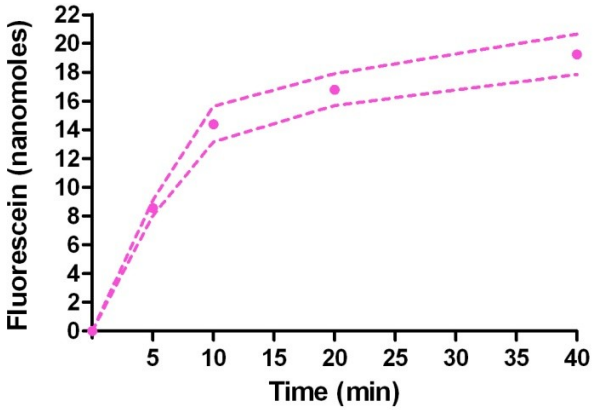

Figure 4.28. Average fluorescein (nanomoles) in whole blood post i.n. fluorescein + chitosan, measured with online high speed microdialysis capillary electrophoresis with laser induced fluorescence detection. Intranasal Dose with Absorption Promoter (rose circles): F (1mM, 50 nanomoles) + Chitosan (0.5% w/v), 50 µL. Each point represents average fluorescein in whole blood sampled via distal tail slice at T = 0 (prior to i.n. dose) and T = 5, 10, 20, and 40 min (post i.n. dose), with the dashed lines above and below representing standard deviation, N=1animal. Data points were normalized based on rat blood volume = 6.86 ± 0.53 mL per/100 g.[2] Electropherograms were recorded every 23.4 seconds.

A comparison of fluorescein (nM) in whole blood post all nasal absorption enhancer i.n. studies was made in Figure 4.29 (nM) and Figure 4.30 (nanomoles).

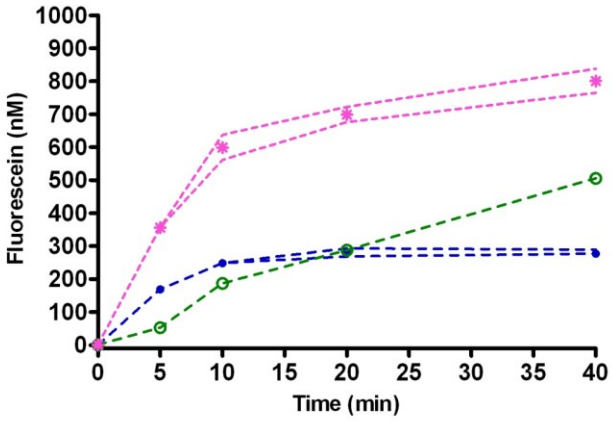

Figure 4.29. Average fluorescein (nM) nasal enhancer comparisons in whole blood measured with online high speed microdialysis capillary electrophoresis with laser induced fluorescence detection. Intranasal Dose with Absorption Promoter Chitosan (rose asterisk): F (1mM, 50 nanomoles) + Chitosan (0.5% w/v), 50 µL, N = 1 animal. Intranasal Dose with Absorption Promoter HPβCD (green, open circles): F (1mM, 50 nanomoles) + HPβCD (9.9% w/v) in aCSF, 50 µL, N = 3 animals. Intranasal Dose (blue solid circles): F (1mM, 50 nanomoles) in aCSF, 50 µL, N = 5 animals. Each point represents average fluorescein in whole blood sampled via distal tail slice at T = 0 (prior to i.n. dose) and T = 5, 10, 20, and 40 min (post i.n. dose), with the dashed lines above and below representing standard deviation, N ≥ 3. Electropherograms were recorded every 23-25 seconds.

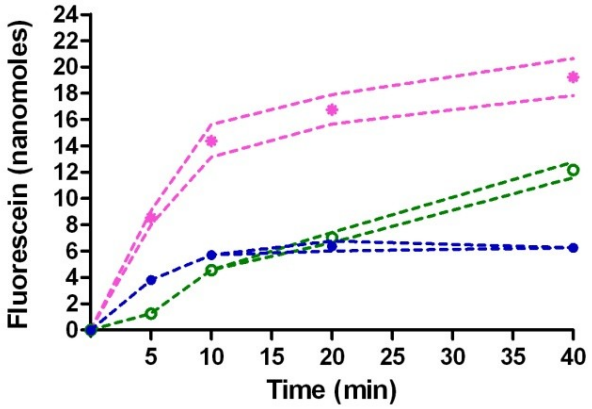

Figure 4.30. Average fluorescein (nanomoles) nasal enhancer comparisons in whole blood measured with online high speed microdialysis capillary electrophoresis with laser induced fluorescence detection. Intranasal Dose with Absorption Promoter Chitosan (rose asterisk): F (1mM, 50 nanomoles) + Chitosan (0.5% w/v), 50 µL, N = 1 animal. Intranasal Dose with Absorption Promoter HPβCD (green, open circles): F (1mM, 50 nanomoles) + HPβCD (9.9% w/v) in aCSF, 50 µL, N = 3 animals. Intranasal Dose (blue solid circles): F (1mM, 50 nanomoles) in aCSF, 50 µL, N = 5 animals. Each point represents average fluorescein in whole blood sampled via distal tail slice at T = 0 (prior to i.n. dose) and T = 5, 10, 20, and 40 min (post i.n. dose), with the dashed lines above and below representing standard deviation, N ≥ 3. Data points were normalized based on rat blood volume = 6.86 ± 0.53 mL per/100 g.[2] Electropherograms were recorded every 23-25 seconds.

Parameter	Intranasal	Dose Corrected Intravenous	Intranasal with HPβCD (9.9% w/v)	Intranasal with Chitosan (0.5% v/v)	Intravenous
Cmax (nM)	6.6 ± 1.1	23.1 ± 2.5	10.6 ± 3.3	1.15 ± 0.9 nM	3.7 ± 0.4
Tmax (min)	81.1 ± 48.1	2.4 ± 0.1	64.3 ± 28.3	58.28	2.4 ± 0.1
Time Post Dose Fluorescein Detected in OB (min)	2.8 ± 0.5	0.8 ± 0.2	7 ± 4	9.62	0.8 ± 0.2
AUC→120 (nmol x min/L)	418.3	1128.0	660.0	44.87	180.5
AUC→40 (nmol x min/L)	78.6	512.9	126.8	12.59	82.1

Table 4.16. Summary of key pharmacokinetic factors in nasal enhancement intranasal studies.

Analyzed pharmacokinetic parameters discussed in this chapter can be found in Table 4.16. Unpaired t test calculations were performed to compare blood AUC i.n. and blood AUC i.n. with chitosan. The differences in the overall fluorescein (nM) blood exposure between i.n. administration of fluorescein and i.n. administration of fluorescein with chitosan were not statistically significant (Table 4.17).

Unpaired t test	
P value	0.0884
P value summary	Ns
Are means signif. different? (P < 0.05)	No
One- or two-tailed P value?	Two-tailed
t, df	t=1.940 df=8

Table 4.17. Statistical comparison of Intranasal AUC→40, blood concentrations to Intranasal Chitosan AUC→40.

Blood volume corrections for variance in animal size were made and i.n. chitosan AUC→40 (nanomoles) was compared to i.n. AUC→40 (nanomoles) (Table 4.18). The

Unpaired t test	
P value	0.0778
P value summary	ns
Are means signif. different? (P < 0.05)	No
One- or two-tailed P value?	Two-tailed
t, df	t=2.022 df=8

Table 4.18. Statistical comparison of Intranasal AUC→40 fluorescein (nanomoles) to blood volume corrected Intranasal Chitosan AUC→40 fluorescein (nanomoles).

results were not statistically significant.

In order to compare the contribution of fluorescein in the OB resulting from intranasal delivery with the nasal enhancers chitosan and HPβCD and the contribution of fluorescein resulting from intravenous delivery, the drug targeting index was calculated (DTI) (Table 4.19). DTI is determined as the ratio of brain AUC/blood AUC after intranasal administration to that after intravenous administration, after being corrected for dose.[25] Intranasal delivery of fluorescein with HPβCD resulted in a 0.79 fold increase in overall drug targeting to the brain compared to intravenous delivery as determined by the

	DTI t = 40 min	**DTP%**	**Bx using nM in Whole Blood**	
Intranasal, Olfactory Bulb	0.56	-78.43	140	
Intranasal with HPβCD, Olfactory Bulb	0.79	-25.93	60	
AUC Fluorescein (nM x min/L)	**Intranasal**	**Intravenous**	**Intranasal HPβCD**	**Intranasal Chitosan**
AUC Brain → 120	418.3	180.5	660	180.5
AUC Brain → 40	78.55	82.07	126.8	12.59
Dose Corrected AUC Brain → 120		1128		
Dose Corrected Brain AUC Brain → 40	78.55	512.9	126.8	12.59
AUC Whole Blood (nM) → 40	9682	5660	11031	11031
AUC Whole Blood (nanomoles) → 40	219.8	116.4	267.4	594.4
AUC Dose Corrected Whole Blood (nM) → 40		35431		
AUC Dose Corrected Whole Blood (nanomoles) → 40	219.8	728.9	267.4	

Table 4.19. Area Under the Curve and Intranasal Drug Targeting Index and Direct Transport Percentage to the Olfactory Bulb

DTI. Intranasal delivery of fluorescein alone resulted in a 0.56 fold increase in overall drug targeting to the brain compared to intravenous delivery as determined by the DTI. DTI of less than 1 is not significant. This implies that there is no overall statistical difference in targeting to the OB between i.n. and i.v. delivery. Intranasal delivery of fluorescein with chitosan resulted in a DTI of 6.8E-05, indicating no direct nose to brain targeting of fluorescein. Intravenous controls were not carried out in this study. The

highest concentrations of fluorescein detected in the blood with application of chitosan to the intranasal fluorescein formulation. Neither chitosan, nor HPβCD resulted in significant brain enhancement via the i.n. delivery over the i.v. delivery of fluorescein to the OB. HPβCD, did however result in a higher brain AUC→120 post i.n. dose, relative to intranasal fluorescein administered without enhancer, with a statistically similar AUC→40 blood value, indicating good potential in its application to intranasal drug delivery nasal enhancement. Direct transport percentage (DTP%), which can be derived from the DTI is a measure of the direct transport from the nose to the brain.[25, 290] The DTP% (Figure 4.31) subtracts the fraction of the brain AUC after intranasal delivery arising from nose-to-blood-to-brain transport (Bx), leaving the fraction of the brain AUC due to direct transport from the nose to the brain via olfactory pathways, trigeminal pathways or other pathways.[25] Unfortunately, fluorescein reached the brain at high concentrations as a result of i.v. administration and with high blood fluorescein levels,

$$\frac{(AUC_{brain})_{i.v.}}{(AUC_{blood})_{i.v.}} = \frac{Bx}{(AUC_{blood})_{i.n.}}$$

$$DTP\% = \frac{(AUC_{brain})_{i.n.} - Bx}{(AUC_{brain})_{i.n.}} \times 100\%$$

Figure 4.31. Calculation of direct transport percent (DTP%).

and hence high AUC, over the first 40 minute time period, DTP% is not a useful tool for calculating what %, if any, of the fluorescein observed in the brain is due to direct nose to brain transport. A comparison of the time taken for fluorescein to reach the olfactory bulb after the dose reveals that nasal enhancers result in a longer time to OB post dose, relative

to intranasal and intravenous application methods. The slower rate of initial increase immediately following i.n. administration indicated in the pharmacokinetic profiles can be interpreted a number of ways. Possibilities include 1) the enhancer formulations increase residency time in the nasal cavity, allowing more drug to potential cross directly to the brain, 2) the process of membrane opening or increasing permeability is slow, which is then followed by a larger increase in rate of fluorescein absorption into the OB or 3) diffusion of fluorescein into the CSF or blood stream, prior to delivery to the brain is a slower process with the enhancers. The continuous increase in fluorescein concentration in the brain with all intranasal dosing techniques was sustained over several hours however, indicating clearance mechanisms typically occurring with intravenous dosing were not as significant a factor. HPβCD studies indicated a significant rise in fluorescein concentrations in the OB approximately 30 minutes post i.n. dosing, possibly related to membrane permeability modification by HPβCD.

Preliminary study of chitosan as a nasal absorption enhancer with fluorescein intranasal delivery indicates it will not be a good compound to use in conjunction with fluorescein. Significant quenching of the fluorescein signal resulted upon mixing with 0.5% chitosan. While the nasal formulation was a viscous gel like solution, potentially increasing residence time of target compounds in the nasal cavity, the solubility of chitosan is low in the physiological pH range, limiting its use with pH dependent fluorescence indicators like sodium fluorescein. With only a single intranasal chitosan study, statistical conclusions are limited. Animal viability during the *in vivo* fluorescein + chitosan study was not high. It is unknown whether this is a result of the chitosan

formulation, an adverse response to the anesthesia and experiment, or unknown variables unique to that particular animal. Results were more promising with intranasal administration of fluorescein with the nasal absorption enhancer hydroxypropyl-β-cyclodextrin. HPβCD (9.9% w/v) used in conjunction with fluorescein (1 mM) for intranasal studies demonstrated statistically significant higher brain exposure to fluorescein over intranasal administration of fluorescein without any permeation enhancer. In addition, sustained levels of fluorescein in the brain were seen in the OB over a period of several hours, without undergoing apparent clearance from the OB. This result is particularly important in drug therapy development. Considerable anatomical differences between human and rats with respect to olfactory epithelium and the brain may influence how the current results translate into human applications, and likely contribute to significant variability between animals of the same species as well. Some small animal models have not translated well to human studies.[172] In rats, the nasal olfactory mucus covers about 50% of the total nasal epithelium as opposed to 5% in humans. The cerebrospinal fluid volume (about 160 mL in humans vs. 0.25 mL in rats) is replaced every 1.5 h in rats compared to every 5 h in humans. The brain interstitial fluid volume is about 260 mL in humans versus 0.3 mL in rats. Therefore, the drug levels achieved in rats by intranasal administration may be an overestimation of what could actually be achieved in humans. Despite anatomical differences between rodents and humans, similar pathways are involved in intranasal delivery to the CNS, at least for IFNb-1b in rats and primates[19] and for melatonin in rats and humans.[218,23] Translation into the clinic is currently underway, with clinical trials of intranasal treatments for

Alzheimer's disease demonstrating success.[157, 158, 291, 292] This is a testament to the fact that the same direct pathways into the CNS utilized in animals are also important and functional in humans.[23] These facts reinforce the necessity of drug bioavailability enhancers like chitosan and hydroxypropyl-β-cyclodextrin for achieving clinically efficacious levels of drug in the human brain.

The high temporal resolution fluorescein assay developed in Chapter 3 of this document indicates it is compatible with the use of nasal absorption permeation enhancers in the study and monitoring of high temporal resolution pharmacokinetic profiles of intranasal drug delivery with high speed online capillary electrophoresis with laser induced fluorescence detection.

CONCLUSIONS

The intranasal route of administration is not a novel approach for drug delivery to the systemic circulation. The novelty lies in using this noninvasive method to rapidly deliver drugs directly from the nasal mucosa to the brain and spinal cord with the aim of treating CNS disorders while minimizing systemic exposure.[23] Application of fluorescein with the nasal absorption enhancer hydroxypropyl-β-cyclodextrin resulted in an increase in delivery of fluorescein to the olfactory bulb when applied in conjunction with intranasally administered fluorescein. It is possible that addition of nasal and membrane permeation enhancers to intranasal drug delivery formulations may circumvent issues associated with high mucosal clearance, low residence time in the nasal cavity, and epithelial membrane impermeability. Increasing brain bioavailability in conjunction with intranasal drug delivery via nasal absorption enhancers and permeability promoters has

high potential for significant improvement in the nasal absorption and rate of transport of drugs from nose to brain. This is of particular importance for treatment of neurological disorders and disease such as Parkinson's, stroke, and Alzheimer's, where delivery of therapeutically relevant levels of drugs to the CNS is essential. High speed online microdialysis capillary electrophoresis with laser induced fluorescence detection monitoring of intranasal delivery of fluorescein with a nasal enhancer has shown the first high temporal resolution pharmacokinetic profiles in the rat olfactory bulb, and can detect relative differences in brain bioavailability of fluorescein when intranasal formulations are modified to improve absorption into the brain. This analytical technique is ideal in its application to developing targeted drug therapies and further elucidating the mechanisms behind nose to brain drug delivery through pharmacokinetic monitoring and analysis.

This work was a collaborative project with Dr. William H. Frey II, Dr. Leah Hanson, and Dr. Jared Fine at the Alzheimer's Research Center at Regions Hospital in St. Paul, MN. The author would like to thank Dr. Shyeilla Dhuria for her time and correspondence regarding pharmaceutical data analysis. Financial support for this research was provided by the University of Minnesota, the Alzheimer's Research Center and National Institutes of Health (Grants GM063533 and NS043304) and is greatly appreciated.

REFERENCES

(1) Shipley, M. T.; Puche, A. C.; Ennis, M. *The olfactory system. In The Rat Nervous System.* ; Academic Press: New York, 2003.
(2) Probst, R. J.; Lim, J. M.; Bird, D. N.; Pole, G. L.; Sato, A. K.; Claybaugh, J. R. *J Am Assoc Lab Anim Sci* **2006**, *45*, 49-52.
(3) Graves, J. D.; Krebs, E. G. *Pharmacology & Therapeutics* **1999**, *82*, 111-121.
(4) Purves, D.; Augustine, G.; Fitzpatrick, D.; Hall, W.; LaMantia, A.-S.; McNamara, J.; Williams, S. M. Eds. *Neuroscience*, 3 ed.; Sinauer Associates, Inc: Sunderland, Massachusetts, 2004.
(5) Snyder, S. H.; Jaffrey, S. R.; Zakhary, R. *Brain Research Reviews* **1998**, *26*, 167-175.
(6) Dirnagle, U.; Iadecole, C.; Moskowitz, M. *Trends in Neurosciences* **1999**, *22*, 391-397.
(7) Czlonkowska, A.; Kurkowska-Jastrzebska, I.; Czlonkowski, A.; Peter, D.; Stefano, G. *Medical Science Monitor* **2002**, *8*, 165-177.
(8) Fedele, E.; Raiteri, M. *Progress in Neurobiology* **1999**, *58*, 89-120.
(9) Hobbs, A. J.; Higgs, A.; Moncada, S. *Annual review of pharmacology and toxicology* **1999**, *39*, 191-220.
(10) Murad, F. *The New England Journal of Medicine* **2006**, *355*, 2003-2011.
(11) Chalimoniuk, M.; Langfort, J.; Lukacova, N.; Marsala, J. *Biochemical and Biophysical Research Communications* **2004**, *324*, 118-126.
(12) Corbin, J.; Fancis, S. *The Journal of Biological Chemistry* **1999**, *274*, 13729-13732.
(13) Vallebuona, F.; Raiteri, M. *Neuroscience* **1993**, *57*, 577-585.
(14) Vallebuona, F.; Raiteri, M. *Journal of Neuroscience* **1994**, *14*, 134-139.
(15) Jedlitschky, G.; Burchell, B.; Keppler, D. *Journal of Biological Chemistry* **2000**, *275*, 30069-30074.
(16) Poulopoulou, C.; Nowak, L. *Journal of Pharmacology and Experimental Therapeutics* **1998**, *286*, 99-109.
(17) Frey, W. H. II.; Liu, J.; Chen, X. Q.; Thorne, R. G.; Fawcett, J. R.; Ala, T. A.; Rahman, Y. E. *DRUG DELIVERY* **1997**, *4*, 87-92.
(18) Thorne, R. G.; Pronk, G. J.; Padmanabhan, V.; Frey, W. H. II. *Neuroscience* **2004**, *127*, 481-496.
(19) Thorne, R. G.; Hanson, L. R.; Ross, T. M.; Tung, D.; Frey, W. H. II. *Neuroscience* **2008**, *152*, 785-797.
(20) Thorne, R. G.; Frey, W. H., 2nd *Clin Pharmacokinet* **2001**, *40*, 907-946.
(21) Hanson, L. R.; Frey, W. H. II. *Bmc Neuroscience* **2008**, *9*, 1-4.
(22) Frey, W. H. II.; Liu, J.; Thorne, R. G.; Rahman, Y. E. *Neurobiology of Aging* **1994**, *15*, S137-S138.
(23) Dhuria, S. V.; Hanson, L. R.; Frey, W. H. II. *Journal of Pharmaceutical Sciences* **2010**, *99*, 1654-1673.
(24) Frey, W. H. II. *Drug Deliv Technol* **2002**, *2*, 46-49.

(25) Dhuria, S. V.; Hanson, L. R.; Frey, W. H. II. *Journal of Pharmaceutical Sciences* **2009**, *98*, 2501-2515.
(26) Liu, X. F.; Fawcett, J. R.; Thorne, R. G.; Frey, W. H. II. *Stroke* **2001**, *32*, 352-352.
(27) Thorne, R. G.; Emory, C. R.; Ala, T. A.; Frey, W. H., 2nd *Brain Res* **1995**, *692*, 278-282.
(28) Klinker, C. C.; Bowser, M. T. *Anal Chem* **2007**, *79*, 8747-8754.
(29) Ciriacks, C. M.; Bowser, M. T. *Neurosci Lett* **2006**, *393*, 200-205.
(30) Ciriacks, C. M.; Bowser, M. T. *Anal Chem* **2004**, *76*, 6582-6587.
(31) O'Brien, K. B.; Esguerra, M.; Klug, C. T.; Miller, R. F.; Bowser, M. T. *Electrophoresis* **2003**, *24*, 1227-1235.
(32) O'Brien, K. B.; Bowser, M. T. *Electrophoresis* **2006**, *27*, 1949-1956.
(33) O'Brien, K. B.; Esguerra, M.; Miller, R. F.; Bowser, M. T. *Anal Chem* **2004**, *76*, 5069-5074.
(34) Bowser, M. T.; Kennedy, R. T. *Electrophoresis* **2001**, *22*, 3668-3676.
(35) Garthwaite, J. *Trends in Neurosciences* **1991**, *14*, 60-67.
(36) Consolo, S.; Cassetti, A.; Uboldi, M. C. *Neuroscience (Oxford)* **1999**, *91*, 51-58.
(37) Schmidt, H. H. H. W.; Lohmann, S. M.; Walter, U. *Biochimica et Biophysica Acta* **1993**, *1178*, 153-175.
(38) Luo, D.; Leung, E.; Vincent, S. *Journal of Neuroscience* **1994**, *14*, 263-271.
(39) Friebe A.; Koesling D. *Circulation Research* **2003**, *93*, 96-105.
(40) Vincent S.; Williams J.; Riner P.; El-Husseini A. *Progress in Brain Research* **1998**, *118*, 27-35.
(41) Ashman, D. F.; Lipton, R.; Melicow, M. M.; Price, T. D. *Biochemical and Biophysical Research Communications* **1963**, *11*.
(42) Goldberg, N. D.; Dietz, S. B.; O'Toole, A. G. *The Journal of Biological Chemistry* **1969**, *244*, 4458-4466.
(43) Ferrendelli, J. A.; Rubin, E. H.; Orr, H. T.; Kinscherf, D. A.; Lowry, O. H. *Analytical Biochemistry* **1977**, *78*, 252-259.
(44) Mao C. C.; Guidotti A.; Costa E. *Brain Research* **1974**, *79*, 510-514.
(45) Rubin, E. H.; Ferrendelli J. A. *Journal of Neurochemistry* **1977**, *29*, 43-51.
(46) Wu, C.-P.; Woodcock, H.; Hladky, S. B.; Barrand, M. A. *Biochemical Pharmacology* **2005**, *69*, 1257-1262.
(47) Marcoli, M.; Cervetto, C.; Paluzzi, P.; Guarnieri, S.; Raiteri, M.; Maura, G. *Neurochemistry International* **2006**, *49*, 12-19.
(48) Hara, S.; Mukai, T.; Mizukami, H.; Kuriiwa, F.; Watanabe, T. *Journal of Pharmacological Sciences* **2007**, *104*, 90-93.
(49) Prast, H.; Philippu, A. *Progress in Neurobiology* **2001**, *64*, 54-68.
(50) Padayatte, P.; Paatanaik, P.; Ma, X.; Van den Akker, F. *Pharmacology and Therapeutics* **2004**, *104*, 8399.
(51) Sampath, J.; Adachi, M.; Hatse, S.; Naesens, L.; Balzarini, J.; Flatley, R.; Matherly, L.; Schuetz, J. *American Association of Pharmaceutical Scientists* **2002**, *4*, 1-9.

(52) Nies, A.; Spring, H.; Thon, W.; Keppler, D.; Jedlitschky, G. *The Journal of Urology* **2002**, *167*, 2271-2275.
(53) Renes, J.; Elisabeth, G. E. d. V.; Jansen, P. L. M.; Mueller, M. *Drug Resistance Updates* **2000**, *3*, 287-3000.
(54) Andric, S. A.; Kostic, T. S.; Stolkilkovic, S. S. *Endocrinology* **2006**, *147*, 3435-3445.
(55) Xu, H.-L.; Gavrilyuk, V.; Wolde, H.; Baughmen, V.; Pellgrino, D. *American Journal of Physiology - Heart and Circulatory Physiology* **2004**, *286*, H2020-H2027.
(56) Boadu, E.; Sager, G. *Scandinavian Journal of Clinical and Laboratory Investigation* **2004**, *64*, 41-48.
(57) Hansen, D.; Malonne, I. D.; Lunte, S.; Lunte, C. *Journal of Pharmaceutical Sciences* **1999**, *88*, 14-27.
(58) Bourne, J. A. *Clin Exp Pharmacol Physiol* **2003**, *30*, 16-24.
(59) Watson, C. J.; Venton, B. J.; Kennedy, R. T. *Anal Chem* **2006**, *78*, 1391-1399.
(60) Davies, M. I.; Cooper, J. D.; Desmond, S. S.; Lunte, C. E.; Lunte, S. M. *Adv Drug Deliv Rev* **2000**, *45*, 169-188.
(61) Wen, X. D.; Qi, L. W.; Chen, J.; Song, Y.; Yi, L.; Yang, X. W.; Li, P. *J Chromatogr B Analyt Technol Biomed Life Sci* **2007**, *852*, 598-604.
(62) Shackman, H. M.; Shou, M.; Cellar, N. A.; Watson, C. J.; Kennedy, R. T. *J Neurosci Methods* **2007**, *159*, 86-92.
(63) Yu, W.; Cheng, Q.; Feng, J.; Li, F. *Pharmazie* **2007**, *62*, 883-891.
(64) Hamani, C.; Luer, M.; Dujovny, M. *Neurological Research* **1997**, *19*, 281-288.
(65) Thompson, J. E.; Vickroy, T. W.; Kennedy, R. T. A. C., 71(13), 2379-2384 *Analytical Chemistry* **1999**, *71*, 2379-2384.
(66) Jing, F. C.; Chen, H.; Li, C. L. *Biomed Environ Sci* **2007**, *20*, 317-320.
(67) Davies, M.; Cooper, J.; Desmond, S.; Lunte, C.; Lunte, S. *Advanced Drug Delivery Reviews* **2000**, *45*, 169-188.
(68) Wang, X. D.; Stenken, J. A. *Analytical Chemistry* **2006**, *78*, 6026-6034.
(69) Chaurasia, C. *Biomedical Chromatography* **1999**, *13*, 317-332.
(70) O'Brien, K.; Esguerra, M.; Miller, R.; Bowser, M. *Analytical Chemistry* **2004**, *76*, 5069-5074.
(71) Gaur, V.; Kumar, A. *Brain Research Bulletin* **2010**, *82*, 57-64.
(72) Jesse, C. R.; Wilhelm, E. A.; Bortolatto, C. F.; Rocha, J. B. T.; Nogueira, C. W. *European Journal of Pharmacology* **2010**, *635*, 135-141.
(73) Kulkarni, S. K.; Dhir, A. *European Journal of Pharmacology* **2007**, *569*, 77-83.
(74) Marte, A.; Pepicelli, I.; Cavallero, A.; Raiteri, M.; Fedele, E. *Journal of Neuroscience Research* **2008**, *86*, 3338-3347.
(75) Powers-Martin, K.; Barron, A. M.; Auckland, C. H.; McCooke, J. K.; McKitrick, D. J.; Arnolda, L. F.; Phillips, J. K. *Journal of Biomedical Science* **2008**, *15*, 801-812.
(76) Zhou, S.; Zuo, H.; Stobaugh, J.; Lunte, C.; Lunte, S. *Analytical Chemistry* **1995**, *67*, 594-599.

(77) Hogan, B.; Lunte, S.; Stobaugh, J.; Lunte, C. *Analytical Chemistry* **1994**, *66*, 596-602.
(78) Bowser, M.; Kennedy, R. *Electrophoresis* **2001**, *22*, 3668-3676.
(79) Yonekura, S.; Iwasaki, M.; Kai, M.; Ohkura, Y. *Journal of Chromatography B-Biomedical Applications* **1994**, *654*, 19-24.
(80) Yonekura, S.; Iwasaki, M.; Kai, M.; Ohkura, Y. *Analytical Sciences* **1994**, *10*, 247-251.
(81) Biggio, G.; Brodie, B. B.; Costa, E.; Guidotti, A. *Proceedings of the National Academy of Sciences of the United States of America* **1977**, *74*, 3592-3596.
(82) 2nd ed.; IUPAC Compendium of Chemical Terminology 2nd Edition, 1997; Vol. 2007.
(83) Llansola, M.; Hernandez-Viadel, M.; Erceg, S.; Montoliu, C.; Felipo, V. *J Neurosci Res* **2009**, *87*, 2351-2355.
(84) Paez, X.; Hernandez, L. *Biopharmaceutics and Drug Disposition* **2001**, *22*, 273-289.
(85) Thompson, J. E.; Vickroy, T. W.; Kennedy, R. T. *Analytical Chemistry* **1999**, *71*, 2379-2384.
(86) Lacroix, M.; Poinsot, V.; Fournier, C.; Couderc, F. *Electrophoresis* **2005**, *26*, 2608-2621.
(87) Chan, S. L.; Fiscus, R. R. *Molecular Human Reproduction* **2003**, *9*, 775-783.
(88) Lada, M.; Kennedy, R. *Analytical Chemistry* **1996**, *68*, 2790-2797.
(89) Perez, S. A.; Colon, L. A. *17* **Electrophoresis**, *2*.
(90) Jorgenson, J. W.; Lukacs, K. D. *Clinical Chemistry* **1981**, *27*, 1551-1553.
(91) Jandik, P.; Bonn, G. *Capillary Electrophoresis of Small Molecules and Ions.* ; VCH Publishers: New York, 1993.
(92) Lada, M. W.; Schaller, G.; Carriger, M. H.; Vickroy, T. W.; Kennedy, R. T. *Analytica Chimica Acta* **1995**, *307*, 217-225.
(93) Lada, M. W.; Kennedy, R. T. *Journal of Neuroscience Methods* **1995**, *63*, 147-152.
(94) Chan, K.; Muschik, G.; Issaq, H. *Electrophoresis* **2000**, *21*, 2062-2066.
(95) Lada, M.; Vickroy, T.; Kennedy, R. *Analytical Chemistry* **1997**, *69*, 4560-4565.
(96) Lada, M. W.; Vickroy, T. W.; Kennedy, R. T. *Journal of Neurochemistry* **1998**, *70*, 617-625.
(97) Ciriacks, C.; Bowser, M. *Analytical Chemistry* **2004**, *76*, 6582-6587.
(98) O'Brien, K.; Esguerra, M.; Klug, C.; Miller, R.; Bowser, M. *Electrophoresis* **2003**, *24*, 1227-1235.
(99) Ciriacks, C.; Bowser, M. *Neuroscience Letters* **2006**, *393*, 200-205.
(100) Cheng, Y. F.; Dovichi, N. J. *Science* **1988**, *242*, 562-564.
(101) Zarrin, F.; Dovichi, N. J. *Anal Chem* **1985**, *57*, 1826-1829.
(102) Zhang, J. Z.; Chen, D. Y.; Wu, S.; Harke, H. R.; Dovichi, N. J. *Clin Chem* **1991**, *37*, 1492-1496.
(103) Khaledi, M. *High-Performance Capillary Electrophoresis: Theory, Techniques, and Applications.* ; John Wiley and Sons, Inc.: New York, 1998.

(104) Li, S. F. Y. *Capillary Electrophoresis: Principles, Practice, and Applications.*; Elsevier: Amsterdam, 1992.
(105) Haugland, R.; Molecular Probes: Eugene, O., 1996. *Handbook of Fluorescent Probes and Research Chemicals, 6th Edition.*, 6th ed.; Molecular Probes: Eugene, OR, 1996.
(106) Alvarez-Coque, M.; Hernandez, M.; Camanas, R.; Fernandez, C. *Analytical Biochemistry* **1989**, *178*, 1-7.
(107) Xu, W.; University of Minnesota: Minneapolis, 2004.
(108) Bantan-Polak, T.; Kassai, M.; Grant, K. *Analytical Biochemistry* **2001**, *297*, 128-136.
(109) Molecular Probes, http://www.invitrogen.com/site/us/en/home/brands/Molecular-Probes.html, 2005.
(110) Frei, R.; Lawrence, J. *Chemical Derivatization in Analytical Chemistry: Volume 2, Separation and Continuous Flow Techniques.* ; Plenum Press: New Yourk, 1982.
(111) Udenfriend, S.; Stein, S.; Boehlen, P.; Dairman, W.; Leimgruber, W.; Weigele, M. *Science* **1972**, *178*, 871-872.
(112) Ohba, Y.; Kai, M.; Nohta, H.; Ohkura, Y., 215-21. *Analytica Chimica Acta* **1994**, *273*, 215-221.
(113) Ohba, Y.; Soda, K.; Kai, M.; Zaitsu, K. *Analytica Chimica Acta* **2000**, *414*, 95-100.
(114) Yonekura, S.; Iwasaki, M.; Kai, M.; Ohkura, Y. *Journal of Chromatography B* **1994**, *654*, 19-24.
(115) Katayama, M.; Matsuda, Y.; Kobayashi, K.; Kaneko, S.; Ishikawa, H. *Biomedical Chromatography* **2006**, *20*, 800-805.
(116) Crescentini, G.; Stocchi, V. *Journal of Chromatography A* **1984**, *290*, 393-399.
(117) Kai, M.; Ohkura, Y.; Yonekura, S.; Iwasaki, M. *Analytical Chimica Acta* **1988**, *207*, 243-249.
(118) Kai, M.; Ohkura, Y. *Analytical Chimica Acta* **1994**, *287*, 75-81.
(119) Isumi, Y.; Akizawa, T.; Matsuda, K.; Umekawa, H.; Kurose, T.; Yoshioka, M. *Journal of Chromatography A* **1998**, *806*, 231-236.
(120) Soda, K.; Ohba, Y.; Zaitsu, K. *Journal of Chromatography B* **2001**, *752*, 55-60.
(121) Ohba, Y.; Soda, K.; Zaitsu, K. *Biological & Pharmaceutical Bulletin* **2001**, *24*, 567-569.
(122) Chen, Z.; Wu, J.; Baker, G.; Parent, M.; Dovichi, N. *Journal of Chromatography A* **2001**, *914*, 293-298.
(123) Hempel, G. *Electrophoresis* **2000**, *21*, 691-698.
(124) Illum, L. *Eur J Pharm Sci* **2000**, *11*, 1-18.
(125) Ross, T. M.; Zuckermann, R. N.; Reinhard, C.; Frey, W. H. *Neuroscience Letters* **2008**, *439*, 30-33.
(126) Ross, T. M.; Martinez, P. M.; Renner, J. C.; Thorne, R. G.; Hanson, L. R.; Frey, W. H. II. *Journal of Neuroimmunology* **2004**, *151*, 66-77.
(127) Hanson, L. R.; Frey, W. H. II. *Journal of Neuroimmune Pharmacology* **2007**, *2*, 81-86.

(128) Pulliam, L.; Sun, B.; Rempel, H.; Hanson, L.; Martinez, P.; Frey, W. *Journal of Neurovirology* **2006**, *12*, 67-67.
(129) Martinez, J. A.; Francis, G. J.; Liu, W. Q.; Pradzinsky, N.; Fine, J.; Wilson, M.; Hanson, L. R.; Frey, W. H. II.; Zochodne, D.; Gordon, T.; Toth, C. *Neuroscience* **2008**, *157*, 908-925.
(130) Alcala-Barraza, S. R.; Lee, M. S.; Hanson, L. R.; McDonald, A. A.; Frey, W. H. II.; McLoon, L. K. *Journal of Drug Targeting* **2010**, *18*, 179-190.
(131) Hanson, L. R.; Hafez, D.; Svitak, A. L.; Burns, R. B.; Li, X. A.; Frey, W. H. II.; Marr, R. A. *Journal of Molecular Neuroscience* **2011**, *43*, 424-427.
(132) Dhuria, S. V.; Hanson, L. R.; Frey, W. H. II *Journal of Pharmacology and Experimental Therapeutics* **2009**, *328*, 312-320.
(133) Corbo, D. C.; Liu, J. C.; Chien, Y. W. *Pharm Res* **1989**, *6*, 848-852.
(134) Carr, D. B.; Goudas, L. C.; Denman, W. T.; Brookoff, D.; Staats, P. S.; Brennen, L.; Green, G.; Albin, R.; Hamilton, D.; Rogers, M. C.; Firestone, L.; Lavin, P. T.; Mermelstein, F. *Pain* **2004**, *108*, 17-27.
(135) Balin, B. J.; Broadwell, R. D.; Salcman, M.; el-Kalliny, M. *J Comp Neurol* **1986**, *251*, 260-280.
(136) Ross, T. M.; Martinez, P. M.; Renner, J. C.; Thorne, R. G.; Hanson, L. R.; Frey, W. H., 2nd *J Neuroimmunol* **2004**, *151*, 66-77.
(137) Liu, X. F.; Fawcett, J. R.; Thorne, R. G.; DeFor, T. A.; Frey, W. H. *Journal of the Neurological Sciences* **2001**, *187*, 91-97.
(138) Liu, X. F.; Fawcett, J. R.; Frey, W. H. II. *Neurology* **2002**, *58*, A389-A389.
(139) Capsoni, S.; Giannotta, S.; Cattaneo, A. *Mol Cell Neurosci* **2002**, *21*, 15-28.
(140) De Rosa, R.; Ancheta Garcia, A.; Braschi, C.; Capsoni, S.; Maffei, L.; Berardi, N.; Cattaneo, A.; Levi-Montalcini, R. *Proceedings of the National Academy of Sciences of the United States of America* **2005**, *102*, 3811-3816
(141) Frey, W. H. II.; Liu, J.; Thorne, R. G.; Rahman, Y. E. *Neurobiology of Aging* **1994**, *15*, S137-S138.
(142) Chen, X. Q.; Fawcett, J. R.; Rahman, Y. E.; Ala, T. A.; Frey, W. H. II. *J Alzheimers Dis* **1998**, *1*, 35-44.
(143) Capsoni, S.; Giannotta, S.; Cattaneo, A. *Proc Natl Acad Sci U S A* **2002**, *99*, 12432-12437.
(144) Jin, K.; Xie, L.; Childs, J.; Sun, Y.; Mao, X. O.; Logvinova, A.; Greenberg, D. A. *Ann Neurol* **2003**, *53*, 405-409.
(145) Kern, W.; Born, J.; Schreiber, H.; Fehm, H. L. *Diabetes* **1999**, *48*, 557-563.
(146) Vilbergsson, S.; Sigurdsson, G.; Sigvaldason, H.; Hreidarsson, A. B.; Sigfusson, N. *Diabet Med* **1997**, *14*, 491-498.
(147) Gozes, I.; Bardea, A.; Reshef, A.; Zamostiano, R.; Zhukovsky, S.; Rubinraut, S.; Fridkin, M.; Brenneman, D. E. *Proc Natl Acad Sci U S A* **1996**, *93*, 427-432.
(148) Dufes, C.; Olivier, J. C.; Gaillard, F.; Gaillard, A.; Couet, W.; Muller, J. M. *Int J Pharm* **2003**, *255*, 87-97.
(149) Li, H.; Yan, Z. Y. *Biomedical Chromatography*, *24*, 1185-1192.
(150) Gozes, I.; Giladi, E.; Pinhasov, A.; Bardea, A.; Brenneman, D. E. *J Pharmacol Exp Ther* **2000**, *293*, 1091-1098.

(151) Gozes, I. *Trends Neurosci* **2001**, *24*, 700-705.
(152) Illum, L. *Journal of Controlled Release* **2003**, *87*, 187-198.
(153) Illum, L. *Drug Discovery Today* **2002**, *7*, 1184-1189.
(154) Benedict, C.; Hallschmid, M.; Hatke, A.; Schultes, B.; Fehm, H. L.; Born, J.; Kern, W. *Psychoneuroendocrinology* **2004**, *29*, 1326-1334.
(155) Benedict, C.; Frey, W. H. II.; Schioth, H. B.; Schultes, B.; Born, J.; Hallschmid, M. *Experimental Gerontology* **2011**, *46*, 112-115.
(156) Benedict, C.; Hallschmid, M.; Schultes, B.; Born, J.; Kern, W. *Neuroendocrinology* **2007**, *86*, 136-142.
(157) Reger, M. A.; Watson, G. S.; Frey, W. H.; Baker, L. D.; Cholerton, B.; Keeling, M. L.; Belongia, D. A.; Fishel, M. A.; Plymate, S. R.; Schellenberg, G. D.; Cherrier, M. M.; Craft, S. *Neurobiology of Aging* **2006**, *27*, 451-458.
(158) Reger, M. A.; Watson, G. S.; Green, P. S.; Baker, L. D.; Cholerton, B.; Fishel, M. A.; Plymate, S. R.; Cherrier, M. M.; Schellenberg, G. D.; Frey, W. H.; Craft, S. *Journal of Alzheimers Disease* **2008**, *13*, 323-331.
(159) Cummings, J. L.; Cole, G. *JAMA* **2002**, *287*, 2335-2338.
(160) Francis, G. J.; Martinez, J. A.; Liu, W. Q.; Xu, K.; Ayer, A.; Fine, J.; Tuor, U. I.; Glazner, G.; Hanson, L. R.; Frey, W. H. II.; Toth, C. *Brain* **2008**, *131*, 3311-3334.
(161) Gluckman, P.; Klempt, N.; Guan, J.; Mallard, C.; Sirimanne, E.; Dragunow, M.; Klempt, M.; Singh, K.; Williams, C.; Nikolics, K. *Biochem Biophys Res Commun* **1992**, *182*, 593-599.
(162) Guan, J.; Williams, C.; Gunning, M.; Mallard, C.; Gluckman, P. *J Cereb Blood Flow Metab* **1993**, *13*, 609-616.
(163) Liu, X. F.; Fawcett, J. R.; Hanson, L. R.; Frey, W. H., 2nd *J Stroke Cerebrovasc Dis* **2004**, *13*, 16-23.
(164) Pardridge, W. M. *Arch Neurol* **2002**, *59*, 35-40.
(165) Pardridge, W. M. *Adv Exp Med Biol* **2002**, *513*, 397-430.
(166) Brasnjevic, I.; Steinbusch, H. W.; Schmitz, C.; Martinez-Martinez, P. *Prog Neurobiol* **2009**, *87*, 212-251.
(167) Soane, R. J.; Frier, M.; Perkins, A. C.; Jones, N. S.; Davis, S. S.; Illum, L. *International Journal of Pharmaceutics* **1999**, *178*, 55-65.
(168) Hinchcliffe, M.; Illum, L. *Adv Drug Deliv Rev* **1999**, *35*, 199-234.
(169) in 't Veen, J. P. M.; van den Berg, M. P.; Romeijn, S. G.; Verhoef, J. C.; Merkus, F. W. H. M. *Eur J Pharm Biopharm* **2005**, *61*, 27-31.
(170) Sarkar, M. A. *Pharm Res* **1992**, *9*, 1-9.
(171) Artursson, P.; Lindmark, T.; Davis, S. S.; Illum, L. *Pharmaceutical Research* **1994**, *11*, 1358-1361.
(172) Davis, S. S.; Illum, L. *Clinical Pharmacokinetics* **2003**, *42*, 1107-1128.
(173) Nonaka, N.; Farr, S. A.; Kageyama, H.; Shioda, S.; Banks, W. A. *J Pharmacol Exp Ther* **2008**, *325*, 513-519.
(174) Jansson, B.; Bjork, E. *J Drug Target* **2002**, *10*, 379-386.
(175) Graff, C. L.; Zhao, R.; Pollack, G. M. *Pharm Res* **2005**, *22*, 235-244.
(176) Banks, W. A.; During, M. J.; Niehoff, M. L. *J Pharmacol Exp Ther* **2004**, *309*, 469-475.

(177) Shipley, M. T. *Brain Res Bull* **1985**, *15*, 129-142.
(178) Baker, H.; Spencer, R. F. *Exp Brain Res* **1986**, *63*, 461-473.
(179) Luzzati, V.; Benoit, E.; Charpentier, G.; Vachette, P. *J Mol Biol* **2004**, *343*, 199-212.
(180) Broadwell, R. D.; Balin, B. J. *J Comp Neurol* **1985**, *242*, 632-650.
(181) Hanson, L. R.; Martinez, P. M.; Taheri, S.; Kamsheh, L.; Mignot, E.; Frey, W. H. II. *Drug Delivery Technology* **2004**, *4*, 66-70.
(182) Hanson, L. R.; Roeytenberg, A.; Martinez, P. M.; Coppes, V. G.; Sweet, D. C.; Rao, R. J.; Marti, D. L.; Hoekman, J. D.; Matthews, R. B.; Frey, W. H. II.; Panter, S. S. *Journal of Pharmacology and Experimental Therapeutics* **2009**, *330*, 679-686.
(183) Vaka, S. R.; Sammeta, S. M.; Day, L. B.; Murthy, S. N. *J Pharm Sci* **2009**, *98*, 3640-3646.
(184) Soane, R. J.; Hinchcliffe, M.; Davis, S. S.; Illum, L. *International Journal of Pharmaceutics* **2001**, *217*, 183-191.
(185) Madara, J. L.; Dharmsathaphorn, K. *J Cell Biol* **1985**, *101*, 2124-2133.
(186) Hadley, W. M.; Dahl, A. R. *Drug Metab Dispos* **1983**, *11*, 275-276.
(187) Li, G.; Yuan, W.; Fu, B. M *J Biomech* **2010**, *43*, 2133-2140.
(188) Pardridge, W. M. *NeuroRx* **2005**, *2*, 3-14.
(189) Pardridge, W. M. *Jpn J Pharmacol* **2001**, *87*, 97-103.
(190) Pardridge, W. M. *Mol Biotechnol* **2005**, *30*, 57-70.
(191) Hawkins, B. T.; Ocheltree, S. M.; Norwood, K. M.; Egleton, R. D. *Neuroscience Letters* **2007**, *411*, 1-5.
(192) Graff, C. L.; Pollack, G. M. *J Pharm Sci* **2005**, *94*, 1187-1195.
(193) Alford, R.; Simpson, H. M.; Duberman, J.; Hill, G. C.; Ogawa, M.; Regino, C.; Kobayashi, H.; Choyke, P. L. *Mol. Imaging* **2009**, *8*, 341-354.
(194) Salem, H.; Loux, J. J.; Smith, S.; Nichols, C. W. *Toxicology* **1979**, *12*, 143-150.
(195) Kozler, P.; Pokorny, J. *Physiol Res* **2003**, *52*, 607-614.
(196) Sun, H. Y.; Miller, D. W.; Elmquist, W. F. *Pharmaceutical Research* **2001**, *18*, 1542-1549.
(197) Nandi, P.; Desaias, D. P.; Lunte, S. M. *Electrophoresis* **2010**, *31*, 1414-1422.
(198) Ravenstijn, P. G. M.; Merlini, M.; Hameetman, M.; Murray, T. K.; Ward, M. A.; Lewis, H.; Ball, G.; Mottart, C.; de Ville de Goyet, C.; Lemarchand, T.; van Belle, K.; O'Neill, M. J.; Danhof, M.; de Lange, E. C. M. *J Pharmacol Toxicol Methods* **2008**, *57*, 114-130.
(199) Bagger, M. A.; Bechgaard, E. *Eur J Pharm Sci* **2004**, *21*, 235-242.
(200) Sjoback, R.; Nygren, J.; Kubista, M. *Spectrochimica Acta Part a-Molecular and Biomolecular Spectroscopy* **1995**, *51*, L7-L21.
(201) Johnson, I.; Spence, M. T. Z., Eds. *Molecular Probes Handbook, A Guide to Fluorescent Probes and Labeling Technologies*, 11th Edition ed.; Invitrogen Life Sciences, 2011.
(202) Mota, M. C.; Carvalho, P.; Ramalho, J.; Leite, E. *Int. Ophthalmol.* **1991**, *15*, 321-326.

(203) Chen, S. C.; Nakamura, H.; Tamura, Z. *Chemical & Pharmaceutical Bulletin* **1979**, *27*, 475-479.
(204) Romanchuk, K. G. *Survey of Ophthalmology* **1982**, *26*, 269-283.
(205) Song, L.; Hennink, E. J.; Young, I. T.; Tanke, H. J. *Biophys J* **1995**, *68*, 2588-2600.
(206) Hillbom, M. E.; Tervo, T. M. T. *Experientia* **1981**, *37*, 936-938.
(207) Tervo, T.; Joo, F.; Palkama, A.; Salminen, L. *Experientia* **1979**, *35*, 252-254.
(208) Sun, H.; Johnson, D. R.; Finch, R. A.; Sartorelli, A. C.; Miller, D. W.; Elmquist, W. F. *Biochemical and Biophysical Research Communications* **2001**, *284*, 863-869.
(209) Chow, H. S.; Chen, Z.; Matsuura, G. T. *J Pharm Sci* **1999**, *88*, 754-758.
(210) Chow, H. H.; Anavy, N.; Villalobos, A. *J Pharm Sci* **2001**, *90*, 1729-1735.
(211) Wang, Y.; Aun, R.; Tse, F. L. *Biopharm Drug Dispos* **1998**, *19*, 571-575.
(212) Sakane, T.; Akizuki, M.; Taki, Y.; Yamashita, S.; Sezaki, H.; Nadai, T. *J. Pharm. Pharmacol.* **1995**, *47*, 379-381.
(213) Agu, R. U.; Vu Dang, H.; Jorissen, M.; Willems, T.; Kinget, R.; Verbeke, N. *Int J Pharm* **2002**, *237*, 179-191.
(214) Pardridge, W. M. *J Neurochem* **1998**, *70*, 1781-1792.
(215) Baba, M.; Oishi, R.; Saeki, K. *Naunyn Schmiedebergs Arch Pharmacol* **1988**, *337*, 423-428.
(216) van den Berg, M. P.; Romeijn, S. G.; Verhoef, J. C.; Merkus, F. W. *J Neurosci Methods* **2002**, *116*, 99-107.
(217) Van den Berg, M. P.; Merkus, P.; Romeijn, S. G.; Verhoef, J. C.; Merkus, F. W. *J Drug Target* **2003**, *11*, 325-331.
(218) van den Berg, M. P.; Merkus, P.; Romeijn, S. G.; Verhoef, J. C.; Merkus, F. W. *Pharm Res* **2004**, *21*, 799-802.
(219) van den Berg, M. P.; Verhoef, J. C.; Romeijn, S. G.; Merkus, F. W. *Eur J Pharm Biopharm* **2004**, *58*, 131-135.
(220) Illum, L.; Jabbal-Gill, I.; Hinchcliffe, M.; Fisher, A. N.; Davis, S. S. *Advanced Drug Delivery Reviews* **2001**, *51*, 81-96.
(221) Merkus, F. W.; Verhoef, J. C.; Marttin, E.; Romeijn, S. G.; van der Kuy, P. H.; Hermens, W. A.; Schipper, N. G. *Adv Drug Deliv Rev* **1999**, *36*, 41-57.
(222) Merkus, F. W.; Verhoef, J. C.; Romeijn, S. G.; Schipper, N. G. *Pharm Res* **1991**, *8*, 588-592.
(223) Schipper, N. G.; Romeijn, S. G.; Verhoef, J. C.; Merkus, F. W. *Pharm Res* **1993**, *10*, 682-686.
(224) Schipper, N. G.; Verhoef, J. C.; De Lannoy, L. M.; Romeijn, S. G.; Brakkee, J. H.; Wiegant, V. M.; Gispen, W. H.; Merkus, F. W. *Br J Pharmacol* **1993**, *110*, 1335-1340.
(225) Na, L.; Mao, S.; Wang, J.; Sun, W. *Int J Pharm* **2010**, *397*, 59-66.
(226) Yang, T.; Hussain, A.; Paulson, J.; Abbruscato, T. J.; Ahsan, F. *Pharm Res* **2004**, *21*, 1127-1136.
(227) Yu, S.; Zhao, Y.; Wu, F.; Zhang, X.; Lu, W.; Zhang, H.; Zhang, Q. *Int J Pharm* **2004**, *281*, 11-23.

(228) Zhang Yi, J. X.-G., Yao Jie *Acta Pharmacologica Sinica* **2001**, *22*, 1051-1056.
(229) Duan, X.; Mao, S. *Drug Discov Today* **2010**, *15*, 416-427.
(230) Vllasaliu, D.; Exposito-Harris, R.; Heras, A.; Casettari, L.; Garnett, M.; Illum, L.; Stolnik, S. *International Journal of Pharmaceutics* **2010**, *400*, 183-193.
(231) Lee, V. H.; Yamamoto, A.; Kompella, U. B. *Crit Rev Ther Drug Carrier Syst* **1991**, *8*, 91-192.
(232) Lee, W. A.; Narog, B. A.; Patapoff, T. W.; Wang, Y. J. *J Pharm Sci* **1991**, *80*, 725-729.
(233) Schipper, N. G.; Verhoef, J. C.; Merkus, F. W. *Pharm Res* **1991**, *8*, 807-814.
(234) Merkus, P.; Guchelaar, H. J.; Bosch, D. A.; Merkus, F. W. *Neurology* **2003**, *60*, 1669-1671.
(235) Marttin, E.; Verhoef, J. C.; Spies, F.; van der Meulen, J.; Nagelkerke, J. F.; Koerten, H. K.; Merkus, F. W. *J Control Release* **1999**, *57*, 205-213.
(236) Gizurarson, S. *Acta Pharm Nord* **1990**, *2*, 105-122.
(237) Ennis, R. D.; Borden, L.; Lee, W. A. *Pharm Res* **1990**, *7*, 468-475.
(238) Zhang, Z. B. *Zhong Xi Yi Jie He Za Zhi* **1991**, *11*, 144-146, 132.
(239) Wong, T. W. *Recent Pat Drug Deliv Formul* **2009**, *3*, 8-25.
(240) Aspden, T. J.; Mason, J. D.; Jones, N. S.; Lowe, J.; Skaugrud, O.; Illum, L. *J Pharm Sci* **1997**, *86*, 509-513.
(241) Tengamnuay, P. S., Amorn; Sailasuta, Achariya; Mitra, Ashim K. *INTERNATIONAL JOURNAL OF PHARMACEUTICS* **2000**, *197*, 53-67.
(242) Mei, D.; Mao, S.; Sun, W.; Wang, Y.; Kissel, T. *Eur J Pharm Biopharm* **2008**, *70*, 874-881.
(243) Luessen, H. L.; de Leeuw, B. J.; Langemeyer, M. W.; de Boer, A. B.; Verhoef, J. C.; Junginger, H. E. *Pharm Res* **1996**, *13*, 1668-1672.
(244) C.R. Behl; H.K. Pimplaskar; A.P. Sileno; J. deMeireles; Romeo, V. D. *Advanced Drug Delivery Reviews* **1998**, *29*, 89-116.
(245) Sailaja A Krishna; Amareshwar P; Chakravarty P *Research Journal of Pharmaceutical, Biologica, and Chemical Sciences* **2010**, *1*, 474-484.
(246) Sinswat, P.; Tengamnuay, P. *Int J Pharm* **2003**, *257*, 15-22.
(247) Dodane, V.; Amin Khan, M.; Merwin, J. R. *Int J Pharm* **1999**, *182*, 21-32.
(248) Illum, L.; Watts, P.; Fisher, A. N.; Hinchcliffe, M.; Norbury, H.; Jabbal-Gill, I.; Nankervis, R.; Davis, S. S. *Journal of Pharmacology and Experimental Therapeutics* **2002**, *301*, 391-400.
(249) Roon, K. I.; Soons, P. A.; Uitendaal, M. P.; de Beukelaar, F.; Ferrari, M. D. *Br J Clin Pharmacol* **1999**, *47*, 285-290.
(250) Haffejee, N.; Du Plessis, J.; Muller, D. G.; Schultz, C.; Kotze, A. F.; Goosen, C. *Pharmazie* **2001**, *56*, 882-888.
(251) Gould, S.; Scott, R. C. *Food Chem Toxicol* **2005**, *43*, 1451-1459.
(252) Liu, J.; Qiu, L.; Gao, J.; Jin, Y. *Int J Pharm* **2006**, *312*, 137-143.
(253) Szejtli, J. *Carbohydrate Polymers* **1990**, *12*, 375-392.
(254) Brewster, M. E.; Hora, M. S.; Simpkins, J. W.; Bodor, N. *Pharm Res* **1991**, *8*, 792-795.

(255) Brewster, M. E.; Vandecruys, R.; Peeters, J.; Neeskens, P.; Verreck, G.; Loftsson, T. *Eur J Pharm Sci* **2008**, *34*, 94-103.
(256) Hirayama, F.; Uekama, K. *Adv Drug Deliv Rev* **1999**, *36*, 125-141.
(257) Asai, K.; Morishita, M.; Katsuta, H.; Hosoda, S.; Shinomiya, K.; Noro, M.; Nagai, T.; Takayama, K. *Int J Pharm* **2002**, *246*, 25-35.
(258) Chavanpatil, M. D.; Vavia, P. R. *Eur J Pharm Biopharm* **2004**, *57*, 483-487.
(259) Shao, Z.; Krishnamoorthy, R.; Mitra, A. K. *Pharm Res* **1992**, *9*, 1157-1163.
(260) Zhang, Y.; Jiang, X. G.; Yao, J. *Acta Pharmacol Sin* **2001**, *22*, 1051-1056.
(261) Bagger, M.; Bechgaard, E. *Int J Pharm* **2004**, *269*, 311-322.
(262) Wang, X.; He, H.; Leng, W.; Tang, X. *Int J Pharm* **2006**, *317*, 40-46.
(263) Czapp, M.; Bankstahl, J. P.; Zibell, G.; Potschka, H. *Epilepsia* **2008**, *49*, 1142-1150.
(264) Li, F.; Feng, J.; Cheng, Q.; Zhu, W.; Jin, Y. *Int J Pharm* **2007**, *328*, 161-167.
(265) Vaka, S. R.; Murthy, S. N. *Pharmazie* **2010**, *65*, 690-692.
(266) Lingeman, H.; Underberg, W. *Detection-Oriented Derivatization Techniques in Liquid Chromatography*; Marcel Dekker, Inc.: New York, 1990.
(267) Hilgier, W.; Anderzhanova, E.; Oja, S. S.; Saransaari, P.; Albrecht, J. *European Journal of Pharmacology* **2003**, *468*, 21-25.
(268) Wu, S.; Dovichi, N. J. *J Chromatogr* **1989**, *480*, 141-155.
(269) Wu, S.; Dovichi, N. J. *Journal of Chromatography* **1989**, *480*, 141-155.
(270) Paxinos, G.; Watson, C., Eds. *The rat brain in stereotaxic coordinates; 4th Edition*; Academic Press: Sand Diego, CA, 1998.
(271) Boehlen, P.; Stein, S.; Udenfriend, S. *Archives of Biochemistry and Physics* **1974**, *163*, 390-399.
(272) Vaca, C. E.; Conradi, M.; Sievertzon, M.; Bergman, J. *Chemico-Biological Interactions* **1994**, *93*, 235-249.
(273) Schneider, F.; Lutun, P.; Couchot, A.; Bilbault, P.; Tempe, J. D. *Intensive Care Med* **1993**, *19*, 99-104.
(274) Rota, M.; Brulot, N.; Rezgui, N.; Labrousse, J.; Allard, D. *Clinica Chimica Acta* **1991**, *201*, 75-82.
(275) Nishikimi, T.; Miura, K.; Minamino, N.; Takeuchi, K.; Takeda, T., 267(1, Pt. 2) *American Journal of Physiology - Heart and Circulatory Physiology* **1994**, *267*, H182-H186.
(276) Chen, H. H.; Grantham, J. A.; Schirger, J. A.; Jougasaki, M.; Redfield, M. M.; Burnett, J. C., Jr. *Journal of the American College of Cardiology* **2000**, *36*, 1706-1712.
(277) Arnal, J. F.; Warin, L.; Michel, J. B. *Journal of Clinical Investigation* **1992**, *90*, 647-652.
(278) Mackenzie, I. M.; Garrard, C. S.; Young, J. D. *Anaesthesia* **2001**, *56*, 326-330.
(279) Galley, H. F.; Le Cras, A. E.; Logan, S. D.; Webster, N. R. *Br J Anaesth* **2001**, *86*, 388-394.
(280) Ferrero, R.; Rodriguez-Pascual, F.; Miras-Portugal, M. T.; Torres, M. *British Journal of Pharmacology* **1999**, *1277*, 779-787.
(281) Kiedrowski, L. *Ann. N.Y. Acad. Sci.* **2007**, *1099*, 383-395.

(282) Suwanwela, N.; Koroshetz, W. J. *Annu. Rev. Med.* **2007**, *58*, 89-106.
(283) Asai, S.; Kunimatsu, T.; Zhao, H.; Nagata, T.; Takahashi, Y.; Ishii, Y.; Kohno, T.; Ishikawa, K. *Clinical Neuroscience and Neuropahtology* **2000**, *11*, 2947-2952.
(284) Obrenovitch, T. P.; Zilkha, E.; Urenjak, J. *Naunyn-Schmiedeberg's Arch. Pharmacol.* **1998**, *357*, 225-231.
(285) Kunimatsu, T.; Asai, S.; Kanematsu, K.; Zhao, H.; Kohno, T.; Misaki, T.; Ishikawa, K. *Brain Research* **1999**, *831*, 273-282.
(286) Satoh, M.; Asai, S.; Katayama, Y.; Kohno, T.; Ishikawa, K. *Brain Research* **1999**, *822*, 142-148.
(287) Jarvis, C. R.; Anderson, T. R.; Andrew, R. D. *Cerebral Cortex* **2001**, *11*, 249-259.
(288) Giorgi, M.; D'Angelo, V.; Esposito, Z.; Nuccetelli, V.; Sorge, R.; Martorana, A.; Stefani, A.; Bernardi, G.; Sancesario, G. *European Journal of Neuroscience* **2008**, *28*, 941-950.
(289) Jeannot, V.; Salmon, J. M.; Deumie, M.; Viallet, P. *J Histochem Cytochem* **1997**, *45*, 403-412.
(290) Zhang, Q.; Jiang, X.; Jiang, W.; Lu, W.; Su, L.; Shi, Z. *Int J Pharm* **2004**, *275*, 85-96.
(291) Reger, M. A.; Watson, G. S.; Green, P. S.; Wilkinson, C. W.; Baker, L. D.; Cholerton, B.; Fishel, M. A.; Plymate, S. R.; Breitner, J. C.; DeGroodt, W.; Mehta, P.; Craft, S. *Neurology* **2008**, *70*, 440-448.
(292) Gozes, I.; Divinski, I. *Curr Alzheimer Res* **2007**, *4*, 507-509.